PROJECTIONS FOR CHANGES IN CLIMATOLOGY AND EXTREME EVENTS OF THE CORDEX-AUSTRALASIA DOMAIN: A DYNAMICAL DOWNSCALING APPROACH

by

Mustafa Tufan Turp

B.S. in Physics, Yıldız Technical University, 2006

M.S. in Computational Science and Engineering, Boğaziçi University, 2010

Submitted to the Institute of Environmental Sciences in partial fulfillment of

the requirements for the degree of

Doctor of Philosophy

in

Environmental Sciences

Boğaziçi University

2021

I dedicate this dissertation to my dear father Halil Şit Turp and my dear grandparents Fetullah Diri and Emine Diri, who passed away during my doctoral studies. Rest in peace!

ACKNOWLEDGEMENTS

I see this dissertation not only as a product of my doctoral studies, but also as a product of the labor of many people who have been involved in my life since the day I was born and contributed to me in many different subjects, either consciously or unconsciously. Therefore, first of all, I would like to thank all the people who have more or less established a place in my life and made me who I am. However, specific to this dissertation, I owe a few special people a debt of gratitude.

I would like to express my first thanks to the precious Prof. M. Levent Kurnaz, who is the only reason I started my academic career and progress without falling on this difficult road. As an academic role model of mine, I have always been proud to be your student. Thank you so much for your guidance, support, teaching, motivation and all the things you have contributed to me with your endless patience.

I would also like to thank my thesis supervisor, Prof. Orhan Yenigün, from whom I took the climate change course at Boğaziçi University for the first time, for his guidance, solution-oriented approaches to problems, motivation and support during my doctoral dissertation.

In addition, I would like to express my gratitude to my jury member Asst. Prof. Tuğba Öztürk, who answered my questions with all her knowledge during the formation and progress of my doctoral dissertation and helped improve the dissertation with his suggestions, and to Prof. Ali Kerem Saysel, who never denied her support through sharing ideas and information during my student life at Boğaziçi University. I also sincerely thank my esteemed jury members Prof. Nadim Copty and Prof. Mete Tayanç for their contribution during the completion of my dissertation.

Of course, during this long journey, people need more social and moral support as well as academic support. At this point, my dear friend and academic buddy Dr. Nazan An and her precious husband Barış An are the people who deserve the most special thanks. You have always been a sister and brother to me in my sadness, happiness, illness, health, moodiness, spoiledness, misery, stubbornness. Laughing and achieving together with you has always made this life more valuable for us. From now on, we will continue to make life valuable for us all together.

I would like to thank my 20-year-old friends Halil İbrahim Özel and Şerafettin Yüksel for putting up with me 24/7 and being two of the best methods of coping with stress, making my life meaningful and never leading me alone.

Moreover, I would like to thank Kamil Çöllü and Zekican Demiralay for their technical support during modeling studies and analysis. As my academic brothers, I think both of you will do very well in this field in the future. Additionally, I would like to thank Prof. Murat Türkeş, one of my extended iklimBU family, for everything he taught us and for his contributions to climate science. I would like to express my gratitude to my dear friends Assoc. Prof. Cenk Demiroğlu and Asst. Prof. Abdullah Akbaş for being by my side at all times and for increasing my academic productivity. Also, I would like to thank Başak Bilgin for her willing support and friendship.

Finally, I would like to express my endless gratitude to my beloved family, which is the reason for my existence and writing these lines. My dear father Halil Şit Turp, whom I lost about a year ago, I am proud to have you surname and from now on, I will always keep it alive with the works I will produce. My dear mother Perihan Turp and my sisters Deniz Turp and Derya Uysal, I could not achieved all of these without your endless love and support. However, I had gains as well as losses during this process. I would also like to thank my dear nephew Mustafa Eymen Uysal, who added joy to my life, and my dear sister's husband Mustafa Uysal. Thank you all!

ABSTRACT

PROJECTIONS FOR CHANGES IN CLIMATOLOGY AND EXTREME EVENTS OF THE CORDEX-AUSTRALASIA DOMAIN: A DYNAMICAL DOWNSCALING APPROACH

Climate change, which is one of the most vital threats to humanity today, will affect many countries on a regional and local scale in terms of common and country-specific areas. In order to adapt to the changing climate, the impacts of climate change in the future should be addressed well. For this reason, joint projects are developed that lead to the production of high resolution climate data in order to accurately determine the impacts of climate change in different parts of the world. In this thesis, within the scope of CORDEX, which is the most prominent of these joint projects today, changes in temperature and precipitation climatology of the Australasia region as well as changes in extreme climate events were examined. For Australasia, one of the least studied regions under the umbrella of CORDEX, the mean air temperature and precipitation changes for three different periods (i.e., 2016 - 2035, 2046 - 2065, 2081 - 2100) were analyzed under three different scenarios (i.e., RCP2.6, RCP4.5, RCP8.5 using global circulation models/global climate models with the approach of multi-model ensemble mean. Later, by using RegCM4.6 regional climate model, low resolution data of HadGEM2-ES and MPI-ESM-MR global climate models were dynamically downscaled to 50 km x 50 km horizontal resolution. Before the future projections were applied in the study, the most suitable Planetary Boundary Layer (PBL) scheme and convective parameterization of the RegCM4.6 model for the region were determined. Accordingly, the RegCM4.6 model was employed using the BATS landuse scheme with the Holtslag PBL scheme and the mixed convective parameterization which is the Tiedtke scheme over lands and the Emanuel scheme over oceans. With RegCM4.6 driven by HadGEM2-ES and MPI-ESM-MR outputs, mean, minimum and maximum temperatures and total precipitation of Australasia have been examined under the RCP4.5 and RCP8.5 scenarios for the periods of 2011-2040, 2041-2070, and 2071-2099 with respect to the reference period of 1971 - 2000. In another part of the study, using the NEX-GDDP dataset with a horizontal resolution of 0.25° x 0.25°, the temperature and precipitation extreme indices for the Australasia region were computed via the RCP4.5 and RCP8.5 scenario outputs of the ACCESS1-0 and MPI-ESM-LR models. While very hot days, tropical nights and heatwaves are used as temperature extremes, very heavy precipitation days, simple daily intensity and consecutive dry days are used for precipitation extremes. The changes in extreme climate events have been analyzed for 2016-2035, 2046-2065, and 2081-2100 with respect to the reference periods of 1981-2000.

The results of the analysis show that there will be increasingly higher temperatures in Australasia towards the end of the century. It is concluded that the mean temperature increase expectation of approximately 1.5 - 3 ℃ may be around 5 ℃ at the end of the century and this value can reach up to 7 ℃ for the maximum temperature. It appears that the expected warming may be greater as we approach the end of the century and move from the most optimistic to the most pessimistic scenario. On the other hand, the change in precipitation varies greatly depending on the period and sub-region. Average ±20 % change in precipitation may occur as 50 % or more increases or 30 % or more decreases in some places. In addition to the change in mean temperature and precipitation, it is clear that there will be an increase in temperature and precipitation extremes for the Australasia region. These results indicate that Australasia will have a future in which hot days and nights, heatwaves are more frequent, and the days with heavy precipitation are more common. In conclusion, it is certain that changes in both mean values and extreme climate events pose a very high risk in terms of human health, ecosystems and ecosystem services, habitats and limited agricultural areas in the region.

ÖZET

CORDEX-AVUSTRALASYA BÖLGESİNİN KLİMATOLOJİSİ VE EKSTREM OLAYLARINDAKİ DEĞİŞİMLERİN PROJEKSİYONU: DİNAMİK ÖLÇEK KÜÇÜLTME YAKLAŞIMI

Günümüzde insanlığın maruz kaldığı en önemli tehditlerin başında gelen iklim değişikliği, bölgesel ve yerel ölçekte birçok ülkeyi ortak ve ülkelere özgü alanlarda oldukça olumsuz etkileyecektir. Değişen iklime uyum gösterilebilmesi için gelecekte iklim değişikliğinin neden olacağı etkileri de iyi tespit etmek gerekir. Bu nedenle iklim değişikliğinin dünyanın farklı yerlerindeki etkilerini doğru bir şekilde tespit edebilmek için yüksek çözünürlüklü iklim verilerinin üretilmesine ön ayak olan ortak projeler geliştirilmektedir. Bu tezde de günümüzde bu ortak projelerin en önemlisi olan CORDEX kapsamında Avustralasya bölgesinin sıcaklık ve yağış klimatolojilerindeki değişimlerin yanı sıra ekstrem iklim olaylarındaki değişimler incelenmiştir. CORDEX çatısı altında en az çalışılan bölgelerden biri Avustralasya için, öncelikle çoklu model ortalaması yaklaşımıyla küresel dolaşım modelleri/küresel iklim modelleri kullanılarak üç farklı senaryo (RCP2.6, RCP4.5 ve RCP8.5) altında üç farklı dönem (2016 - 2035, 2046 - 2065, 2081 - 2100) için ortalama hava sıcaklığı ve yağış değişimleri analiz edilmiştir. Daha sonra RegCM4.6 bölgesel iklim modeli kullanılarak HadGEM2-ES ve MPI-ESM-MR küresel iklim modellerinin düşük çözünürlüklü verileri dinamik ölçek küçültme yaklaşımı ile 50 km x 50 km yatay çözünürlüğüne yükseltilmiştir. Çalışmada gelecek projeksiyonları yapılmadan önce RegCM4.6 modelinin bölge için en uygun Gezegen Sınır Katmanı (PBL) şeması ve konvektif parametrizasyonu tespit edilmiştir. Buna göre RegCM4.6 modeli BATS arazi kullanım şeması ile Holtslag PBL ve karalar üzerinde Tiedtke okyanus üzerinde Emanuel şemalarının olduğu karma konvektif parametrizasyonu kullanılarak çalıştırılmıştır. HadGEM2-ES ve MPI-ESM-MR çıktıları kullanılarak çalıştırılan RegCM4.6 ile Avustralasya bölgesinin ortalama, minimum ve maksimum sıcaklıkları ile toplam yağışı RCP4.5 ve RCP8.5 senaryoları altında 2011 - 2040, 2041 - 2070 ve 2071-2099 dönemleri için 1971 - 2000 referans dönemine kıyasla incelenmiştir. Çalışmanın bir başka kısmında ise 0.25° x 0.25° yatay çözünürlüğe sahip NEX-GDDP veri seti kullanılarak ACCESS1-0 ve MPI-ESM-LR modellerinin RCP4.5 ve RCP8.5 senaryo çıktıları ile Avustralasya bölgesi için sıcaklık ve yağış ekstrem endeksleri hesaplanmıştır. Sıcaklık ekstremleri olarak çok sıcak günler, tropik geceler ve sıcak dalgası kullanılırken, yağış ekstremleri için çok yoğun yağışlı

günler, günlük temel yağış yoğunluğu ve ardışık kuru günler kullanılmıştır. Ekstrem iklim olaylarındaki değişimler 2016 - 2035, 2046 - 2065 ve 2081-2100 için 1981 - 2000 referans dönemine kıyasla incelenmiştir.

Yapılan analiz sonuçları Avustralasya bölgesinde yüzyıl sonuna doğru giderek daha da artan yüksek sıcaklıkların olacağını göstermektedir. Yaklaşık 1.5 - 3 ℃ arasındaki ortalama sıcaklık artışı beklentisinin yüzyıl sonunda 5 ℃ civarında olabileceği ve bu değerinin maksimum sıcaklık için 7 ℃'ye kadar varabileceği söylenebilir. Beklenen ısınmanın yüzyıl sonuna doğru yaklaştıkça ve en iyimserden en kötümser senaryoya geçtikçe daha fazla olabileceği görülmektedir. Buna karşılık, yağıştaki değişim ise dönem ve alt bölgeye bağlı olarak çok fazla değişkenlik göstermektedir. Yağışta ortalama ± % 20 oranındaki değişim, bazı yerlerde % 50 ve üzeri artışlar veya % 30 ve üzeri azalışlar şeklinde olabilecektir. Ortalama sıcaklık ve yağıştaki değişimin dışında Avustralasya bölgesi için sıcaklık ve yağış ekstremlerinde de artış olacağı açıktır. Bu sonuçlar da Avustralasya bölgesini sıcak gün ve gecelerin, sıcak dalgasının sıklaştığı, aynı zamanda şiddetli yağışlı günlerin daha çokça görüldüğü bir geleceğin beklediğine işaret etmektedir. Sonuç olarak, hem ortalama değerler hem de ekstrem iklim olaylarındaki değişimlerin bölgedeki insan sağlığı, ekosistemler ve ekosistem hizmetleri, yaşam alanları ve sınırlı tarım alanları açısından oldukça yüksek risk doğurduğu kesindir.

TABLE OF CONTENTS

LIST OF FIGURES

LIST OF TABLES

LIST OF SYMBOLS/ABBREVIATIONS

Symbol	Explanation	Unit
CH_4	Methane	ppb
CO_2	Carbon dioxide	ppm
F_c	Vertical Eddy Flux	
γ_c	Counter Gradient	
g	Gravitational Acceleration	
h	Height	
$H_2O_{(g)}$	Water vapour	
$\mathrm{i}_1(\mathrm{t},\mathrm{x})$	Element Number x of the Field at Time Step t of the First Input File (model 1)	
$\mathrm{i}_2(\mathrm{t},\mathrm{x})$	Element Number x of the Field at Time Step t of the Second Input File (model 2)	
$\mathrm{i}_\mathrm{n}(\mathrm{t},\mathrm{x})$	Element Number x of the Field at Time Step t of the nth Input File (model n)	
κ	Diffusivity	
k	Von Karman Constant	
K_c	Eddy Diffusivity	
N_2O	Nitrous oxide	ppb
$\mathrm{o}(\mathrm{t},\mathrm{x})$	Element Number x of the Field at Time Step t of Output File (Ensemble Mean)	
O_2	Oxygen	
O_3	Ozone	
p	Pressure	
p_s	Surface Pressure	
p_t	Top Pressure	
Q	Total Water Mixing Ratio	

R_{icr}	Critical Bulk Richardson Number
σ	Sigma
$\dot{\sigma}$	Sigmadot
S	Shear
SO_4	Sulfate
θ_l	Liquid Water Potential Temperature
θ_s	Appropriate Temperature.
θ_v	Virtual Potential Temperature
u	Zonal Wind Component
u_i	Momentum
ϕ_c^0	Surface Temperature or Water Vapor Flux
v	Meridional Wind Component
w_t	Turbulent Convective Velocity
ω	Omega

Abbreviation	**Explanation**
A1	Global and Economy Based Growth Scenario
A2	Regional and Economy Based Growth Scenario
AAO	Antarctic Oscillation
ACCESS1.0	Australian Community Climate and Earth-System Simulator Global Climate Model Version 1.0
ACCESS1.3	Australian Community Climate and Earth-System Simulator Global Climate Model Version 1.3
ADW	Angular-Distance Weighting
Af	Tropical Rainforest Climate
Am	Tropical Monsoon Climate
AR4	Assessment Report 4
AR5	Assessment Report 5

AR6	Assessment Report 6
ATM	RegCM Outputs for Atmosphere
Aw	Tropical Savanna, Wet
B1	Global and Environment Based Growth Scenario
B2	Regional and Environment Based Growth Scenario
Bash	Bourne-again shell
BATS	Biosphere-Atmosphere Transfer Scheme
BATS1e	Biosphere-Atmosphere Transfer Scheme Version 1e
BC	Black Carbon
BCC-CSM1-1	Beijing Climate Center Climate System Model Version 1.1
BCSD	Bias-Correction Spatial Disaggregation
BNU-ESM	Beijing Normal University Earth System Model
BOM	Australian Government Bureau of Meteorology
BSh	Hot Semi-arid Climate
BSk	Cold Semi-arid Climate
BWh	Hot Desert Climate
BWk	Cold Desert Climate
CanESM2	Second Generation Canadian Center for Climate Modelling and Analysis Earth System Model
CCI	Climate Change Initiative
CCM1	Community Climate Model Version 1
CCM2	Community Climate Model Version 2
CCM3	Community Climate Model Version 3
CCSM	Community Climate System Model
CCSM4	US National Centre for Atmospheric Research CCSM Version 4
CDO	Climate Data Operators
CESM1-BGC	NSF-DOE-NCAR Community Earth System Model, Version 1–Biogeochemistry

Cfa	Humid Subtropical Climate
Cfb	Temperate Oceanic Climate
Cfc	Subpolar Oceanic Climate
CHRM	Regional Climate Model of the Swiss Federal Institute of Technology
CLARIS	A Europe-South America Network for Climate Change Assessment and Impact Studies
CLIVAR	Climate and Ocean: Variability, Predictability and Change
CLM3.5	Community Land Model Version 3.5
CLM4.5	Community Land Model Version 4.5
CMCC-CM	Centro Euro-Mediterraneo sui Cambiamenti Climatici Climate Model
CMCC-CMS	Centro Euro-Mediterraneo sui Cambiamenti Climatici Stratosphere-resolving Climate Model
CMIP	Coupled Model Intercomparison Project
CMIP2	Coupled Model Intercomparison Project Phase 2
CMIP3	Coupled Model Intercomparison Project Phase 3
CMIP5	Coupled Model Intercomparison Project Phase 5
CMIP6	Coupled Model Intercomparison Project Phase 6
CNRM-CM5	National Centre for Meteorological Research Climate Model Version 5
CORDEX	Coordinated Regional Climate Downscaling Experiment
CORDEX-CORE	Coordinated Regional Climate Downscaling Experiment - Coordinated Output for Regional Evaluations
COSMO-CLM	The Consortium for Small-scale Modelling- Climate Limited-area Modelling
CPU	Central Processing Unit
CRU	Climatic Research Unit
CRU TS	Climatic Research Unit Gridded Time Series
Csa	Hot-summer Mediterranean Climate
Csb	Warm-summer Mediterranean Climate

CSIRO	Commonwealth Scientific and Industrial Research Organisation
CSIRO-MK3-6-0	Climate System Model of Commonwealth Scientific and Industrial Research Organisation
Cwa	Monsoon-influenced Humid Subtropical Climate
DJF	December - January - February
DOE	United States Department of Energy
EC-EARTH	European community Earth-System Model
ECMWF	European Centre for Medium-Range Weather Forecasts
ENIAC	Electronic Numerical Integrator and Computer
ENSEMBLES	Ensemble-based Predictions of Climate Changes and their Impacts
ENSO	El Niño Southern Oscillation
ERA-Interim	Global reanalysis climate data produced by the ECMWF
ESM	Earth System Model
ET	Expert Team
ETCCDI	Expert Team on Climate Change Detection and Indices
EURO	Europe
FAR	First Assessment Report
GCM	General Circulation Model / Global Climate Model
GFDL-CM3	Climate Model of Geophysical Fluid Dynamics Laboratory Version 3
GFDL-ESM2G	NOAA Geophysical Fluid Dynamics Laboratory Earth System Model Version 2G
GFDL-ESM2M	National Oceanic and Atmospheric Administration Geophysical Fluid Dynamics Laboratory Model
GHCN	Global Historical Climatology Network
GISS	Goddard Institute for Space Studies
GISS-E2-R	NASA Goddard Institute for Space Studies E2-R Model
GMFD	Global Meteorological Forcing Dataset
GMTED2010	Global Multi-resolution Terrain Elevation Data 2010

GrADS	Grid Analysis and Display System
HadGEM2-AO	United Kingdom Met Office Hadley Centre Aerosol and Ocean Model
HadGEM2-CC	United Kingdom Met Office Hadley Centre Carbon Cycle Model
HadGEM2-ES	United Kingdom Met Office Hadley Centre Earth System Model
HGE-4.5	HadGEM2-ES under RCP4.5 scenario
HGE-8.5	HadGEM2-ES under RCP8.5 scenario
HIRHAM	Regional Climate Model of the Danish Meteorological Institute
ICBC	Initial and Boundary Condition
ICTP	Abdus Salam International Centre for Theoretical Physics
INMCM4	Russian Institute for Numerical Mathematics Climate Model Version 4
IOD	Indian Ocean Dipole
IPCC	Intergovernmental Panel on Climate Change
IPSL-CM5A-LR	Institut Pierre Simon Laplace Climate Model CM5A-LR
IPSL-CM5A-MR	Institut Pierre Simon Laplace Model CM5A-MR
IS92	IPCC 1992 Scenarios
ITCZ	Intertropical Convergence Zone
JCOMM	Joint Technical Commission for Oceanography and Marine Meteorology
JJA	June - July - August
MAM	March - April - May
MED	Mediterranean
MENA	Middle East and North Africa
MIROC5	University of Tokyo, National Institute for Environmental Studies, and Japan Agency for Marine-Earth Science and Technology (MIROC) Version 5
MIROC-ESM	University of Tokyo, National Institute for Environmental Studies, and Japan Agency for Marine-Earth Science and Technology (MIROC) Earth System Model

MIROC-ESM-CHEM	University of Tokyo, National Institute for Environmental Studies, and Japan Agency for Marine-Earth Science and Technology (MIROC) Earth System Model Chemistry
MIT	Massachusetts Institute of Technology
MJO	Madden-Julian Oscillation
MM4	Mesoscale Model Version 4
MM5	Mesoscale Model Version 5
MPI-4.5	MPI-ESM-MR under RCP4.5 scenario
MPI-8.5	MPI-ESM-MR under RCP8.5 scenario
MPI-ESM-LR	Max Planck Institute for Meteorology Earth System Model LR
MPI-ESM-MR	Max Planck Institute for Meteorology Earth System Model MR
MRI-CGCM3	Meteorological Research Institute Coupled Global Climate Model Version 3
NARCCAP	North American Regional Climate Change Assessment Program
NASA	National Aeronautics and Space Administration
NCAR	National Center for Atmospheric Research
NCCS	NASA Center for Climate Simulation
NCEI	National Centers for Environmental Information
NCEP	National Centers for Environmental Prediction
NCL	NCAR Command Language
NetCDF	Network Common Data Form
NEX-GDDP	NASA Earth Exchange Global Daily Downscaled Projections
NOAA	National Oceanic and Atmospheric Administration
NorESM1-M	Norwegian Climate Centre Earth System Model M
NSF	National Science Foundation
OC	Organic Carbon
PBL	Planetary Boundary Layer
PNNL	Pacific Northwest National Lab

ppb	parts per billion
ppm	parts per million
PRUDENCE	Prediction of Regional Scenarios and Uncertainties for Defining European Climate Change Risks and Effects
PSU/NCAR	Pennsylvania State University/National Center for Atmospheric Research
QGIS	Quantum Geographic Information System
RAD	RegCM Outputs for Radiation
RCA	Rossby Centre Regional Climate Model
RCM	Regional Climate Model
RCP	Representative Concentration Pathway
RCP2.6	Representative Concentration Pathway 2.6
RCP4.5	Representative Concentration Pathway 4.5
RCP6.0	Representative Concentration Pathway 6.0
RCP8.5	Representative Concentration Pathway 8.5
RegCM	Regional Climate Model System maintained by the Abdus Salam International Center for Theoretical Physics Earth System Physics section
RegCM1	RegCM Version 1
RegCM2	RegCM Version 2
RegCM2.5	RegCM Version 2.5
RegCM3	RegCM Version 3
RegCM4	RegCM Version 4
RegCM4.5	RegCM Version 4.5
RegCM4.6	RegCM Version 4.6
REMO	Regional Climate Model of the Max-Planck-Institute of Meteorology
RESM	Regional Earth System Model
RMSE	Root Mean Square Error

ROMS	Regional Ocean Modeling System
RRTM	Rapid Radiative Transfer Model
SA90	IPCC 1990 Scenario A
SAM	Southern Annular Mode
SAR	Second Assessment Report
SDD	Statistical-Dynamical Downscaling
SEA	South East Asia
SON	September - October - November
SPCZ	South Pacific Convergence Zone
SRES	Special Report on Emission Scenarios
SRF	RegCM Outputs for Surface
SSP	Shared Socio-economic Pathway
SSP1	Shared Socio-economic Pathway with low challenges
SSP2	Shared Socio-economic Pathway with intermediate challenges
SSP3	Shared Socio-economic Pathway with high challenges
SSP4	Shared Socio-economic Pathway with predominantly adaptation challenges
SSP5	Shared Socio-economic Pathway with predominantly mitigation challenges
SST	Sea Surface Temperature
STS	RegCM Outputs for Statistical Daily Surface
SUBEX	Subgrid Explicit Moisture Scheme
TAR	Third Assessment Report
UDEL	University of Delaware
UN	United Nations
UNFCCC	United Nations Framework Convention on Climate Change
UW	University of Washington
UW-PBL	University of Washington Planetary Boundary Layer

WCRP	World Climate Research Programme
WGI	Working Group I
WMO	World Meteorological Organization
WRFP/WRFG	Weather Research & Forecasting Model PNNL/Grell

1. INTRODUCTION

With the Industrial Revolution, because of the extensive use of fossil fuels on a global scale, excessive accumulation in the atmospheric carbon dioxide has caused an increase in the average temperature of Earth and a rapid climate change has been observed all around the world. Carbon dioxide emission due to extensive use of fossil fuels, which was regarded as the pivotal environmental issue in the world in 1979 ("Costs and benefits of carbon dioxide", 1979; WMO, 1979), has maintained its importance progressively and became the most crucial threat of the 21st century. Climate change is not just an environmental threat today. It has been directly or indirectly effective in numerous fields, including health, agriculture, forests, water resources, coastal areas, and other natural areas, and has been the main cause of devastating losses, not only for humanity but for all species. The concentration of atmospheric carbon dioxide, which is the principal greenhouse gas, has reached over 410 ppm (parts per million) levels today with an acceleration increasing from 280 ppm value during the Industrial Revolution period and it tends to increase rapidly. When the warmest 20 years of the global records are listed, the warmest 19 years took place in the first two decades of the millennium (Table 1.1 and Table 1.2). For instance; as seen in Table 1.1, according to National Oceanic and Atmospheric Administration (NOAA) National Centers for Environmental Information (NCEI) data, the global average temperature was 1 ℃ warmer in 2016 compared to the 1901 - 2000 reference period and 0.98 ℃ warmer in 2020. Similarly, as seen in Table 1.2, according to National Aeronautics and Space Administration (NASA) data, 2016 and 2020 have been recorded as the warmest year together so far. According to NASA, global average temperatures in both 2016 and 2020 were 1.02 ℃ warmer than the 30-year base period between 1951 and 1980.

Table 1.1. List of the top-warmest years on global record by NOAA NCEI (Data source: NOAA NCEI, 2021).

Rank	**Year**	**Anomaly (°C)**	**Rank**	**Year**	**Anomaly (°C)**
1	2016	1.00	**11**	1998	0.65
2	2020	0.98	**12**	2003	0.64
3	2019	0.95	**12**	2006	0.64
4	2015	0.93	**12**	2009	0.64
5	2017	0.91	**12**	2012	0.64
6	2018	0.83	**13**	2002	0.62
7	2014	0.74	**13**	2007	0.62
8	2010	0.72	**14**	2004	0.58
9	2013	0.68	**15**	2001	0.57
10	2005	0.67	**15**	2011	0.57

Table 1.2. List of the top-warmest years on global record by NASA (Data source: NASA, 2021a).

Rank	**Year**	**Anomaly (°C)**	**Rank**	**Year**	**Anomaly (°C)**
1	2016	1.02	**10**	2009	0.66
1	2020	1.02	**11**	2006	0.64
2	2019	0.98	**11**	2012	0.64
3	2017	0.92	**12**	2002	0.63
4	2015	0.90	**13**	2003	0.62
5	2018	0.85	**14**	1998	0.61
6	2014	0.75	**14**	2011	0.61
7	2010	0.72	**15**	2001	0.54
8	2005	0.68	**15**	2004	0.54
8	2013	0.68	**15**	2008	0.54
9	2007	0.67	**16**	1997	0.46

The global average temperature trend in the 1980 - 2020 period indicates an increase of 0.8 °C every 10 years (Figure 1.1). Moreover, the increasing trend of the last 40 years is also remarkable

(Figure 1.1 and Figure 1.2). Although the ranking of the global warmest years varies slightly depending on the reference period and the data source, these small changes in the ranking do not change the fact that the year 2000 and beyond experienced an extreme warming on a global scale, except for 1997 - 1998 and 2014 - 2016, which coincided with the most severe periods of El Niño Southern Oscillation (ENSO). Beyond all these, another striking point is that the top 7 warmest years until 2020, whether it be NOAA data or NASA data, are the last 7 years between 2014 and 2020. As in 2019 and 2020, the next 8 years between 2020 and 2028 are also expected to be among the top 10 warmest years on a global scale (Arguez et al., 2020).

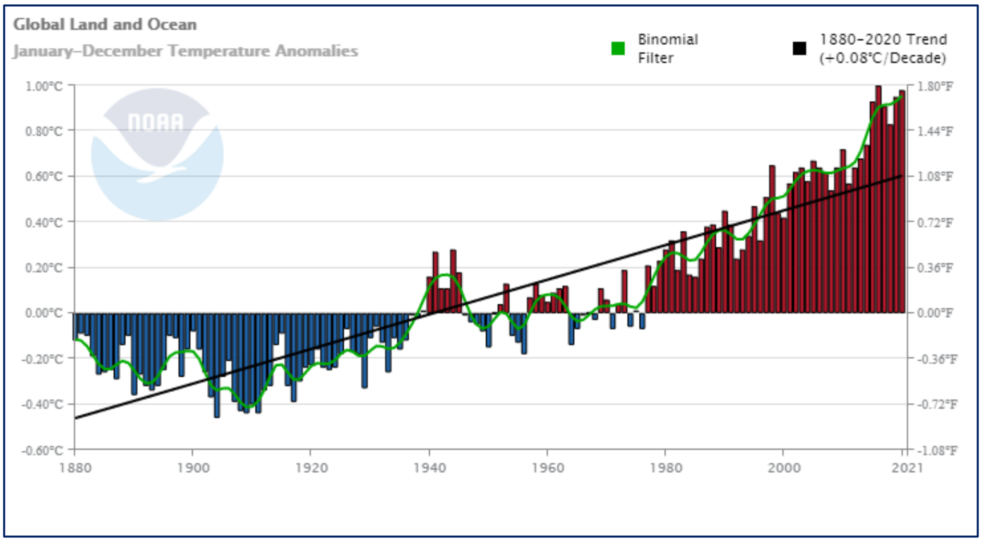

Figure 1.1. Annual global average temperature anomalies and trend for the period of 1880 - 2020 (Plotted via NOAA NCEI (2021)). In the graph, the blue colored columns show colder years compared to the 20th century average, and the red colored columns show warmer years compared to the same reference period. The green solid line also shows the smooth trend (using binomial filter).

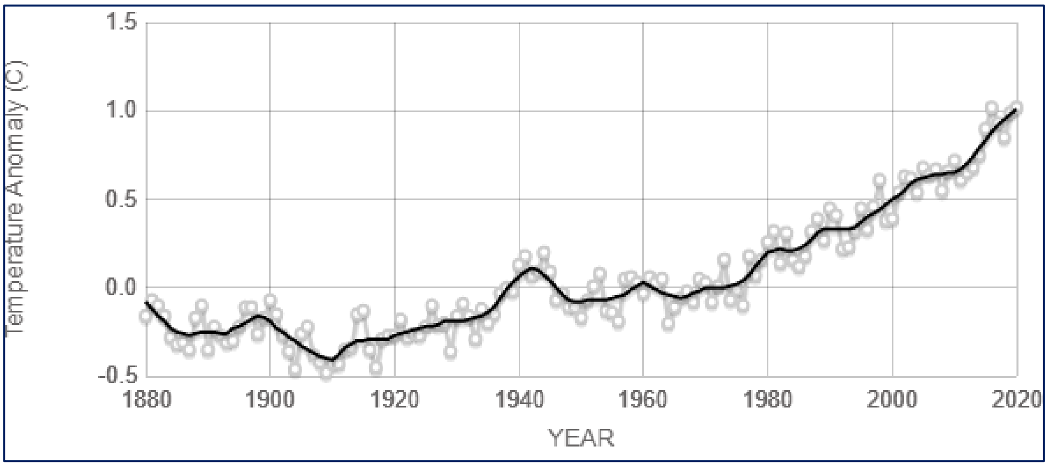

Figure 1.2. Annual global average temperature anomalies and trend for the period of 1880 - 2020 (Plotted via NASA (2021a)). In the graph, the hollow gray bubbles show the annual anomalies in global average temperatures compared to 1951 - 1980, and the black solid line shows the smooth trend (using locally weighted scatterplot smoothing approach).

Climate change is defined in the United Nations Framework Convention on Climate Change (UNFCCC) as "*a change of climate which is attributed directly or indirectly to human activity that alters the composition of the global atmosphere and which is in addition to natural climate variability observed over comparable time periods*" (UNFCCC, 1992). Adverse effects of climate change are also defined as "*changes in the physical environment or biota resulting from climate change which have significant deleterious effects on the composition, resilience or productivity of natural and managed ecosystems or on the operation of socio-economic systems or on human health and welfare*" (UNFCCC, 1992). In the 1st Working Group Section (WGI) of the Fifth Assessment Report (AR5) (IPCC, 2013) announced by the Intergovernmental Panel on Climate Change (IPCC), which published the most up-to-date scientific, technical and socioeconomic information in regular reports with the contribution of a large number of scientists, it is declared that the climate system is undoubtedly warming and it is very likely (at least 95 % probability) that more than half of the increase in mean surface temperatures since the middle of the 20th century is caused by the increase in human-made greenhouse gas emissions. Furthermore, it is stated that this finding is based on stronger and more concrete evidence than the previous IPCC Assessment Report (Assessment Report 4 -AR4-). In other words, the AR5, with the growing evidence of the human effect on climate as against the AR4, states that the primary reason for the warming observed since the middle of the 20th century is very likely humankind.

According to the AR5, warming in our climate system is unquestionable and extraordinary changes in Earth's climate have been observed for many years since the 1950s (IPCC, 2013).

During this period, the atmosphere and the oceans have become warmer, the amount of snow and ice has become smaller, the sea level has risen and the greenhouse gas levels have increased. In the Northern Hemisphere, the 30-year period between 1983 and 2012 was probably the hottest three decades of the last 1400 years (IPCC, 2013; Türkeş, 2013). The global mean surface temperature increased by 0.89 °C between 1901 and 2012, which is the longest period in which regional trends can be calculated sufficiently (IPCC, 2013; Türkeş, 2013). During this period, almost the entire globe was warmed. In addition, changes in extreme climate events have been observed since the 1950s. For instance; while the number of cold days decreases on a global scale, the number of hot days increases. The frequency and/or intensity of heatwaves and heavy precipitation events have increased in many regions of the world. The oceans are warming, and the global mean sea level rose 19 cm between 1901 and 2010 (IPCC, 2013; Türkeş, 2013). In the last 20 years, Greenland and Antarctic ice cover have lost mass; glaciers have shrunk all over the world. The concentrations of carbon dioxide (CO_2), methane (CH_4) and nitrous oxide (N_2O) gases in the atmosphere have reached unprecedentedly high levels of the last 800 thousand years (Figure 1.3). Carbon dioxide emissions, primarily due to the use of fossil fuels and secondary net land use change, increased by 40 % compared to the pre-industrial period (IPCC, 2013; Türkeş, 2013). In addition, 30 % of anthropogenic carbon dioxide emission is absorbed by the oceans, causing acidification in the oceans (IPCC, 2013; Türkeş, 2013).

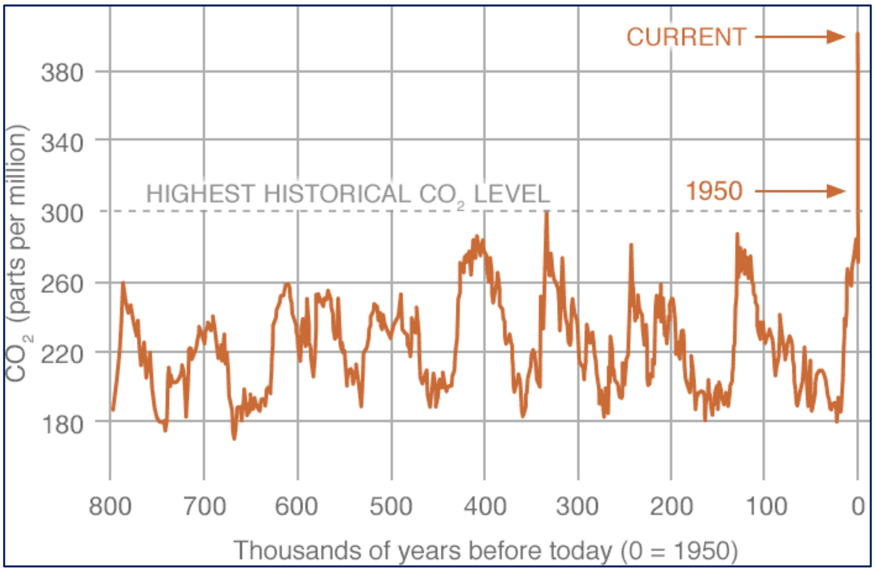

Figure 1.3. Historical global atmospheric carbon dioxide concentration in parts per million (ppm) (Reproduced from NASA (2021b)).

Considering the direct and indirect connections of climate change to climatic, biological and social disasters in the light of all this information, studies that provide information about possible climate conditions by projecting future climate conditions are vital. The climate system, which has a very complex structure since it contains many variables, cycles, processes and interactions together, is a very large and difficult problem in terms of modeling in this context. Another factor which makes this problem difficult is that it is strenuous and complicated to predict the prospective behavior of human beings. Therefore, the reliability of climate change studies carried out by considering various scenarios in terms of possible behaviors of human beings is higher. According to the new scenario sets (Representative Concentration Pathways – RCPs) used in the fifth report of the IPCC (Meinshausen et al., 2011; van Vuuren et al., 2011a), the changes expected in the climate are similar to the AR4 in terms of magnitude and patterns, considering the distinctnesses between these scenarios (IPCC, 2013; Türkeş, 2013). Based on the AR5, an increase in global surface temperature is likely to exceed 1.5 °C under new scenarios (RCP4.5, RCP6.0, and RCP8.5) except for the RCP2.6 scenario by the end of this century with respect to the period of 1850 - 1900 (IPCC, 2013). Considering only the RCP6.0 and RCP8.5 scenarios, warming is likely to exceed 2 °C by the end of the 21st century. According to the RCP4.5 scenario, it is more likely to not exceed 2 °C. Global warming will continue after 2100 in the projection made based on all scenarios except RCP2.6. Warming will continue to show interannual to decadal variability and it will not show regional homogeneity. According to the report in question, the global average surface temperature increase in the 2016 - 2035 period will likely be in the range of 0.3 - 0.7 °C compared to the 1986 - 2005 period. In terms of natural internal variability, short-term increases in seasonal average and annual average temperatures are expected to be very likely higher in tropical and subtropical belts than in mid-latitudes.

It is very valuable to bring together the above-mentioned changes in climate and the impacts of climate change observed and projected all over the world under the leadership of the IPCC and periodically presenting them in a consensus. However, since the topographical and geographical features of each region and each country differ from each other, and the levels of vulnerability to climate change are distinct, the need for regional studies is highlighted, particularly in determining the impacts of climate change.

Coordinated Regional Climate Downscaling Experiment (CORDEX), which was created to carry out these regional studies within the framework of a functional academic cooperation, provides the creation of significant scientific resources within the IPCC reports by initiating the realization of current climate change projections. Although there are increasingly various studies within the frame of CORDEX initiative, most of these studies mainly focus on the domains of Africa, Europe, and the Mediterranean. This situation creates a handicap in terms of evaluating the vulnerability of some regions or sub-regions to climate change. For instance, as recommended by Evans (2011), performing unique simulations for the CORDEX-Australasia by different groups must be urgently fostered. Apart from Evans (2011), Perkins-Kirkpatrick et al. (2016) also strongly emphasized that an international comprehensive collaboration is required to understand the change in heatwaves over Australia better. The current situation of regional climate change and modeling studies and the aforementioned scientific suggestions also provide a basis for the formation of this thesis.

1.1. Literature Review

As stated in the previous section and as it is well known, it is certain that Earth has been warming. When the data on the large time scale by the beginning of the 20th century to the first decade of the millennium are examined, it is obvious that there is a warming trend in all seasons, particularly during winter (Donat et al., 2013, 2014). In essence, the destructive effects of temperature and precipitation changes rather than the increase in the global mean temperature are vital in terms of environment and society. As shown in Figure 1.4, it is necessary to perceive a warming world not only as an increase in mean temperatures but as an increased probability of seeing hotter and extremely hot temperatures than average. Observations also fall in with this fact, which means warm temperature extremes have continued to increase, whereas there is a decreasing trend in cold temperature extremes (Alexander, 2016).

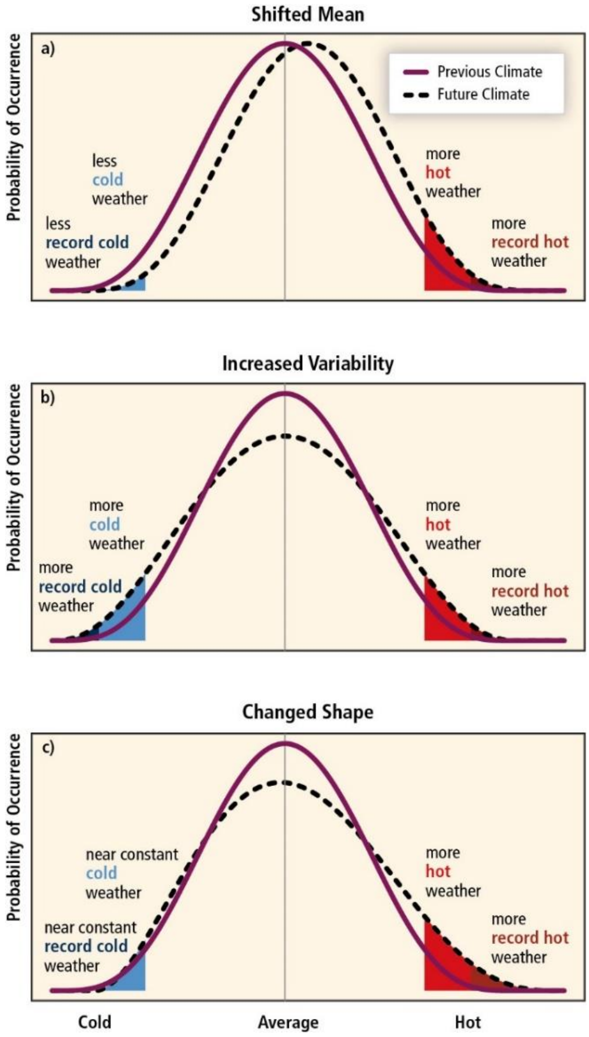

Figure 1.4. Change in probability of occurrence for temperature extremes: (a) shifted mean, (b) increased variability, and (c) changed shape (IPCC, 2012).

Temperature and precipitation extremes become more severe, more frequent, and longer-lasting under a changing climate (Seneviratne et al., 2012). Although precipitation extremes show more significant variability relative to temperature extremes, the increasing heavy precipitation trend seems to be more dominant than the decreasing trend (Donat et al., 2013). Temperature extremes occur much faster than projected by climate models (Li et al., 2018). Therefore, the sectoral effects of extreme events may be greater than expected (Schewe et al., 2019).

The observation results highlight warmer and wetter conditions globally in the 20th century (Alexander et al., 2006). According to Perkins et al. (2012), the frequency, intensity, and duration of heatwaves and warm spells between 1950 and 2011 have been increased globally. In addition, the probability of heatwaves occurring at very short intervals in succession becomes more likely in the future (Baldwin et al., 2019). Similarly, both observation and climate model results reveal that excessive precipitation has risen globally, regardless of the dry or humid region from 1951 to 2010

(Donat et al., 2016). Analysis results based on the GCMs in CMIP5 indicate that there will be an increase in the intensity of precipitation in the world, and this increase will be more pronounced, especially in extra-tropical regions (Bador et al., 2018).

Before moving on to the observed and projected changes for the Australasia domain identified above on a global scale, the term Australasia should be underlined. The term Australasia can basically be defined as a name given to the geographical region comprising Australia, New Zealand, and New Guinea. In terms of CORDEX, it should be noted that it includes some island countries, large and small, around these main countries. Regardless of how large the scale is, Australia, with its largest landmass, is the primary focus of this domain in any case.

As of 2020, Australia has warmed an average of 1.44 ℃ in the last 110 years (CSIRO and BOM, 2020). In Australia, which gets warmer above the global average, it is seen that temperature increases have been higher particularly since the second half of the 20th century (CSIRO and BOM, 2020). While 2019 was recorded as the warmest year in Australia's historical records, 7 years in the period of 2013 - 2019 were among the top 9 warmest years in Australia’s historical records (CSIRO and BOM, 2020). In Australia, not only mean temperatures have increased, but also extreme temperatures. For instance, in 2019, the number of extremely hot days was more than 3 times higher than in the last century (CSIRO and BOM, 2020). Alongside the increase in extreme temperatures, extremely cold days in Australia have decreased across the continent, except in the southwestern and southeastern parts of the country (CSIRO and BOM, 2020). For instance, observation results for the period of 1910 - 2018 show an increase in the number of days above 40 °C (Figure 1.5) and a decrease in the number of days below 10 °C (Figure 1.6) in Australia (BOM, 2020). By the way, the extreme temperature indices calculated from the minimum temperatures increase more noticeably than the extreme temperature indices calculated from the maximum temperatures for Australia (Jacob and Walland, 2016).

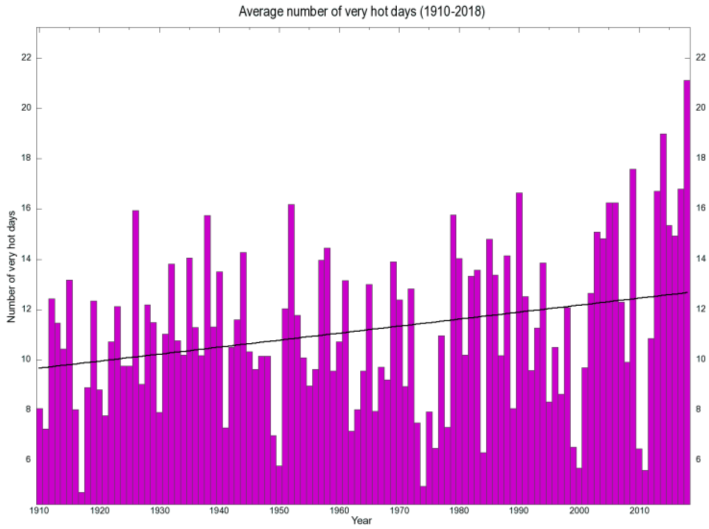

Figure 1.5. Annual time series of the number of days above 40 °C (Plotted via BOM (n.d.-a)).

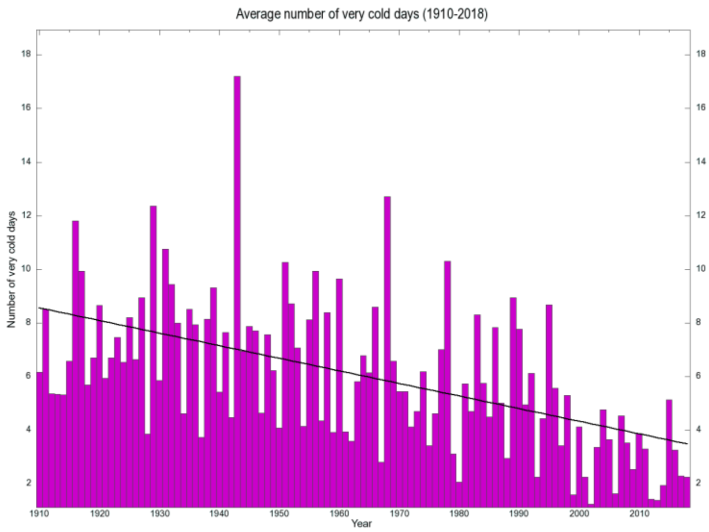

Figure 1.6. Annual time series of the number of days below 10 °C (Plotted via BOM (n.d.-b)).

It has been determined that the significant increase in the number and intensity of temperature and precipitation extremes in Australia in the second half of the 20th century has been observed again on a larger time scale between the beginning of the 20th century and the beginning of the 21st century (Collins et al., 2000; Alexander and Arblaster, 2009; Cowan et al., 2014; Alexander and Arblaster, 2017). In the southwest of Australia, precipitation has decreased by 16 % during April - October and 20 % during May - July in the last 50 years (CSIRO and BOM, 2020). In the southeast of Australia, precipitation has decreased by 11 % in the last 20 years between April and October (CSIRO and BOM, 2020). While there have been record declines in precipitation in some parts of the southwest and southeast of the continent, in the northern parts of the continent there has been some increase since 1970 (CSIRO and BOM, 2020). The change in precipitation shows much more variation on a regional scale compared to temperature. One of the most basic information we know about precipitation is that the moisture holding capacity of the warm air will also be higher. Based on the Clausius-Clapeyron relation, this determination is based on the view that each degree of temperature increase boosts the probability of precipitation by approximately 7 % (Trenberth et al., 2003). In a recent study, it is stated that the ratio of this relationship between precipitation and air temperature may be more than we think, and that the relationship between precipitation and dew point temperature can be a more accurate approach to explain heavy precipitation relative to the relationship between precipitation and air temperature (Ali et al., 2021). Regardless of the degree of the relationship between precipitation and temperature, it is clear that increasing temperatures also cause an increase in the severity and frequency of extreme precipitation events. In Australia, particularly short-term extreme precipitation events have started to be seen more intensely in recent years. Hourly extreme precipitation has been reported to increase by about 10 %, but more in the northern part of the continent (CSIRO and BOM, 2020). The changes in the precipitation regime of Australia also affect the basins and indicate a decrease in the streamflow in these basins (e.g., the Murray–Darling Basin, the South Australian Gulf, and the South East Coast, etc.) since the last quarter of the last century (CSIRO and BOM, 2020). On the other hand, in the north where precipitation increased, for instance, in the Tanami–Timor Sea Coast drainage division, an increase trend was observed in streamflow in the same period (CSIRO and BOM, 2020).

It can also be said that changes in temperature, precipitation, and humidity have caused increases in the frequency and duration of bushfires, which are vital for Australia, over the past 7 decades (CSIRO and BOM, 2020). The risk of bushfire is particularly severe and critical in the southeastern part of the continent. The number of bushfires, an essential natural disaster for Australia, tends to increase with climate change (Sharples et al., 2016). This increase may be associated with an increase in the frequency of severe Indian Ocean Dipole (IOD) events due to global warming (Cai et al., 2014). As in this example, the connection of not only bushfires but also other climatic disasters with changes in large-scale processes occurring over the Pacific and Indian Oceans, especially ENSO, should not be ignored (Westra et al., 2016). Specifically, ENSO has a significant impact on the Australian heatwaves and therefore in the northern-northeastern parts of the country undergo long-time blazing heatwaves, which also have an early start, whereas the southeastern part is less affected by ENSO (Perkins et al., 2015; Loughran et al., 2019). Similarly, the effects of ENSO in the summer season, and the IOD and Southern Annular Mode (SAM) in the spring and winter seasons are dominant on Australia’s excessive precipitation (King et al., 2014). Additionally, the number of tropical cyclones in Australia has been decreased since 1982, which generally increases in the years when El Niño is seen and decreases in the years when La Niña is seen (CSIRO and BOM, 2020). In conclusion, when analyzing extreme climate events in Australia, seasonal and regional variations and large-scale processes should be considered very well.

In New Zealand in the southwestern Pacific Ocean, mean temperatures, which have increased by almost 1 ℃ in the last 100 years, are expected to increase by at least 1 - 2 ℃ in the future (Office of the Prime Minister's Science Advisory Committee, 2013). Although these 1 - 2 ℃ increases may seem insignificant, it can be said that this increase in mean temperatures will boost the negative impact of climate change on northern and southern islands of New Zealand in terms of extreme climate events (Office of the Prime Minister's Science Advisory Committee, 2013). It is predicted that precipitation, which varies a lot spatially as is the case with everywhere, will not change much across New Zealand. For instance, precipitation is expected to increase by 5 % in the period of 2030-2050 in the western part of South Island with respect to the period of 1980-2000, whereas it is expected to decrease at the same rate in the eastern and northern parts of North Island (Office of the Prime Minister's Science Advisory Committee, 2013). Climate change, which has an impact on the form of an increase in temperatures and a decrease or increase in precipitation, is projected to cause an increase in strong winter winds in New Zealand at the end of the current century (Office of the Prime Minister's Science Advisory Committee, 2013). Since the climatic variations in precipitation and temperature in New Zealand have been correlated with the large-scale variations in ENSO and SAM (Salinger and Mullan, 1999; Salinger and Griffiths, 2001; Ummenhofer and England, 2007; Ummenhofer et al., 2009), those teleconnections must always be considered during climate change analyzes.

Also in Papua New Guinea, another country in the southwestern Pacific Ocean, temperatures are increasing consistently with global warming. In addition to the fact that the trend of increase in minimum temperature is stronger than the trend of increase in maximum temperature, therefore, the number of warm extreme events also increases, and the number of cold extreme events decreases (PACCSAP, 2015). It is indicated that the number of cyclones in the country has decreased but there has been an increase in their severity (PACCSAP, 2015). While the temperature of the country is expected to increase up to 1.1 ℃ in the next decade, it is predicted that the wind speed of cyclones will increase by up to 11 % and their precipitation will strengthen by about 20 % at the end of the century (PACCSAP, 2015). Papua New Guinea, where the sea level has risen by an average of 7 mm/year since 1993, will inevitably be affected by the sea level rise and frequent and severe extreme climate events caused by climate change in the future (PACCSAP, 2015).

Indonesia should also be mentioned partially, as it is located within the boundaries of the expanded Australasia domain with many islands. The main reason why Indonesia is partially mentioned is that it is essentially located in the South-East Asia (SEA) domain, the newest region of CORDEX (Region 14). It has been stated that since 1990, the mean temperatures in Indonesia increased by about 0.3 ℃ and the annual total precipitation decreased 2 - 3 % on the overall average (Case et al., 2007; World Bank Group, 2021a). In Indonesia, during the 1960 - 2006 period, the number of hot nights and days increased by more than 20 %, while the number of cold nights decreased by about 7 % (Ministry of Foreign Affairs of the Netherlands, 2018). Considering the regional variability of precipitation, there is a decrease in the southern regions of the country and an increase in the northern regions (Case et al., 2007; World Bank Group, 2021a). In addition, the seasonality of precipitation in these regions has also changed (Ministry of Foreign Affairs of the Netherlands, 2018), causing an increase in wet season precipitation in the south and a decrease in dry seasons in the north (Case et al. 2007; World Bank Group, 2021a). Drought events in the country are also seen more frequently after 1960 (Ministry of Foreign Affairs of the Netherlands, 2018). Indonesia is among the climate change hotspots in the current century for both intermediate and high emission trajectories (Diffenbaugh and Giorgi, 2012). In Indonesia, the temperature is expected to increase by an average of 0.2 - 0.3 ℃ per decade in the future (Case et al., 2007; World Bank Group, 2021b). It is also predicted that the increase in temperatures may reach much higher levels depending on the sub-region, period, and scenario (Ministry of Foreign Affairs of the Netherlands, 2018; World Bank Group, 2021b). While an increase in total annual precipitation is expected in many islands of Indonesia, decreases of up to 15 % are projected in the southern parts (World Bank Group, 2021b). The islands of Sumatra and Borneo, which are home to the world's most diverse rainforests, are projected to be wetter at a rate varying between 10 % and 30 % in the period of December - February towards the end of the century due to the change in the seasonality of precipitation (World Bank Group, 2021b). However, it is foreseen that June - August period will be 5 - 15 % drier in Jakarta (Case et al., 2007). In addition, Indonesia will inevitably be affected by the negative impact of climate change on extreme events. For instance, it is projected that the increase observed in the number of hot nights and days will climb more towards the end of the century and cold nights will not be observed after 2060 (Ministry of Foreign Affairs of the Netherlands, 2018). To be specific, while severe droughts may be seen particularly in the south of the country, severe floods caused by heavy precipitation and cyclones with decreasing frequency but increasing in intensity are also expected in the future (Ministry of Foreign Affairs of the Netherlands, 2018). Considering the role of ENSO and IOD in precipitation variability in Indonesia (Aldrian, 2002; Nur'utami and Hidayat, 2016; Hendrawan et al., 2019), as in other countries of the Pacific Ocean, it should also be considered that changes in ENSO and IOD may cause changes in the characteristics of extreme events. Lastly, another significant impact of climate change is that the coastal zones where the majority of the population lives in Indonesia and the agricultural areas and ecosystem in these zones are under serious danger due to the rise in sea level (Measey, 2010).

According to the optimistic scenario (RCP2.6), annual temperature averages in North Australia are expected to increase by 0.4 to 2.4 ℃ by the end of the century, 0.3 to 1.5 ℃ in South Australia/New Zealand, and 0.2 to 1.9 ℃ in Southeast Asia (Christensen et al., 2013). According to the pessimistic scenario (RCP8.5), annual temperature averages are expected to increase between 0.5 and 5.8 ℃ in the north of Australia, 0.4 to 5 ℃ in South Australia/New Zealand, and 0.3 to 4.9 ℃ in Southeast Asia (Christensen et al., 2013). Looking at Australasia's precipitation change projections, it is expected that both increase and decrease can occur within the same region. According to the optimistic scenario, the reduction in annual precipitation in North Australia could reach 24 % by the end of the century, or there could be an increase of up to 10 % (Christensen et al., 2013). The change rate, which is at most 19 % decrease in the South Australia/New Zealand region, is expected to increase by 8 % in some sub-regions (Christensen et al., 2013). Similarly, for the Southeast Asia region, the decrease in precipitation is expected to reach 5 %, and the increase in precipitation is expected to rise to 10 % (Christensen et al., 2013). The expected precipitation variation intervals for the pessimistic scenario are -51 % to 33 % for North Australia, -33% to 15% for South Australia/New Zealand, -7% to 29% for Southeast Asia (Christensen et al., 2013).

Even though the models contain some uncertainties and biases, they are quite good at modeling Australia's temperature and precipitation extremes in terms of their overall performance (Tozer et al., 2019). Although precipitation projections vary widely depending on the models and regions, the overall inference of CMIP5 models is that Australia will have more frequent flood and heatwave and longer drought risks in the future (Johnson et al., 2016; Dey et al., 2019). When both RCP4.5 and RCP8.5 scenarios are taken into consideration, it is stated that the increase in warm and dry extremes and decrease in cold extremes will become more evident in Australia until the end of this century (Cowan et al., 2014; Alexander and Arblaster, 2017). It is evident that this negative impact will be even more severe in RCP8.5. Heatwaves are becoming scorching, longer-lasting, and more frequent and, furthermore, climate change is making them worse in terms of their impacts on people, property, communities, and the environment (Steffen et al., 2014; Perkins-Kirkpatrick et al., 2016; Herold et al., 2018). Future winter warm spells in Australia will rise in frequency and duration at a greater rate than summer heatwaves, and that the hottest events will become increasingly sweltering for both seasons by the end of this century (Cowan et al., 2014). In Australia, the share of heatwaves (approximately 55 % for 1900 - 2011) is very high in deaths caused by natural disasters such as heatwaves, floods, tropical cyclones/willy willies and storms, bushfires, and earthquakes (Coates et al., 2014). As climate change will cause Australian state capitals to be exposed to at least threefold more heatwaves in the future, there is an increased risk of mortality from exceptional temperatures in these populated areas (Herold et al., 2018). It also means reduced wheat yield for Australia in the future (Herold et al., 2018). On the other hand, the processes related to wind hazards contain more uncertainty, it is also expected that wind hazards will decrease in the north and south regions of Australia and increase in the eastern parts of the continent (Walsh et al., 2016).

It is projected that there will be an increase in the severity and number of extreme precipitation events in northwestern and southeastern regions of Australia, particularly in the spring and summer seasons (CSIRO, 2010, 2012; Alexander and Arblaster, 2017; Dey et al., 2018). A significant rising trend for winter dry days in the southwest of Western Australia is expected (Alexander and Arblaster, 2017). In addition, according to White et al. (2010), in a vast area of Tasmania, not only will the frequency and intensity of precipitation increase, but also their recurrence time will be shortened. Moreover, it is deemed that heavy one-day and two-day precipitation events in Tasmania will be experienced more often than now (White et al., 2010). This situation increases the flood risk for Tasmania. Moreover, the flood risk caused by excessive precipitation and the associated damage is especially crucial for the southeast of Australia, which is densely populated (Ashcroft et al., 2019).

Last but not least, the number of marine heatwave events has increased and their duration has been prolonged with the increasing sea surface temperature globally (Marin et al., 2021). Hence, the Tasman Sea is one of the hotspots most affected by this global change, with the contribution of the local climate variability of the region (Marin et al., 2021). Additionally, ocean acidification caused by increased CO_2 concentration entirely threatens the ecosystem of the Pacific Ocean (Lenton et al., 2018). Warmer sea temperatures cause coral bleaching, which in turn destroying many coral reefs. Thus, Australia's Great Barrier Reef, the world's largest coral reef system, is now in danger (Reisinger et al., 2014; Fabricius et al., 2020).

1.2. Objective and Design of the Thesis

As stated in the introduction and literature review sections, climate change and climate modeling studies require an international joint effort. Sharing the data and knowledge produced in climate science is an indispensable element of the road maps to be drawn in combating climate change. Working of various groups with multifarious models and scenarios at different regional scales in climate research is one of the most critical stages of this element. Within the scope of CORDEX, which is the most concrete example of joint efforts, data and information sharing in climate science, it is emphasized that the priority should be given to the less studied domains rather than the studies that prioritize Africa, Europe and MENA domains. The Australasia domain, denoted as Region 9 within the framework of CORDEX, is one of the least studied domains within the scope of CORDEX. Prior to the establishment of CORDEX and up to the early years of CORDEX, studies remained specific to Australia and its sub-regions (e.g. CSIRO, 2007; Perkins et al., 2007; Murphy and Timbal, 2008; Alexander and Arblaster, 2009; Evans and McCabe, 2010; Smith and Chandler, 2010; Vaze et al., 2011; Evans et al., 2012; Evans and McCabe, 2013; Evans et al., 2014, etc.). Comprehensive studies are required for both the continent and the surrounding islands. The motivation for the emergence of this thesis is that the region, which includes many island countries vulnerable to climate change in the Pacific Ocean, has not been projected with different parameterizations and schemes of various models within the scope of CORDEX. The main purpose of the thesis is to examine the general climatology of the Australasia region in a changing climate by making projections of the region with higher resolution compared to global models within the scope of CORDEX. However, not only general climatology, but also the change in extreme weather events, which is very valuable in understanding the impact dimension of climate change, are also discussed. At all these stages, the content of the research was enriched by using different models, parameterizations, schemes, approaches, data, and scenarios. Furthermore, a large data set resource that can be used by different sectors and individuals in the future was provided.

Following the introduction (Chapter 1), the thesis is organized as follows: Chapter 2 describes the domain, data, and the analysis methods of the study. It also describes climate modeling in a technical detail with historical development process. The results of the thesis are presented in Chapter 3. As the first output of the thesis, assessment of projected changes in temperature and precipitation climatology over the domain via multi-model ensemble mean of CMIP5 models are presented in Chapter 3.1. Then, in Chapter 3.2, the results of the changes in extreme climate events over the CORDEX-Australasia domain using the NEX-GDDP dataset are given. Chapter 3.3 evaluates the RegCM4.6 performances to set the most reliable run for the CORDEX-Australasia domain. Lastly, future projections for changes in climatology of the CORDEX-Australasia domain are provided in Chapter 3.4, following by the discussion in Chapter 4 and conclusion in Chapter 5.

2. DATA AND METHODOLOGY

2.1. Domain and Data

2.1.1. Global Initiatives for Climate Modeling and Coordinated Regional Climate Downscaling Experiment (CORDEX)

As mentioned earlier, it is the best way to progress by comparing different models whenever possible to achieve accurate results about a region's climate projections. However, such a detailed study requires a lot of time and computer power. In this respect, it is the most reasonable solution to attempt international cooperation of different institutions using various models. Since the effects of climate change exhibit varied characteristics in different domains and time scales, regional based works are significantly critical to detect the climate change signals properly. Within this context, various international projects such as PRUDENCE (Christensen et al., 2007), ENSEMBLES (van Der Linden and Mitchell, 2009), NARCCAP (Mearns et al., 2009), and CLARIS (Menéndez et al., 2010) have been conducted around the world. Coordinated Regional Climate Downscaling Experiment (CORDEX) is also one of those multi-partner initiatives which were constituted in 2008 by the World Climate Research Programme (WCRP) (Giorgi et al., 2009; Evans, 2011). CORDEX totally involves 14 distinct domains (Table 2.1) and it assembles data of at least 50 km x 50 km downscaled regional climate projections for almost all parts of the globe (Figure 2.1).

Table 2.1. List of CORDEX domains.

CORDEX ID	Domain
Region 1	South America
Region 2	Central America
Region 3	North America
Region 4	Europe (EURO)
Region 5	Africa
Region 6	South Asia
Region 7	East Asia
Region 8	Central Asia
Region 9	Australasia
Region 10	Antarctica
Region 11	Arctic
Region 12	Mediterranean (MED)
Region 13	Middle East & North Africa (MENA)
Region 14	South East Asia (SEA)

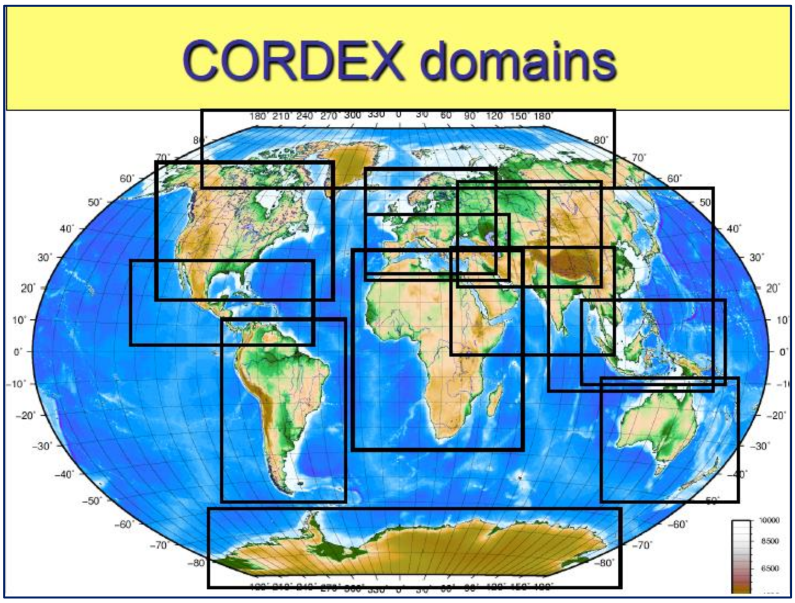

Figure 2.1. CORDEX Domains (Adapted from Giorgi (2019)).

Although CORDEX's core domain is Africa, projection studies have been carried out for each domain with different scenarios and models by various groups (Giorgi and Gutowski Jr., 2015). In the early years of CORDEX, priority was given as 50 km x 50 km resolution under RCP4.5 and RCP8.5 scenarios. However, 25 km x 25 km resolution under RCP2.6 scenario is being studied in recent years and the new target is to reduce the grid resolution to 12.5 km x 12.5 km under actual GCMs and scenarios (Gutowski Jr. et al., 2016; Giorgi et al., 2017; Remedio et al., 2019).

The dynamical downscaling section of this thesis has been realized with the 50 km grid space based on the RCP4.5 and RCP8.5 scenarios as well as the historical run for the Australasia domain, one of the least studied domains of CORDEX. CORDEX-Australasia is a vast domain that comprises mainly Australia, New Zealand, and Papua New Guinea while it also covers the islands in the Pacific Ocean, such as New Caledonia, Fiji, Tonga, Tuvalu, and Vanuatu as well. Although Indonesia is included in the domain, it is actually examined in detail within the South-Asia domain of CORDEX. In the non-rotated pole coordinate system, the minimal domain for CORDEX-Australasia is defined between longitudes 89.25°E and 153.43°W and latitudes 52.36°S and 12.21°N (Figure 2.2). However, within the scope of this thesis, a slightly expanded domain has been chosen for CORDEX-Australasia (Figure 2.3).

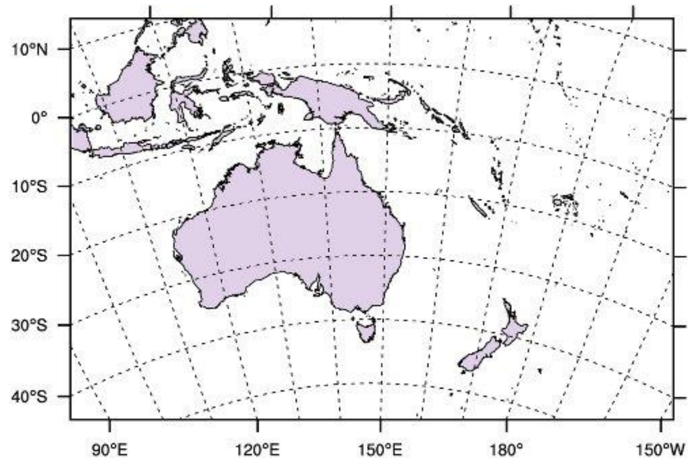

Figure 2.2. Minimal domain for CORDEX-Australasia (Reproduced from http://cordex-australasia.wikidot.com/rcm-domains).

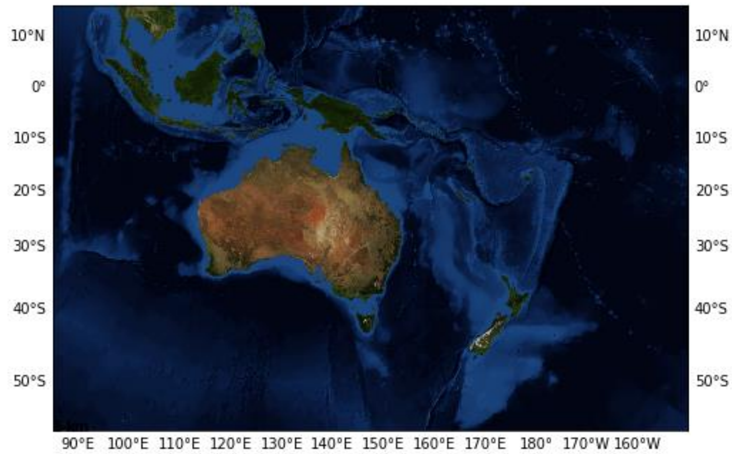

Figure 2.3. Expanded domain for CORDEX-Australasia.

2.1.1.1. Climate of Australasia. The climate of Australasia varies from tropical monsoonal and arid to moist temperate and alpine (Figure 2.4). The Australasia region includes both low latitude and mid-latitude climate types since it covers both hemispheres. Based on the Köppen-Geiger climate classification, it includes three main climate types in the general definition: tropical moist climate (A), dry climate (B), and moist mid-latitude climates with mild winters (C) (Peel et al., 2007; Türkeş, 2010; Ahrens and Henson, 2018). The largest land part of the region, which consists of island countries in the Pacific and Indian ocean, is the continental country, i.e., Australia. According to the Köppen-Geiger climate classification, desert climate (BWk and BWh) prevails in Australia's mid-west part, located between 15°S - 30°S latitudes. The hot and dry desert climate (BWh), which covers a significant part of Australia, and the cold and dry desert climate (BWk), is replaced by the hot and dry steppe climate (BSh) towards the north and east. In the northernmost part of the country, tropical wet climate with rainy summers and dry winters (Aw), in other words, savanna climate can be seen. While some small places in the northeastern Australia experience wet temperate climate with dry winters and extremely hot long summers (Cwa), the humid subtropical climate type (Cfa), defined as wet temperate with very hot long summers, is dominant in the east of the country. The prevailing climate type in Southeastern Australia, Tasmania, and New Zealand is the marine west coast climate (Cfb), a wet temperate climate with its long and cool summers. As well as the cool and dry steppe climate (BSk), the wet temperate Mediterranean climate (Csb) with hot and dry summers is also seen on the coasts of South Australia. Wet temperate Mediterranean climate (Csa) with scorching and dry summers is another climate type experienced in Southwest Australia. When we look at the island countries in the equatorial belt, it is seen that the dominant climate type in Papua New Guinea and Indonesia is a humid equatorial climate (Af and Am). It is evident that the climate type (Af), which is defined as the very moist equatorial rain climate, prevails in a much broader region than the monsoon type equatorial rain forest climate type (Am). Towards 15°N latitudes, tropical wet (Aw), and tropical monsoon type (Am) moist equatorial climates are observed.

General characteristics of climate types in the region are stated as follows (Türkeş, 2010; Ahrens and Henson, 2018):

- Humid Equatorial Climate (Af & Am): In humid equatorial climates between 10°N - 10°S latitudes, thunderstorms due to convective movements caused by strong surface warming and heavy rains are observed. Tropical and equatorial rain forests are dominant as vegetation in places with such climates.

- Tropical Desert and Steppe Climates (BWh & BSh): Tropical desert and steppe climates that are seen between latitudes 15°N(S) - 35°N(S) have extremely arid, arid, and semi-arid conditions characterized by high maximum temperatures and moderate annual temperature differences.

- West Coast Desert Climate (BWk & BWh): The west coast desert climate, which is seen between latitudes 15°N(S) - 30°N(S), is extremely dry, relatively cool, and foggy and prevails in the west coast belts. Daily and annual temperature differences are insignificant in these coasts.

- Tropical Wet-Dry Climate (Aw & Cwa): Tropical wet-dry climate that is seen between latitudes of 5°N(S) - 25°N(S) is a tropical climate where a humid season occurs in high sun time and a dry season in low sun time due to the displacement of moist air masses with dry air masses.

- Moist Subtropical Climate (Cfa): In the humid subtropical climate seen between latitudes 20°N(S) - 35°N(S), a moist marine tropical air mass prevails on the eastern edges of the continents. While high temperatures and abundant precipitation are seen in summer, winters are cool. Mid-latitude cyclones appear to be frequent and effective.

- Marine West Coast Climate (Cfb & Cfc): The marine west coast climate, which is seen between latitudes 40°N(S) - 60°N(S), has a high cloud amount and is rainy in all seasons. Precipitation reaches the maximum in winter, and daily and annual temperature differences are low.

- Mediterranean Climate (Csa & Csb): In the Mediterranean climate between the latitudes of 30°N(S) - 45°N(S), summers are hot and dry, and winters are cool and rainy. Daily and annual temperature differences are moderate. Temperature differences and spring precipitation are relatively increased towards the east and the continental interior regions.

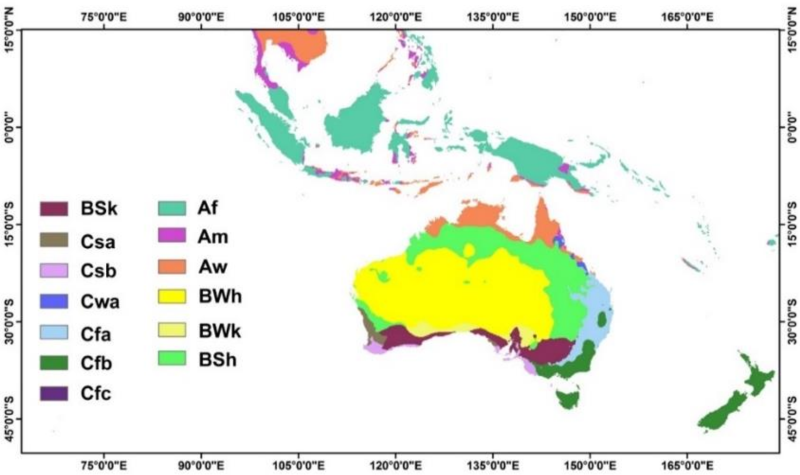

Figure 2.4. The Köpper-Geigen climate classification for the Australasia domain (It was drawn using data provided by Peel et al. (2007)).

2.1.1.2. Climate Drivers of Australasia. In the winter, dry air flows from the arid interior regions of the mainland towards the intertropical convergence zone (ITCZ) cause arid or low precipitation conditions in Australia's northern part (Türkeş, 2010). In summer, the humid air currents that move from the Indian ocean to the ITCZ ensure wet conditions prevail throughout the ITCZ by pulling rising air currents (Türkeş, 2010).

A small monsoon system is influential in the north of the Australian continent. In the Australian monsoon circulation, the north and northwest winds carry warm and humid marine air to the northern coastal regions of Australia in the summer months (November - March) and cause fertile summer rain in these regions (Türkeş, 2010). In the winter season, since the ITCZ shifts to the north of the equator, the southern dry and hot air currents originating from the hot and continental inner regions of the Australian continent are prominent in the coastal regions of northern Australia (Türkeş, 2010). Therefore, arid conditions prevail in the north in winter.

Subtropical anticyclones seen on the South Atlantic and the Indian Ocean are concentrated towards the west of Australia. Although it changes seasonally, approximately 40 anticyclones are seen in Australia every year (Barry and Chorley, 2009). The number of anticyclones in spring and summer is higher than in autumn and winter. The frequency of anticyclonic centers is generally the highest among the latitudes of 30°S in winter and 35 - 40°S in summer (Barry and Chorley, 2009). Among the anticyclones are low-pressure troughs, also called the polar front. Within these troughs, the subtropical jet flow accelerates, especially in winter, by curling up at the equator and produces upper air depressions that move towards the southeast and marine polar air flows from the south (Barry and Chorley, 2009). High-pressure conditions on Australia cause high temperatures in the central and western parts of the continent, especially in the summer. These pressures reduce the average amount of precipitation (Barry and Chorley, 2009). In winter, upper air depressions bear rain to the southeastern regions and southwestern Australia along the anticyclonic fronts. In the summer, the ITCZ moves southward into a monsoon trough, which gives rise to a rainy season in northern Australia, and the southeast trade winds on the shore bear rain to the east coast.

New Zealand is also associated with climate systems like in southern Australia (Figure 2.5). Anticyclones separated by troughs cross the area on average once a week (Barry and Chorley, 2009). The movement of anticyclones is directed towards the east and reaches a speed of around 30 km/h (Barry and Chorley, 2009). Anticyclones are associated with stagnant air, light winds, sea breezes, and slight fog. The airflow in the southwest direction on the east edge of the high-pressure cell is generally cool and marine, and drizzles are observed in the south or southeast. On the west side of the cell, the airflow is generally in the north or northwest direction and creates soft and humid conditions. Increased high-pressure conditions in the autumn cause a drier season. If a wave of depression occurs on the cold front in the west of New Zealand, it usually moves to the south of the country, moving towards the front in the southeast direction. It may take 1.5 or 2 days for depression over New Zealand to leave the country, which means prolonged rain conditions (Barry and Chorley, 2009). The Southern Alps predominantly control the amount of precipitation. While mountains facing the west or northwest receive average annual precipitation of over 2500 mm, total precipitation in some parts of the South Island exceeds 10000 mm (Barry and Chorley, 2009). The eastern lee regions have much lower precipitation (Barry and Chorley, 2009). While the North Island of New Zealand has maximum winter precipitation, the South Island has a more variable seasonal maximum under southwestern depressions (Barry and Chorley, 2009).

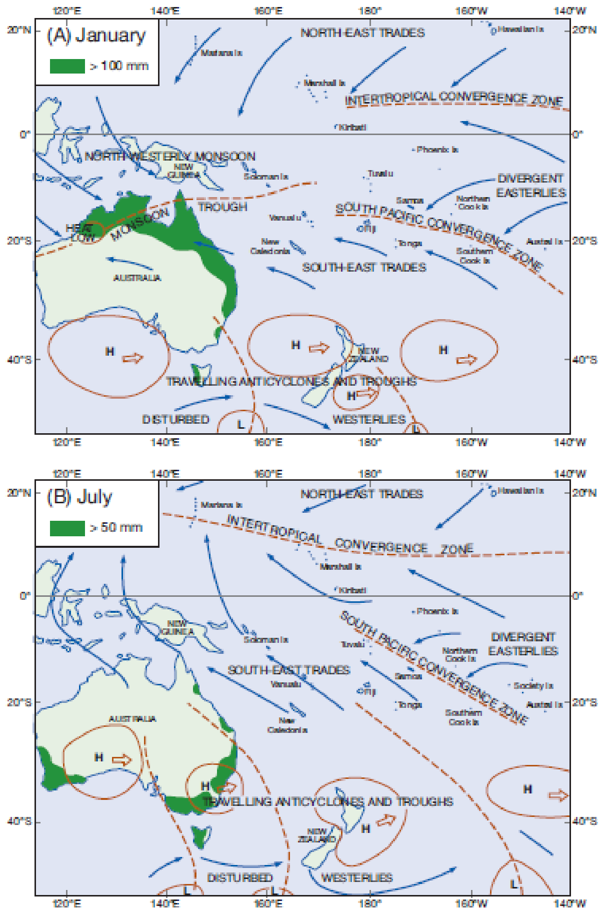

Figure 2.5. Climate systems in Australasia. Green areas are the places where mean monthly precipitation is (a) over 100 mm in January, (b) over 50 mm in July (Reproduced from Barry and Chorley (2009). The original versions of the maps were drawn by Salinger et al. (1995) after Steiner (1980)).

El Niño Southern Oscillation (ENSO), Indian Ocean Dipole (IOD), the Madden-Julian Oscillation (MJO), and the Antarctic Oscillation (AAO) are the main drivers of Australasia’s exceedingly variable climate (Figure 2.6). In the negative ENSO, in other words, during the La Niña period, the sea surface temperature increases more and causes cloudy and rainy weather conditions along the equatorial Pacific in the north of Australia (BOM, n.d.-c). During La Niña, June - November precipitation in the central, northern, and eastern regions of Australia are above the seasonal average (BOM, n.d.-c). La Niña means low daytime temperatures, a wide risk of flooding, and more tropical cyclones for Australia. If ENSO is positive, in other words, in El Niño, the focus of convection weakening over Australia, Papua New Guinea, and Indonesia shifts from the Australia/Indonesia region to the central Pacific Ocean (BOM, n.d.-c). After the trade winds lose their strength, June - November precipitation decreases in the eastern regions of Australia and causes drier conditions in most parts of the country, especially in the eastern areas (BOM, n.d.-c). El Niño means high temperatures and more heatwave, cloudless nights, prolonged frost risk, strong sea breezes, and less tropical cyclone for Australia, and drought risk for the northern and eastern Australia. The temperature differences in the western and eastern parts of the tropical Indian Ocean are also very influential on Australia’s precipitation patterns. If the western part of the tropical Indian Ocean is warmer than the eastern part, that is, in the IOD positive phase, the amount of winter-spring precipitation is lower than normal in central and southern Australia (BOM, n.d.-d). While the west and south of Australia become warmer, minimum temperatures increase in southeast Australia and pose a risk of forest fires. When IOD switches to a negative phase, the winter-spring precipitation in eastern and southern Australia and minimum temperatures in northern Australia increases (BOM, n.d.-d). The rise in the amount of precipitation naturally also increases the risk of flooding. MJO, which can be seen at any time of the year, generally affects Australia in October - April (BOM, n.d.-e). It may cause an increase or decrease in both precipitation and temperatures, depending on the region where it occurs. During the active period of MJO, tropical cyclones can be seen more, trigger El Niño, strengthen or weaken monsoon rains (BOM, n.d.-e). AAO, which is formed by the changes of western winds and weather systems in the north-east direction on the Southern Ocean and can show a week and a few months bears more precipitation to the east of Australia when it is positive in summer (BOM, n.d.-f). When AAO is positive in winter, there is more precipitation in the east and less precipitation in the southern coast (BOM, n.d.-f). Tasmania, which receives more precipitation than normal in the positive phase of AAO, receives less than usual in winter. While there is less precipitation in eastern and southeastern Australia in the summer, the risk of spring heatwave increases in southern Australia when AAO is negative (BOM, n.d.-f). When AAO is negative in winter, the southwestern and southeast regions of Australia receive more precipitation, and less precipitation occurs in some eastern parts (BOM, n.d.-f).

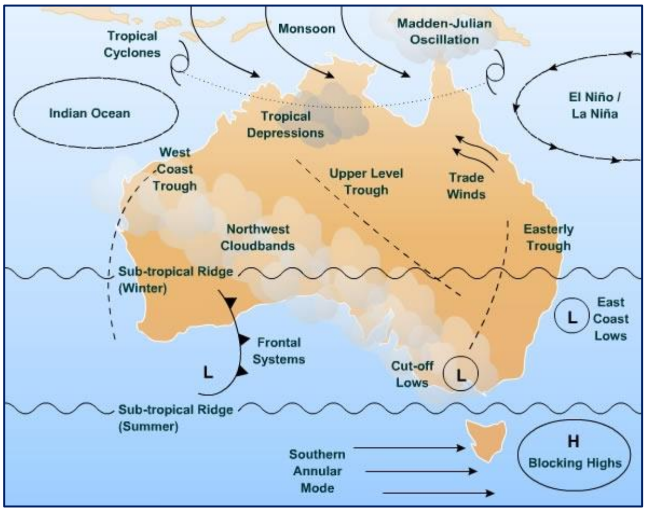

Figure 2.6. Main climate drivers of Australia (Reproduced from BOM, n.d.-g).

2.1.2. Scenario Processes from Past to Present and Representative Concentration Pathways (RCPs)

Today, different research centers and many scientists in different countries of the world carry out individual and joint projects and conduct studies that predict the future climate conditions of the world. Since the aim is to portray the possible climate conditions of the future, the critical point here is how to determine the future climate. For this reason, the extent to which the anthropogenic greenhouse gas emissions, which are the main cause of the current climate change, will change in the future and how much of the atmospheric amount of the energy coming from the sun will increase in the Earth is the first part that should be foreseen. Hence, various scenarios are prepared and future atmospheric greenhouse gas concentrations are estimated. In order to make climate projections about the future, it is necessary to envisage how humanity will take measures against global climate change. At this point, scientists create various scenarios depending on the development and change of economic systems. These scenarios include wide range from the most optimistic scenario to the most pessimistic scenario. In other words, all these scenarios can be expressed as continuing the existing living conditions without compromise, making some compromises or continuing vital activities with a complete lifestyle change.

The scenarios used in climate models have been altered under different names by changing with divergent perspectives and approaches over time. Climate scientists used time-dependent scenarios in GCMs until the early 1990s (Moss et al., 2010). The equilibrium climate scenarios and the emission scenarios set, the IPCC 1990 Scenario A (SA90) (IPCC, 1990), were used in the IPCC's First Assessment Report (FAR). The IPCC proposed new emission scenarios in 1992 to increase the functionality of GCMs. The IPCC 1992 scenarios (IS92) (Leggett et al., 1992) were used in the Second Assessment Report of the IPCC (SAR) (IPCC, 1996). As from the IS92, much has changed in the understanding of future greenhouse gas emissions and possible changes in climate. For this reason, the IPCC decided to prepare a new series of emission scenarios in 1996, with a wider usage area than the IS92, to be included in the 3rd Assessment Report (TAR) (IPCC, 2001). Therefore, these new scenarios, which can enable the testing of the climate and environmental consequences of future greenhouse gas emissions and the evaluation of alternative mitigation and adaptation strategies, namely the SRES (Special Report on Emission Scenarios), were developed by Nakićenović et al. (2000) to be used as a basis for climate projections in the TAR. These scenarios covered up-to-date information on advanced emission limit values and changes in the world economy, including the assessment of different values and trends in technological changes, the spread of the area of different economic development projections, and the narrowing in income gap between developed and developing countries. The SRES, which was gathered under four main groups under the names A1, A2, B1, and B2, were separated according to the demographic, social, economic, and technological change narratives. Scenarios A1 and A2 of the SRES characterize high emissions, while scenarios B1 and B2 describe relatively low emissions. Scenario sets of both IS92 and SRES were used in the 4th Assessment Report (AR4) of the IPCC (IPCC, 2007).

In its last published report (AR5) (IPCC, 2013), the IPCC changed its perspective and utilized the Representative Concentration Pathways (RCPs) (Meinshausen et al., 2011; van Vuuren et al., 2011a) in the projection studies instead of emission scenarios. There are four pathways which are named RCP2.6, RCP4.5, RCP6.0, and RCP8.5 from optimistic to pessimistic respectively. The numbers adjacent to the abbreviation RCP denote the radiative forcing values (W/m^2) by the year 2100. RCP2.6 (van Vuuren et al., 2007, 2011b) reaches its peak in the mid-century and then follows a decreasing trend. RCP4.5 (Smith and Wigley, 2006; Clarke et al., 2007; Wise et al., 2009) and RCP6.0 (Fujino et al., 2006; Hijioka et al., 2008) follows a stabilization pathway. The radiative forcing value in RCP4.5 is stabilized at the end of the century. RCP8.5 (Riahi et al., 2007, 2011) emissions follow a continuously increasing pathway until 2100, so the radiative forcing level mounts up by the end of the century. The radiative forcing levels of RCPs in different years are given in Table 2.2.

Table 2.2. Total radiative forcing levels for RCPs excluding mineral dust and land albedo effect (Full data is available at the RCP web-database http://www.iiasa.ac.at/web-apps/tnt/RcpDb).

Scenario	**Unit**	**Year**			
		2000	**2020**	**2050**	**2100**
RCP2.6	W/m^2	1.723	2.584	2.998	2.714
RCP4.5	W/m^2	1.723	2.579	3.766	4.309
RCP6.0	W/m^2	1.723	2.480	3.521	5.481
RCP8.5	W/m^2	1.723	2.665	4.762	8.388

If we evaluate the RCPs in terms of greenhouse gas concentrations, it is predicted that the lowest concentrations will occur in RCP2.6 and the highest concentrations in RCP8.5 (Table 2.3). RCP2.6 is a decisive and radical pathway to minimize greenhouse gas emissions in the way of mitigating the effects of climate change. Nevertheless, according to the RCP2.6, CO_2 concentration is expected to reach a peak value in the middle of the century and get to approximately 421 ppm at the end of the century (Figure 2.7). It is certain that this value will be reached in the first quarter of this century. RCP4.5 and RCP6.0 pathways, which have medium range concentrations, require further mitigation efforts compared to the highly optimistic RCP2.6. RCP8.5, which is seen as the most pessimistic of these pathways, is known as the business-as-usual scenario today. According to the RCP8.5, the use of fossil fuel is as intense as it is today and sufficient steps are not taken to combat climate change, and the CO_2 concentration will reach approximately 936 ppm at the end of this century.

Table 2.3. CO_2, CH_4, and NO_2 concentrations according to RCP scenarios.

GHG	Scenario	Unit	Year			
			2000	2020	2050	2100
CO_2	RCP2.6	ppm	368.865	412.068	442.700	420.895
	RCP4.5	ppm	368.865	411.129	486.535	538.358
	RCP6.0	ppm	368.865	409.360	477.670	669.723
	RCP8.5	ppm	368.865	415.780	540.543	935.874
CH_4	RCP2.6	ppb	1751.022	1730.518	1451.540	1253.628
	RCP4.5	ppb	1751.022	1801.434	1833.094	1576.346
	RCP6.0	ppb	1751.022	1785.791	1894.850	1649.396
	RCP8.5	ppb	1751.022	1923.671	2739.985	3750.685
N_2O	RCP2.6	ppb	315.850	329.208	341.896	344.016
	RCP4.5	ppb	315.850	329.983	350.608	372.274
	RCP6.0	ppb	315.850	330.202	354.592	406.265
	RCP8.5	ppb	315.850	331.514	367.220	435.106

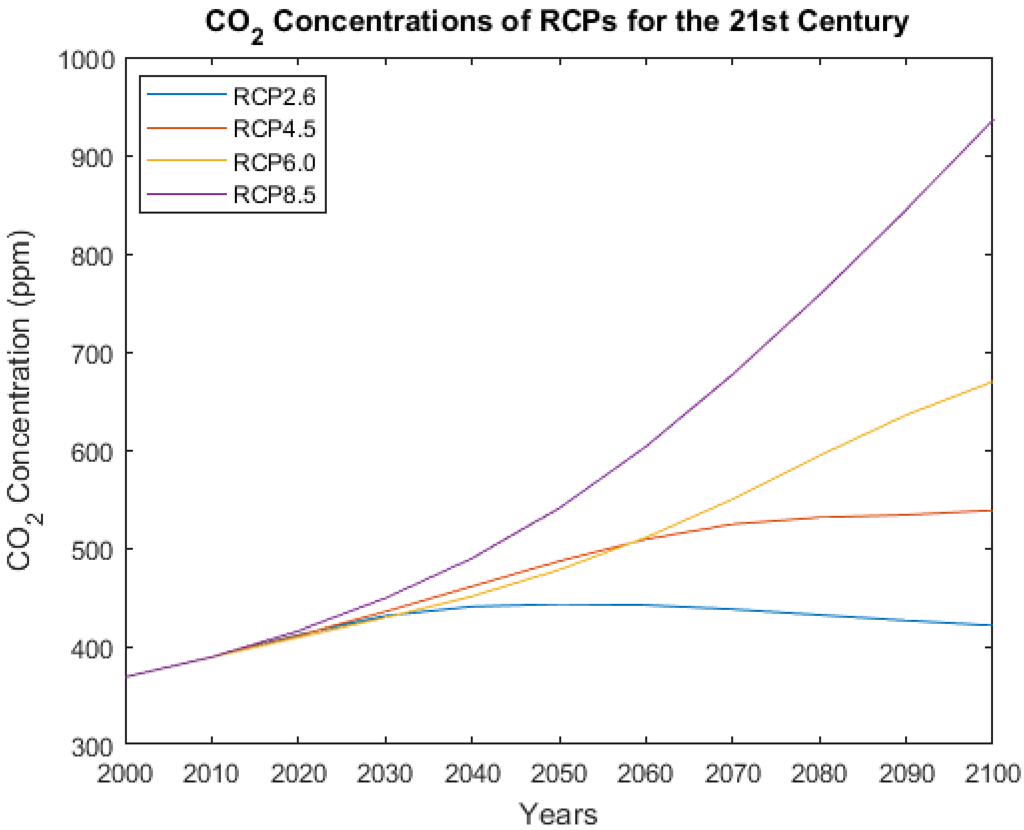

Figure 2.7. CO_2 concentration trends under RCP2.6, RCP4.5, RCP6.0, and RCP8.5 between 2000 and 2100.

With the 6th Assessment Report (AR6), which is planned to be released due 2022, IPCC has made the transition to new scenario sets as well as RCPs (Figure 2.8). These storylines, called Shared Socio-economic Pathways (SSPs), consist of five pathways that take into account various challenges for mitigation and adaptation (Kriegler et al., 2012; O'Neill et al., 2014). They are SSP1 with low challenges, SSP2 with intermediate challenges, SSP3 with high challenges, SSP4 with predominantly adaptation challenges, and SSP5 with predominantly mitigation challenges.

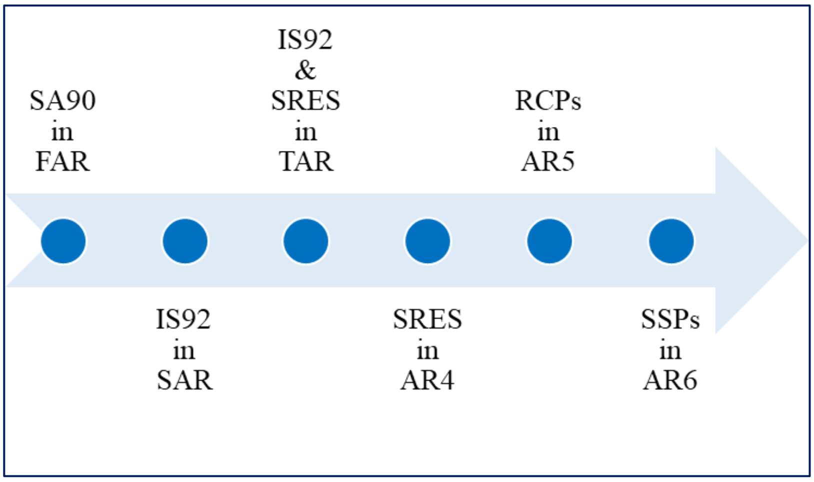

Figure 2.8. Timeline of IPCC scenario sets.

In this thesis, projection studies have been carried out considering RCP4.5 and RCP8.5, which are the most widely used scenarios in the literature recently. However, RCP2.6, which was emphasized in the studies after the Paris Agreement (United Nations, 2015) in line with the 1.5 - 2 °C warming target of the states, was also used in a part of the thesis, although it may seem difficult to realize scientifically in today's conditions.

2.1.3. Coupled Model Intercomparison Project Phase 5 (CMIP5)

Like many other complex systems, climate studies have to rely on models as well. Simple models can give us the main ideas of how the system works, but we need more sophisticated models to get into the details. These sophisticated models are closer to reality, but they need to have more computer power and longer simulation time. Rapid and widespread realization of climate modeling, which has become very expensive in terms of time and computer costs, has a critical role in determining the climate conditions that occur and are likely to happen and the effects of climate change. Therefore, it becomes more of an issue that different people and institutions around the world act hand in hand. In this way, joint climate change projects, which are conducive to the functioning of climate change studies in the world more regularly and effectively, enable the comparison of climate models realized by various climate groups in different parts of the world. The best known and most important of these joint projects is known as the Coupled Model Intercomparison Project (CMIP). The CMIP, which was first implemented in 2008 by the World Climate Research Program (WCRP) with the cooperation of 20 modeling groups, has been updated over time and continued to develop in several phases. Since the day it was founded, factors such as the increase in the number of groups contributing to modeling studies, newly developed scenarios and models, development of existing models have brought the CMIP to the sixth phase and got the name CMIP6. In this thesis, the GCMs in the CMIP5, which form the basis of the IPCC's last published report AR5 and will continue to contribute to AR6, were used. CMIP5 contains data produced by GCMs with different resolutions developed by various climate modeling groups in different countries such as USA, Canada, China, Australia, Japan, Germany, France. The pattern correlation graphs in Figure 2.9 comparing the performance of CMIP5 data in temperature and precipitation projections with CMIP2 and CMIP3 show that CMIP5 is more accurate in representing the pattern of temperature and precipitation than its previous phases (IPCC, 2013). Accordingly, the pattern correlations of surface temperature are very close to 1, being higher than precipitation in all three phases of CMIP. However, CMIP5 pattern correlations are the highest for both climate variables.

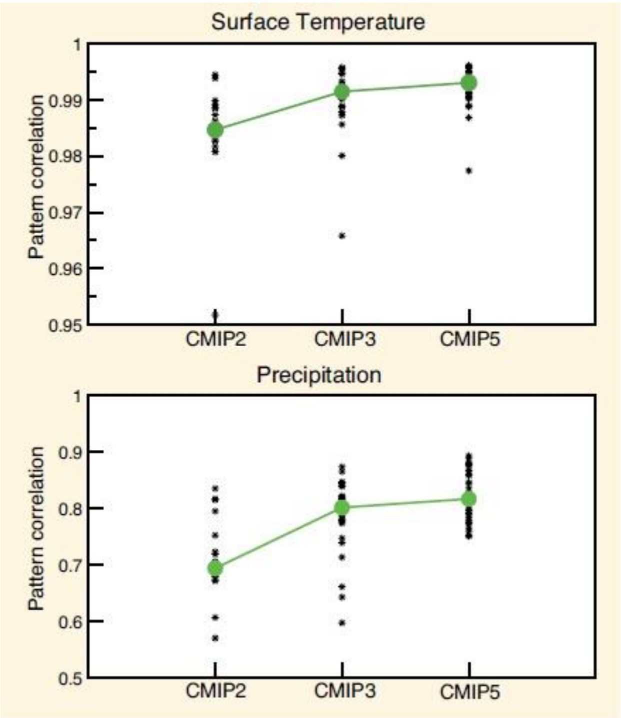

Figure 2.9. Pattern correlations for surface temperature and precipitation in different phases of CMIP (Reproduced from Flato et al. (2013)).

These datasets are used individually in macro-scale studies, as well as micro-scale, that is, they are used as input by RCMs in regional and local studies and reduced to a scale that can represent the climate of that region more realistically. In the dynamic downscaling approach, which is the main study of this thesis, two common models in CMIP5, MPI-ESM-MR and HadGEM2-ES, were used. In other parts of the thesis, different CMIP5 models are also used and these models are specified in the relevant sections.

2.1.4. Climatic Research Unit Gridded Time Series (CRU TS)

Climatic Research Unit Gridded Time Series (CRU TS), hereinafter CRU, is a global monthly gridded observation dataset prepared by the University of East Anglia in England. The CRU provides data for 10 different climate variables at 0.5° x 0.5° grid resolution for the entire world for the period from the 20th century to the present (Harris et al., 2020). The variables in the CRU dataset are: mean air temperature (°C), maximum air temperature (°C), minimum air temperature (°C), diurnal air temperature range (°C), precipitation rate (mm/month), potential evapotranspiration (mm/day), vapour pressure (hPa), cloud cover (%), wet days (days), and frost days (days/month). CRU enables the comparison of model and observation data for reference periods in climate studies by making the station data covering all terrestrial areas in the world, except Antarctica, gridded with the angular-distance weighting (ADW) interpolation method.

2.1.5. ERA-Interim

ERA-Interim dataset is global scale grid reanalysis climate data produced by the European Centre for Medium-Range Weather Forecasts (ECMWF). ERA-Interim data has approximately 80 km (approximately 0.7° x 0.7°) horizontal and 60 levels vertical grid resolution for 1979 - 2019 period (Simmons et al., 2006; Dee et al., 2011). ERA-Interim dataset is prepared using data and models of all observation networks in the world, especially satellite data. ERA-Interim provides climate data with higher temporal resolution (at least 6 hours) for much more climate variables compared to CRU data. ERA-Interim is used as an input in regional climate models and enables comparison of different variables for reference periods in the validation of the models. ERA-Interim dataset has recently been named ERA5 by increasing the grid size to approximately 9 km.

2.1.6. University of Delaware (UDEL) Global Climate Data

University of Delaware Global Climate Data, hereinafter UDEL, is a global monthly gridded observation dataset prepared by the University of Delaware in the United States of America. Using only in situ observations like CRU data, the UDEL dataset provides gridded observation data for the whole world by interpolating the precipitation and mean temperature values, which are the two basic variables of climate, to 0.5° x 0.5° grid resolution on a monthly basis (Willmot and Matsuura, 2001). UDEL makes use of the stations within the Global Historical Climatology Network (GHCN) (Vose et al., 1992) and the station measurements and archives of different institutions in the world on the basis of the station records of Legates and Willmot (1990a, 1990b). Using these data, UDEL creates an alternative gridded observation dataset to CRU on a global scale by employing Shepard's distance-weighting method (Shepard, 1968). In this way, it is possible to compare with different observation datasets for the validation of models in climate modeling studies.

2.1.7. The United States National Centers for Environmental Prediction/The National Centers for Atmospheric Research (NCEP/NCAR) Reanalysis I

NCEP/NCAR Reanalysis I is another global scale grid reanalysis climate data jointly produced by the United States National Center for Environmental Prediction (NCEP) and the National Center for Atmospheric Research (NCAR). NCEP/NCAR Reanalysis I, whose first version covers a time period from 1948 to the present, is based on the entire observation network in the world as in ERA-Interim. There is another version of the NCEP/NCAR Reanalysis I dataset, which includes a time period from 1979 to the present. This dataset, prepared in cooperation with NCEP and the United States Department of Energy (DOE), is briefly known as NCEP/DOE Reanalysis II (Kanamitsu et al., 2002). NCEP/NCAR Reanalysis I (Kalnay et al., 1996) with a time resolution of 6 hours and grid resolution of 1.875° x 1.875° (2.5° x 2.5° for some parameters) provides an alternative to ERA-Interim data in climate studies. NCEP/NCAR Reanalysis I, which has 17 pressure levels, and 28 sigma levels, offers the opportunity to benefit from various climate parameters such as air temperature, precipitation, relative humiditiy, and three-dimensional wind speed.

2.1.8. The National Aeronautics and Space Administration (NASA) Earth Exchange Global Daily Downscaled Projections (NEX-GDDP) Dataset

The National Aeronautics and Space Administration (NASA) Earth Exchange Global Daily Downscaled Projections (NEX-GDDP) dataset is prepared by the Climate Analytics Group and

NASA Ames Research Center and distributed by the NASA Center for Climate Simulation (NCCS). The NEX-GDDP dataset provides high resolution (0.25° x 0.25° grid size) data for three fundamental climate variables (i.e., maximum temperature, minimum temperature, and precipitation) on a daily basis for the years between 1950 and 2100 (2099 for two models), using the 21 GCM data (Table 2.4) included in CMIP5 (Thrasher and Nemani, 2015). In the NEX-GDDP dataset, the historical data of GCMs for the 1950 - 2005 past period and the RCP4.5 and RCP8.5 scenario outputs of the GCMs for the future period of 2006 - 2100 statistically downscaled to a finer resolution using the Bias-Correction Spatial Disaggregation (BCSD) method (Wood et al., 2002, 2004; Maurer and Hidalgo, 2008; Thrasher et al., 2012, 2013; Maraun and Widmann, 2018). In the BCSD method, firstly GCM data were compared with the Global Meteorological Forcing Dataset (GMFD) observation data (Sheffield et al., 2006), and bias correction was done with quantile mapping approach (Thrasher et al., 2012), then corrected data were interpolated to 0.25° x 0.25° (approximately 25 km x 25 km) grid points.

Table 2.4. List of GCMs included in the NEX-GDDP (Thrasher and Nemani, 2015).

GCMs in the NEX-GDDP		
ACCESS1-0	CSIRO-MK3-6-0	MIROC-ESM
BCC-CSM1-1	GFDL-CM3	MIROC-ESM-CHEM
BNU-ESM	GFDL-ESM2G	MIROC5
CanESM2	GFDL-ESM2M	MPI-ESM-LR
CCSM4	INMCM4	MPI-ESM-MR
CESM1-BGC	IPSL-CM5A-LR	MRI-CGCM3
CNRM-CM5	IPSL-CM5A-MR	NorESM1-M

Although NEX-GDDP dataset, which has a short history, has been used very little in the literature, it has recently been preferred as a data source in various studies (Bao and Wen, 2017; Turp et al., 2017; Raghavan et al., 2018; Sahany et al., 2019; Kumar et al., 2020). High resolution retrospective and prospective data of the NEX-GDDP are used in the 5th chapter of the thesis to examine the changes in some temperature and precipitation extremes for the Australasia region.

2.2. Climate Modeling

Identifying and anticipating the potential direct and/or indirect effects of climate change, which is one of the most important problems of today's world on a global scale, that we are currently experiencing or will experience in the future is crucial to adapt climate change and to mitigate its impacts. As climate change poses an increasing threat to Earth, scientific studies that have been conducted in this area have focused on modeling studies aimed at future climate forecasts, especially in the last quarter century. Today, various research centers and many scientists in different countries of the world carry out individual and joint projects for predicting the future climate conditions of the world.

Climate scientists understand the past climate and project the future climate through the use of climate models. Climate models are dynamic and highly complex mathematical tools based on the fundamental laws of physics (Newton's laws, thermodynamic laws, etc.) that take into account all atmospheric-ocean-land interactions and all feedbacks and cycles on global and local scales. In the early twentieth century, modeling studies, which started with simple equations and basic parameters to make weather forecasts, were developed with the help of developing science and technology to create more complex and reliable climate models. Currently, the most advanced climate models are the so-called “General Circulation Models” or “Global Climate Models” (GCMs). These models take into account the movements of Earth's atmosphere and ocean on a global scale and include atmospheric-ocean interactions. These models simply divide the world into a range of boxes (grid or raster), allowing us to obtain climate data about any point of the world. The critical point here is how to determine the future climate. Therefore, the extent to which greenhouse gas emissions, which are the main cause of the current climate change, will change in the future, and how much atmospheric concentrations will increase and warm the Earth trapping the energy, should be envisaged. For this purpose, various scenarios are prepared to predict future atmospheric greenhouse gas concentrations. These scenarios are called RCP (Representative Concentration Pathway) and provide a range of optimistic and pessimistic future predictions from low greenhouse gas emissions to high greenhouse gas emissions. Thus, by using RCP scenarios, the future climate of many different regions of the world is predicted with the help of global models. This provides information on the future state of the climate if there is a reduction behavior in greenhouse gas emissions or no effort is made, and we continue business as usual.

There are over 60 different global models developed and used by 30 different research groups around the world. All these models are operated in different grid sizes (resolution). Current models have an average resolution of 150 km. Although this resolution is better than that of previous models (200 - 350 km), regional and local studies require higher resolution data. For this, the output from the global model is dynamically reduced to higher resolutions (10 - 50 km) using “Regional Climate Models” (RCMs). In other words, the results obtained from the global models are used as input of the regional models and the most useful data sets are obtained for the region of interest.

Sometimes a reanalysis model for hindcasting and a regional climate model for very high resolution output can be a parent model instead of a GCM.

In this section, the issue of climate modeling, of which general introduction is mentioned above, is examined. First of all, a short history of climate modeling is explained. Afterwards, global and regional climate models are explained and RegCM regional climate model used in the study is detailed.

2.2.1. A Brief History of Climate Modeling

Climate models are grounded on weather forecasting models. Climate models should resolve long-term processes much better than weather forecasting models (Neelin, 2011). In 1904, Norwegian scientist Vilhelm Bjerknes declared the idea that weather forecasts should be built upon the laws of physics (Bjerknes, 1904; Jacobson, 2005; Gramelsberger, 2009; Volken and Brönnimann, 2009). Although this idea is not truly original, Bjerknes has developed this idea a little more (Jewell, 1984; Nebeker, 1995; Jacobson, 2005). Bjerknes expresses weather with seven basic variables (i.e., temperature, three components of wind, density, water content (humidity), and pressure) and states that the changes in these variables can be calculated using the fundamental physics equations (i.e., the thermodynamic energy equation, the hydrostatic equation, the continuity equation, Newton's second law of motion, and the ideal gas law) currently known. Unlike Bjerknes, who suggested graphical techniques rather than analytical solutions to meteorological equations, British scientist Lewis Fry Richardson developed analytical solutions to these equations in the first quarter of the 20th century (Richardson, 1922; Jacobson, 2005; Lynch, 2006). In this respect, Richardson is considered the first developer of numerical weather forecasts.

At the suggestion of John von Neumann in 1946 (Jacobson, 2005), the first numerical weather forecast was made under the leadership of Jule Charney using the world's first electrically powered computer with electronic data processing capacity - ENIAC (Electronic Numerical Integrator and Computer) (Charney, 1949, 1951). In 1956, Norman Phillips run a general circulation model based on a two-level quasi-geostrophic structure (Phillips, 1956). Phillips' model is known as the first GCM. In the 1960s and 1970s, general circulation model developing groups began to form. For instance, one of the most important was formed in 1964 at the National Center for Atmospheric Research (NCAR) under the leaderships of Warren Washington and Akira Kasahara, making the NCAR the world's leading climate modeling center (Jacobson, 2005; Lynch, 2008). In 1965, Joseph Smagorinsky and Syukuro Manabe from the United States Weather Bureau (today it is known as

Geophysical Fluid Dynamics Laboratory) developed a simple three-dimensional (3D) model that uses basic equations for a 9-level atmosphere vertically (Weart, 2004). Although the results of this model contain many deficiencies and errors in detail, other groups started to contribute to modeling with the belief that such models can produce useful results. Again in 1965, Yale Mintz and Akio Arakawa from the University of California developed a model similar to the model of Smagorinsky and Manabe (Weart, 2004). Following these attempts, Akira Kasahara and Warren Washington presented a new GCM based on height instead of pressure for vertical coordinate (Kasahara and Washington, 1967). Another milestone for climate modeling was the coupling atmospheric model with ocean model by Syukuro Manabe and Kirk Bryan (Manabe and Bryan, 1969). In 1972, for the first time, the United Kingdom's national meteorological service (the UK Met Office) provided proper precipitation forecasts by using a 10-level primitive equation model, where physical processes were handled more comprehensively and accurately (Lynch, 2008). In the mid-70s, Manabe et al. (1975) advanced their previous modeling research and simulated global climate on a more realistic topography for the entire world. Since the 1970s, many research centers and scholars in different parts of the world have been working to improve climate models (Edwards, 2011). During this period, few attempts have been made to investigate the role of change in CO_2 concentration (Hausfather, 2020). Studies involving projections at different scenarios accelerated (Manabe and Wetherald, 1975; Manabe and Stouffer, 1980; Washington and Meehl, 1984; Wilson and Mitchell, 1987; Hansen et al., 1988). While the improvement of GCMs continued at that time (Edwards, 2011), regional climate models started to be developed as of the end of 1980s, which started to produce higher resolution data (Giorgi, 2019). With the development of regional climate models in the late 80s (Giorgi, 2019), progress in both climate science and computer technology have enabled us to develop today's state-of-the-art models (Edwards, 2011; Rockel, 2015; Giorgi, 2019; Tapiador et al., 2020). In the 30-year period since the 1990s, especially with the publication of IPCC reports, climate models have evolved to the Earth System Models (ESMs) with high resolution and complex structures that take account of aerosols, carbon cycle, dynamic vegetation, atmospheric chemistry, and land ice as well as atmosphere, ocean, sea ice, and land surface interactions (Figure 2.10) (Giorgi, 1995; Edwards, 2011; IPCC, 2013; Giorgi and Gao, 2018; Giorgi, 2019).

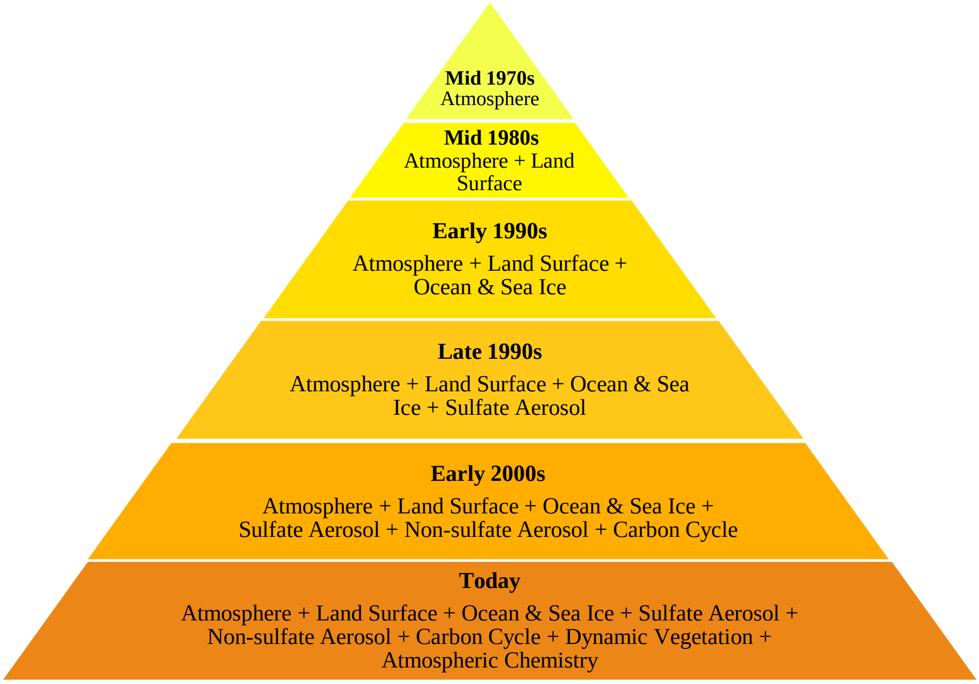

Figure 2.10. A brief illustration of the development process of climate modeling (IPCC, 2001).

2.2.2. General Circulation Models

GCM stands for global climate model or general circulation model. These two terms are used interchangeably. GCMs are more precisely the coupling models of the atmosphere and ocean circulations (Figure 2.11). GCMs simulate the evolution of the Earth's climate system over time describing the interactions of components with each other to create the Earth’s complex climate variability and change. Essentially, GCMs project the impacts of anthropogenic greenhouse gases and aerosols on future climate over a century or more.

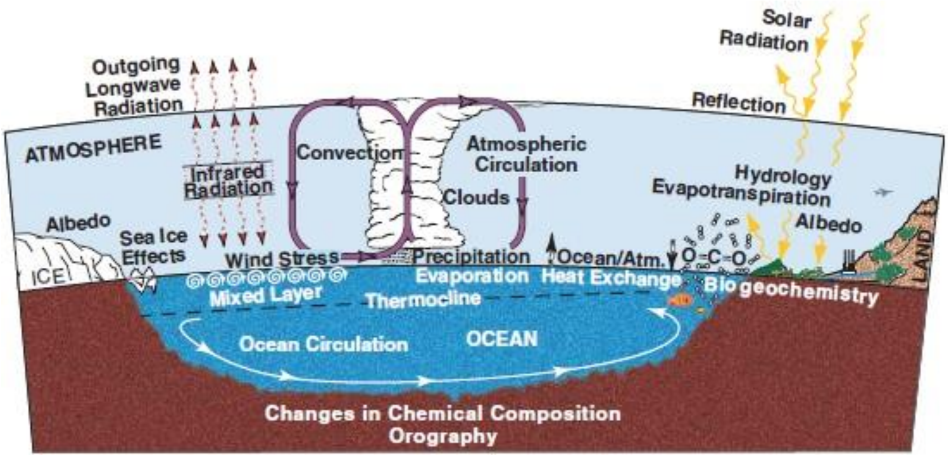

Figure 2.11. Components of the climate system (Reproduced from Neelin (2011)).

GCMs are composed of numerical representations of the atmosphere, ocean, sea, ice, land, surface and other processes (Figure 2.12). The interactions and processes among all these components are expressed by the solution of mathematical equations of these processes based on the basic laws of physics.

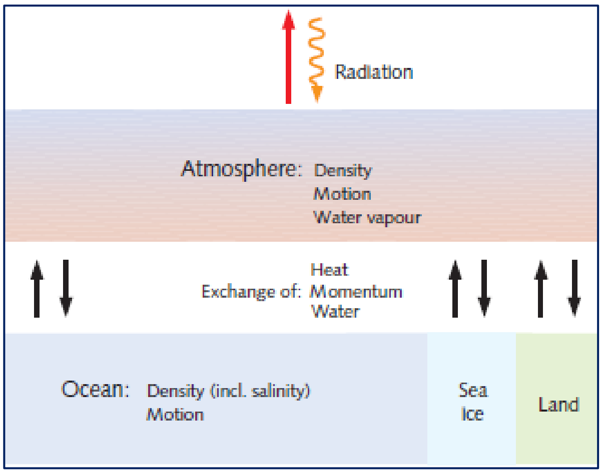

Figure 2.12. Interactions and processes between the components in a GCM (Reproduced from Houghton (2009)).

The climate system equations can solely be solved with up-to-date computers. The main approach behind the computations of those equations is to discretize the entire domain to grid cells (Neelin, 2011). The grid size as well as the grid number of the model determines the horizontal and vertical resolutions of the model (Figure 2.13). As shown in Figure 2.14, a typical GCM has a horizontal resolution determined by differences between latitudes and longitudes and a vertical resolution determined by pressure differences (Neelin, 2011).

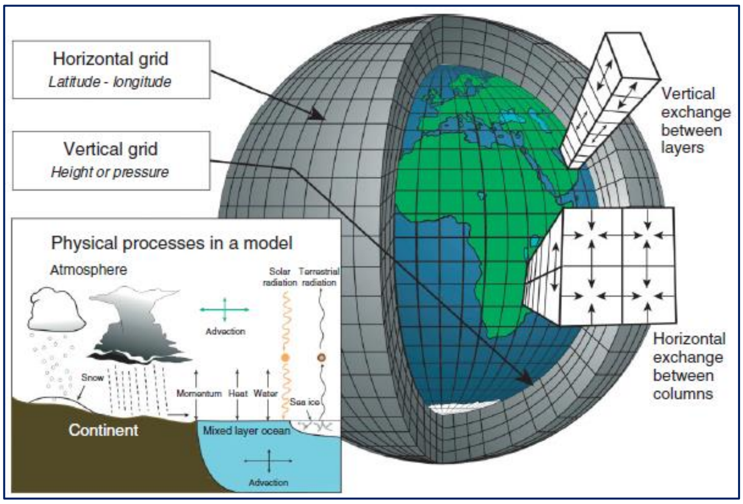

Figure 2.13. A schematic drawing for the Cartesian gridding in a typical GCM (Reproduced from Edwards (2011). Illustrated by Courtney Ritz and Trevor Burnham).

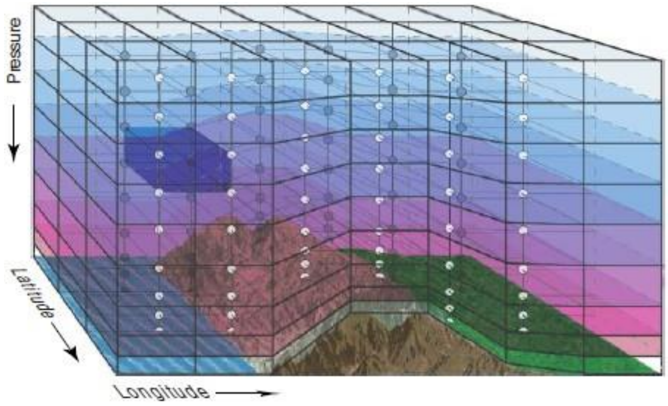

Figure 2.14. Horizontal and vertical resolutions in a GCM (Reproduced from Neelin (2011)).

Phillips’ two-level quasi-geostrophic model is known as the first general circulation model (Phillips, 1956; Lynch, 2008). After Phillips' attempt, the most important step in the global climate model was taken by Kasahara and Washington (1967). NCAR's two-layer global circulation model, based on Richardson's dynamical approach, was successfully run for a period of more than three months. As explained in the previous section, especially Manabe et al. (1975) and afterwards, the development of GCMs gradually continued. GCMs have reached more advanced levels, as computers have been further developed and enable faster and larger data calculations. The grid sizes of the first GCMs, which are approximately 500 km, have decreased almost fivefold today (Giorgi, 2019; Demory et al., 2020). While the GCMs used in the Fourth Assessment Report (AR4) of the IPCC have an average horizontal resolution of 300 km, the GCMs with an average resolution of 150 km were used in the Fifth Assessment Report (AR5). Current models have a horizontal resolution of about 100 km and a vertical level between 20 and 30 (National Research Council, 2012; Demory et al., 2020). GCMs with higher horizontal resolutions below 100 km and vertical resolutions up to 100 levels are now becoming available (National Research Council, 2012; Demory et al., 2020). GCMs have presently been altering to high resolution Regional Earth System Models (RESMs) for recent years (Giorgi, 2019).

GCMs, which form the basis of climate modeling, are improving their skills to simulate the Earth’s climate with each passing day. In the literature on the comparison studies, there seems to be general agreement that GCMs give results consistent with the observations about the changes and variations in climate variables (Reichler and Kim, 2008; Hausfather et al., 2020). Even though the resolution of GCMs has enormously increased, they still have to go hand in hand with RCMs since their core structure is not suitable for direct regional or local simulations as well as the high computational costs.

2.2.3. Climate Model Downscaling

It is known that topography and meteorological processes at regional scale cannot be represented very well in the GCMs (Maraun and Widmann, 2018). On the other hand, many users need climate data on smaller scales than the GCM grid sizes and this can be achieved through downscaling the GCM outputs (Figure 2.15). Downscaling is basically applied in two ways: statistically using statistical regression models or dynamically using high-resolution regional climate models. In addition to these two fundamental approaches, a hybrid downscaling approach, which uses both these two approaches, is also operated as a third way.

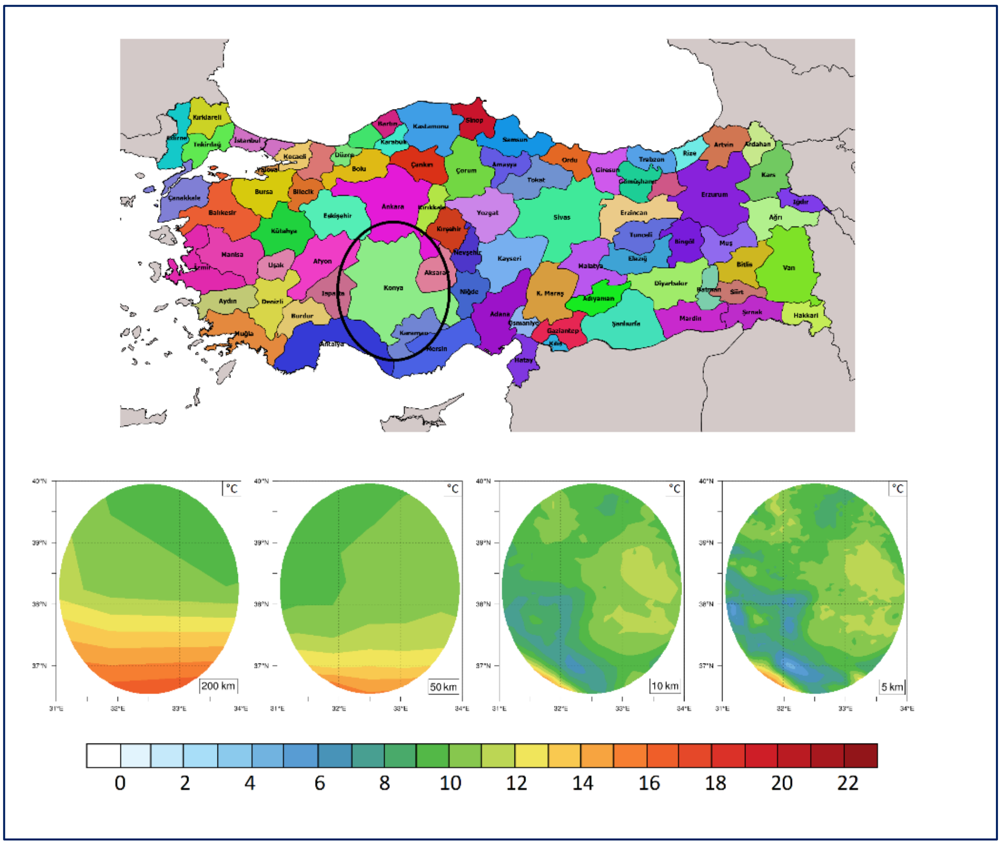

Figure 2.15. An example of downscaling at different resolutions (from 200 km to 50 km, 10 km, and 5 km).

2.2.3.1. Comparison of Downscaling Methods: Statistical, Dynamical, and Hybrid Approaches. The purpose of downscaling is to translate the information produced by the GCMs to regional and local scales. As previously mentioned, GCMs typically provide climate data over very large grid cells, often 100 - 300 km in size. As most people work on much more local scales (below 50 km), it is necessary to use any downscaling technique to get the needed data at finer scales.

Firstly, the relationships between global and regional climate patterns can be found by comparing model projections and actual climate observations. Then, these relationships can be statistically described (Maraun and Widmann, 2018). The next step for projecting changes at the regional or local level based on the GCM output is to apply these statistical relationships to future climate projections assuming that the statistical relationships observed in the past will continue in the future (Zorita and von Storch, 1999). The basic principle in statistical downscaling is to establish a statistical model showing the mathematical relationship between a predictor and a predictand (Maraun and Widmann, 2018). Here, the predictand defines the high resolution, in other words, the downscaled climate variable, and the predictor defines the low resolution climate variable. Thus, the relationship between a low resolution GCM output and a high resolution downscaled output is provided empirically. Statistical downscaling techniques generally fall into three categories; transfer functions (more widely known as regression methods), weather typing (also known as pattern classification or analogues), and weather generators (Wilby and Wigley, 1997; Zorita and von Storch, 1999; Wilby et al., 2004; Lanzante et al., 2018; Maraun and Widmann, 2018). Transfer functions are often the simplest statistical downscaling methods. They include regression-based techniques such as multiple regression, canonical correlation analysis, and artificial neural networks (Wilby et al., 2004; Maraun and Widmann, 2018). A linear or nonlinear relationship between the GCM outputs and the observations are built in these techniques. All transfer functions have one aspect in common; they build a direct relationship between the observations and the GCMs for the same region. Weather typing or analogue techniques such as Monte Carlo experiments, fuzzy classification, self-organizing maps are the other methods for statistical downscaling (Wilby et al., 2004; Maraun and Widmann, 2018). Weather typing methods are based on synoptic meteorology (Hewitson and Crane, 1996; Maraun and Widmann, 2018). Unlike transfer functions, weather typing uses the large-scale atmospheric patterns from a GCM to build that relationship with observations. Lastly, one of the most known statistical downscaling methods is the weather generators such as spell length methods, stochastic methods, and Markov chain (Wilby et al., 2004; Maraun and Widmann, 2018). Weather generators rely on the probability distribution of climate variables depending on their temporal dependency (Maraun and Widmann, 2018).

Although application of statistical downscaling seems more advantageous and practical since it requires less computational power, it is in need of very high quality observation data to establish an accurate relationship between the predictor and the predictand (Mearns et al., 1999). Statistical downscaling also makes it difficult to achieve realistic regional results for a heterogeneous and/or high topography. In this case, dynamical downscaling is the best alternative (Beniston, 2003). Dynamical downscaling is a preferred approach to obtain high resolution climate data for a limited area via RCMs based on physical equations, just like GCMs (Wilby and Wigley, 1997; Rummukainen, 2010; Maraun and Widmann, 2018). Like statistical downscaling, dynamical downscaling depends on the GCM information being reliable. Dynamical downscaling can consistently demonstrate the mesoscale weather systems and microclimates as well as the interactions among several variables (IPCC, 2007). Since dynamical downscaling is an approach based on physical equations, they have higher reliability (IPCC, 2007).

As with any downscaling technique, there are advantages and disadvantages. Statistical downscaling does not take a lot of intensive computer power and can typically be performed on one computer, or a small server, while dynamical downscaling often requires multiple servers and super-computing. The relatively inexpensive nature of statistical downscaling makes it easier to downscale more GCMs than dynamical downscaling. Statistical downscaling can be flexibly crafted for a specific purpose. Observations are a key part of statistical downscaling, and those observations provide information on past events in a region of interest (Mearns et al., 1999). Most statistical downscaling techniques focus on a long observational record to build a robust statistical relationship. This is a weakness if you are interested in changes to things like soil moisture. Statistical downscaling assumes a stationary relationship which means the cross-scale relationship described will be valid in the future (Mearns et al., 1999; IPCC, 2007). This particular assumption may not be valid, particularly close to the end of the century, given that climate change may alter the way the climate currently functions. Statistical downscaling is also lack of rational interaction among the different variables (IPCC, 2007). Results from statistical downscaling can be directly affected by the errors of the GCM. If the GCM has errors in a particular region of interest, those errors can be translated to the results of statistical downscaling as well. Achieving reliable climate output at high resolution on a regional scale is possible by considering the factors affecting the climate of that region properly during downscaling (Murphy, 1999). In this context, the better and meticulously considered the drivers that may affect the climate of the region, especially orography, wetlands and land structure, the more quality climate information is obtained. Dynamical downscaling is more advantageous in this respect. The main handicap of dynamical downscaling is to be computationally expensive (Mearns et al., 1999). While it depends on the quality of the nested GCM, where the initial and boundary conditions are defined, it also needs different parameterizations for each domain examined (Mearns et al., 1999). Yet, it is a great advantage that it can be applied to every region for every resolution (from 1 km to 50 km) without data limitation (Mearns et al., 1999; IPCC, 2007).

In addition to these two principal downscaling methods, a hybrid approach involving both methods can also be used. The hybrid approach is usually referred to as statistical-dynamical downscaling (SDD) in the literature (Frey-Buness et al., 1995; Maraun and Widmann, 2018; Tapiador et al., 2020). SDD is basically applied in three steps: 1- to classify large-scale weather types, 2- dynamical downscaling, 3- weighting of dynamically downscaled outputs by using the frequencies of classified large-scale weather types in the first step (Frey-Buness et al. 1995; Maraun and Widmann, 2018). Originally it was provided to be used more widely by Frey-Buness et al. (1995) based on the approaches developed by Wippermann and Gross (1981) and Heimann (1986) on wind climatology. After Frey-Buness et al. (1995), the hybrid approach has been widely used as an alternative to statistical and dynamical downscaling methods, commonly in studies related to wind climatology (Mengelkamp et al., 1997; Fuentes and Heimann, 2000; Heimann, 2001; Pinto et al., 2010; Reyers et al., 2015; Schubert et al., 2017; Hoffmann et al., 2018). The hybrid approach can be advantageous for convenient domains in terms of saving time and need of strong computing power infrastructure of the RCMs.

In conclusion, the GCMs and downscaling techniques all have their strengths and weaknesses, and the best option to use them depending on the application field. Systematic seasonal and spatial variations besides their marginal, spatio-temporal and multivariable aspects should be rigorously evaluated to select the viable model because those aspects show whether the model has an added value (Maraun and Widmann, 2018). Although there is no perfect model, climate decision makers can use a group of the data sets produced by those models to examine the range of possible climates that they might face in the future.

2.2.4. Regional Climate Models

As mentioned in the previous section, dynamical downscaling is performed with RCMs, software tools developed using physical equations. RCMs are driven using initial and boundary conditions from a GCM (Houghton, 2009). In other words, RCMs are one-way nesting tools. Since RCMs are more useful in representing local-scale orographic, coastal, and inland processes (Jones et al., 1995; Christensen and Christensen, 2007; Maraun et al., 2010), they produce precise results particularly for the heterogeneous terrains. Adequately modeling of complex topography and uplands is the foremost issue in terms of modeling (Giorgi and Mearns, 1991; Beniston, 2003). RCMs improve the low-resolution global outputs of GCMs, which are insufficient to represent the regional or local climate, to a much higher resolution depending on the required details over the studied domain. RCMs generally downscale the coarser grid size of over 100 km to a resolution of 10-50 km (Figure 2.16). However, it is possible to make dynamical downscaling up to resolutions below 10 km when it is needed to get local climate information. Today's state-of-the-art RCMs, capable of downscaling up to 1 km horizontal resolution, basically have two types: hydrostatic and non-hydrostatic. In hydrostatic RCMs, a minimum 10 km grid size can be reached, while non-hydrostatic versions are able to have a resolution below 10 km. In addition, double nesting must be made in order to reach the finer resolution in hydrostatic models. The double nesting technique is simply that the RCM is first run with low resolution GCM outputs and then run one more time with the outputs from this first simulation. To illustrate, a 150 km resolution GCM output is first downscaled to 50 km via an RCM, then 50 km model outputs are used as input for the same RCM to obtain a higher resolution (10 km) data. Whether 50 km, 10 km or 1 km resolution, simulations of high or very high resolution climate data via RCMs are very demanding in terms of computational power and data storage capacity as well as simulation time.

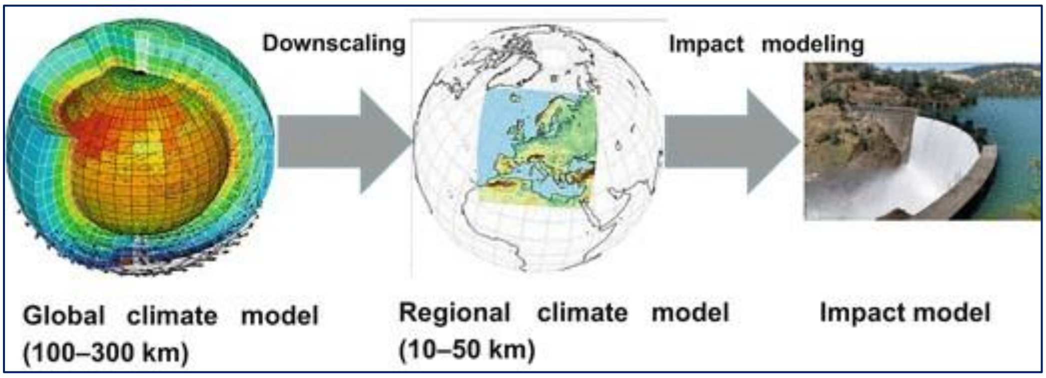

Figure 2.16. An illustration of the role of downscaling (Reproduced from Vautard (2018)).

RCMs are highly sensitive to the boundary conditions produced by the GCMs to which they are nested. Hence, the numerical solutions embedded in the dynamical core of the RCMs can be termed as a Dirichlet problem since they solve the partial differential equations for a limited area based on the initial and boundary conditions defined by the GCMs (Tapiador et al., 2020). There are various RCMs (e.g. HIRHAM, CHRM, COSMO-CLM, RegCM, REMO, RCA, WRFP/WRFG, etc.) developed by a variety of research centers in the world (Tapiador et al., 2020). RCMs differ from each other by their physical and mathematical approaches such as vertical levels, schemes, parameterizations, map projections, and calendar types. The projected domain and period, chosen parent GCM, schemes and parameterizations used in RCM may have discrepant or similar results in different models. So this is why multiple simulations (e.g. different schemes and parameterizations, GCMs, scenarios etc.) should be tested and compared with each other.

It is very valuable for an RCM to make the most accurate climate projections in the shortest time. Hence an RCM always has to be updated and upgraded. The more an RCM is developed by a larger team, the more it will develop and become widespread (Tapiador et al., 2020). As the usage of the RCMs becomes widespread, the deficiencies are also completed and improved to make them better. These improvements can be not only in the dynamical core of the model, but also in the code (Tapiador et al., 2020).

RCMs, which started to be developed and employed increasingly as of 1989 (Dickinson et al., 1989; Giorgi and Bates, 1989; Giorgi, 1990), have reached a high level in the past three decades and continue to be advanced further (Giorgi, 2019, Tapiador et al., 2020). RCMs do not merely address regional or local climate change signals, climate variability, or impacts of climate change on extreme climate events. They also produce the input to be used in impact studies (Woth et al., 2006; Meleux et al., 2007; Olesen et al., 2007; Teutschbein and Seibert, 2010; Endler and Matzarakis, 2011; Bedia et al.; 2013; Rodó et al., 2013; Tobin et al., 2015; Pal and Eltahir, 2016; Coppola et al., 2018) that are vital for climate change adaptation strategies.

2.2.4.1. RegCM. RegCM is an open source and user friendly regional climate model currently being developed by the Abdus Salam International Centre for Theoretical Physics (ICTP) (Pal et al., 2007). RegCM has been effectively applied to several domains (i.e., the Mediterranean, Africa, North America, Central America, South America, East Asia, Central Asia, South Asia, Europe) by a variety of regional climate change and climate variability studies (Gao et al., 2002; Chen et al., 2003; Öztürk et al., 2011; Almazroui, 2012; Giorgi et al., 2012; Gu et al., 2012; Ozturk et al., 2012; Coppola et al., 2014; Giorgi, 2014; Giorgi et al., 2014; Mariotti et al., 2014; Turp et al., 2014a; Sylla et al., 2016; Ozturk et al., 2017, 2018) over the last two decades. It has also been extensively used by many impact studies in recent years (Batista et al., 2016; Demiroglu et al., 2016a, 2016b; An et al., 2018; Demiroglu et al., 2018; Reboita et al., 2018; Gao et al., 2019; Song et al., 2019; Zaninelli et al., 2019; An et al., 2020; Li et al., 2020; Persaud et al., 2020; Venetsanou et al., 2020; Demiroglu et al., 2021).

2.2.4.1.1. A Brief History of RegCM. In 1987, the U.S. Department of Energy launched a feasibility project on the future climate conditions of the Yucca Mountain in Nevada, which is planned to be utilized for the radioactive waste disposal (Barron, 1987; Carter, 1987; Mahony, 2017; Giorgi, 2019). NCAR's CCM1 (Community Climate Model version 1) (Williamson et al., 1987) used in the Yucca Project was found to be inadequate in modeling the regional climate because of its too coarse resolution, which is approximately 500 km grid size (Dickinson et al., 1989; Mahony, 2017; Giorgi, 2019). Upon the proposal of Dickinson et al. (1989), higher resolution (60 km grid size) data was obtained for the Yucca Mountain using the MM4 (Mesoscale Model version 4) (Anthes et al., 1987), which is the limited area model developed by the PSU/NCAR (Pennsylvania State University/National Center for Atmospheric Research). Next, one-month simulations for the western United States (Giorgi and Bates, 1989; Giorgi, 1990) and for Europe (Giorgi et al., 1990) using the MM4 also formed the first version of modern RegCM. One-month simulations were followed by multiyear simulations (Giorgi et al., 1993a; Giorgi et al., 1994).

Biosphere-Atmosphere Transfer Scheme (BATS) (Dickinson et al., 1986) was used for the land surface scheme of RegCM1, which took its dynamical structure from MM4 and its physical structure from CCM1 and MM4. RegCM1 has also been upgraded to RegCM2 (Giorgi et al., 1993b, 1993c), with upgrading of CCM1 and MM4 to CCM2 (Hack et al., 1993) and MM5 (Grell et al., 1994) respectively. RegCM2.5 was developed in the late 90s with the coupling of the lake model and tracer transport scheme. Its dynamics consisted of MM5, while its physics comprised CCM3 (Kiehl, 1996) and MM5. Several years later, RegCM3 (Pal et al., 2007) was built thanks to coupling chemistry/aerosol scheme, sub-grid land-surface scheme, and enhancement in convective and non-convective precipitation, air-sea fluxes. Additionally, RegCM has become more popular with the third-generation version, making the model suitable for parallel computing with the updates made in the code. In the next modified version (RegCM4), RegCM's CCM3 and MM5 based structure was preserved, and some improvements in its dynamics and physics continued to be made. The most significant alterations in RegCM4 were the integration of the new planetary boundary layer scheme (PBL) and land surface scheme (Giorgi et al., 2012). In RegCM4, UW-PBL (University of Washington PBL) (Grenier and Bretherton 2001; Bretherton et al., 2004) was added as an alternative to the modified Holtslag PBL (Holtslag et al., 1990) scheme and CLM3.5 (Community Land Model version 3.5) (Tawfik and Steiner, 2011) scheme was added as an alternative to the BATS land surface scheme. More details in aerosol and atmospheric chemistry processes were described in RegCM4 as well (Giorgi et al., 2012). Again, the model code was updated to make the software more efficient and user friendly. In the past three decades, several major and minor versions of RegCM have been released (Figure 2.17). Finally, RegCM, now available in version 4.7, is no longer just a hydrostatic model, but also provides its users with the non-hydrostatic option as of RegCM4.5 (Giorgi et al., 2016).

Dynamical downscaling subject to this study was conducted using RegCM4.6. Therefore, an in-depth framework of RegCM4.6 is described in the following section before presenting simulation results.

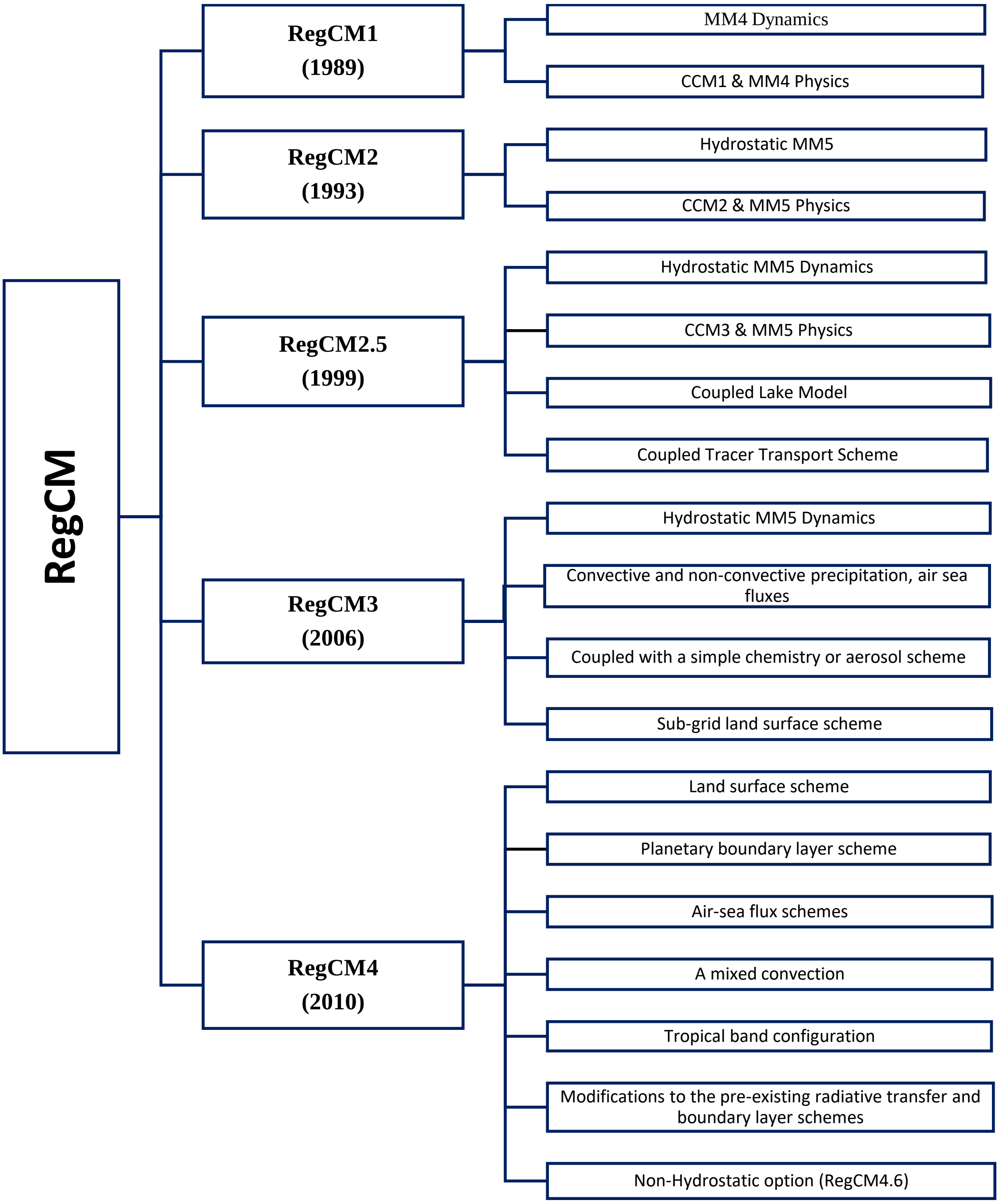

Figure 2.17. The development stages of RegCM.

2.2.4.1.2. Modeling Steps of RegCM. RegCM's simulation process is simply based on the principle of making calculations on a more detailed topography by use of the fundamental parameters from a parent GCM. The underlying mechanism for RegCM is divided into three processing parts: pre-processing, main-processing, and post-processing (Figure 2.18). Elevation, sea surface temperature (SST), land use as terrain variables and air temperature, atmospheric pressure, specific humidity, zonal and meridional wind velocity as initial and boundary conditions (ICBCs) are identified to the model during the pre-processing phase. In this step, the input files for the simulation are created by interpolating terrain variables and ICBCs to study area (domain) on a suitable map projection horizontally and sigma coordinate system vertically. That is to say, the pre-processing phase is an initialization stage for the model. After the pre-processing phase, RegCM starts the simulations by executing the input files. During the main-processing phase, tens or hundreds of terabytes of climate data (Table 2.5) are produced as a result of simulations lasting at least several months depending on the domain size, the grid resolution of the data, and the computer capacity. More Central Processing Unit (CPU) capacity will also reduce simulation time. After the simulation phase is over, the post-processing phase starts and therefore the data obtained in the NetCDF (Network Common Data Form) format is converted to the format needed in the desired time scale for the variable(s) of interest, and analyzed with various computation and visualization tools such as CDO (Climate Data Operators), NCL (NCAR Command Language), GrADS (Grid Analysis and Display System), QGIS (Quantum Geographic Information System), and Bash (Bourne-again shell) Scripting.

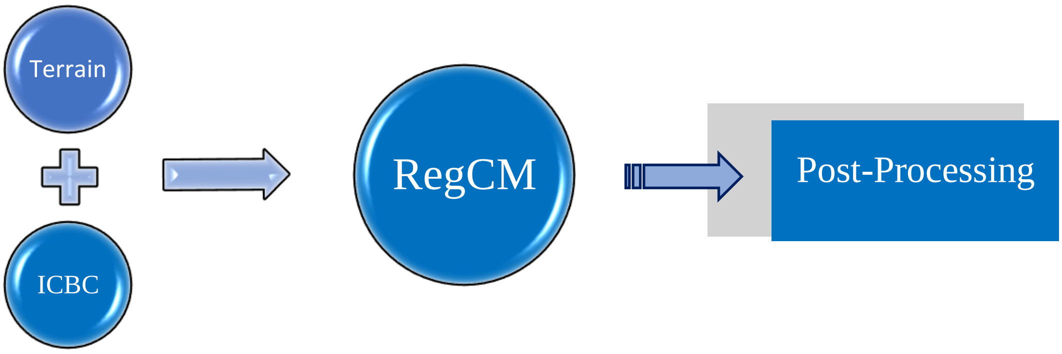

Figure 2.18. A brief illustration of processes in RegCM.

Table 2.5. RegCM outputs for surface (SRF), radiation (RAD), statistical daily surface (STS), and atmosphere (ATM) variables.

SRF	RAD	STS	ATM
Surface Pressure (hPa)	Longitude on Cross Points (degrees_east)	Surface Pressure (hPa)	Surface Pressure (hPa)
Surface wind stress (N/m^2)	Latitude on Cross Points (degrees_north)	Maximum surface temperature (K)	Total rain precipitation flux (kg/m^2 s)
Ground surface temperature (K)	Land Mask (1)	Minimum surface temperature (K)	Ground surface temperature (K)
Foliage canopy temperature (K)	Surface Model Elevation (m)	Maximum total precipitation flux (kg/m^2 s)	Total soil water (kg/m^2)
Total precipitation flux (kg/m^2 s)	Surface Pressure (hPa)	Mean total precipitation flux (kg/m^2 s)	Zonal component of wind (westerly) (m/s)
Total evapotranspiration flux (kg/m^2 s)	Surface net downward shortwave flux (W/m^2)	Duration of sunshine (s)	Meridional component of wind (southerly) (m/s)
Liquid water equivalent of snow thickness (kg/m^2)	Surface net upward longwave flux (W/m^2)	Minimum of surface pressure (hPa)	Air Temperature (K)
Sensible heat flux (W/m^2)	Clearsky top of atmosphere net downward shortwave flux (W/m^2)	Mean surface pressure (hPa)	Pressure velocity (hPa/s)
Net upward longwave energy flux (W/m^2)	Clearsky surface net downward shortwave flux (W/m^2)	Maximum 2-meter temperature (K)	Specific humidity in air (kg/kg)
Net downward shortwave energy flux (W/m^2)	Clearsky top of atmosphere net upward longwave flux (W/m^2)	Minimum 2-meter temperature (K)	Mass fraction of cloud liquid water (kg/kg)
Surface downward longwave flux in air (W/m^2)	Clearsky net upward longwave flux (W/m^2)	Mean 2-meter temperature (K)	Relative Humidity (%)
Surface downward shortwave flux in air (W/m^2)	Top of atmosphere incoming shortwave flux (W/m^2)	Maximum speed of 10m wind (m/s) Runoff flux (kg/m^2 s)	
Convective precipitation flux (kg/m^2 s)	Net top of atmosphere upward shortwave flux (W/m^2)	Runoff flux (kg/m^2 s)	
Atmospheric Boundary Layer thickness (m)	Total cloud fraction (1)		
Surface albedo to direct shortwave radiation (1)	Total columnar liquid water content (kg/m^2)		
Surface albedo to diffuse shortwave radiation (1)	Total columnar ice water content (kg/m^2)		
Duration of sunshine (s)	Top of atmosphere net upward longwave flux (W/m^2)		
Snow Melt (kg/m^2)	Cloud fractional cover (1)		
Anemometric zonal (westerly) wind component (m/s)	Cloud liquid water path (g/m^2)		
Anenometric meridional (southerly) wind component (m s-1)	Shortwave radiation heating rate (K/s)		
Near surface air temperature (K)	Longwave radiation heating rate (K/s)		
Near surface air specific humidity (1)			
Near surface relative humidity (%)			
Moisture content of the soil layers (kg/m^2)			
Moisture content of the soil layers (kg/m^2)			
Runoff flux (kg/m^2 s)			
Runoff flux (kg/m^2 s)			

2.2.4.1.3. Description of RegCM4.6. RegCM has the options to be run with two dynamic structures as hydrostatic and non-hydrostatic since its 4.5 version was released. Climate projections for the Australasia domain realized in this thesis were made using hydrostatic RegCM4.6. Therefore, only the hydrostatic version is explained in this section, which describes the basic physical structure of RegCM (Table 2.6).

Table 2.6. Physical structure of RegCM4.6.

Dynamics	Hydrostatic
	Non-hydrostatic
Radiation	CCM3
	RRTM
Large Scale Precipitation	SUBEX
	Explicit Microphysics
Cumulus Convection	Anthes-Kuo
	Grell
	MIT-Emanuel
	Tiedtke
	Kain-Fritsch
	Mix
Planetary Boundary Layer	Modified Holtslag
	UW-PBL
Land Surface	BATS
	CLM
Ocean Fluxes	BATS1e Monin-Obukhov
	Zeng
	COARE Bulk Flux Algorithm
Coupled Ocean	MIT Ocean Model
	ROMS
Lake Model	1D Thermal Lake Model
Aerosols	OC-BC-SO_4
	Dust
	Sea Salt
Elevation	GMTED2010

RegCM, which takes its dynamic structure from MM5, uses the horizontal Arakawa-B grid structure and the sigma-p coordinate system vertically (Elguindi et al., 2014; Giorgi et al., 2016). Arakawa-B is one of the five horizontal grid types recommended by Arakawa (1972). As shown in Figure 2.19, some variables are calculated at the midpoint of the grid in the B-type grid scheme, while others are calculated at the corner points. According to the Arakawa-B scheme, u and v wind velocity components are distributed to the middle point of the grid, and variables such as air temperature, specific humidity, and atmospheric pressure are distributed to the corner points.

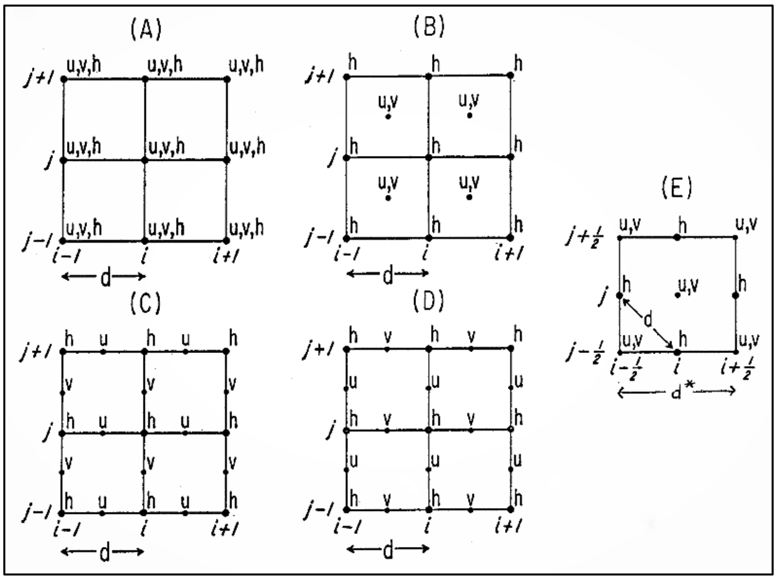

Figure 2.19. Arakawa's horizontal grid types (Reproduced from Arakawa (1972)).

Sigma (σ) coordinate system, which is frequently employed in mesoscale models, is also used to define the vertical levels of RegCM since its dynamics is already from the MM5 (Elguindi et al., 2014). The σ coordinate system vertically divides the atmosphere into pressure levels, with 1 at the top and 0 at the bottom, following the domain's terrain (Figure 2.20) (Dudhia et al., 2005).

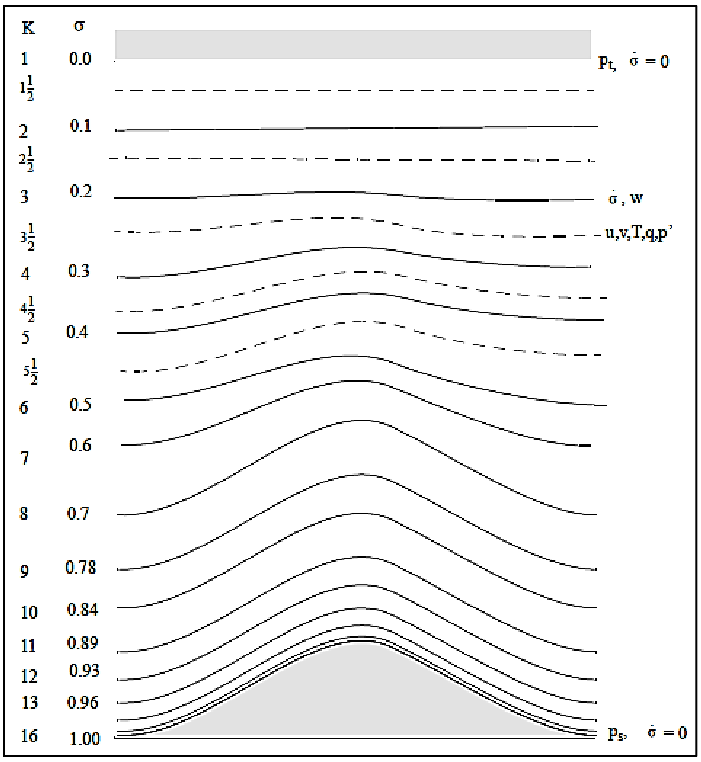

Figure 2.20. Sigma (σ) coordinate system for the vertical levels of RegCM (Reproduced from Dudhia et al. (2005)).

RegCM has 23 vertical levels, but it is generally driven with 18 levels for the hydrostatic core and 23 levels for the non-hydrostatic core (Elguindi et al., 2014; Giorgi et al., 2016). The σ coordinate of the pressure value at any level is calculated by the formula given in Equation 2.1, in which p, p_t, and p_s denote any pressure, top pressure, and surface pressure values in the atmosphere, respectively (Dudhia et al., 2005; Elguindi et al., 2014):

$$\sigma = \frac{(p - p_t)}{(p_s - p_t)} \tag{2.1}$$

In the RegCM preprocessing phase, that is, before the model starts running, the basic variables from the parent model, SST, and topographic values are horizontally and vertically interpolated according to aforementioned approaches and a particular map projection. RegCM includes four types of map projection options for regridding: Normal Mercator, Lambert Conformal, Polar Stereographic, and Rotated Mercator (Elguindi et al., 2014). The appropriate map projection to be used in the model depends on the location of the domain. Thus, it is suggested to use Normal Mercator for low latitudes around 30° north and south of the equator, Lambert Conformal for mid-latitudes around 45°, and Polar Stereographic for high latitudes extending across the 75°, and Rotated Mercator for the areas outside these domains specifically spanning 45° latitudes (Elguindi et al., 2014; Giorgi et al., 2016). Within the scope of the thesis, Rotated Mercator map projection was used for the Australasia domain. Figure 2.21 illustrates the Australian domain drawn using each map projection.

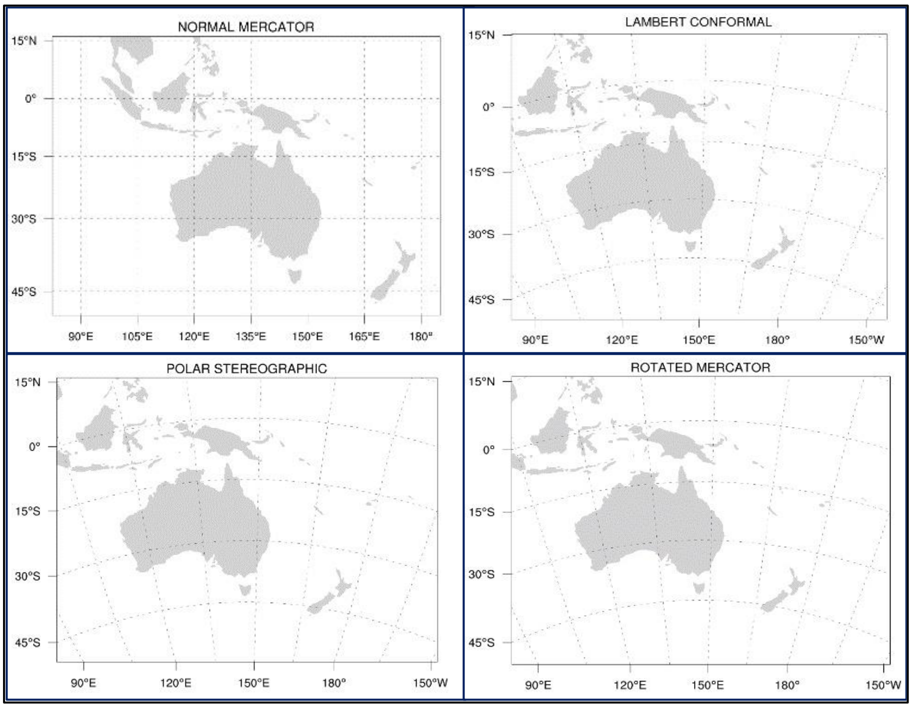

Figure 2.21. Australasia with different map projections.

Dynamic structure of the RegCM4.6's hydrostatic option has several fundamental equations (Elguindi et al., 2014) as described in detail by Grell et al. (1994) for MM5: hydrostatic equation, horizontal momentum equations, continuity equation, sigmadot ($\dot{\sigma}$) equation, thermodynamic equation, and omega (ω).

Computations for all processes within the climate system are described in the model using approximately representations called parameterizations. Although these parameterizations are an important source of uncertainty, they are still very useful to represent the climate system properly as much as possible. In today's state-of-the-art climate models, the number and options of parameterizations, which are constantly being developed, enhance depending on the level of sophistication and complexity of the model.

In the thesis, RegCM's radiation and land surface parameterizations were not changed in the phase of regional climate modeling and the default schemes of the model were used. RegCM has long been using the radiation scheme developed for CCM3 (Kiehl et al., 1996) as the default scheme. A Rapid Radiative Transfer Model (RRTM) (Mlawer et al., 1997) is another option for the radiative scheme in RegCM. It can be concisely expressed that the CCM3 radiation scheme (Briegleb, 1992) uses the 18-spectral intervals for oxygen (O_2), ozone (O_3), water vapour ($H_2O(g)$), and carbon dioxide (CO_2), adopting the delta-Eddington (δ-Eddington) approximation (Joseph et al., 1976) for scattering and absorption of solar radiation (Kiehl et al., 1996; Elguindi et al., 2014). It also considers the role of other greenhouse gases, aerosols, and cloud ice (Elguindi et al., 2014). RRTM is a favorable alternative to the CCM3 radiation scheme. It is a novel radiation scheme which uses a correlated k-method for both shortwave and longwave fluxes (Mlawer et al., 1997). It might be useful to reduce the radiative biases and to investigate the impacts of aerosols for exhaustive and convection-permitting modeling.

One of the essential steps of RegCM is to define the land use surface scheme to the model for the domain of interest. In this way, the surface structure of the domain where the high resolution data will be obtained is defined and it is provided that the surface-atmosphere interaction processes are calculated in the most accurate way. RegCM4.6 has two land surface models, BATS version 1e (BATS1e) (Dickinson et al., 1993) and CLM version 4.5 (CLM4.5) (Oleson et al., 2013). In the thesis, the use of default BATS1e was preferred instead of CLM4.5. BATS1e in RegCM4.6 has 20 distinct vegetation types (Table 2.7) which include three soil layers with various texture kinds from sand to clay and different soil color from light to dark (Dickinson et al., 1993; Giorgi et al., 2012;

Elguindi et al., 2014). BATS1e is a highly improved land use model in terms of soil moisture and solar radiation fluxes. CLM4.5, which seems to be a more complex surface model compared to BATS1e, causes RegCM to need approximately 20 % more computation time (Giorgi et al., 2012).

Table 2.7. Vegetation types in BATS1e.

Crop/Mixed Farming	Evergreen Broadleaf Tree	Semi-desert	Evergreen Shrub
Short Grass	Tall Grass	Ice Cap/Glacier	Deciduous Shrub
Evergreen Needleleaf tree	Desert	Bog/Mash	Mixed Woodland
Deciduous Needleleaf Tree	Tundra	Inland Water	Forest/Field Mosaic
Deciduous Broadleaf Tree	Irrigated Crop	Ocean	Water & Land Mixture

2.2.4.1.4. Planetary Boundary Layer Schemes in RegCM4.6. Planetary Boundary Layer (PBL) is the lowest layer of the atmosphere, about 1 km above the ground. As the lowest part of the troposphere, PBL is the closest part of the atmosphere to the ground and it is directly affected by the heating and cooling processes on the ground surface. The connection of the processes on the surface with the turbulent fluxes in PBL is one of the most important aspects in climate models. Numerical definitions of turbulent fluxes in PBL in RegCM are made with two different schemes: Holtslag PBL and the University of Washington (UW) turbulence closure model.

Holtslag PBL: Holtslag PBL is the first nonlocal scheme used in RegCM to describe heat, moisture, and momentum transfer processes between surface and atmosphere. In the first RegCM version, the local scheme was used (Deardoff, 1972; Pal et al., 2007), but in later versions Holtslag PBL was preferred. The nonlocal PBL is more appropriate, since it better performs the physical processes between surface and atmosphere under dry convective states (Holtslag and Boville, 1993). Holtslag PBL is a 1st order diagnostic scheme that is based on the nonlocal diffusion approach and takes into account the opposite gradient in unstable atmospheric conditions (Holtslag et al., 1990; Elguindi et al., 2014). Analyzes have observed that the Holtslag PBL scheme calculates the upward moisture transfer too much and this situation causes less moisture on the surface and more moisture at the top of the PBL (Elguindi et al., 2014). Similarly, it has been determined that under very stable atmospheric conditions, immoderate heat, moisture and momentum transport cause incorrect calculation of temperature inversions in layers close to the surface (Elguindi et al., 2014). This situation results in high temperature biases, especially in places in the high latitudes of the northern hemisphere such as Siberia and Canada. In order to eliminate these two negative situations mentioned above, some corrections were made in the Holtslag PBL parameterization with RegCM4, and better processing of vertical exchanges between surface and atmosphere was achieved. It is still used as a favorite PBL in modeling studies as a one-dimensional multilayer model, since it does not require much computational capacity. Formula given in Equation 2.2 is used in calculation of vertical eddy flux in Holtslag PBL.

$$F_c = -K_c\left(\frac{\partial C}{\partial z} - \gamma_c\right) \tag{2.2}$$

F_c: vertical eddy flux, K_c: eddy diffusivity, z: height inside PBL, γ_c: countergradient.

The eddy diffusivity (K_c) formula is given in Equation 2.3:

$$K_c = kw_t z\left(1 - \frac{z}{h}\right)^2 \tag{2.3}$$

k: von Karman constant, w_t: turbulent convective velocity, h: PBL height.

The formula of temperature and water vapour's countergradient term (γ_c) is given in Equation 2.4:

$$\gamma_c = C\frac{\phi_c^0}{w_t h} \tag{2.4}$$

C: constant (= 8.5), ϕ_c^0: surface temperature or water vapor flux.

The PBL height (h) is calculated using the formula given in Equation 2.5:

$$h = \frac{\mathrm{R_{icr}}[u(h)^2 + v(h)^2]}{\left(\frac{g}{\theta_s}\right)[\theta_v(h) - \theta_s]} \tag{2.5}$$

R_{icr}: critical bulk Richardson number, u: zonal wind component, v: meridional wind component, g: gravitational acceleration; θ_v: virtual potential temperature, θ_s: appropriate temperature.

The UW Turbulence Closure Model: Apart from Holtslag PBL, another PBL scheme that can be used in RegCM is the UW turbulence closure model (the UW model). Unlike Holtslag PBL, the

UW model is a local scheme. The UW model, which enables stratocumulus clouds and coastal fog to be better defined in the model, is a 1.5-order prognostic scheme (Grenier and Bretherton, 2001; Bretherton et al., 2004; Elguindi et al., 2014). It provides an alternative parameterization for shallow cumulus convection (Bretherton et al., 2004; McCaa and Bretherton, 2004). Based on the local diffusion approach, the UW model allows calculating vertical transfers both within and outside PBL boundaries (Elguindi et al., 2014). It also represents the physical processes between surface and atmosphere in dry convective conditions (Grenier and Bretherton, 2001). However, unlike the 1st order models, the UW model uses turbulence kinetic energy to describe diffusivites (Elguindi et al., 2014). Basically, the UW model first determines the boundary layer height as the process step and then calculates the surface turbulent kinetic energy. It then predicts changes in surface turbulent kinetic energy, determines the diffusivites at each height, and finally predicts the change in each prognostic quantity (Elguindi et al., 2014). The UW PBL model solves the following equations (Equation 2.6, Equation 2.7, Equation 2.8, and Equation 2.9) at each time step:

$$\left.\frac{\partial u_i}{\partial t}\right|_{BL} = \frac{\partial}{\partial z}\left[\kappa z S_m(z)\sqrt{2e(z)}\,\frac{\partial u_i}{\partial z}\right] \tag{2.6}$$

$$\left.\frac{\partial \theta_l}{\partial t}\right|_{BL} = \frac{\partial}{\partial z}\left[\kappa z S_h(z)\sqrt{2e(z)}\,\frac{\partial \theta_l}{\partial z}\right] \tag{2.7}$$

$$\left.\frac{\partial Q}{\partial t}\right|_{BL} = \frac{\partial}{\partial z}\left[\kappa z S_h(z)\sqrt{2e(z)}\,\frac{\partial Q}{\partial z}\right] \tag{2.8}$$

$$\left.\frac{\partial \chi_j}{\partial t}\right|_{BL} = \frac{\partial}{\partial z}\left[\kappa z S_h(z)\sqrt{2e(z)}\,\frac{\partial \chi_j}{\partial z}\right] \tag{2.9}$$

u_i: momentum, θ_l: liquid water potential temperature, Q: total water mixing ratio, κ: diffusivity, S: shear.

2.2.4.1.5. Convective Parameterizations. RegCM has three basic parameterization alternatives for the calculation of convective precipitation: Anthes-Kuo scheme, Grell scheme, MIT-Emanuel scheme, Tiedtke scheme, and Kain-Fritsch scheme. In addition, the Grell scheme is represented by two different closure types, Arakawa-Schubert and Fritsch-Chappell. The Betts-Miller scheme, which has not been operated until now, although it is included in RegCM's name list, is therefore not mentioned in this section. With the fourth version of RegCM, one of the most striking features added to the model is that the convective parameterizations can be selected separately on land and ocean. This option, called mixed convection, allows the model to run with convection parameterization whichever scheme fits best on land and ocean.

Anthes-Kuo Scheme: Kuo scheme is the most well-established parameterization approach used for convective precipitation (Kuo, 1965, 1974; Raymond and Emanuel, 1993). RegCM uses a modified version of Kuo scheme, namely, the Anthes-Kuo scheme (Anthes, 1977; Anthes et al., 1987). When the moisture convergence in an air column exceeds a specific value and a convectively unstable vertical sounding occurs, the Anthes-Kuo scheme's convective activity kicks in (Elguindi et al., 2014). In the Anthes-Kuo scheme, a certain part of the air column is moistened and the remaining part turns into precipitation. The humidity rate of the air column is also calculated depending on the average relative humidity. Since evapotranspiration in the previous time step will moisten the lower atmosphere, it is indirectly added to the moisture convergence. In this case, with increasing evepotranspiration, it turns into an increasing amount of precipitation, assuming that the air column is unstable. The latent heat arising from the condensation is distributed between the upper and lower layers of the cloud so that the maximum heating is accumulated in the upper part of the cloud layer (Elguindi et al., 2014). In addition, by adding the horizontal diffusion term and time release constant to the scheme, moisture redistribution and instantaneous latent heat transfer are prevented, thus avoiding the formation of numerical point storms (Elguindi et al., 2014). In the Anthes-Kuo scheme, as the altitudes of the cloud at the lower and upper levels are not specified, the cloud types are not defined and the calculations for cloud dynamics and microphysics are not made (Jacobson, 2005). Although still present in the model, the Anthes-Kuo scheme is rarely preferred over other cumulus parameterizations available, as it produces poorer precipitation (Giorgi et al., 2012).

Grell Scheme: Simple but useful Grell scheme is the most preferred cumulus parameterization in RegCM. Like the Arakawa-Schubert cumulus parameterization, the Grell scheme treats the circulation of clouds as two fixed directions, up and down (Grell, 1993; Grell et al., 1994; Elguindi et al., 2014). The Grell scheme is activated when the rising air parcel reaches the moist convection level (Giorgi et al., 2012). Except for the upper and lower parts of the air circulation, no direct mixing occurs between the cloudy air parcel and its environment (Elguindi et al., 2014). Entrainment and detrainment processes are not seen along the edges of the cloud in the Grell scheme where the mass flux is constant with height (Elguindi et al., 2014). In the Grell scheme, where moistening and heating are determined by the detrainment processes and mass movements in the upper and lower parts of the cloud, the cooling effect of the descending moist air is also taken into account (Elguindi et al., 2014). In RegCM, the Grell scheme offers two different closure type options: Arakawa-Schubert and Fritsch-Chappell. In the Arakawa-Schubert closure type, there is a two-layer approach as the layer where the cloud is formed and the subcloud mixing layer (Jacobson, 2005). Additionally, many clouds are formed in the cloud layer and all these clouds combine in an air column to form a cloud group (Jacobson, 2005). The Fritsch-Chappell closure type, on the other hand, has been developed for the correct consideration of mesoscale convective systems in climate models (Fritsch and Chappell, 1980; Fritsch and Kain, 1993). In the Arakawa-Schubert closure type, the buoyant energy is released instantly at each time step, while in the Fritsch-Chappell closure type it is released every 30 minutes (Arakawa and Schubert, 1974; Fritsch and Chappell, 1980; Arakawa and Cheng, 1993; Fritsch and Kain, 1993; Giorgi et al., 2012). Another major difference between these two closure types is the approach between atmosphere, convective fluxes, and precipitation nexus (Elguindi et al., 2014). The Arakawa-Schubert closure type associates convective fluxes and precipitation with tendencies in the state of the atmosphere, while the Fritsch-Chappell closure type associates convective fluxes with the atmosphere’s instability degree. However, both closure types establish a statistical equilibrium between convection and large-scale processes (Elguindi et al., 2014).

<u>MIT-Emanuel Scheme</u>: The MIT-Emanuel scheme, originally designed by Emanuel (1991) to describe cumulus convection in large-scale models, was later developed (Emanuel and Živković-Rothman, 1999) and integrated into the model as of the 3rd generation RegCM (Pal et al., 2007; Giorgi et al., 2012). The MIT-Emanuel scheme is the most complicated approach that can be used for convective precipitation parameterization in RegCM (Giorgi et al., 2012). The MIT-Emanuel scheme takes up and down convective fluxes at the subcloud scale, assuming that mixing in clouds occurs heterogeneously and intermittently (Elguindi et al., 2014). In the MIT-Emanuel scheme, convection begins when the neutral buoyancy level exceeds the cloud base level (Elguindi et al., 2014). With the ascending air parcel between the neutral buoyancy level and the cloud base level, some of the condensed moisture turns into precipitation, while the remaining part provides cloud formation (Elguindi et al., 2014). It is also considered that the cloud is mixed with the air within its environment. The MIT-Emanuel scheme takes into account the simplified ice processes, allowing the water in the cloud to automatically turn into rain water (Giorgi et al., 2012). Transport of passive traces is also deemed in the MIT-Emanuel scheme (Elguindi et al., 2014).

<u>Tiedtke Scheme</u>: Just like the MIT-Emanuel scheme, the Tiedtke scheme deals with convective transport in more detail. The Tiedtke scheme, which is included in the model with actual versions of RegCM, is activated when the air parcel exceeds a certain environment temperature. The Tiedtke scheme was first developed with an idea that suggests the mass flux approach for more accurate

cumulus parameterization in large-scale models (Tiedtke, 1989). The Tiedtke scheme represents the cloud ensemble as a one-dimensional bulk model, also taking into account downstream and upstream airflows (Tiedtke, 1989). Moreover, many types of convection (i.e., penetrative convection, shallow convection, and midlevel convection) are included in the Tiedtke scheme (Tiedtke, 1989). Bulk cloud mass flux approach in penetrative and midlevel convections is based on large-scale moisture convergence, whereas shallow convection is based on surface evaporation (Tiedtke, 1989). The Tiedtke scheme, which realistically represents the convective heating fields and surface fluxes, has become a very useful scheme for climate models (Tiedtke, 1989, 1996). The Tiedtke scheme also performs more reliably in terms of the hydrological cycle.

Kain-Fritsch Scheme: The Kain-Fritsch scheme is a cumulus convection scheme developed based on the Fritsch-Chappell closure approach (Kain and Fritsch, 1990, 1993; Kain, 2004). It is simply defined as a one-dimensional bulk plume model that includes entrainment and detrainment processes (Kain and Fritsch, 1990). In the Kain-Fritsch scheme, the bidirectional movement of air mass between clouds and the environment of clouds is regulated vertically layer by layer (Kain and Fritsch, 1990, 1993). Conservation of mass, thermal energy, total humidity, and momentum that are not required during most of the implementation phases of the Fritsch-Chappell closure have become elaborately applied in the Kain-Fritsch scheme (Kain and Fritsch, 1993). The Kain-Fritsch scheme is a mass flux convection parameterization that includes vertical momentum dynamics to predict the instability of the atmosphere, the existence of suitable instability conditions for the growth of the cloud, and the characteristics of the convective cloud (Kain, 2004). The Kain-Fritsch scheme has been further developed, especially thanks to innovations such as activation of shallow convection and changes in the formulation of rising and sinking air (Kain, 2004).

3. RESULTS

3.1. Assessment of Projected Changes in Temperature and Precipitation Climatology over the CORDEX-Region 9 via Multi-Model Ensemble Mean of CMIP5 Models

Even though we have highly sophisticated climate models today, none of them are perfect. In this respect, they are still a simplified version of reality. As mentioned by Maraun and Widman (2018) with reference to Stainforth et al. (2007), climate models have uncertainties due to different reasons (i.e., forcing uncertainty, model imperfection, and internal climate variability). Despite all the shortcomings and uncertainties, today's models perform very successfully and usefully (Flato et al., 2013; Hausfather et al., 2020). Since the performance of the models can change temporally and spatially, it is best to compare as many models as possible in climate change studies. One of the most basic approaches of the studies carried out with various climate models in climate science is to reveal the performance of each model individually and to talk about the common results at the regional scale by considering the average of all models. Multi-model ensemble mean approach is one of the approaches used in climate change studies as a method that improves the performance of the models and reduces the bias (Tebaldi and Knutti, 2007; Parker, 2013; Herger et al., 2018). In this context, multi-model ensemble approach, which has been used in various studies before (IPCC, 2013; Sillmann et al., 2013a, 2013b; Turp et al., 2014b, 2015, 2016a; Turp and Kurnaz, 2017; Ahmed et al., 2019), has been evaluated under three different scenarios (i.e., RCP2.6, RCP4.5, and RCP8.5) and periods (i.e., 2016 - 2035, 2046 - 2065, and 2081 - 2100) for air temperature and precipitation projections using CMIP5 models for Australasia. CDO program was used in calculating multi-year seasonal means and multi-model ensemble means. According to the definition of CDO program (Schulzweida, 2020), the multi-model ensemble mean is formulated as follows (Equation 3.1):

$$o(t, x) = \text{mean}\{i_1(t, x), i_2(t, x), \ldots, i_n(t, x)\} \tag{3.1}$$

Here, $i_1(t, x)$: element number x of the field at time step t of the first input file (model 1)

$i_2(t, x)$: element number x of the field at time step t of the second input file (model 2)

$i_n(t, x)$: element number x of the field at time step t of the nth input file (model n)

$o(t, x)$: element number x of the field at time step t of output file (ensemble mean)

3.1.1. CMIP5 Multi-Model Projection of the Changes in Air Temperature and Precipitation Climatology over the CORDEX-Australasia Domain under the RCP2.6 Scenario

In this section, the seasonal and spatial performances of both individual and multi-model ensemble means of eight different GCM outputs (Table 3.1), which are included in the CMIP5 and run under the RCP2.6 scenario, were compared with CRU observation data as a first step. Secondly, using the multi-model ensemble means, the projection results for three future periods (i.e., near-term, mid-term, and long-term) were evaluated. Since each model has a different horizontal resolution, all models were interpolated (Jones, 1998) to a mutual 1° x 1° horizontal resolution for comparison. While the past period comparisons were made for the period of 1981 - 2000, the future projection changes were investigated for the periods of 2016 - 2035, 2046 - 2065, and 2081 - 2100 with respect to the reference period of 1981 - 2000.

Table 3.1. CMIP5 models used in multi-model ensemble mean approach under the RCP2.6 scenario.

Model Name	Modeling Group	Horizontal Resolution (lat x lon)
BCC-CSM1.1	Beijing Climate Center, China Meteorological Administration	2.7906° x 2.8125°
CanESM2	Canadian Centre for Climate Modelling and Analysis	2.7906° x 2.8125°
CNRM-CM5	Centre National de Recherches Météorologiques/Centre Européen de Recherche et Formation Avancée en Calcul Scientifique	1.4008° x 1.40625°
CSIRO-Mk3.6.0	Commonwealth Scientific and Industrial Research Organization & Queensland Climate Change Centre of Excellence	1.8653° x 1.875°
GFDL-ESM2G	NOAA Geophysical Fluid Dynamics Laboratory	2.0225° x 2°
GISS-E2-R	NASA Goddard Institute for Space Studies	2° x 2.5°
HadGEM2-ES	Met Office Hadley Centre & Instituto Nacional de Pesquisas Espaciais	1.25° x 1.875°
NorESM1-M	Norwegian Climate Centre	1.8947° x 2.5°

3.1.1.1. Benchmarking CMIP5 Model Performances for Seasonal Air Temperature and Precipitation Climatology under the RCP2.6 Scenario. When we look at the temperature bias of each model seasonally (Figure 3.1), it was seen that some models have cold bias, whereas some models have warm bias. When the temperature spatial mean values of each model were compared with the CRU observation value, the NorESM1-M model has the highest bias (between -1.5 ℃ and -2 ℃) in the December - January - February (DJF) period, while the GISS-E2-R in March - April - May (MAM) and September - October - November (SON) seasons and the CNRM-CM5 model in June - July - August (JJA) were highly biased (varying from -1.2 ℃ to +1.4 ℃). If the models are evaluated in terms of bias, it was found that the most successful models are CSIRO-Mk3.6.0 in DJF, HadGEM2-ES in MAM, GFDL-ESM2G in JJA, and CanESM2 in SON. When the multi-model ensemble means were calculated and compared with the observation, it was concluded that the temperature bias for all four seasons reduces reasonably against the individual bias of many models. In the seasons of DJF, MAM, and JJA, the multi-model ensemble mean had a cold bias below 0.5 °C, while it had a warm bias very close to zero in SON.

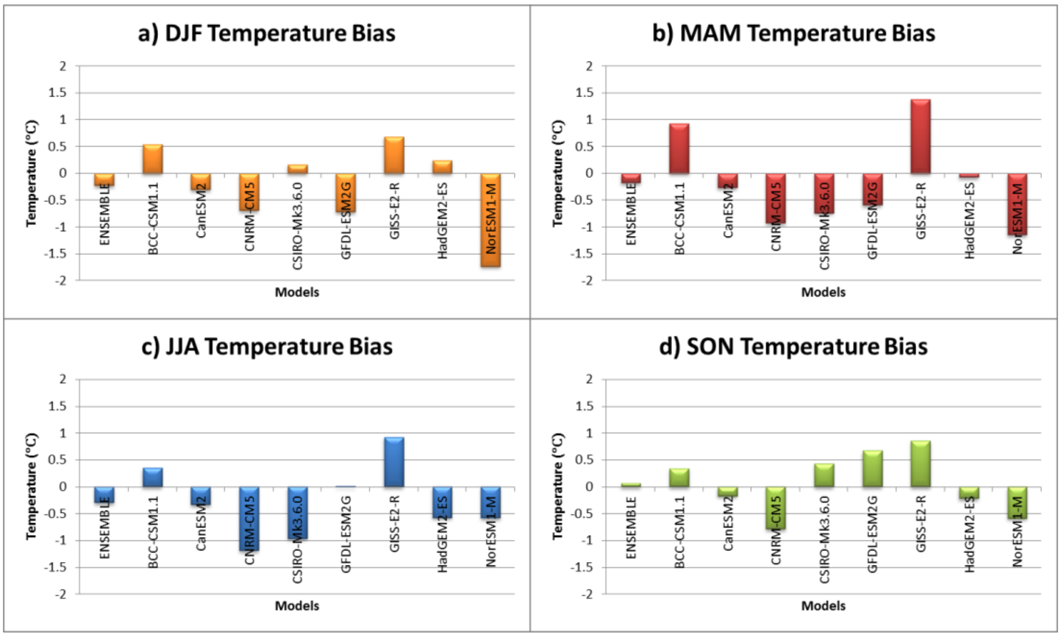

Figure 3.1. Seasonal air temperature bias for models used in the multi-model ensemble mean approach under the RCP2.6 scenario (i.e., December - January - February (DJF), March - April - May (MAM), June - July - August (JJA), and September - October - November (SON) seasons).

If we look at the spatial pattern of the multi-model ensemble mean bias (Figure 3.2), cold bias appears more dominant, especially in all seasons except SON. While the cold bias exceeding 4 °C is remarkable towards the equatorial regions, cold bias dominates Papua New Guinea for four seasons, except for a few local points. Contrary to Papua New Guinea, while New Zealand has warm bias for all four seasons, warm bias is more common in the coastal areas of Australia, mainly in the southeastern coasts and Tasmania state. Cold bias is more significant over the arid areas of Australia.

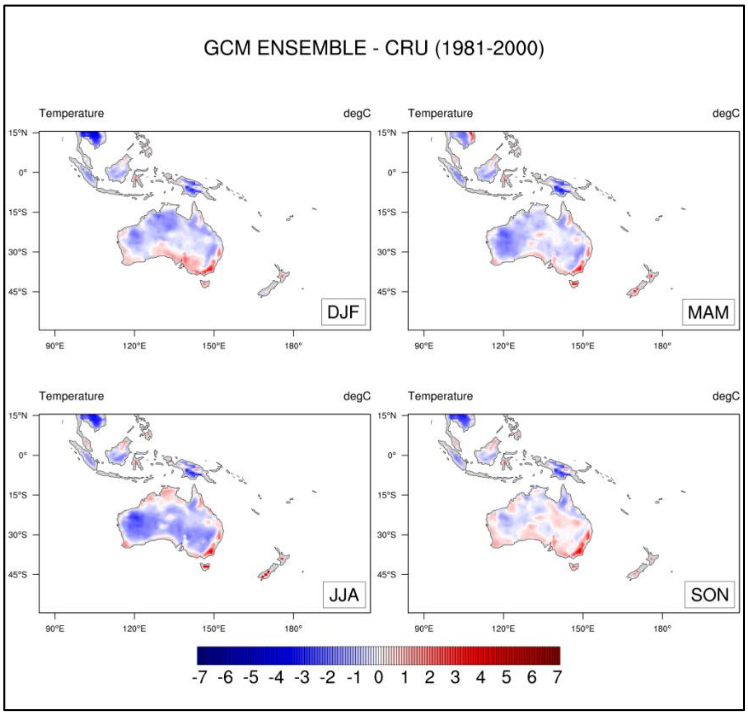

Figure 3.2. Spatial pattern of the multi-model ensemble mean bias in seasonal air temperature for the models used under the RCP2.6 scenario (i.e., December - January - February (DJF), March - April - May (MAM), June - July - August (JJA), and September - October - November (SON) seasons).

The precipitation bias of the models (Figure 3.3) shows predominantly overestimation in the DJF and MAM seasons. Besides, precipitation biases are lower in the JJA and SON seasons. When the individual biases are viewed seasonally, it is clear that the most precipitation biases are seen in GFDL-ESM2G and NorESM1-M models in DJF, GFDL-ESM2G in MAM, GISS-E2-R in JJA, HadGEM2-ES and GISS-E2-R in SON. It is noteworthy that the precipitation bias is relatively low in the models in the season of JJA, followed by the precipitation bias in SON compared to the DJF and MAM seasons of the year. When multi-model ensemble mean is also calculated, it is seen that precipitation bias, like the temperature, has decreased to more reasonable levels compared to the levels which individual models have. Here, overestimation occurs in multi-model ensemble mean for all four seasons. The satisfying performance of the models in the JJA and SON seasons is reflected in the multi-model ensemble as well, minimizing the bias in these seasons to be almost zero. The high bias of the models in the DJF season causes the multi-model ensemble mean value to be above the bias values of some models in this period.

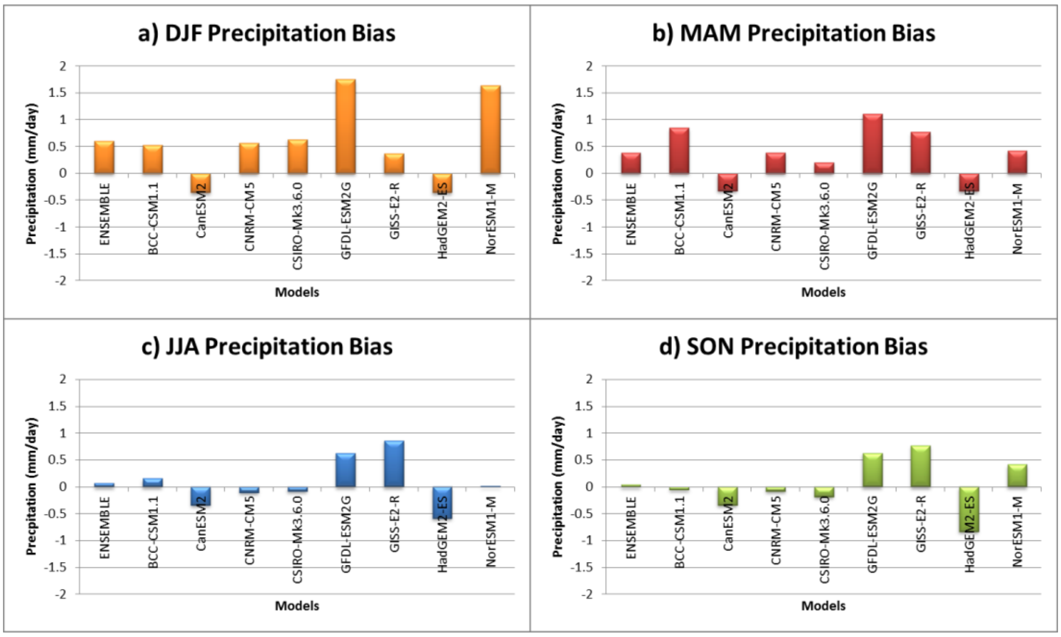

Figure 3.3. Seasonal precipitation bias for models used in the multi-model ensemble mean approach under the RCP2.6 scenario (i.e., December - January - February (DJF), March - April - May (MAM), June - July - August (JJA), and September - October - November (SON) seasons).

As the spatial distribution of precipitation bias is examined (Figure 3.4), it is seen that there is almost no bias in regions where there usually is low precipitation. In the JJA and SON seasons, there is up to 3 mm/day of underestimation in the southwest and northwest coasts of Australia. Precipitation bias is more remarkable in places with high topography like Papua New Guinea and in areas with a tropical climate like Indonesia and Malaysia. For example, whilst Papua New Guinea has up to about 7 mm/day throughout New Guinea Highlands depending on the season, there are also up to 7 mm/day underestimation in JJA towards the central and southern parts of the country. On the other hand, on Borneo, Asia’s third largest island, there are often underestimates of over 2 mm/day.

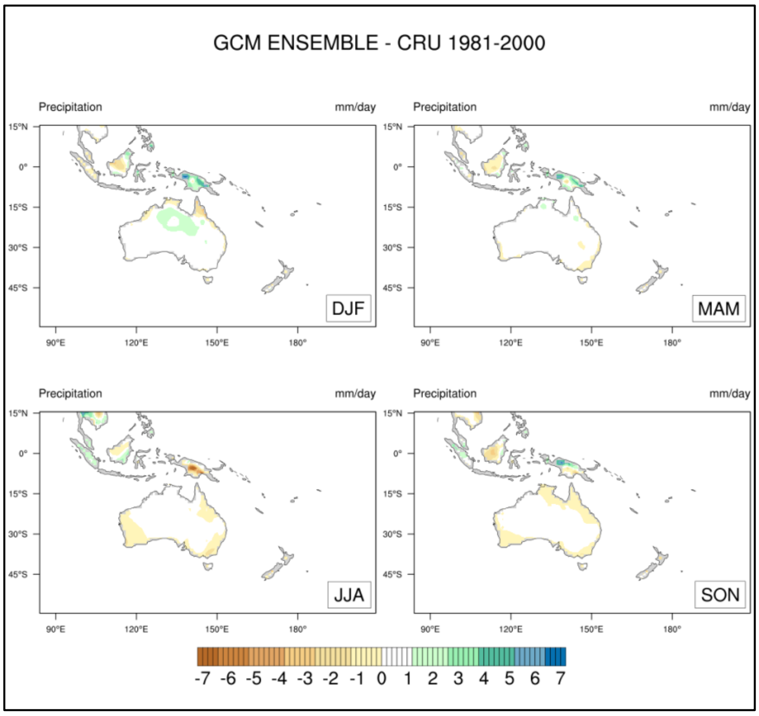

Figure 3.4. Spatial pattern of the multi-model ensemble mean bias in seasonal precipitation for the models used under the RCP2.6 scenario (i.e., December - January - February (DJF), March - April - May (MAM), June - July - August (JJA), and September - October - November (SON) seasons).

<u>*3.1.1.2. CMIP5 Multi-Model Ensemble Mean Projections for Seasonal Changes in Air Temperature Under the RCP2.6 Scenario.*</u> Looking at the seasonal temperature change maps foreseen in Australasia (Figure 3.5, Figure 3.6, and Figure 3.7), an increase in temperature is expected as the time progresses in all four seasons. Even in RCP2.6, which is the most optimistic case among the climate scenarios, it is predicted that the temperatures will increase to almost 2 °C in Australasia depending on the region, season, and period. It is anticipated that the increase in temperature, which is more prominent in the western and eastern parts of Australia in the near future, will be more significant in almost all seasons in the middle of the continent and around Indonesia. It is estimated that the temperatures will become hotter at the end of the century, and there will be much more temperature increase, especially in the western parts of Australia in the DJF and MAM seasons. At the end of the century, in the austral summer season, increases close to 2 °C are projected in the southeast region, which is the most populated zone, and it is remarkable.

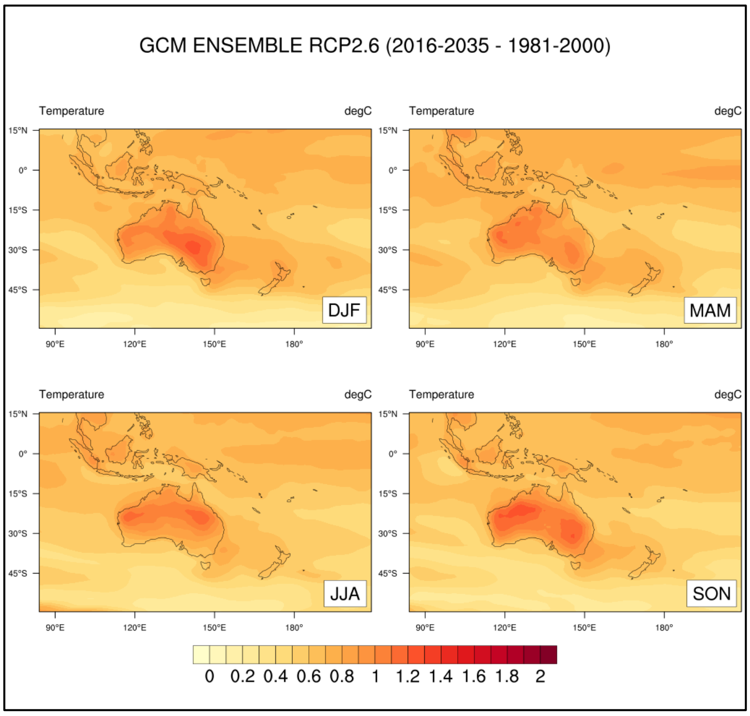

Figure 3.5. Temperature change projections of the multi-model ensemble mean based on RCP2.6 scenario for the period of 2016 - 2035 with respect to the reference period of 1981 - 2000: (i) December - January - February (DJF), (ii) March - April - May (MAM), (iii) June - July - August (JJA), and (iv) September - October - November (SON) seasons.

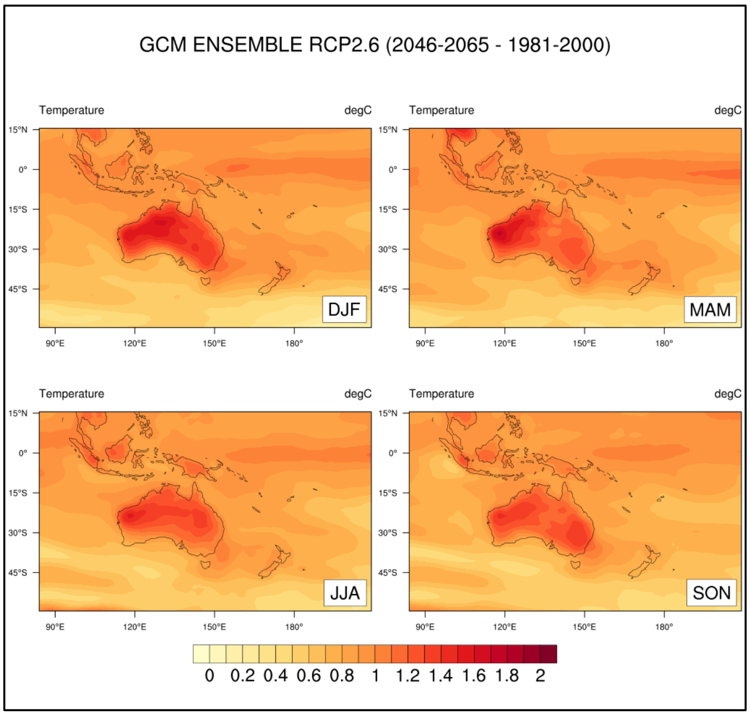

Figure 3.6. Temperature change projections of the multi-model ensemble mean based on RCP2.6 scenario for the period of 2046 - 2065 with respect to the reference period of 1981 - 2000: (i) December - January - February (DJF), (ii) March - April - May (MAM), (iii) June - July - August (JJA), and (iv) September - October - November (SON) seasons.

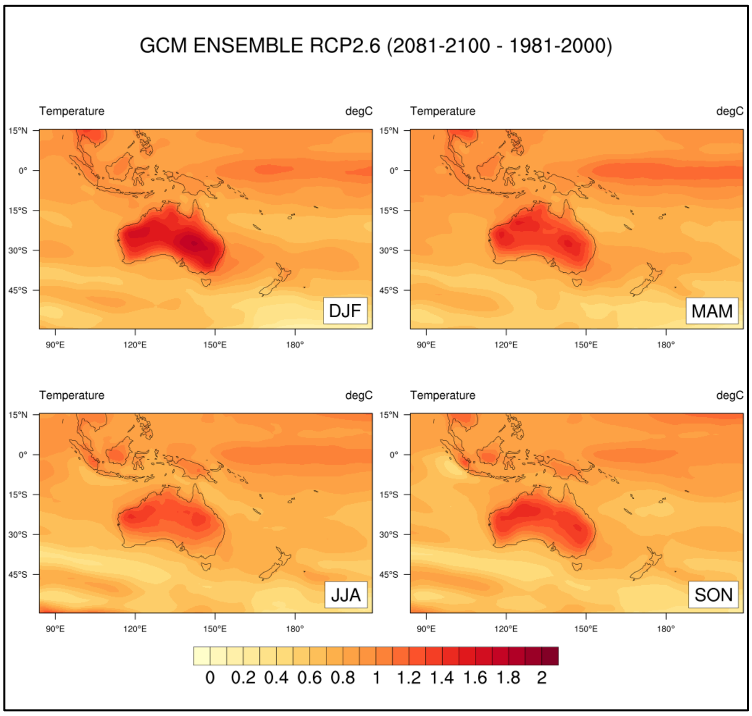

Figure 3.7. Temperature change projections of the multi-model ensemble mean based on RCP2.6 scenario for the period of 2081 - 2100 with respect to the reference period of 1981 - 2000: (i) December - January - February (DJF), (ii) March - April - May (MAM), (iii) June - July - August (JJA), and (iv) September - October - November (SON) seasons.

When the spatial means of the changes in temperature in which the spatial distribution is seen in the maps above are examined, it is predicted that the temperature increases expected to be above 0.5 °C in 2016 - 2035 (Figure 3.8) will exceed 0.75 °C in the future periods of 2046 - 2065 (Figure 3.9) and 2081 - 2100 (Figure 3.10) compared to the 1981 - 2000 period. It is also observed that the temperature variation range in DJF, which corresponds to the summer period for the southern hemisphere, is much wider compared to other periods. In this period, there may be minimal temperature changes, which can be neglected in some places, and in some regions, increases approaching 2 °C will be in question in time.

To summarize, it is projected that temperatures in the Australasia region will increase between 0 and 2 °C in DJF and MAM seasons, 0.1 - 1.5 °C in JJA season, and 0.2 - 1.5 °C in SON, compared to the past 1981 - 2000 period.

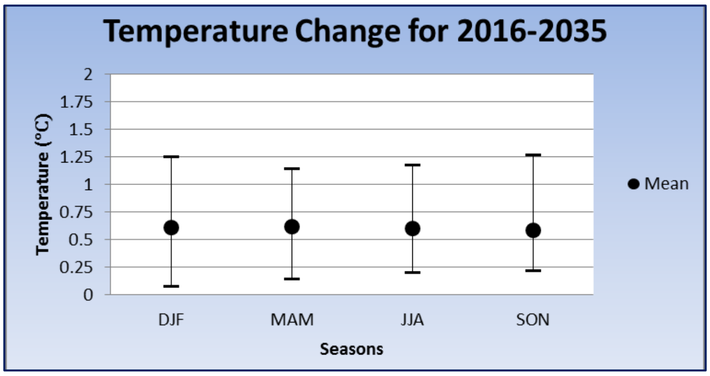

Figure 3.8. Seasonal change in temperature over the Australasia domain using the multi-model ensemble mean based on RCP2.6 scenario for the period of 2016 - 2035 with respect to the reference period of 1981 - 2000: (i) December - January - February (DJF), (ii) March - April - May (MAM), (iii) June - July - August (JJA), and (iv) September - October - November (SON) seasons.

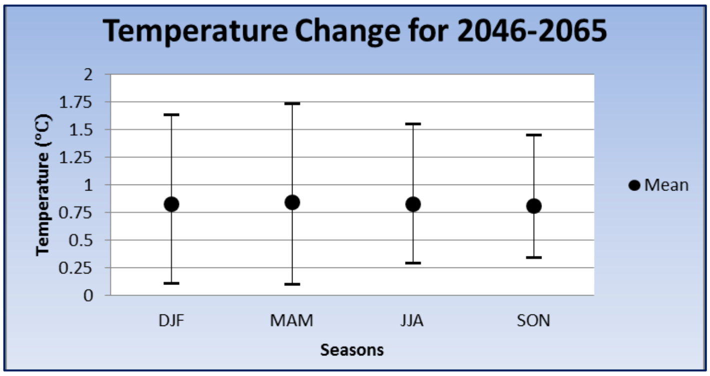

Figure 3.9. Seasonal change in temperature over the Australasia domain using the multi-model ensemble mean based on RCP2.6 scenario for the period of 2046 - 2065 with respect to the reference period of 1981 - 2000: (i) December - January - February (DJF), (ii) March - April - May (MAM), (iii) June - July - August (JJA), and (iv) September - October - November (SON) seasons.

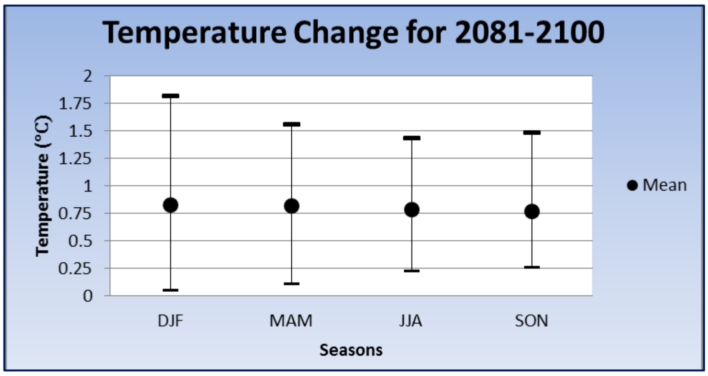

Figure 3.10. Seasonal change in temperature over the Australasia domain using the multi-model ensemble mean based on RCP2.6 scenario for the period of 2081 - 2100 with respect to the reference period of 1981 - 2000: (i) December - January - February (DJF), (ii) March - April - May (MAM), (iii) June - July - August (JJA), and (iv) September - October - November (SON) seasons.

<u>3.1.1.3. CMIP5 Multi-Model Ensemble Mean Projections for Seasonal Changes in Precipitation Under the RCP2.6 Scenario.</u> Looking at the seasonal future projections of the multi-model ensemble mean results for precipitation (Figure 3.11, Figure 3.12, and Figure 3.13), the expectation of both a small decrease and a small increase in all periods and seasons stands out in the Australia region. In Australia, which is the mainland of the region, a precipitation reduction of around 1 mm/day is predicted in the JJA and SON seasons in the 2016 - 2035 period in almost the entire continent. It is estimated that a similar decrease may occur in the arid interior parts of the continent during the same period, DJF season. According to the medium-term future forecast, a decrease expectation that has become more evident on the Indian Ocean will spread to a broader area, including Indonesia and Malaysia. In the SON season of 2046 - 2065, a decrease of up to 1.5 mm/day in precipitation in the southeast of Australia and an increase of up to 1 mm/day in other regions of Australia is predicted. In 2081 - 2100, there is a region in the east-northeast of Papua New Guinea and the Solomon Islands, where precipitation increase of 1 to 2 mm/day is expected. In this period, an increase in the southern region of New Zealand and a decrease in the northern region are predicted in all four seasons. In particular, in JJA and SON, an average decrease in precipitation is expected throughout Australia.

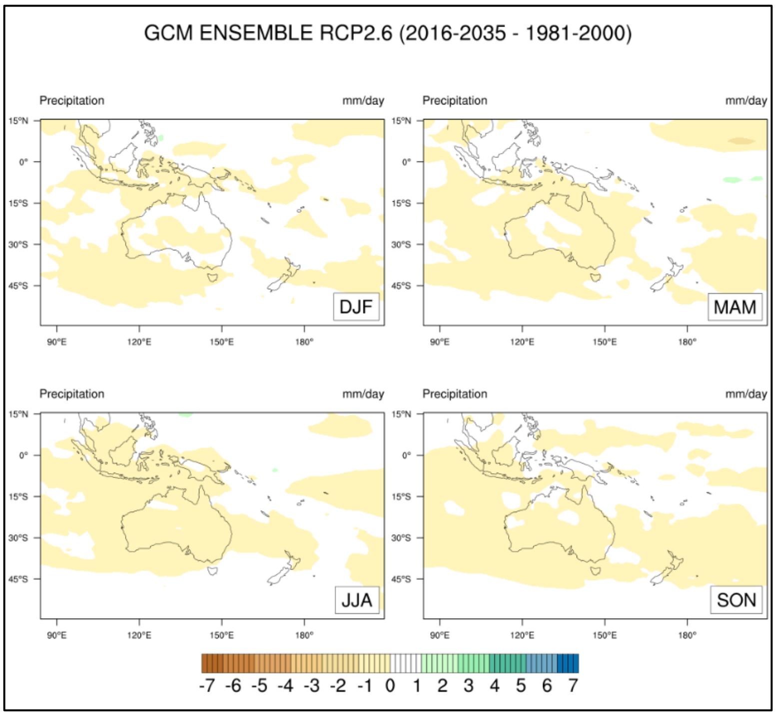

Figure 3.11. Precipitation change projections of the multi-model ensemble mean based on RCP2.6 scenario for the period of 2016 - 2035 with respect to the reference period of 1981 - 2000: (i) December - January - February (DJF), (ii) March - April - May (MAM), (iii) June - July - August (JJA), and (iv) September - October - November (SON) seasons.

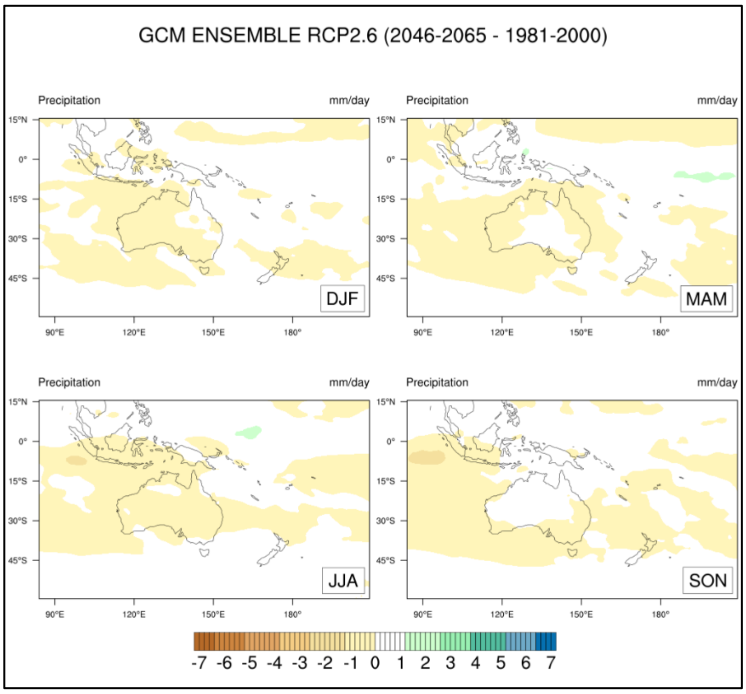

Figure 3.12. Precipitation change projections of the multi-model ensemble mean based on RCP2.6 scenario for the period of 2046 - 2065 with respect to the reference period of 1981 - 2000: (i) December - January - February (DJF), (ii) March - April - May (MAM), (iii) June - July - August (JJA), and (iv) September - October - November (SON) seasons.

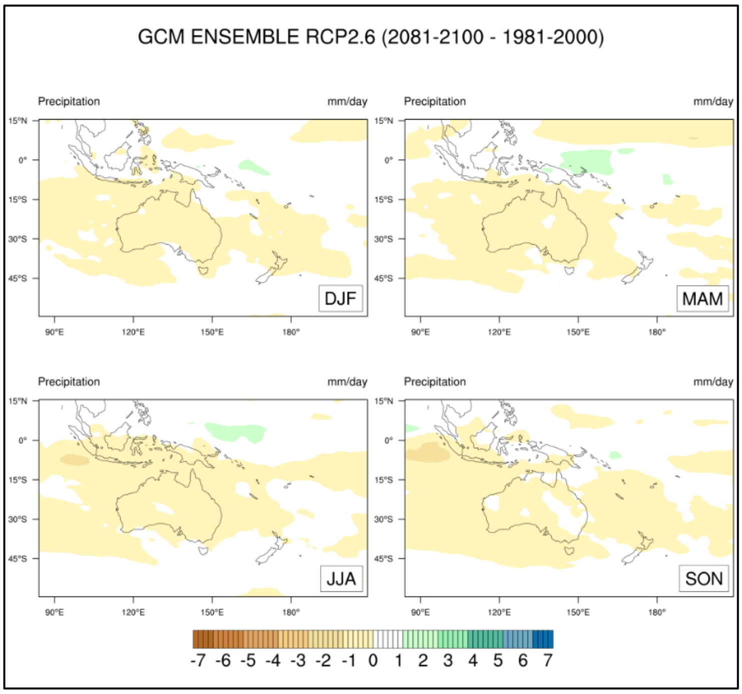

Figure 3.13. Precipitation change projections of the multi-model ensemble mean based on RCP2.6 scenario for the period of 2081 - 2100 with respect to the reference period of 1981 - 2000: (i) December - January - February (DJF), (ii) March - April - May (MAM), (iii) June - July - August (JJA), and (iv) September - October - November (SON) seasons.

When the results are evaluated in terms of the spatial mean (Figure 3.14, Figure 3.15, and Figure 3.16), it is expected that the average precipitation change will increase by around 1 % in the 2016 - 2035 period , excluding JJA and SON and in the 2081 - 2100 period excluding SON. In the periods of 2016 - 2035 JJA and SON and 2081 - 2100 SON, when the average decrease is expected, this amount of decrease remains below 1 %. The most important part to be considered in precipitation change results is the high variability. As can be seen in the precipitation variability tables, depending on the seasons, up to 50 % increase in precipitation can be observed, as well as a decrease over 30 %. For example, although the average precipitation change in the JJA season of 2046 - 2065 is around 1 %, it is seen that there are places within the domain where both an increase of up to 50 % and a decrease of up to 25 % is predicted.

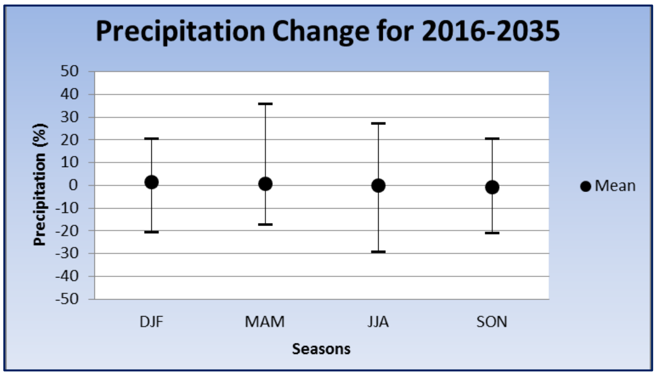

Figure 3.14. Seasonal change in precipitation over the Australasia domain using the multi-model ensemble mean based on RCP2.6 scenario for the period of 2016 - 2035 with respect to the reference period of 1981 - 2000: (i) December - January - February (DJF), (ii) March - April - May (MAM), (iii) June - July - August (JJA), and (iv) September - October - November (SON) seasons.

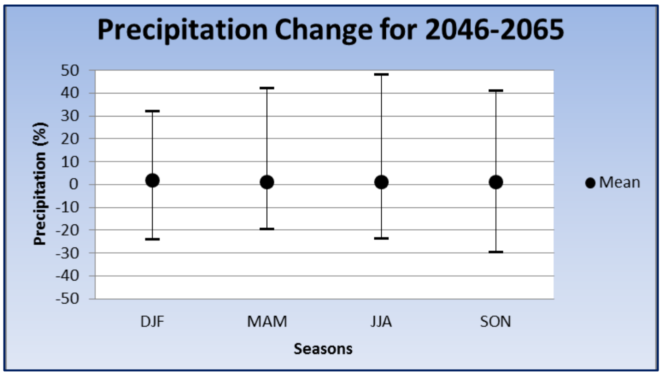

Figure 3.15. Seasonal change in precipitation over the Australasia domain using the multi-model ensemble mean based on RCP2.6 scenario for the period of 2046 - 2065 with respect to the reference period of 1981 - 2000: (i) December - January - February (DJF), (ii) March - April - May (MAM), (iii) June - July - August (JJA), and (iv) September - October - November (SON) seasons.

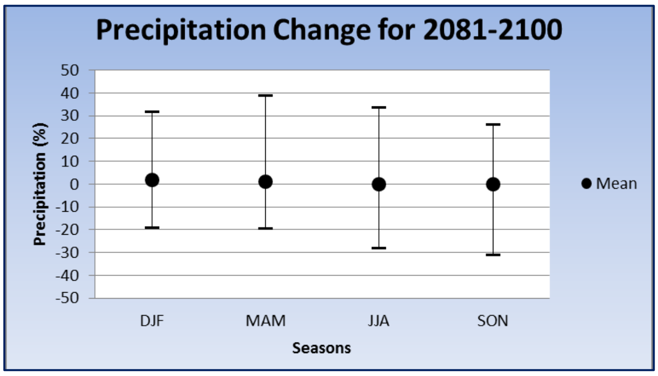

Figure 3.16. Seasonal change in precipitation over the Australasia domain using the multi-model ensemble mean based on RCP2.6 scenario for the period of 2081 - 2100 with respect to the reference period of 1981 - 2000: (i) December - January - February (DJF), (ii) March - April - May (MAM), (iii) June - July - August (JJA), and (iv) September - October - November (SON) seasons.

3.1.2. CMIP5 Multi-Model Projection of the Changes in Air Temperature and Precipitation Climatology over the CORDEX-Australasia Domain Under the RCP4.5 Scenario

In this section, an analysis similar to the previous section was made using 14 GCMs under the RCP4.5 scenario (Table 3.2). Again, the seasonal and spatial performances of both individual and multi-model ensemble means of 14 different GCM outputs, which are included in the CMIP5 and run under the RCP4.5 scenario, were compared with CRU observation data. Then, using the multi-model ensemble means, the projection results for three future periods (i.e., near-term, mid-term, and long-term) were evaluated. This time, in order to have a common grid size, the horizontal resolution of all models and observational data was bilinearly interpolated to 0.75° x 0.75° by taking into account the resolution of CMCC-CM. While the past period comparisons were made for the period of 1981 - 2000, the future projection changes were investigated for the periods of 2016 - 2035, 2046 - 2065, and 2081 - 2100 with respect to the reference period of 1981 - 2000.

Table 3.2. CMIP5 models used in multi-model ensemble mean approach under RCP4.5 and RCP8.5 scenarios.

Model Name	**Modeling Group**	**Horizontal Resolution (lat x lon)**
ACCESS1.0	Commonwealth Scientific and Industrial Research Organisation, Australia & Bureau of Meteorology, Australia	1.25° x 1.875°
ACCESS1.3	Commonwealth Scientific and Industrial Research Organisation, Australia & Bureau of Meteorology, Australia	1.25° x 1.875°
CMCC-CM	Centro Euro-Mediterraneo per I Cambiamenti Climatici	0.7484° x 0.75°
CMCC-CMS	Centro Euro-Mediterraneo per I Cambiamenti Climatici	3.7111° x 3.75°
CNRM-CM5	Centre National de Recherches Meteorologiques/Centre Europeen de Recherche et Formation Avancees en Calcul Scientifique	1.4008° x 1.40625°
EC-EARTH	EC-EARTH consortium	1.1215° x 1.125°
HadGEM2-AO	Met Office Hadley Centre	1.25° x 1.875°
HadGEM2-CC	Met Office Hadley Centre	1.25° x 1.875°
HadGEM2-ES	Met Office Hadley Centre & Instituto Nacional de Pesquisas Espaciais)	1.25° x 1.875°
MIROC-ESM	Japan Agency for Marine-Earth Science and Technology, Atmosphere and Ocean Research Institute (The University of Tokyo) & National Institute for Environmental Studies	2.7906° x 2.8125°
MIROC-ESM-CHEM	Japan Agency for Marine-Earth Science and Technology, Atmosphere and Ocean Research Institute (The University of Tokyo) & National Institute for Environmental Studies	2.7906° x 2.8125°
MPI-ESM-LR	Max-Planck-Institut für Meteorologie	1.8653° x 1.875°
MPI-ESM-MR	Max-Planck-Institut für Meteorologie	1.8653° x 1.875°
MRI-CGCM3	Meteorological Research Institute	1.12148° x 1.125°

<u>3.1.2.1. Benchmarking CMIP5 Model Performances for Seasonal Air Temperature and Precipitation Climatology Under the RCP4.5 and RCP8.5 Scenarios.</u> When the spatial mean of the temperature values of 14 models used in RCP4.5 and RCP8.5 projections are compared with the observation data for the 1981 - 2000 reference period (Figure 3.17), in DJF 10 models contain warm bias and 4 models cold bias, in MAM 9 models include warm bias and 5 models cold bias, in JJA 6 models contain warm bias and 8 models cold bias, and in SON 8 models include warm bias and 6 models cold bias. While EC-EARTH model shows the highest bias (-2.4 °C) in DJF, it is seen that the least bias (0.04 °C) is in MPI-ESM-LR. It is concluded that the highest bias is in the EC-EARTH model in other seasons, just as in the DJF season. According to the bias comparisons, the EC-EARTH model has a cold bias of approximately 2 °C in MAM, 1.3 °C in JJA and 1.6 °C in SON. When the models with the least bias among 14 models are examined seasonally, it is clear that the most realistic model in all four seasons is MPI-ESM-LR. MPI-ESM-LR model shows 0.06 °C warm bias in DJF, 0.15 °C warm bias in MAM, 0.02 °C cold bias in JJA and lastly 0.04 °C warm bias in SON according to seasonal order. In addition, ACCESS1.3 model also has a 0.02 °C cold bias in JJA season just like MPI-ESM-LR. Apart from the individual performance of all models, when the multi-model ensemble mean results are compared with the CRU observation data, it is clear that for all four seasons the bias decreases considerably and approaches zero, and this situation provides an improvement as if there is almost no bias in taking a multi-model ensemble.

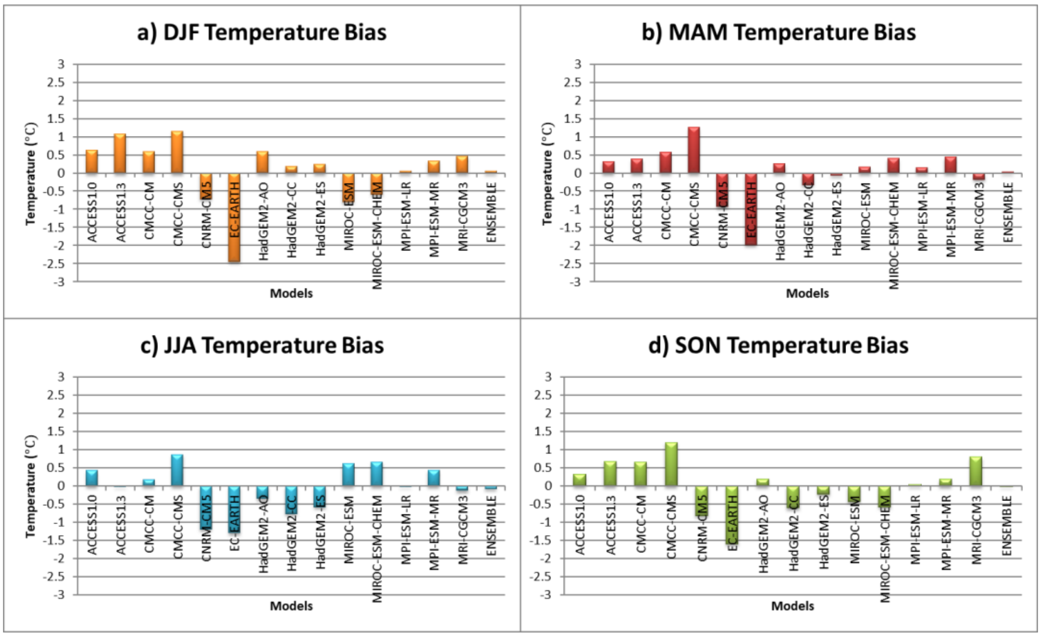

Figure 3.17. Seasonal air temperature bias for models used in the multi-model ensemble mean approach under the RCP4.5 and RCP8.5 scenarios.

When the spatial distribution of the multi-model ensemble mean values are mapped seasonally (Figure 3.18), warm bias of up to 7 °C can be seen in the Australasia domain, as well as cold bias of up to 4 °C. A cold bias is dominant in all seasons in the equatorial region. Especially in Papua New Guinea, which has a high topography, biases reach their maximum values, while cold biases are observed in all seasons around Indonesia and the Gulf of Thailand (except for the MAM season for Cambodia and Vietnam). There is a warm bias of approximately 5 °C for MAM in Vietnam. Towards 45°S latitude, that is, on the southern coasts of Australia, Tasmania and New Zealand, there is generally a warm bias. While the north-northwest parts of Australia have cold bias during the DJF and MAM seasons, the warm bias in the DJF in the southeast of Australia are also striking. On the mountainous southeast coast of Australia, warm bias of up to 5 ℃ is observed in the SON season.

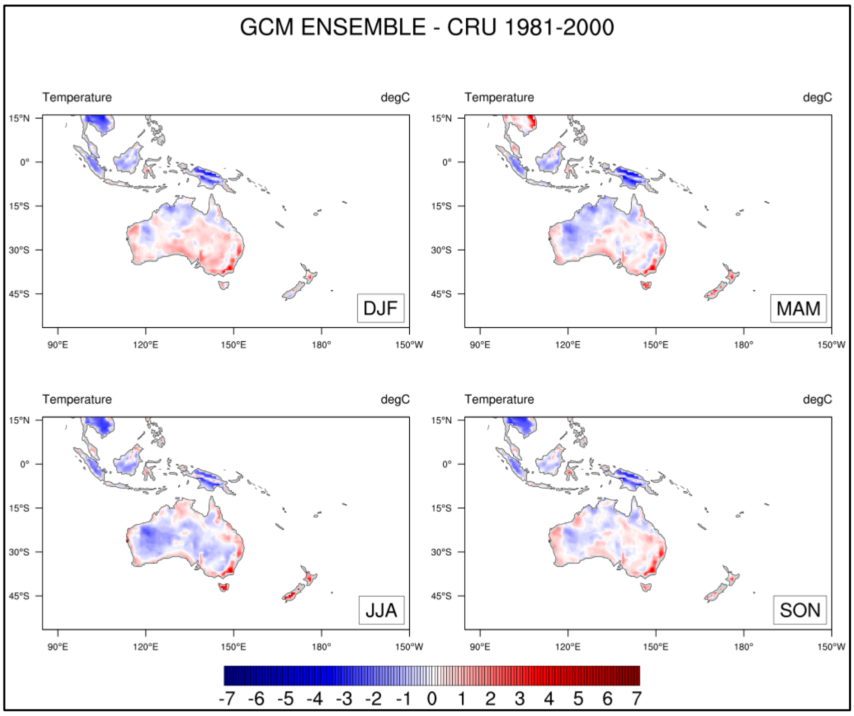

Figure 3.18. Spatial pattern of the multi-model ensemble mean bias in seasonal air temperature for the models used under the RCP4.5 and RCP8.5 scenarios (i.e., December - January - February (DJF), March - April - May (MAM), June - July - August (JJA), and September - October - November (SON) seasons).

When the spatial means of the precipitation values of the 14 models used in the RCP4.5 and RCP8.5 projections are compared with the observation data for the 1981 - 2000 reference period (Figure 3.19), it is found that the model results are generally biased in the direction of underestimation. Looking at Figure 3.19, while DJF has half overestimation and half underestimation, in MAM 5 models have overestimation, and 9 models underestimation, in JJA 5 models have overestimation, and 9 models underestimation and in SON 3 models have overestimation and 11 models underestimation. CMCC-CM is the model with the highest bias in all four seasons. The CMCC-CM model predicts precipitation 1.5 mm/day less than normal in the DJF and SON seasons and it predicts precipitation 0.9 mm/day more in the MAM season and 0.8 mm/day more in the JJA season. In terms of individual performances of the models, HadGEM2-AO for DJF and MAM, MPI-ESM-MR for JJA and CNRM-CM5 for SON stand out as the most realistic models according to the seasons. When the multi-model ensemble mean is calculated and compared with the CRU observation data, it is seen that the bias is very close to zero especially in the DJF and MAM seasons. Multi-model ensemble mean underestimates precipitation in the spatial mean 0.1 mm/day for JJA and 0.3 mm/day in SON. As a result, it is clear that bias decreases when the multi-model ensemble mean is taken in the precipitation results.

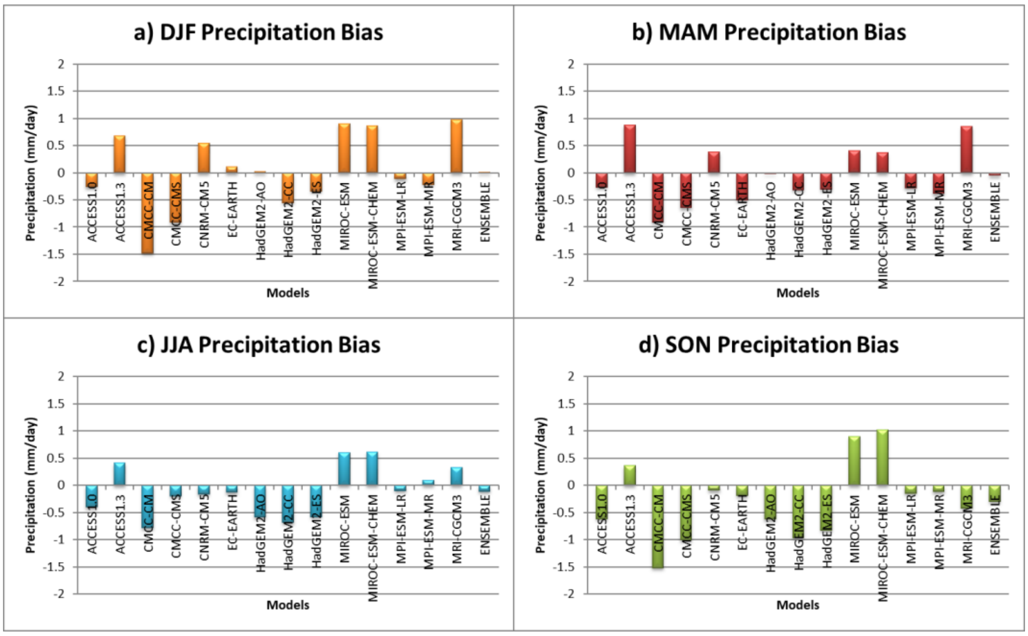

Figure 3.19. Seasonal precipitation bias for models used in the multi-model ensemble mean approach under the RCP4.5 and RCP8.5 scenarios (i.e., December - January - February (DJF), March - April - May (MAM), June - July - August (JJA), and September - October - November (SON) seasons).

When the multi-model ensemble mean is calculated, the spatial mean values show quite a few bias, however, when the spatial distribution of the results is examined, it is seen that there are higher biases in some parts of the domain and lower bias in some parts (Figure 3.20). According to the 1981 - 2000 reference period, while precipitation bias for all four seasons in most of Australia remained in the range of 0 - 1 mm/day, northern Australia has an underestimation of up to 6 mm/day in DJF. While underestimation is common in Indonesia and its surroundings, overestimation is present in northern and southern parts of Papua New Guinea during the DJF, MAM and SON seasons. In JJA, there is underestimation up to 6 mm/day in the central area of Papua New Guinea. There is generally an underestimation for New Zealand.

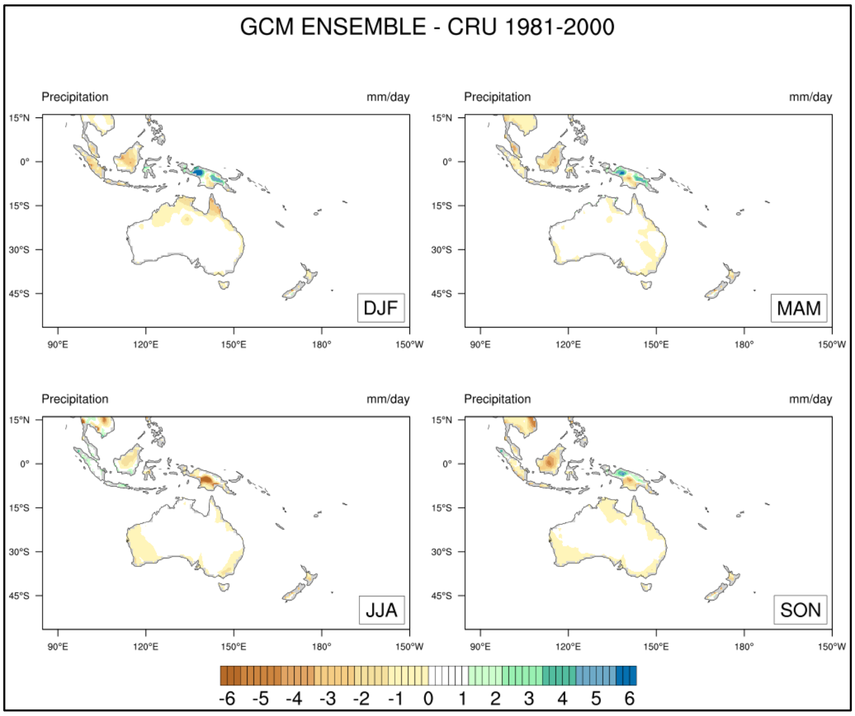

Figure 3.20. Spatial pattern of the multi-model ensemble mean bias in seasonal precipitation for the models used under the RCP4.5 and RCP8.5 scenarios (i.e., December - January - February (DJF), March - April - May (MAM), June - July - August (JJA), and September - October - November (SON) seasons).

3.1.2.2. CMIP5 Multi-Model Ensemble Mean Projections for Seasonal Changes in Air Temperature Under the RCP4.5 Scenario. When the short, medium- and long-term future projections of the multi-model ensemble mean results are analyzed according to the RCP4.5 scenario (Figure 3.21, Figure 3.22, and Figure 3.23), an increasing temperature rise is expected towards the end of the century. While there is an expectation of an average increase of 0.5 °C in each season in the period of 2016 - 2035, it is seen that this increase may reach 1.5 - 2 °C in the northern and western parts of Australia. Similarly, during the MAM season, a temperature increase of 1.5 °C is predicted in the northern hemisphere of the domain in Southern Thailand, Cambodia and Vietnam.

When the 2046 - 2065 period is switched, it is clear that the temperature increases are higher for all four seasons compared to the 2016 - 2035 period. While nearly twice as much warming is projected as in the previous period on average, there may be temperature rises of 2.5 - 3 °C around

Australia and the Gulf of Thailand. In this period, particularly in DJF and SON, more warming is foreseen in the inner regions of Australia.

By the end of the century, it is seen that the temperature increase will become more severe for the whole domain. While 1.5 °C temperature increases are expected in the whole region, it is seen that this increase, which may be at least 0.5 - 0.7 °C seasonally, can reach 3 - 3.5 °C depending on the season. It is expected that temperature increases will be higher in the west-northwest regions of Australia during the MAM season and in the inner parts of the country away from the mountainous coastal regions in the DJF and SON. In this period, it is seen that the expected warming in the small island countries on the Pacific Ocean may reach 2 °C. In addition, looking at the overall projections, it can be said that the highest regional temperature increases will be in the SON season.

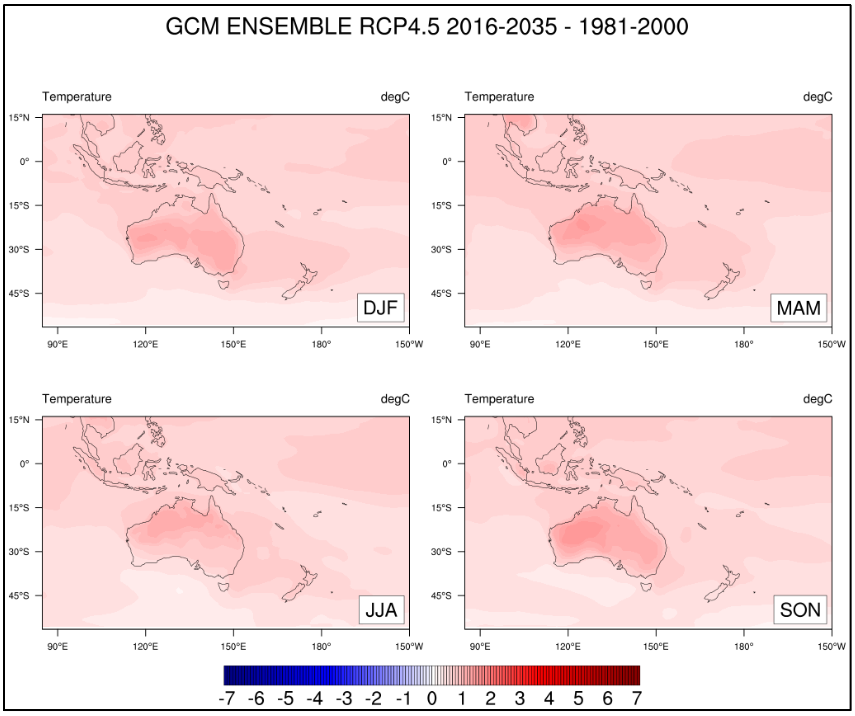

Figure 3.21. Temperature change projections of the multi-model ensemble mean based on RCP4.5 scenario for the period of 2016 - 2035 with respect to the reference period of 1981 - 2000: (i) December - January - February (DJF), (ii) March - April - May (MAM), (iii) June - July - August (JJA), and (iv) September - October - November (SON) seasons.

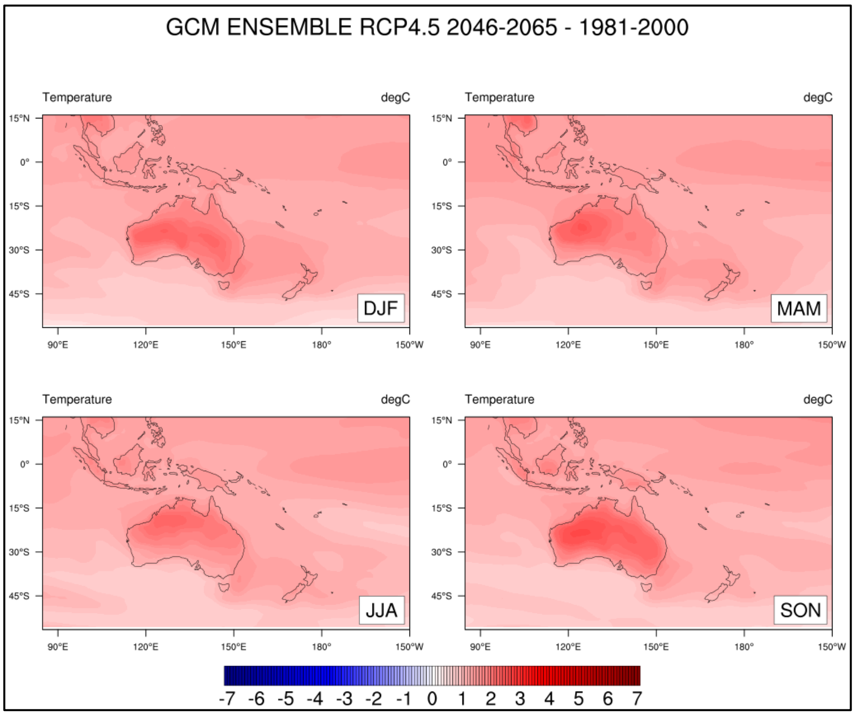

Figure 3.22. Temperature change projections of the multi-model ensemble mean based on RCP4.5 scenario for the period of 2046 - 2065 with respect to the reference period of 1981 - 2000: (i) December - January - February (DJF), (ii) March - April - May (MAM), (iii) June - July - August (JJA), and (iv) September - October - November (SON) seasons.

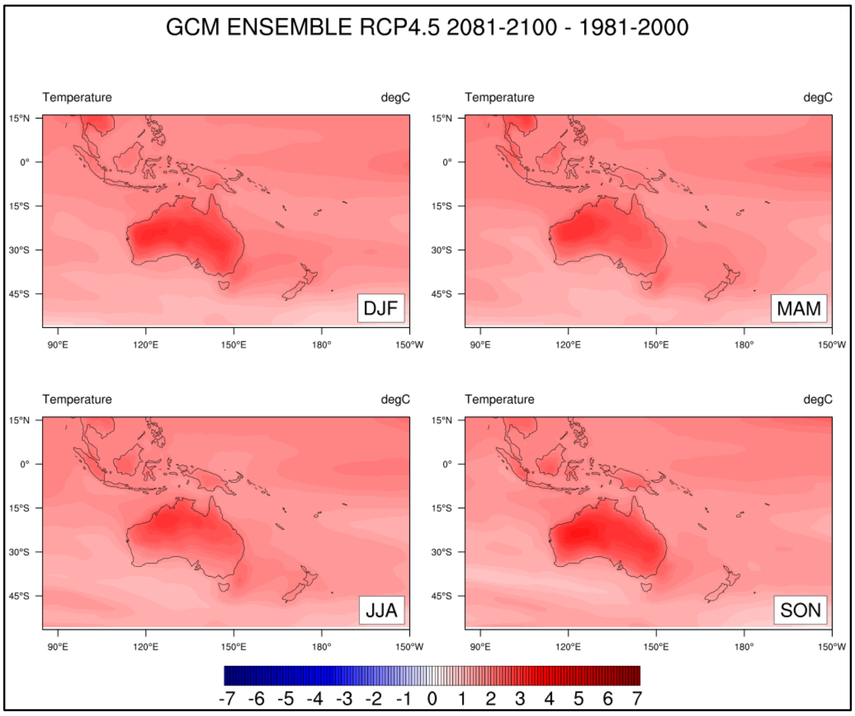

Figure 3.23. Temperature change projections of the multi-model ensemble mean based on RCP4.5 scenario for the period of 2081 - 2100 with respect to the reference period of 1981 - 2000: (i) December - January - February (DJF), (ii) March - April - May (MAM), (iii) June - July - August (JJA), and (iv) September - October - November (SON) seasons.

3.1.2.3. CMIP5 Multi-Model Ensemble Mean Projections for Seasonal Changes in Precipitation Under the RCP4.5 Scenario. When the multi-model ensemble mean precipitation projections for RCP4.5 are examined (Figure 3.24, Figure 3.25, and Figure 3.26), it is predicted that there will be both a little decrease and a very little increase regionally, except for the significant increases in certain seasons in the medium- and long term. In the near term, it is estimated that there will be an average decrease of 1 mm/day in Australia and its surroundings and the part of the domain in the northern hemisphere except for a small region in the north of Australia during the MAM season. In the MAM season of 2046 - 2065, it is seen that the projected increase of around 3 mm/day in an area starting from the north of Papua New and Solomon Islands and continuing along the equatorial region over the Pacific Ocean, will also include an area covering the oceanic island countries such as Micronesia, Palau, Nauru in the JJA season of the same period. It appears that the decrease in JJA over a wide area up to 40° latitudes in the southern hemisphere will continue to be seen in the SON, except for some small areas in the northeast and southeast of Australia. In the period of 2046 - 2065, it is obvious that the possible increase in the equatorial region, especially east of 150°E longitude, will spread to a wider area in the last 20 years of the century. It is also seen that the expected decrease in the low and middle latitude regions of the southern hemisphere in the JJA and SON seasons of 2046 - 2065 will be similar in 2081 - 2100.

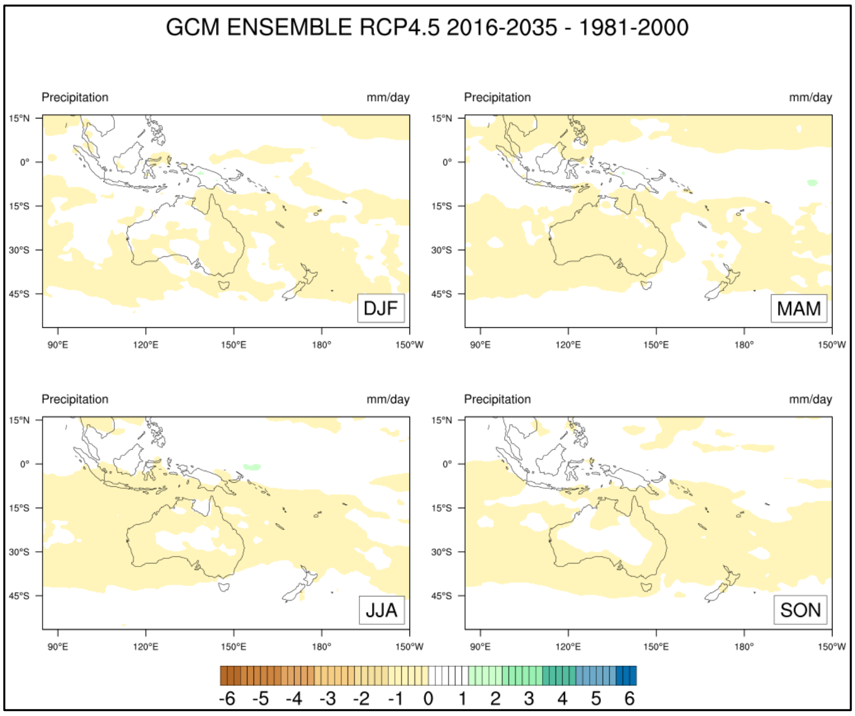

Figure 3.24. Precipitation change projections of the multi-model ensemble mean based on RCP4.5 scenario for the period of 2016 - 2035 with respect to the reference period of 1981 - 2000: (i) December - January - February (DJF), (ii) March - April - May (MAM), (iii) June - July - August (JJA), and (iv) September - October - November (SON) seasons.

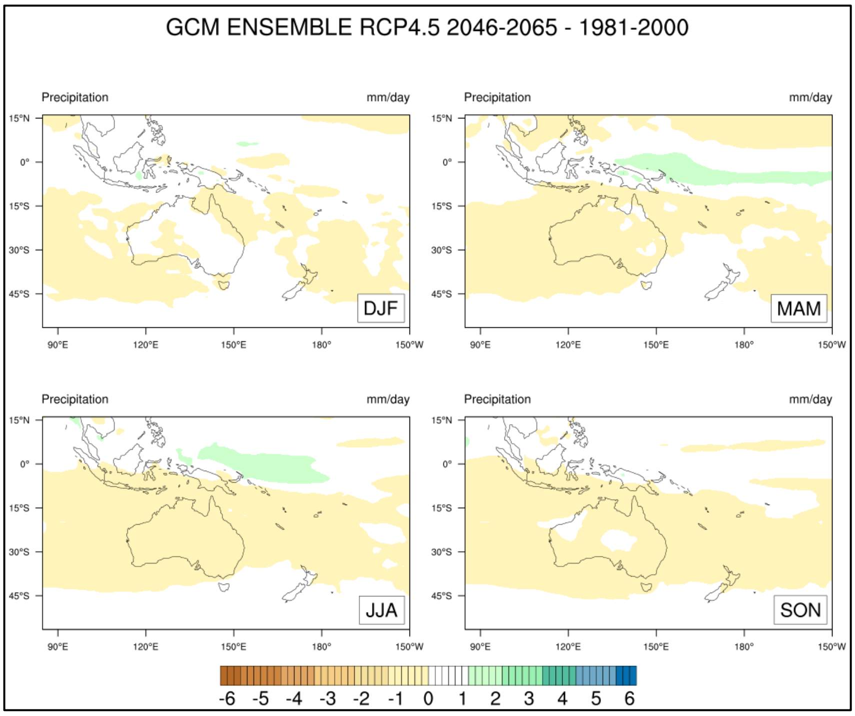

Figure 3.25. Precipitation change projections of the multi-model ensemble mean based on RCP4.5 scenario for the period of 2046 - 2065 with respect to the reference period of 1981 - 2000: (i) December - January - February (DJF), (ii) March - April - May (MAM), (iii) June - July - August (JJA), and (iv) September - October - November (SON) seasons.

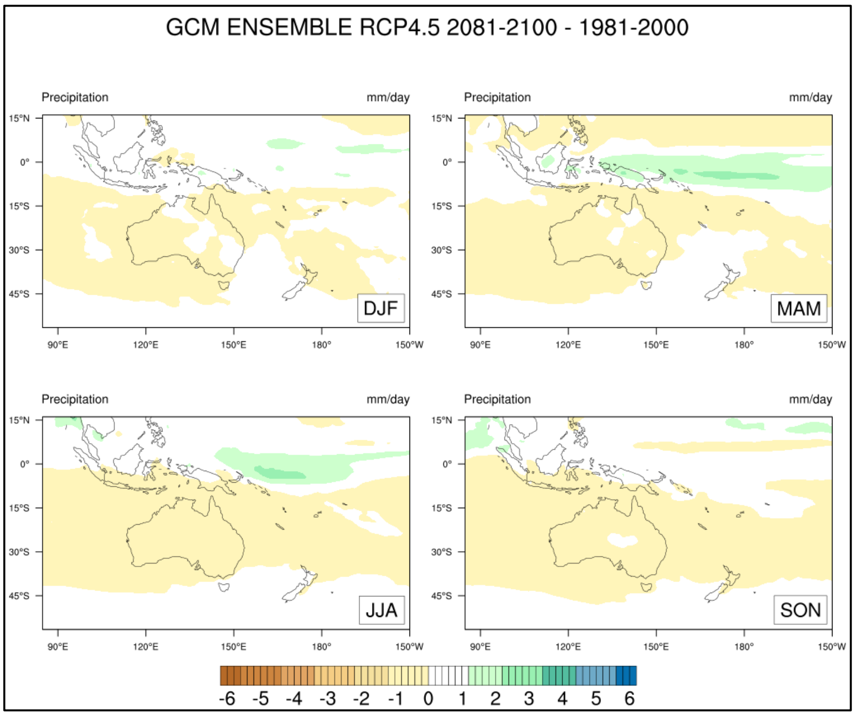

Figure 3.26. Precipitation change projections of the multi-model ensemble mean based on RCP4.5 scenario for the period of 2081 - 2100 with respect to the reference period of 1981 - 2000: (i) December - January - February (DJF), (ii) March - April - May (MAM), (iii) June - July - August (JJA), and (iv) September - October - November (SON) seasons.

3.1.3. CMIP5 Multi-Model Projection of the Changes in Air Temperature and Precipitation Climatology over the CORDEX-Australasia Domain under the RCP8.5 Scenario

The analysis results in this section are also obtained for the RCP8.5 scenario using the same models, periods, and approach used for the RCP4.5 scenario in the previous section. According to the RCP8.5 scenario, which is the most pessimistic among the RCPs, it is expected that the increase in temperatures will be much higher than the RCP4.5 scenario except in the near-term. Just like the RCP4.5 projection, the RCP8.5 projection also shows that as time progresses, the temperature increase will be even much higher.

3.1.3.1. CMIP5 Multi-Model Ensemble Mean Projections for Seasonal Changes in Air Temperature Under the RCP4.5 Scenario. It is seen that the projection results calculated with RCP8.5 are similar to the projection results calculated with RCP4.5 for the period 2016 - 2035 (Figure 3.27). This can be explained by the differentiation between scenarios starting after 2040 and the effects becoming more distinguishable in the second half of the century. According to the RCP8.5 scenario, the multi-model ensemble mean temperature changes foresee an average of 0.7 °C of warming in all seasons in the near future, while it can be said that this warming may be seasonally below 0.7 °C in some regions and above 1.5 °C in some regions. It is seen that the warming in this period is predominantly evident in Australia. When it comes to the period of 2046 - 2065 (Figure 3.28), it is seen that the mean temperature increase expectation for all seasons will be above the highest expectations in the RCP4.5 scenario. For the period 2046 - 2065, the RCP8.5 projection predicts an average warming of 1.7 °C. However, there may be temperature increases of more than 3 °C in the northwest region of Australia for all four seasons and in Southern Thailand, Cambodia, and Vietnam during the MAM season. Similarly, in SON, there is an expectation of an increase in temperature approaching 4 °C in west-northwest Australia. Among the multi-model ensemble mean future projections, the period 2081 - 2100 of the RCP8.5 scenario shows the most radical increase in temperatures (Figure 3.29). While a minimum temperature increase of 1 degree is expected in this period, it is expected that this increase will approach 7 °C seasonally in some places. For example, in SON, most of Australia will encounter temperatures 6 °C warmer than the 1981 - 2000 mean. During this period when the entire domain will be exposed to very high temperatures in all seasons, the highest temperatures will be seen not only in Australia but also in the equatorial region. In the period of 2081 - 2100, where an average of 3 °C of warming is expected, the small island countries in the Pacific Ocean will also be exposed to a temperature increase of 1-3 °C. Also, looking at the overall projections, it can be said that the regional maximum temperature increases will be in the SON season as in the RCP4.5 scenario.

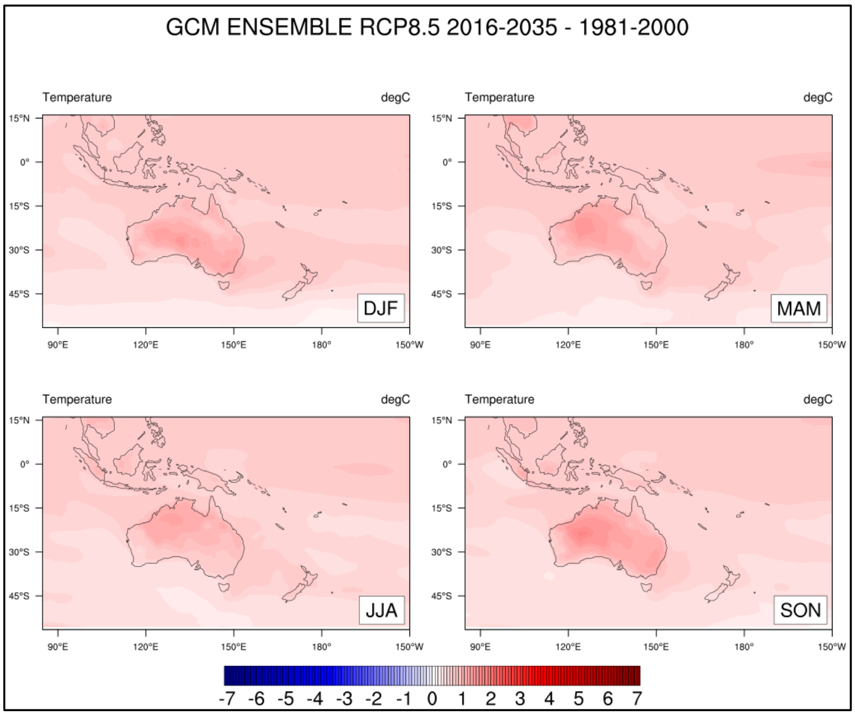

Figure 3.27. Temperature change projections of the multi-model ensemble mean based on RCP8.5 scenario for the period of 2016 - 2035 with respect to the reference period of 1981 - 2000: (i) December - January - February (DJF), (ii) March - April - May (MAM), (iii) June - July - August (JJA), and (iv) September - October - November (SON) seasons.

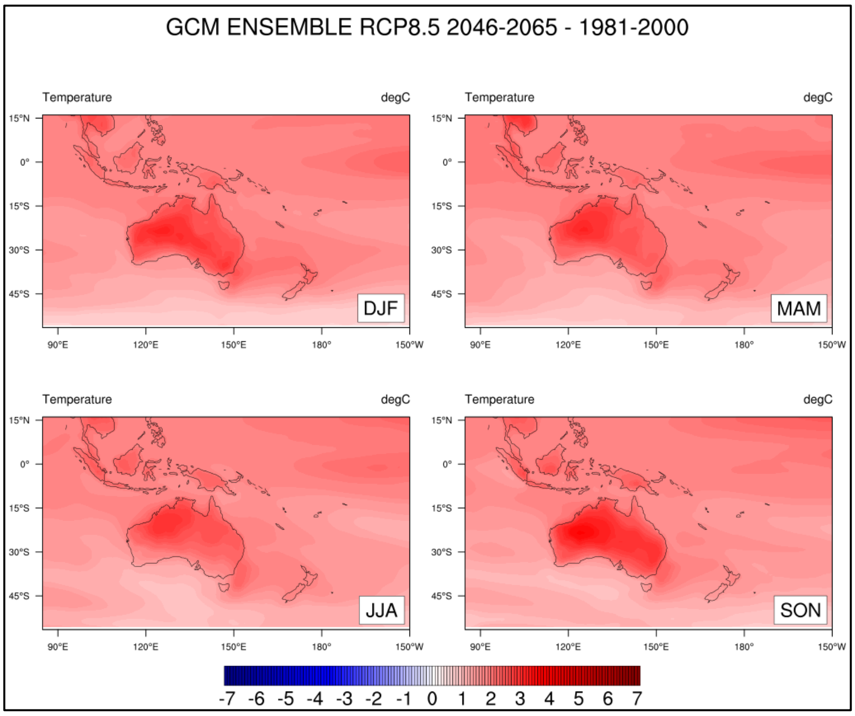

Figure 3.28. Temperature change projections of the multi-model ensemble mean based on RCP8.5 scenario for the period of 2046 - 2065 with respect to the reference period of 1981 - 2000: (i) December - January - February (DJF), (ii) March - April - May (MAM), (iii) June - July - August (JJA), and (iv) September - October - November (SON) seasons.

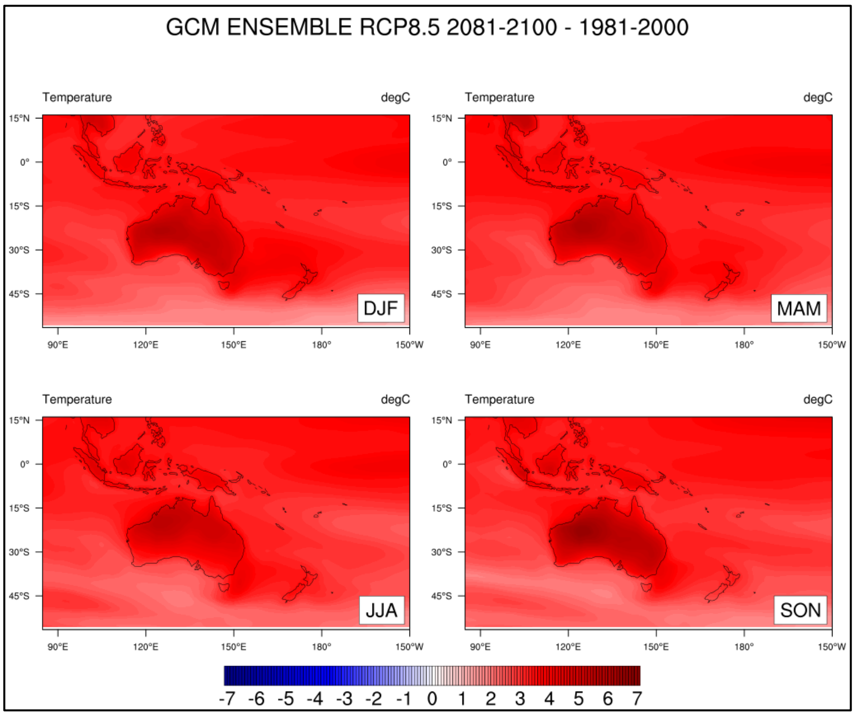

Figure 3.29. Temperature change projections of the multi-model ensemble mean based on RCP8.5 scenario for the period of 2081 - 2100 with respect to the reference period of 1981 - 2000: (i) December - January - February (DJF), (ii) March - April - May (MAM), (iii) June - July - August (JJA), and (iv) September - October - November (SON) seasons.

3.1.3.2. CMIP5 Multi-Model Ensemble Mean Projections for Seasonal Changes in Precipitation Under the RCP8.5 Scenario. The multi-model ensemble mean results of the projections calculated under the RCP8.5 scenario predict that there will be slightly more precipitation in Australasia, equatorial region and over the ocean towards 45°S latitude compared to the 1981 - 2000 period and less on terrestrial areas, particularly Australia (Figure 3.30, Figure 3.31, and Figure 3.32). As in the RCP4.5 projection, the increase in precipitation over the equatorial area of the Pacific Ocean is remarkable. This increase will be effective in a wider area and at a higher level, especially in the MAM of the 2046 - 2065 period and in all seasons of the 2081 - 2100 period. For example, looking at the mean of the last 30 years of the JJA season of the century, it is seen that the precipitation increase on the ocean where small island countries such as Micronesia, Nauru, and Marshall Islands are located can reach 6 mm/day.

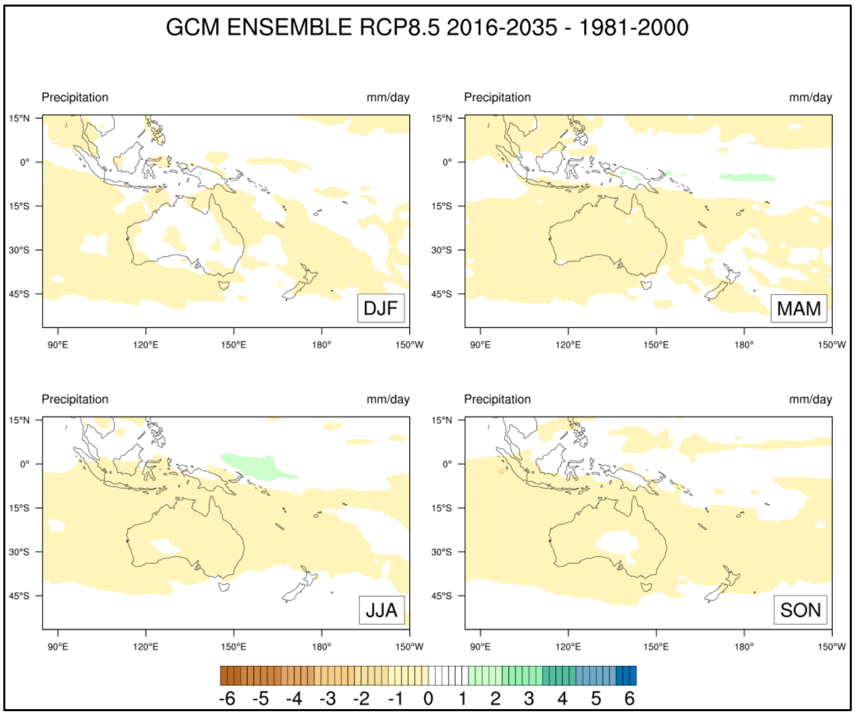

Figure 3.30. Precipitation change projections of the multi-model ensemble mean based on RCP8.5 scenario for the period of 2016 - 2035 with respect to the reference period of 1981 - 2000: (i) December - January - February (DJF), (ii) March - April - May (MAM), (iii) June - July - August (JJA), and (iv) September - October - November (SON) seasons.

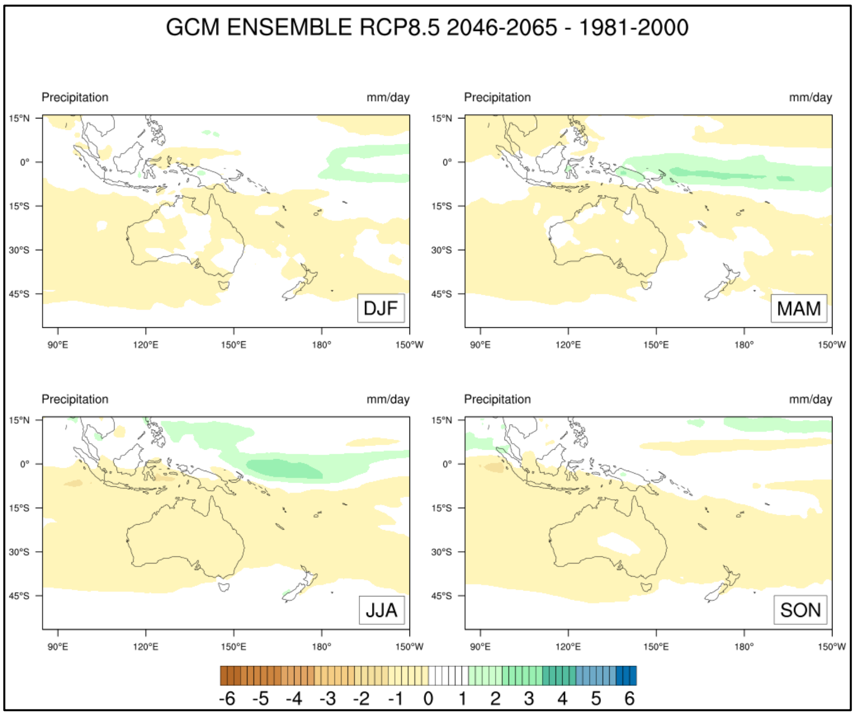

Figure 3.31. Precipitation change projections of the multi-model ensemble mean based on RCP8.5 scenario for the period of 2046 - 2065 with respect to the reference period of 1981 - 2000: (i) December - January - February (DJF), (ii) March - April - May (MAM), (iii) June - July - August (JJA), and (iv) September - October - November (SON) seasons.

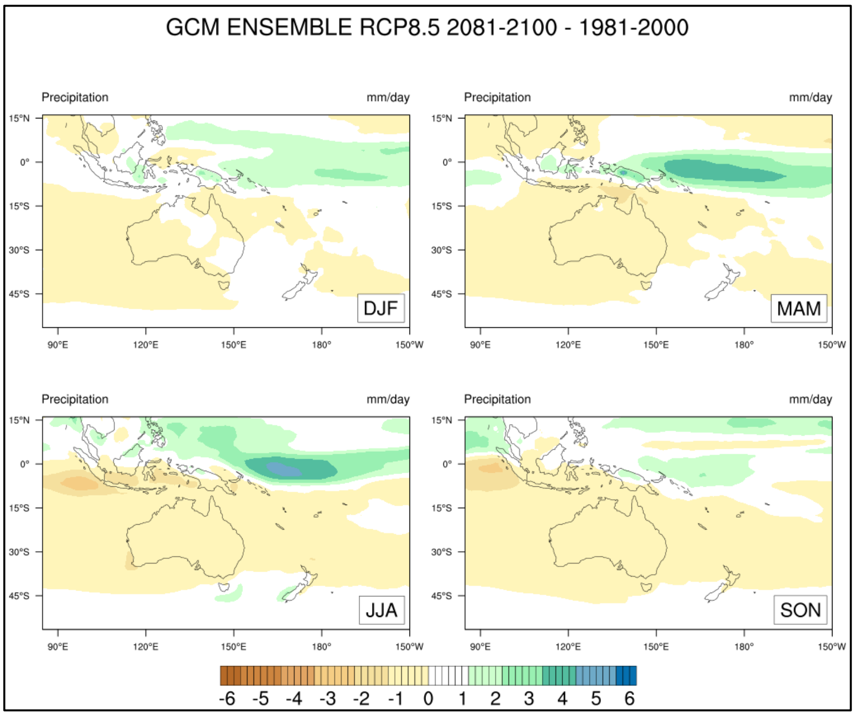

Figure 3.32. Precipitation change projections of the multi-model ensemble mean based on RCP8.5 scenario for the period of 2081 - 2100 with respect to the reference period of 1981 - 2000: (i) December - January - February (DJF), (ii) March - April - May (MAM), (iii) June - July - August (JJA), and (iv) September - October - November (SON) seasons.

To summarize, it can be said that there will be an increasing temperature increase from the near future to the far future when the temperature projection results are evaluated for three different periods under the RCP4.5 and RCP8.5 scenarios by calculating the multi-model ensemble means of different GCMs (Figure 3.33). It is also clear that the temperature increases according to the RCP8.5 scenario will be higher compared to the RCP4.5 scenario, especially at the end of the century. The seasonal difference in spatial temperature means is not very evident in all periods, and the temperature increase values (0.6 - 0.7 °C) in both scenarios in the 2016 - 2035 period are very close to each other. The greenhouse gas concentration values of both scenarios are not very distinguishable from each other during this period, and this situation may explain that the effect on temperature is close to each other for both scenarios. It is seen that the mean temperature increases of 1.2 - 1.3 °C for RCP4.5 in the period of 2046 - 2065 will be 1.7 °C for RCP8.5. In the period 2081 - 2100, RCP4.5 scenario will reach this increase value envisaged by the RCP8.5 scenario in the period 2046 - 2065. The most terrifying of the temperature projections is the RCP8.5 scenario for the period 2081 - 2100. The temperature projection made for the year 2081 - 2100 under the RCP8.5 scenario indicates that the temperatures in Australasia will increase on average 3.1 - 3.2 °C compared to the 1981 - 2000 period.

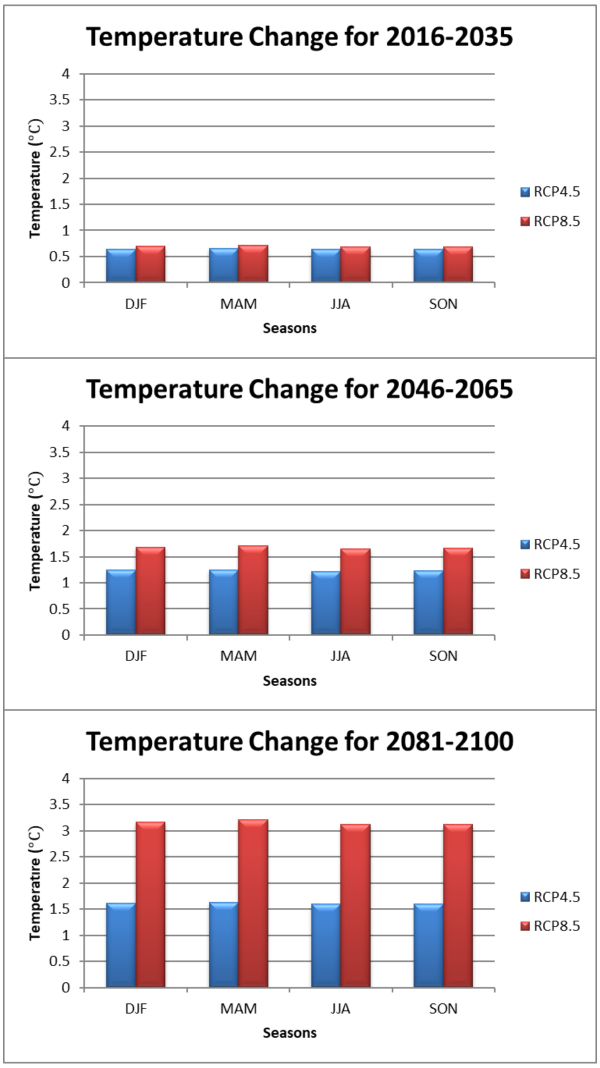

Figure 3.33. Temperature changes for multi-model ensemble mean based on the RCP4.5 and RCP8.5 scenarios for the periods of 2016 - 2035, 2046 - 2065, and 2081-2100 with respect to the reference period of 1981 - 2000.

When the multi-model ensemble means of different GCMs are calculated and the precipitation projection results under RCP4.5 and RCP8.5 scenarios are evaluated for three different periods in the future, they show more seasonal variation in contrast to temperature changes (Figure 3.34). Since spatial means are taken into account, an increase can be mentioned for Australasia under both scenarios. This should not cause us to ignore the seasonal and spatially varying decrease expectations stated in the previous sections. According to the RCP4.5 scenario, the average increase expectation in precipitation in the 2016 - 2035 period is higher than the RCP8.5 scenario in DJF, MAM, and SON seasons. Particularly in SON, this increase can be approximately 2.5 times. It is seen that the values increase as time passes and the scenario worsens in precipitation changes as well as in temperature changes. In the period of 2046 - 2065, according to the RCP8.5 scenario, it is expected that the increase expectation, which is slightly above 0.15 mm/day in DJF, MAM and JJA seasons, will be between 0.05 - 1 mm/day in the SON season. According to the RCP4.5 scenario in the aforementioned period, the increase of approximately 0.15 mm/day in DJF and JJA seasons will remain below this value in the other two seasons. When we look at the far future, it is predicted that the highest average precipitation increase expectation according to the RCP8.5 scenario will realize in DJF (over 0.3 mm/day) and in JJA (approximately 0.2 mm/day) according to the RCP4.5 scenario. For both scenarios, the highest increase in precipitation in all seasons is expected to occur in the period 2081 - 2100.

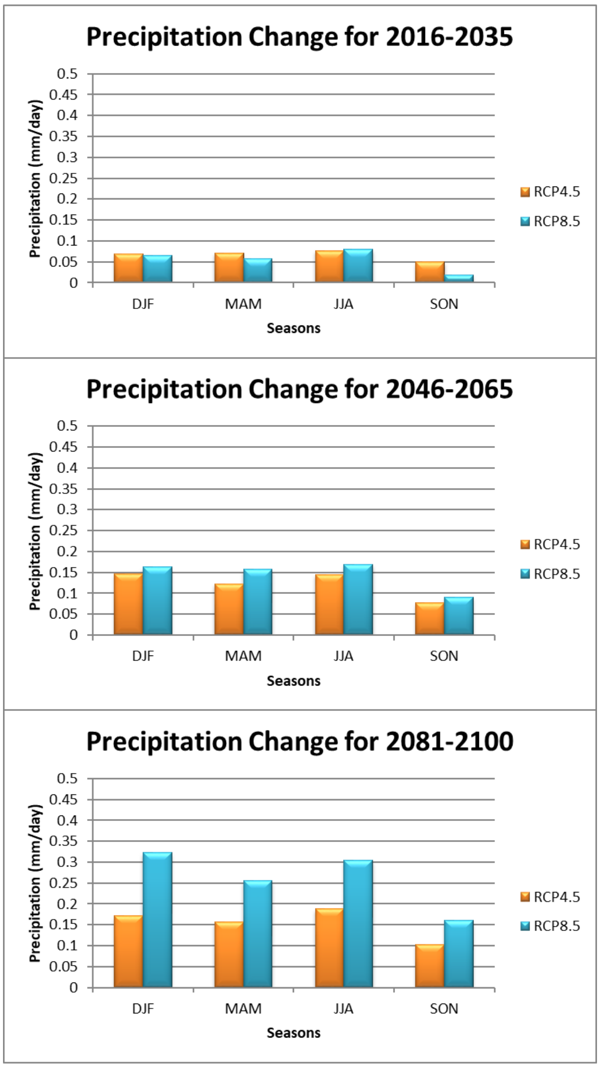

Figure 3.34. Precipitation changes for multi-model ensemble mean based on the RCP4.5 and RCP8.5 scenarios for the periods of 2016 - 2035, 2046 - 2065, and 2081-2100 with respect to the reference period of 1981 - 2000.

3.2. Changes in Extreme Climate Events Over the CORDEX-AUSTRALASIA Domain Using the NEX-GDDP Dataset

In this part, different extreme indices are used for the analysis of temperature and precipitation extremes. The indices created by the Joint CCI/CLIVAR/JCOMM Expert Team (ET) on Climate Change Detection and Indices (ETCCDI) are based on the selection and definition of extreme indices. Twenty seven core indices have been defined by the ETCCDI to understand the impact of climate change on extreme temperature and precipitation events (Karl et al., 1999; Peterson et al., 2001). These indices, which the World Meteorological Organization (WMO) also suggests to be used (Klein Tank, 2009), have become the most basic elements in the research of extreme climate events for various regions in the literature (Frich et al., 2002; Peterson et al., 2002; Klein Tank, 2004; Aguilar et al., 2005; Vincent et al., 2005; Zhang et al., 2005; Haylock et al., 2006; Turp et al., 2016b; Ezer et al., 2017; Turp et al., 2017). Although common index definitions are made globally, these indices can be modified according to the characteristics of the region studied. Considering this point, totally six indices were used to define both temperature and precipitation extremes for the Australasia region (Table 3.3). These indices were created by combining general indices defined by the ETCCDI with indices defined by the BOM for Australia (BOM, n.d.-h) While very hot days (vhd), very hot nights/tropical nights (tn), and heat waves (hw) were used for temperature extremes, very heavy precipitation days (vhp), simple daily intensity (sdi), and consecutive dry days (cdd) were used for precipitation extremes. The definition and unit of each index is given in Table 3.3.

Table 3.3. Definitions of temperature and precipitation extreme indices.

Extreme type	Index Name	Definition	Unit
Temperature	Very Hot Days	The number of days where maximum temperature is above 40 ℃.	days/year
Temperature	Tropical Nights	The number of days where minimum temperature is above 25 ℃.	days/year
Temperature	Heatwave	The number of heatwave periods where in intervals of at least 5 consecutive days the daily maximum temperature is more than 5 ℃ with respect to the 95th percentile of the maximum temperature in the reference period.	periods/year
Precipitation	Very Heavy Precipitation	The number of days where daily precipitation amount is above 30 mm.	days/year
Precipitation	Simple Daily Intensity	The rate of total precipitation amount to the number of wet days, which means the daily precipitation amount is above 1 mm.	mm/day
Precipitation	Consecutive Dry Days	The number of the period of the days where daily total precipitation amount is consecutively below 1 mm with more than 5 days.	periods/year

Since the NEX-GDDP dataset is a global and daily high-resolution dataset, it contains approximately 12 TB of data in total. Since it is impossible to use all of this size of data within the framework of the restrictive available technical possibilities (e.g. online downloading of data, the storage capacity of the data), not all of the data was used in the study. For this reason, only two of the 21 GCMs included in the NEX-GDDP dataset were selected. The performance evaluation results of CMIP5 data previously made by BOM in modeling the climate of Australia were taken into consideration in this selection. In this context, ACCESS1 and MPI-ESM-LR, which are the two most accurate models for producing temperature and precipitation data for Australia, are used.

3.2.1. Evaluation of Prospective Changes in Temperature Extremes for the CORDEX-Australasia Domain Using the NEX-GDDP Dataset

Prospective changes in temperature extremes for the Australasia domain were evaluated using three different indices: very hot days, tropical nights (very hot nights), and heatwave. The changes projected to likely occur in the three future periods (i.e., 2016 - 2035, 2046 - 2065, and

2081 - 2100) compared to the reference period (1981 - 2000) in these three indices were calculated for both optimistic (RCP4.5) and pessimistic (RCP8.5) scenarios and mapped separately according to both climate models (i.e., ACCESS1-0 and MPI-ESM-LR).

When the change in the number of very hot days is examined firstly (Figure 3.35 and Figure 3.36), an increase is expected according to both models. According to both models, it is seen that this increase will become more severe towards the end of the century. Besides, the projected increase in the MPI-ESM-LR model is slightly higher than the projected increase in the ACCESS1-0 model. While the expected average increase in the period of 2016 - 2035 is similar in both scenarios, when it comes to 2046 - 2065 and 2081 - 2100, the RCP8.5 scenario predicts more increase than the RCP4.5 scenario. According to both models, the number of days above 40 ℃ in the future will be more than 0 - 10 days per year in the spatial average. It is seen that this increase expectation can reach the highest values in places outside the northeast-east-south coasts of Australia (inland areas where tropical desert and steppe climate prevails and in the west and northwest parts). For example, according to both models, it can be said that the amount of increase in the last two decades of the century may reach 100 %, according to RCP4.5 and 200 % according to RCP8.5. In the same period, similar results can be seen in humid and tropical climates such as the island of Sumatra in Indonesia and Thailand.

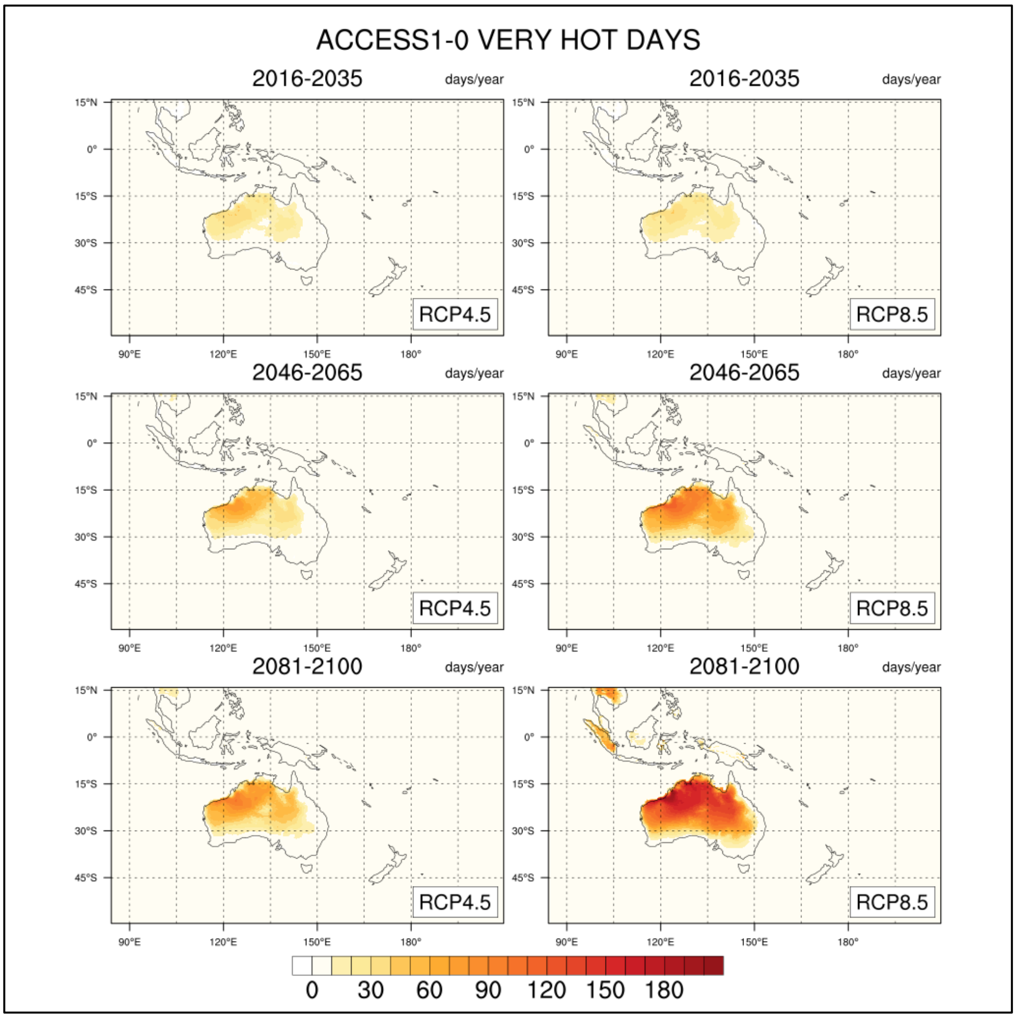

Figure 3.35. Changes in the number of very hot days for the ACCESS1-0 model under the RCP4.5 and RCP8.5 scenarios for the periods of 2016 - 2035, 2046 - 2065, and 2081-2100 with respect to the reference period of 1981 - 2000.

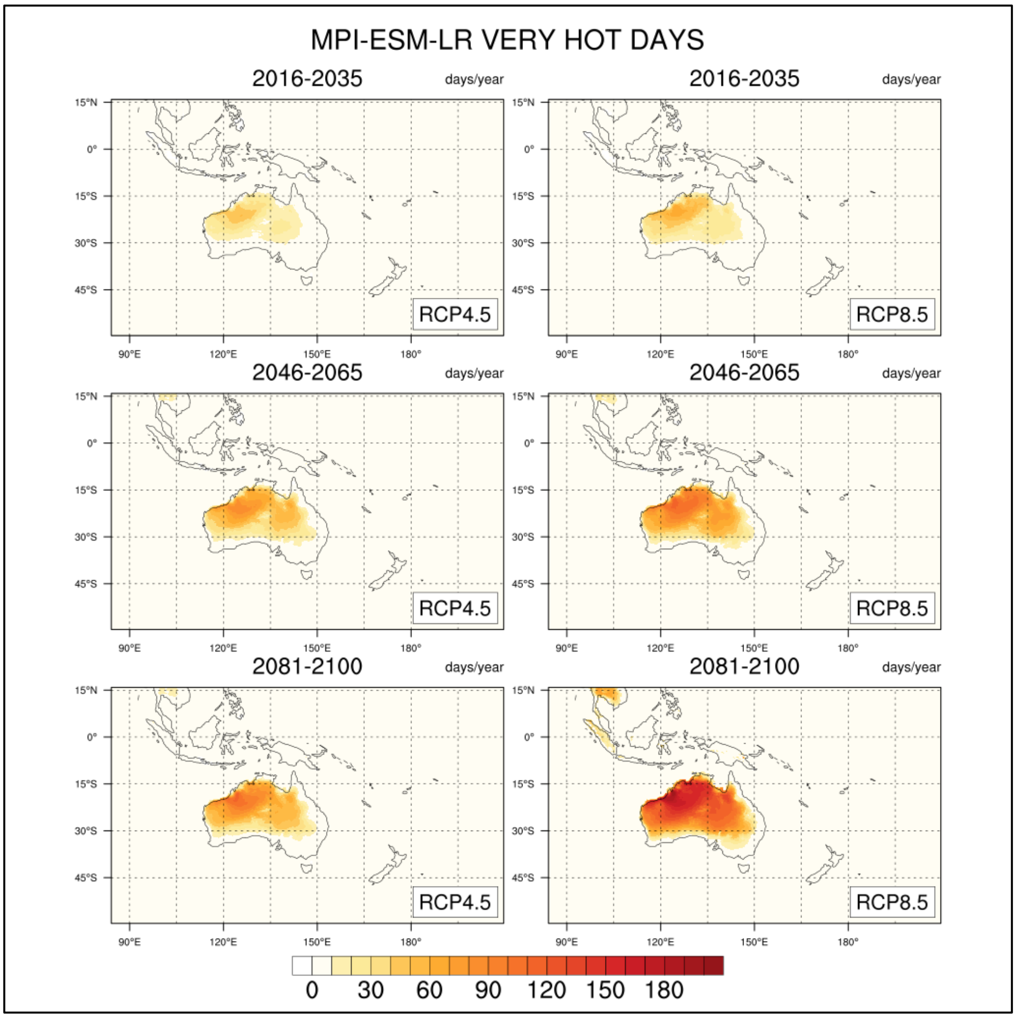

Figure 3.36. Changes in the number of very hot days for the MPI-ESM-LR model under the RCP4.5 and RCP8.5 scenarios for the periods of 2016 - 2035, 2046 - 2065, and 2081-2100 with respect to the reference period of 1981 - 2000.

The variation in the number of tropical nights also shows a pattern similar to the change in the number of very hot days (Figure 3.37 and Figure 3.38). The results of both models show that nighttime temperatures in the Australasia domain will reach above 25 °C in the future. It can be said that this increase expectation will be higher in the RCP8.5 scenario compared to the RCP4.5 scenario and will increase very much, particularly in the long term (2081 - 2100). Also, the MPI-ESM-LR model predicts further increases compared to the ACCESS1-0 model. Considering all these findings, the MPI-ESM-LR model foresees the highest increase in tropic nights under the RCP8.5 scenario for the 2081 - 2100 period. In this period, not only the amount of increase but also the width of the spread area is remarkable. As in very hot days, there is not much difference between models and scenarios in 2016 - 2035. However, in the RCP4.5 scenario, the increase reaching an average of 20 days/year towards the end of the century. Under the RCP8.5 scenario, it is around 40 days/year for ACCESS1-0 and it is seen that it can get approximately 50 days/year for

MPI-ESM-LR. It is inevitable that tropical nights, which show a significant increase in the region between 30°S - 15°N latitudes, will significantly increase, particularly from the north of Australia to Papua New Guinea, Indonesia, Malaysia, and Thailand. Towards the end of the century, night temperatures above 25 °C are expected in some places along the equatorial region throughout the year.

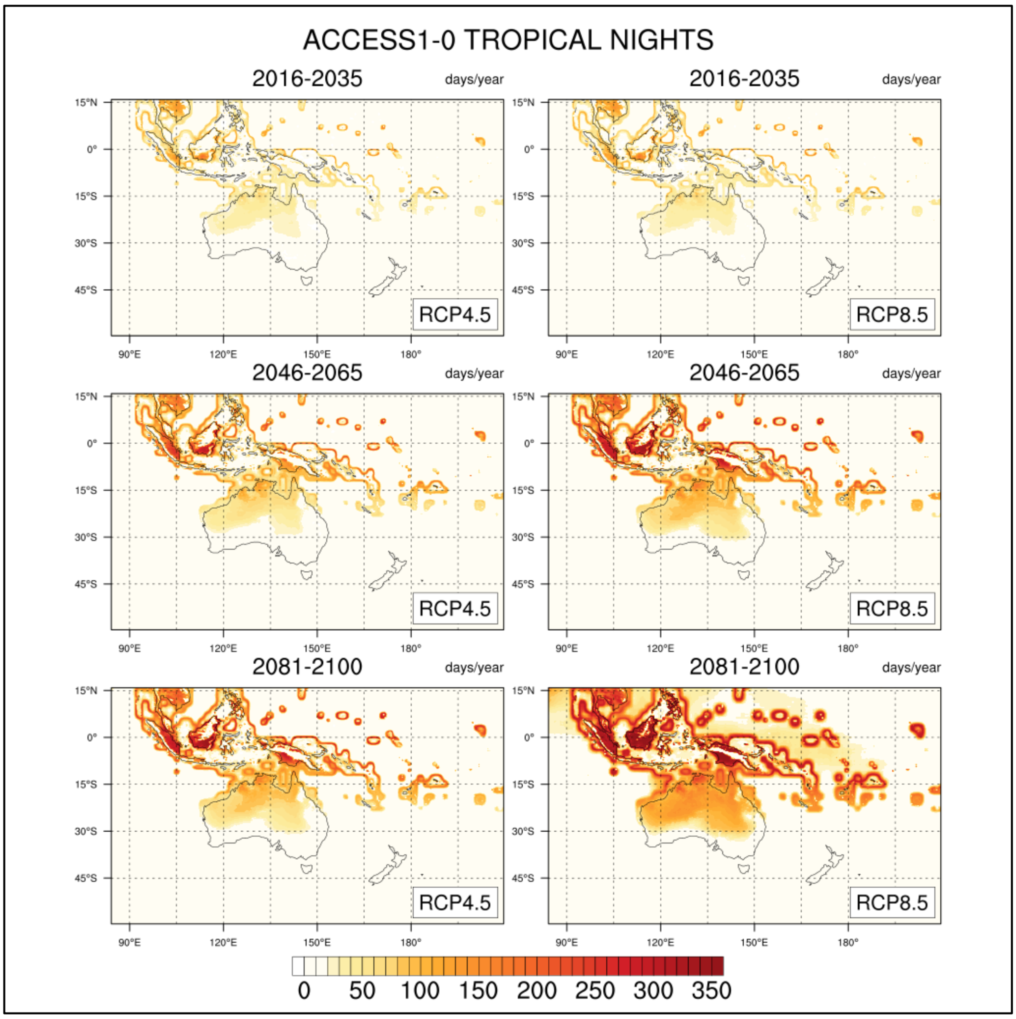

Figure 3.37. Changes in the number of tropical nights for the ACCESS1-0 model under the RCP4.5 and RCP8.5 scenarios for the periods of 2016 - 2035, 2046 - 2065, and 2081-2100 with respect to the reference period of 1981 - 2000.

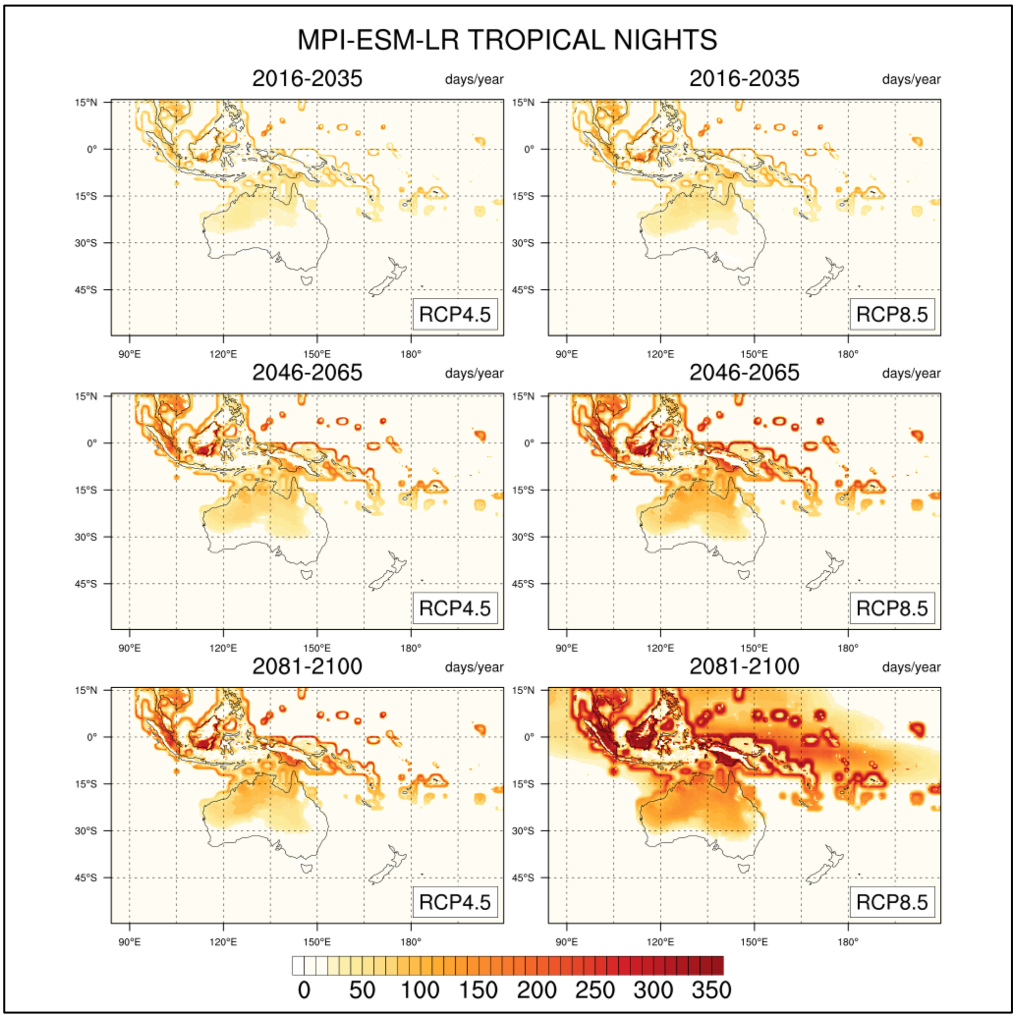

Figure 3.38. Changes in the number of tropical nights for the MPI-ESM-LR model under the RCP4.5 and RCP8.5 scenarios for the periods of 2016 - 2035, 2046 - 2065, and 2081-2100 with respect to the reference period of 1981 - 2000.

Finally, when the changes in the number of heatwaves for Australasia are examined (Figure 3.39 and Figure 3.40), it is seen that the heatwaves will increase as both models and scenarios predict. In both models, the change in heatwave has a similar pattern in temporal and spatial terms. In the periods of 2016 - 2035 and 2046 - 2065, the increase in the number of heatwaves, which become more evident in the tropical zone between 15°N and 15°S latitudes, is expected to be influential in a wider area by 2081 - 2100, including other places in the south of the southern region. The average increase expectation, which is similar to each other in both scenarios and models for the 2016 - 2035 period (approximately 3 periods/year), is approximately 5 periods/year for RCP4.5 and about 6 periods/year for RCP8.5 for the 2046 - 2065 period. It is estimated. By the end of the century, it is predicted that the increase in heatwaves will be around 6 periods/year for RCP4.5 and 7 periods/year for RCP8.5 when both models are considered. Considering both scenarios and periods, although the predictions of the MPI-ESM-LR model are slightly higher than the

ACCESS1-0, this difference can be regarded as negligible. The expectation of the maximum increase in the number of heatwaves will reach 15 - 16 periods/year from the second half of the century, particularly according to the pessimistic scenario. This high increase expectation is concentrated around Indonesia, Philippines, Papua New Guinea, and Micronesia.

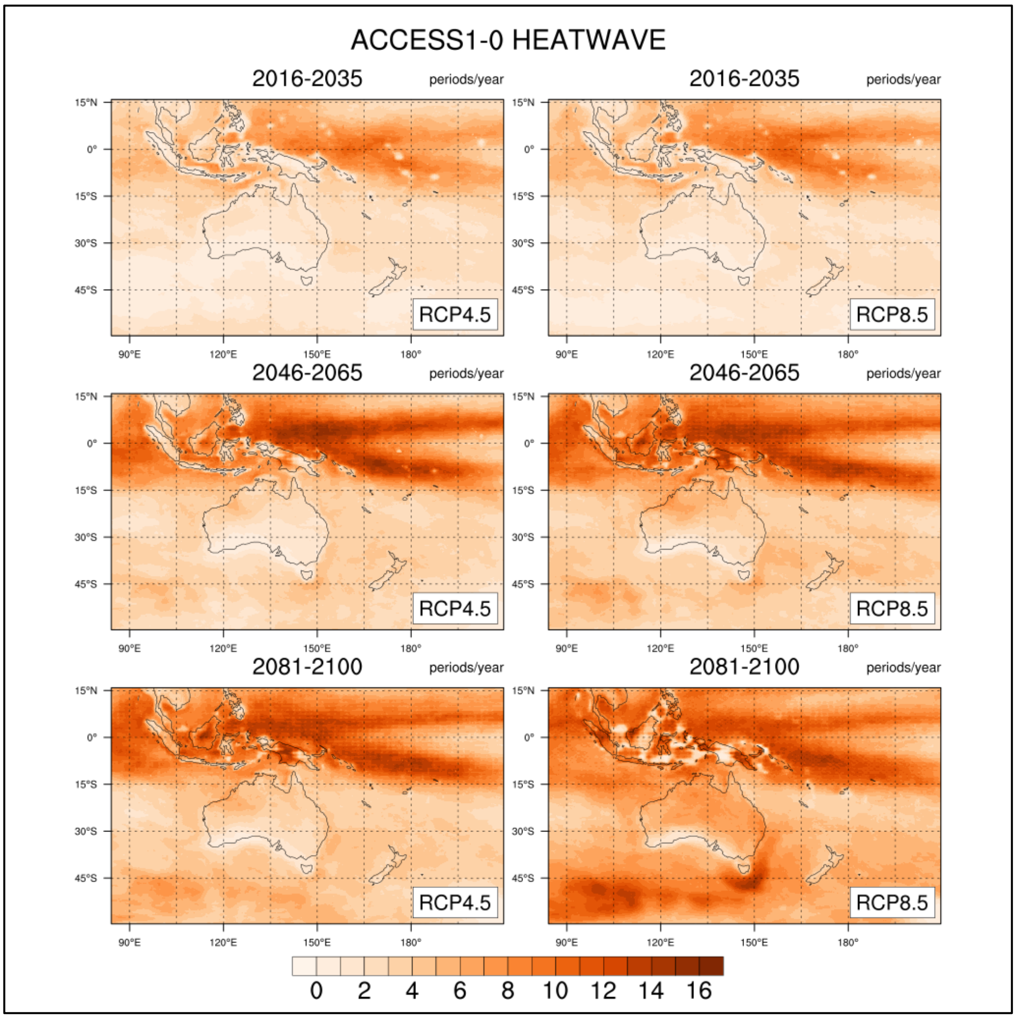

Figure 3.39. Changes in the number of heatwaves for the ACCESS1-0 model under the RCP4.5 and RCP8.5 scenarios for the periods of 2016 - 2035, 2046 - 2065, and 2081-2100 with respect to the reference period of 1981 - 2000.

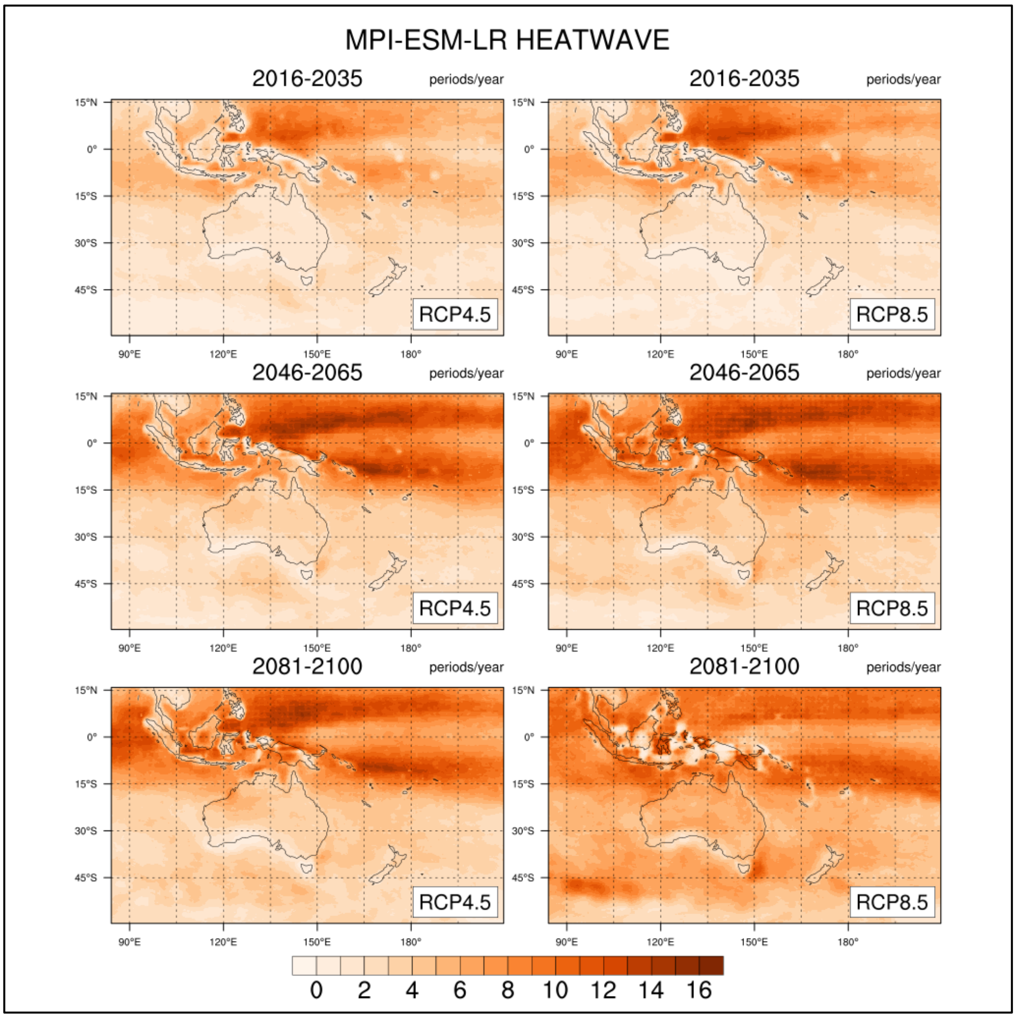

Figure 3.40. Changes in the number of heatwaves for the MPI-ESM-LR model under the RCP4.5 and RCP8.5 scenarios for the periods of 2016 - 2035, 2046 - 2065, and 2081-2100 with respect to the reference period of 1981 - 2000.

3.2.2. Evaluation of Prospective Changes in Precipitation Extremes for the CORDEX-Australasia Domain Using the NEX-GDDP Dataset

Prospective changes in precipitation extremes for the Australasia domain were evaluated using three different indices: very heavy precipitation, simple daily intensity, and consecutive dry days. As with temperature extremes, the changes in precipitation extremes projected to likely occur in the three future periods (i.e., 2016 - 2035, 2046 - 2065, and 2081 - 2100) compared to the reference period (1981 - 2000) in these three indices were calculated for both optimistic (RCP4.5) and pessimistic (RCP8.5) scenarios and mapped separately according to both climate models (i.e., ACCESS1-0 and MPI-ESM-LR).

First, when the change in the number of days with heavy precipitation is examined (Figure 3.41 and Figure 3.42), ACCESS1-0 and MPI-ESM-LR model results show different patterns in terms of periods and scenarios. Considering the spatial average, while a less reduction is expected in the RCP4.5 scenario result of the ACCESS1-0 model, the increases that may exceed 10 days/year are expected in the RCP8.5 scenario of the same model. According to ACCESS1-0, periodic differences are not very striking in terms of average values; yet, it can be seen that the expected average increase slightly rises when moving from the near future to the far future. Considering all three periods together, the decreases of approximately 5 days/year in the RCP8.5 scenario in Australia, the largest land part in the region, draw attention. This decrease expectation, which is dominant in the RCP8.5 scenario, except for the north and southeastern coasts of the country, is more in the form of a fragmented pattern towards the inner regions of the continent in the RCP4.5 scenario. Contrary to the expectation of a decrease in the number of days with precipitation above 30 mm in Australia, there is a predominant increase expectation on the ocean. According to the RCP4.5 scenario, it is seen that the increase expectation, which is around 5 days/year for all three periods, when the RCP8.5 scenario is switched, Australasia can reach 70 days/year in the equatorial region between 15°N and 15°S latitudes. According to the MPI-ESM-LR model, it can be said that the increases and decreases for both scenarios are similar. Although a minimal increase is expected in terms of spatial average throughout the region according to the RCP8.5 scenario, the results of both scenarios of the model point to the decrease showing a heterogeneous pattern on the Indian and the Pacific Ocean. It is expected that decreases around 5 days/year spread over a wider area, particularly on the Indian Ocean during 2046 - 2065 and 2081 - 2100 periods, will be seen in some inner and coastal parts of the continent. Contrary to this decrease expectation, according to the MP-ESM-LR model RCP8.5 scenario, the number of days with extreme precipitation events in Indonesia’s Borneo and Sulawesi islands and Papua New Guinea may increase by 20 days/year or more in 2046 - 2065 and 2081 - 2100 periods.

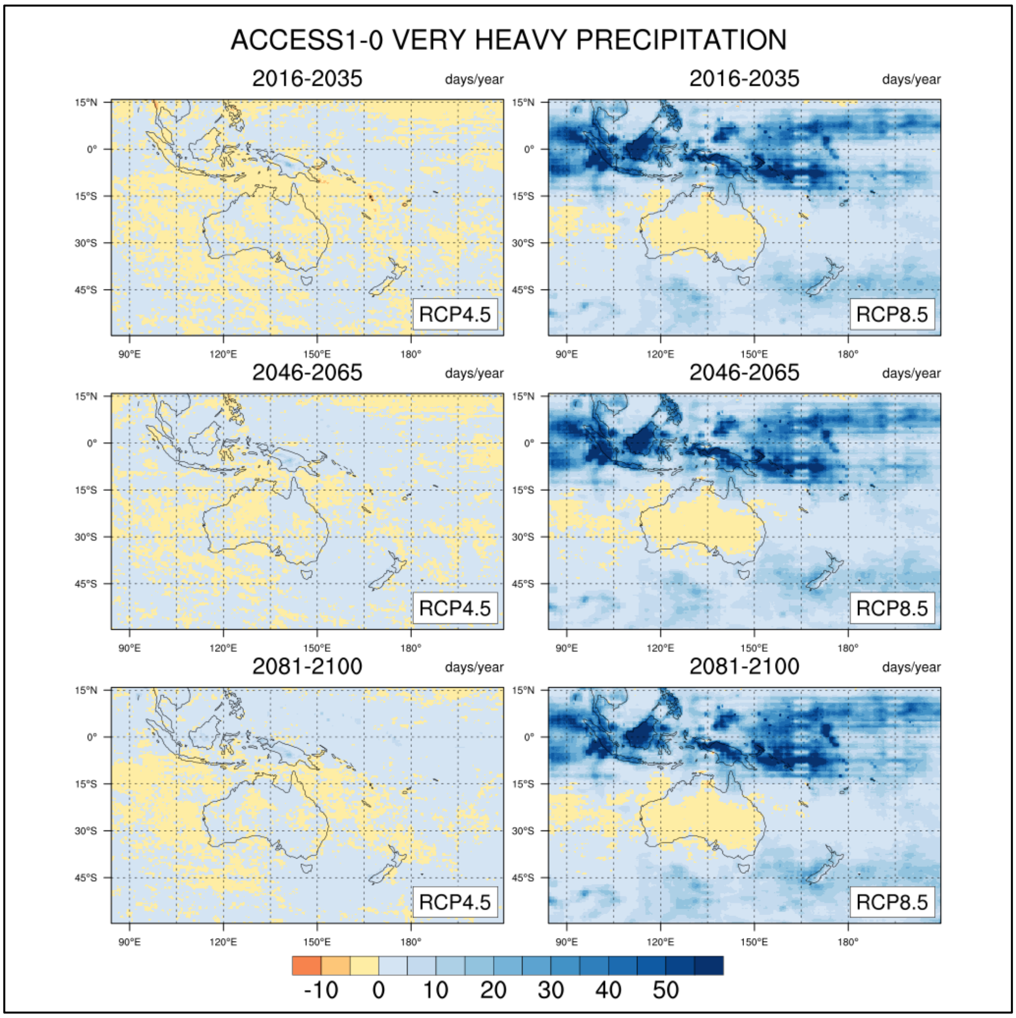

Figure 3.41. Changes in the number of days with very heavy precipitation for the ACCESS1-0 model under the RCP4.5 and RCP8.5 scenarios for the periods of 2016 - 2035, 2046 - 2065, and 2081-2100 with respect to the reference period of 1981 - 2000.

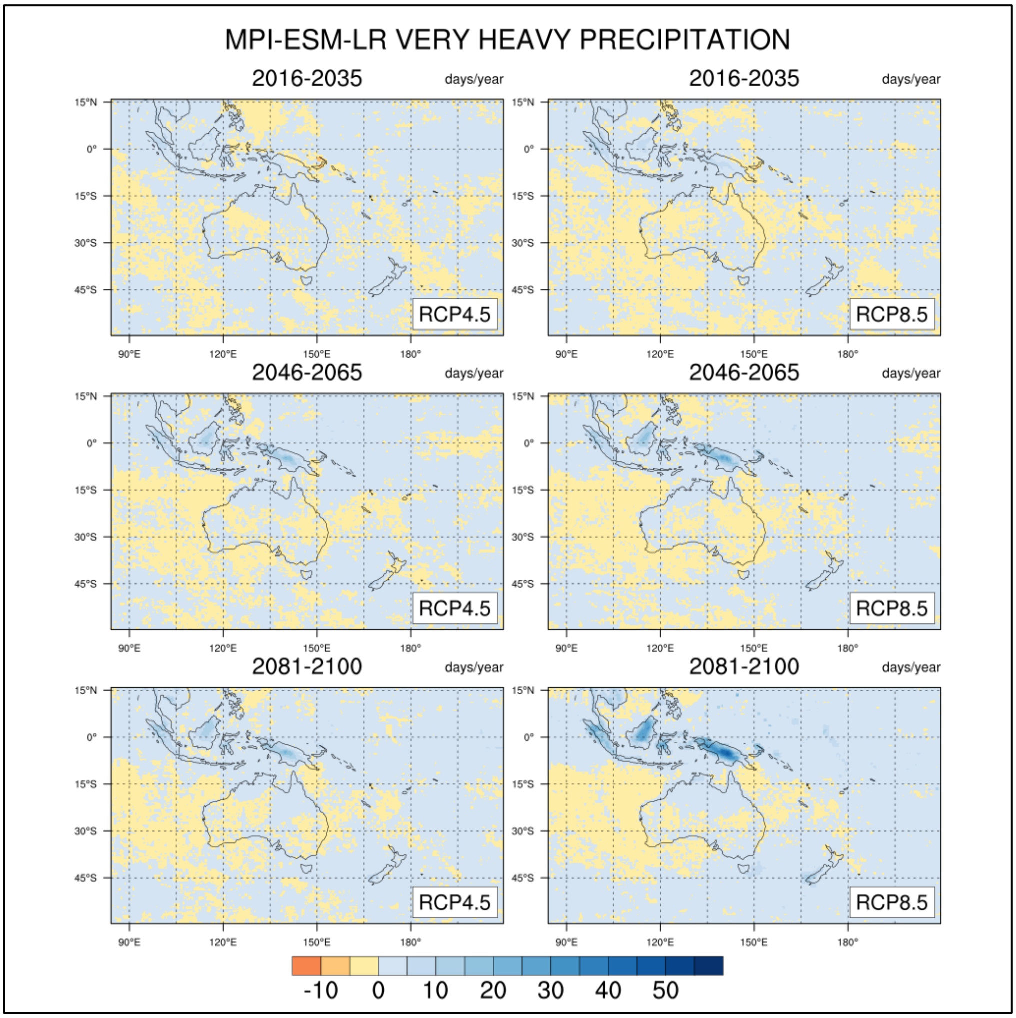

Figure 3.42. Changes in the number of days with very heavy precipitation for the MPI-ESM-LR model under the RCP4.5 and RCP8.5 scenarios for the periods of 2016 - 2035, 2046 - 2065, and 2081-2100 with respect to the reference period of 1981 - 2000.

After analyzing the change in the number of days with extreme precipitation, when the change in the simple daily intensity is examined (Figure 3.43 and Figure 3.44), an increase in precipitation intensity is expected throughout Australasia. Nonetheless, there will be a decrease, particularly in some areas over the ocean. According to the ACCESS1-0 model results, it is seen that the increase in precipitation intensity in the range of 0 - 5 mm/day under the RCP4.5 scenario will exceed an average of 5 mm/day for the RCP8.5 scenario. For both scenarios, it is expected that the increase in the simple daily intensity value will be slightly higher when going from the near future to the distant future. According to RCP8.5, the increase in the future, particularly in the region from the northern coast of Australia up to 15°N, is remarkable. It is seen that in these periods, simple daily intensity can increase up to 70 mm/day in these places. Contrary to these places, according to the RCP4.5 scenario results of the same model, there is a decrease expectation for the Indian Ocean in the west of Australia and the Pacific Ocean in the east. It can be said that this decrease of 5 - 10 mm/day will be influential in the inner parts of Australia in all three periods. It is expected that this decrease in the RCP4.5 scenario may be seen in the inner parts of the continent, losing its impact on the ocean when it comes to the RCP8.5 scenario. The change in simple daily intensity gives results on average similar to each other in both RCP4.5 and RCP8.5 scenarios, according to the MPI-ESM-LR model. For both scenarios, the expected increase between 0 - 5 mm/day is slightly higher in the RCP8.5 scenario compared to the RCP4.5 scenario. Unlike the ACCESS1-0 model, the MPI-ESM-LR model is likely to increase in the Australia continent. In both scenarios, a decrease in precipitation intensity is expected over the Indian Ocean in the west of Australia and the Pacific Ocean in the east for all three periods. This decrease is predicted to be in the range of 0 - 5 mm/day.

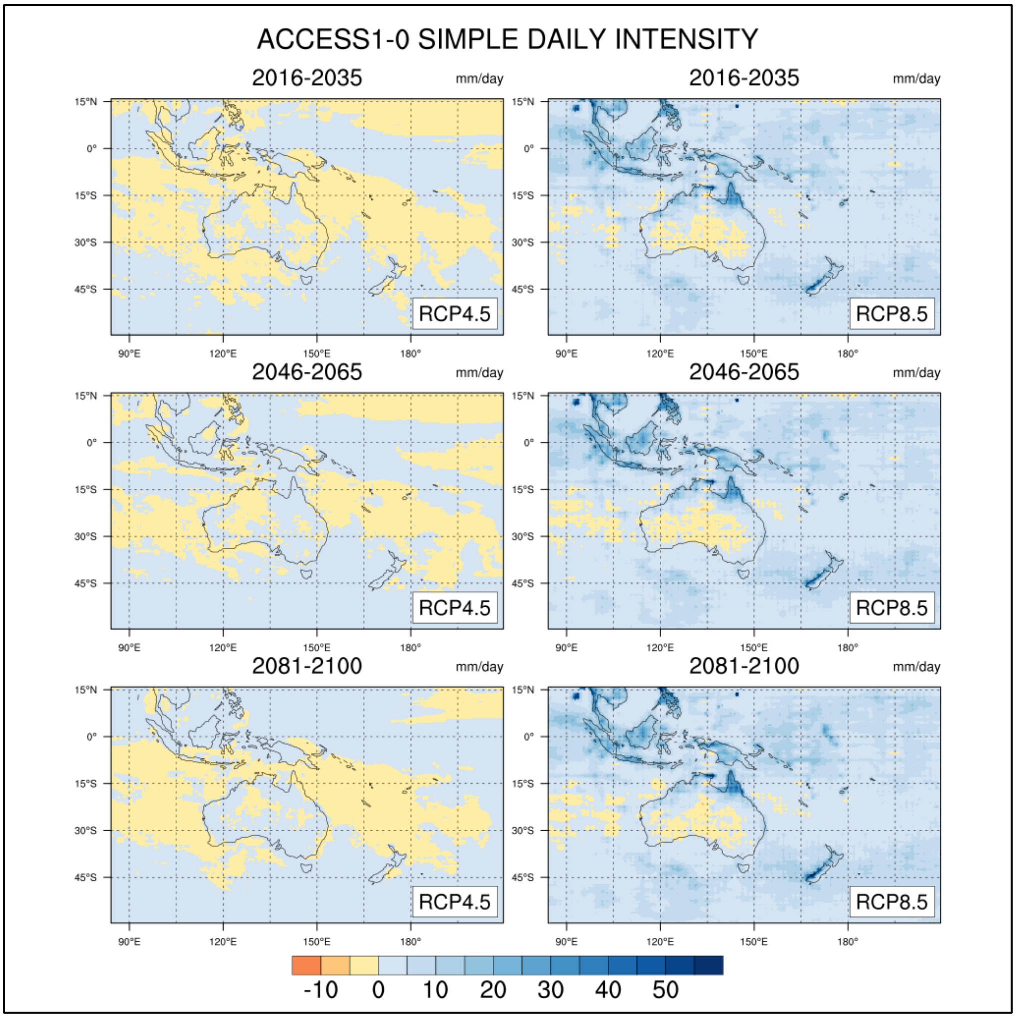

Figure 3.43. Changes in the simple daily intensity for the ACCESS1-0 model under the RCP4.5 and RCP8.5 scenarios for the periods of 2016 - 2035, 2046 - 2065, and 2081-2100 with respect to the reference period of 1981 - 2000.

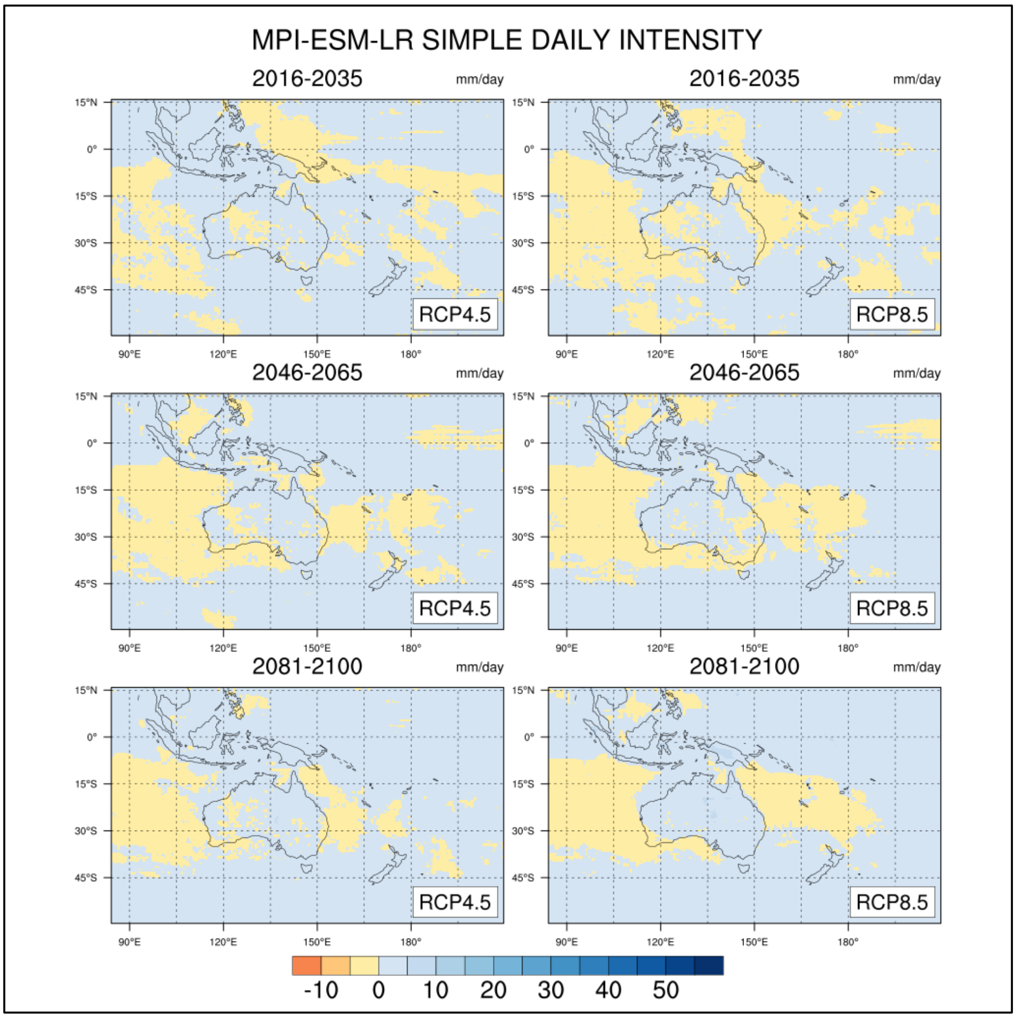

Figure 3.44. Changes in the simple daily intensity for the MPI-ESM-LR model under the RCP4.5 and RCP8.5 scenarios for the periods of 2016 - 2035, 2046 - 2065, and 2081-2100 with respect to the reference period of 1981 - 2000.

Finally, when the changes in the consecutive dry days are examined (Figure 3.45 and Figure 3.46), both the optimistic and pessimistic scenario predictions of both models foresee very little change in terms of the regional average. It is seen that the negligible decrease and increase values, which are predominantly over the ocean, appear as a more significant change in the direction of decrease on the Australian continent. It is clear that the expected reduction in Australia, according to the ACCESS1-0 model, will reach approximately 10 periods/year. Considering the RCP4.5 scenario predictions of ACCESS1-0, it should be noted that the expected decrease from the east of longitude 150°E along the equator line between 1 - 5 periods/year periodically may be in the form of drops up to 10 periods/year in RCP8.5 scenario for Australia. It is seen that the amount of decrease will rise significantly from the inner parts of Australia towards the south. Again, for the same model and the same scenario, a decrease in the consecutive dry days is expected on the Indian Ocean in western Australia. According to the pessimistic scenario of the same model, there are expectations of an increase of approximately 4 periods/year and more on New Zealand and other Polynesia islands on South Pacific. When it comes to the MPI-ESM-LR model, it is seen that the amount of decrease can vary between 3 and 7 periods/year periodically with the most severe form. These decreases will become dominant in the south of 45°S latitude for the RCP8.5 scenario in the same periods as the inner and southern parts of Australia according to both scenarios, especially in 2046 - 2065 and 2081 - 2100. According to the MPI-ESM-LR model, when both scenarios are taken into consideration, the periodic increase between 3 and 8 periods/year is more evident, especially in 2046 - 2065 and 2081 - 2100 periods, but can be seen along the equatorial line from the east of longitude 150°E in all three periods. At this point, the results of the MPI-ESM-LR model and the ACCESS1-0 model differ.

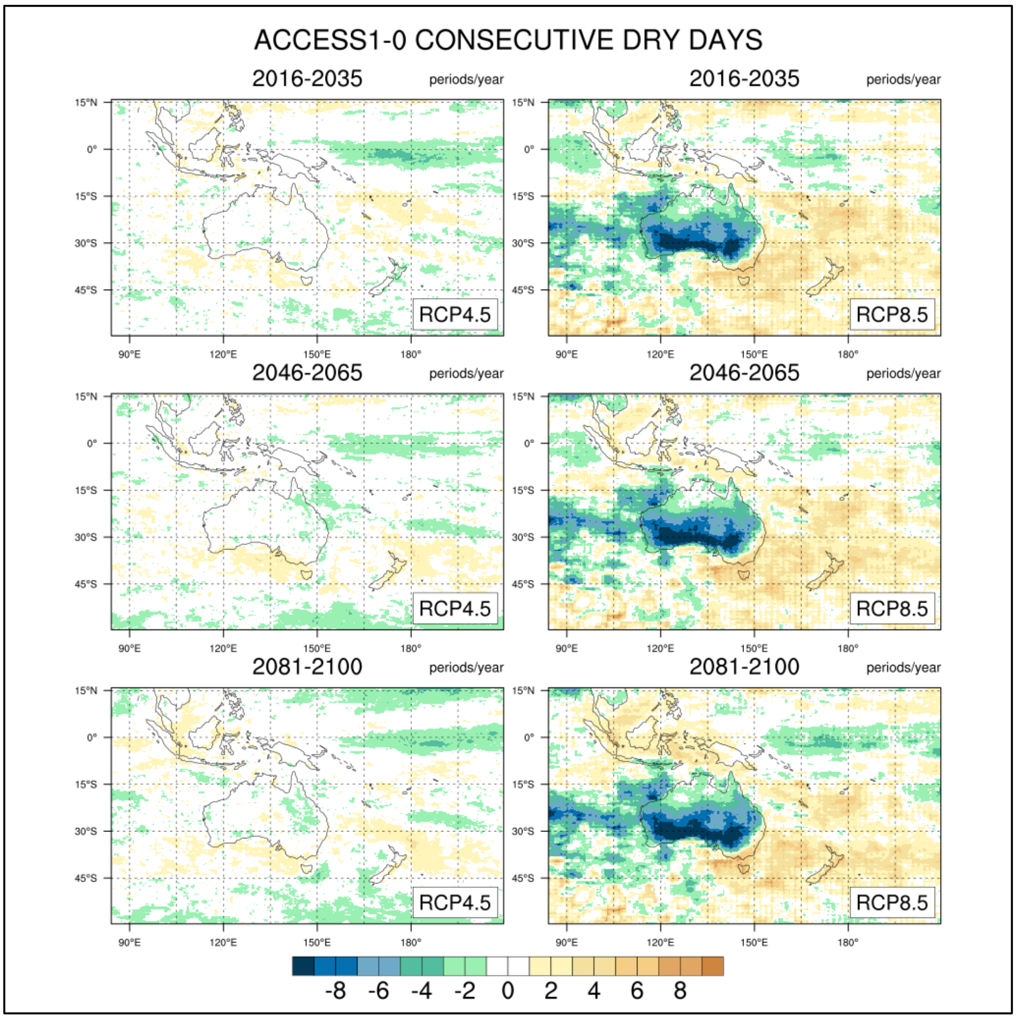

Figure 3.45. Changes in the consecutive dry days for the ACCESS1-0 model under the RCP4.5 and RCP8.5 scenarios for the periods of 2016 - 2035, 2046 - 2065, and 2081-2100 with respect to the reference period of 1981 - 2000.

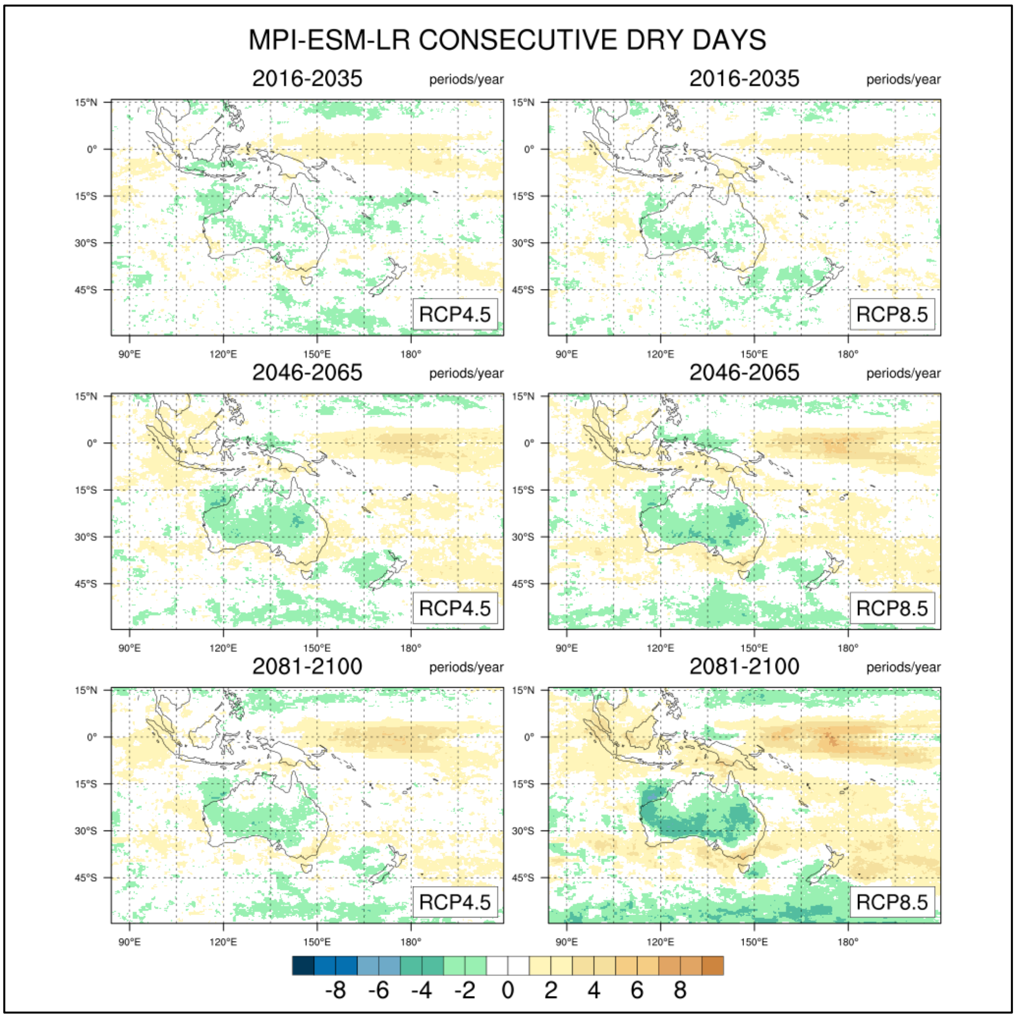

Figure 3.46. Changes in the consecutive dry days for the MPI-ESM-LR model under the RCP4.5 and RCP8.5 scenarios for the periods of 2016 - 2035, 2046 - 2065, and 2081-2100 with respect to the reference period of 1981 - 2000.

3.3. Evaluation of RegCM4.6 for the CORDEX-AUSTRALASIA Domain

Climate models have parametric and structural uncertainties. In order to be able to rely on the outcomes of future projections of climate models, we first expect it to model the current climate in the most accurate way. In other words, we can run a climate model for past and future climate after validating the climate model.

Climate models cannot perform small-scale and complex processes in the atmosphere in the same reality as they exist in nature. Hereby, processes that are difficult to express and complex in climate models are defined by some simplifications with various approaches and approximate calculations. We can also call it parameterization of the model. In order for a climate model to give the most realistic and accurate results, choosing the most appropriate alternative scheme in the model is the first step that should be taken into consideration and applied. In this step, the climate model is run for a short term (3-5 years) for a reference period, where we can make observational comparisons under different scheme options. These short-term outputs are compared with the in situ observation or reanalysis data, and the most appropriate schemes are selected by evaluating the value of the results in terms of temporal and spatial distribution. However, after this validation process, the climate model can be used for long-term simulations for the past and the future.

The height distribution of clouds is very critical in cumulus convection parameters (Holton, 2004). The main reason for this is that diabatic heating is dependent on the distribution of cloud heights at local scale (Holton, 2004). Condensation heating caused by cumulus convection is one of the most important problems, especially in terms of tropical meteorology (Holton, 2004).

In this context, in this part of the study, a pair of PBL and cumulus convection schemes that can model the regional climate in the most appropriate conditions had been determined before long-term climate simulations were conducted for the Australasia domain. RegCM has two alternative schemes for PBL and seven alternative schemes for cumulus convection (Table 3.4).

Table 3.4. Possible Schemes in RegCM4.6.

Planetary Boundary Layer Schemes	Convection Schemes
Holtslag (Holtslag, 1990), UW PBL (Bretherton et al., 2004; McCaa and Bretherton, 2004)	Kuo (Anthes, 1977) Grell - Arakawa & Schubert (Grell, 1993; Grell et al. 1994) Grell - Fritsch & Chappell (Grell, 1993; Fritsch and Chappell, 1980) Emanuel (Emanuel, 1991; Emanuel and Zivkovic-Rothman, 1999) Tiedtke (Tiedtke, 1996) Kain-Fritsch (Kain and Fritsch, 1990; Kain, 2004) Mixed (e.g. Grell over land and Emanuel over ocean)

RegCM offers the mixed scheme option as the seventh alternative, separate on lands and oceans, as well as using the same scheme both on lands and oceans in the part of the cumulus convective scheme. It has been determined that the Emanuel scheme over land generates higher precipitation than normal, while the Grell scheme over tropical oceans generates less precipitation than normal (Giorgi et al., 2012). For this reason, the mixed cumulus convection scheme using the Grell scheme on lands and the Emanuel scheme on oceans has been proposed as the most reasonable option (Giorgi et al., 2012). The Kain-Fritsch scheme, which is grounded on the Grell scheme, is not considered for oceans either. In addition, the Kuo scheme, which was active with the first version of RegCM, was not considered in the study because it was insufficient to calculate precipitation compared to other alternative schemes (Giorgi et al., 2012). In the light of all this information, six different possibilities were taken into consideration for the cumulus convective scheme, as the Grell scheme and the Tiedtke scheme with two closure types on lands, the Emanuel and Tiedtke schemes and on oceans. Considering these six different preferences and two different PBL schemes, a total of 12 different test runs were designed and run for the 1983-1987 period. While choosing this period, attention has been paid to the selection of the periods when ENSO, which has a very important impact on the Australasia domain, is neutral or weak (Meyers et al., 2007; Jacob and Walland, 2016; Null, 2021). In the analysis of the test run outputs made with 12 different parameterizations (Table 3.5), the year 1983 was accepted as spin-up year and the analyzes were made to cover the period of 1984-1987.

Table 3.5. Test runs for the evaluation of RegCM4.6 for the CORDEX-Australasia domain.

RUN ID	**PBL SCHEME**	**LAND_CS**	**OCEAN_CS**
RUN1 (R1)	Holtslag	Grell-Arakawa&Schubert	Emanuel
RUN2 (R2)	Holtslag	Grell-Fritsch&Chappell	Emanuel
RUN3 (R3)	Holtslag	Tiedtke	Emanuel
RUN4 (R4)	Holtslag	Grell-Arakawa&Schubert	Tiedtke
RUN5 (R5)	Holtslag	Grell-Fritsch&Chappell	Tiedtke
RUN6 (R6)	Holtslag	Tiedtke	Tiedtke
RUN7 (R7)	UW	Grell-Arakawa&Schubert	Emanuel
RUN8 (R8)	UW	Grell-Fritsch&Chappell	Emanuel
RUN9 (R9)	UW	Tiedtke	Emanuel
RUN10 (R10)	UW	Grell-Arakawa&Schubert	Tiedtke
RUN11 (R11)	UW	Grell-Fritsch&Chappell	Tiedtke
RUN12 (R12)	UW	Tiedtke	Tiedtke

First of all, ERA-Interim reanalysis dataset was used under 12 different parameterizations and the multiyear means of temperature and precipitation outputs of RegCM operated for a short time were taken for the period of 1984-1987. Then, a comparison was made with the values of the same variables obtained from three different observation datasets (i.e. CRU, UDEL, and NCAR) for the same period. ERA-Interim's temperature and precipitation data with a horizontal resolution of approximately 80 km were dynamically reduced to a resolution of 50 km using RegCM4.6. All data sets must have the same grid resolution in order to make comparisons between data. For this reason, the CRU, UDEL, and NCAR datasets were bilinearly interpolated into RegCM's 50 km resolution grid structure. In addition to the calculation of spatial correlation coefficient, variation ratio, Root

Mean Square Error (RMSE), and bias as benchmarks, Taylor diagrams (Taylor, 2001) were drawn with reference to the NCAR dataset.

When the 12 different test run outputs obtained from the climate model are compared statistically with CRU, UDEL, and NCAR data (Table 3.6), it is obvious that the smoothest and compatible results for both temperature and precipitation are seen with NCAR reanalysis data. Comparison results with the CRU and UDEL observation datasets show higher bias, higher RMSE, higher variation ratio, and smaller correlation coefficient values. In contrast, comparisons made with NCAR reanalysis data appear to have lower bias, lower RMSE, lower variation ratio, and higher correlation coefficient values. At this point, it should not be forgotten that Australasia domain includes mostly the ocean as well as the terrestrial areas. Analysis results were given for all reference datasets. However, instead of datasets containing only in situ observational data such as CRU and UDEL, NCAR reanalysis data including all terrestrial and oceanic areas of the domain were considered as a reference dataset.

3.3.1. Parametrization Results of RegCM4.6 for Temperature

The spatial correlation coefficients between RegCM temperature outputs and CRU, UDEL, and NCAR outputs gave very good results for all test runs (between 0.82 and 0.99). It is seen that these coefficients reach almost 1 between the NCAR dataset and RegCM. Variation ratios also have values close to 1. It turns out that the RMSE values and bias values are also low. R1, R2, and R3 stand out as the best three models in terms of variation ratio, RMSE, and bias values. RegCM temperature results appear to contain cold bias, which varies between -0.5 ℃ and -1.5 ℃. It is also clearly seen in the Taylor diagram drawn for the annual mean temperature that the temperature estimated with RegCM gives very good results for all test runes (Figure 3.47). All sub models contain results close to the reference value. Although RegCM test run results give similar results in terms of temperature, considering all the comparisons, it is seen that the R3 model is the best model with low bias and RMSE values, variation ratio and correlation coefficients close to 1. Briefly, in RegCM4.6 it was found that the most suitable PBL scheme for temperature is Holtslag, the cumulus convective scheme is Tiedtke over lands and Emanuel over oceans.

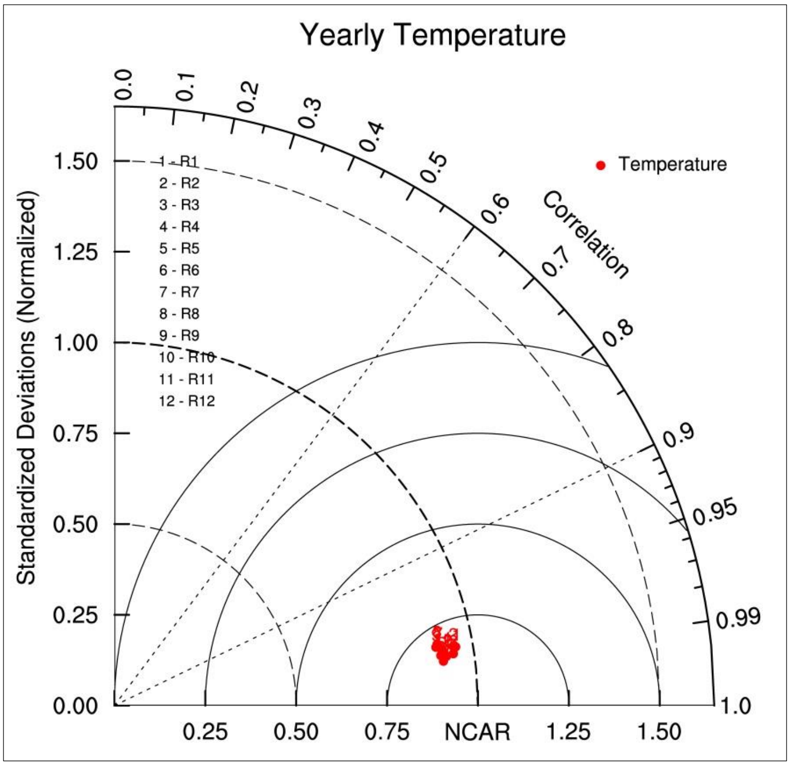

Figure 3.47. Taylor diagram for annual temperature.

3.3.2. Parametrization Results of RegCM4.6 for Precipitation

When the precipitation values, which are one of the most difficult variables to model in climate models, are examined, results that are less reliable than the temperature values are obtained. It is seen that the spatial correlation coefficients between RegCM output and CRU, UDEL, and NCAR outputs varied between 0.07 and 0.46. The highest correlation coefficients belong to R3, R6, R10, R11, and R12. Despite the relatively low correlation coefficients, variation ratio values are quite reassuring in terms of capturing precipitation patterns, especially when the NCAR dataset is taken as a basis. At this point, again, the first three test runs give the best results. It can be said that RMSE and bias values give very reasonable and reliable results when NCAR data is taken as reference. Yet, it is obvious that RegCM precipitation results include overestimation. For a domain affected by global-scale weather movements, the bias in precipitation values between approximately 3 % and 40 % (according to NCAR reference data) makes the model results acceptable in terms of precipitation. It appears that at least three biases in precipitation are R6 (2.88 %), R4 (12.68 %), and R5 (16.02 %), respectively. When looking at the Taylor diagram drawn for annual precipitation to make it easier to decide which model is the best for precipitation, R3 test run value stands out (Figure 3.48). Just like temperature, it was found that the most suitable PBL scheme for precipitation in RegCM4.6 was Holtslag and the cumulus convective scheme was Tiedtke over lands and Emanuel over oceans.

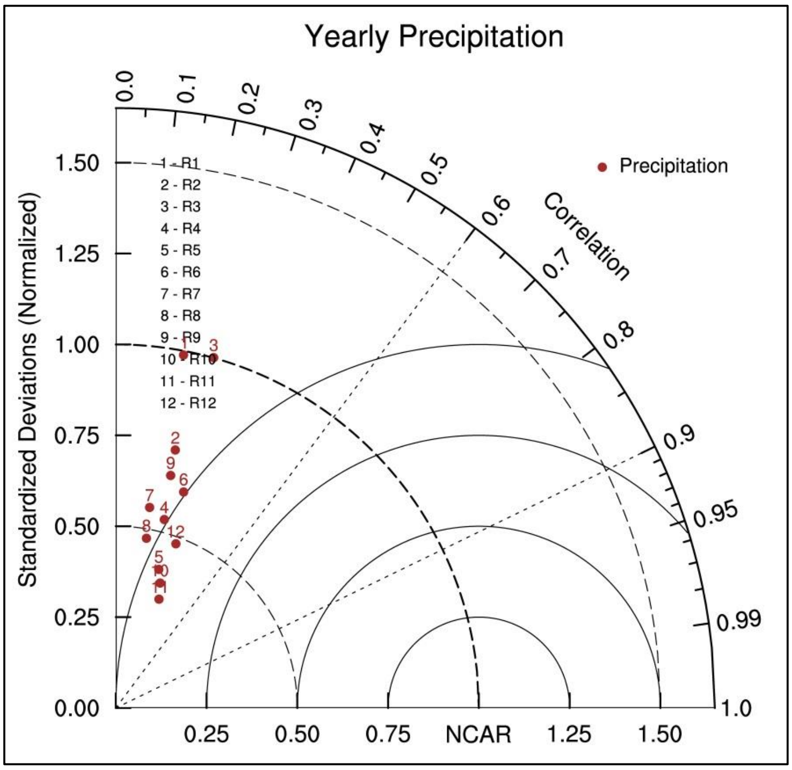

Figure 3.48. Taylor diagram for annual precipitation.

Table 3.6. Statistical comparison of test runs with observation and reanalysis datasets for the baseline period (1984 - 1987).

Precipitation	**Correlation**	**R1**	**R2**	**R3**	**R4**	**R5**	**R6**	**R7**	**R8**	**R9**	**R10**	**R11**	**R12**
	CRU	0.212	0.306	0.410	0.234	0.286	0.404	0.074	0.113	0.370	0.147	0.211	0.431
	UDEL	0.245	0.341	0.443	0.265	0.317	0.451	0.076	0.120	0.411	0.145	0.217	0.463
	NCAR	0.189	0.225	0.270	0.250	0.297	0.300	0.167	0.178	0.230	0.335	0.370	0.344
	Variation Ratio	**R1**	**R2**	**R3**	**R4**	**R5**	**R6**	**R7**	**R8**	**R9**	**R10**	**R11**	**R12**
	CRU	0.618	0.456	0.626	0.335	0.250	0.390	0.350	0.297	0.411	0.228	0.201	0.301
	UDEL	0.749	0.552	0.759	0.406	0.303	0.472	0.424	0.360	0.498	0.276	0.244	0.365
	NCAR	0.989	0.728	1.001	0.535	0.399	0.623	0.559	0.474	0.657	0.365	0.322	0.481
	RMSE (mm/month)	**R1**	**R2**	**R3**	**R4**	**R5**	**R6**	**R7**	**R8**	**R9**	**R10**	**R11**	**R12**
	CRU	154.03	116.07	141.26	121.84	98.36	118.63	115.09	98.88	112.18	105.82	96.76	100.02
	UDEL	159.51	117.16	150.06	119.84	91.70	120.79	108.88	88.65	112.34	96.16	84.40	98.18
	NCAR	98.03	89.54	93.90	90.38	84.96	89.60	88.66	85.74	87.47	80.03	77.72	80.46
	Bias (%)	**R1**	**R2**	**R3**	**R4**	**R5**	**R6**	**R7**	**R8**	**R9**	**R10**	**R11**	**R12**
	CRU	134.05	149.82	90.77	89.72	112.45	72.16	84.13	91.67	85.81	49.83	51.21	69.89
	UDEL	184.11	202.96	129.20	129.08	156.82	109.47	122.50	131.15	124.42	80.23	81.28	105.05
	NCAR	35.99	39.52	21.60	12.68	16.02	2.88	36.88	38.70	31.77	18.13	18.05	18.81
Temperature	**Correlation**	**R1**	**R2**	**R3**	**R4**	**R5**	**R6**	**R7**	**R8**	**R9**	**R10**	**R11**	**R12**
	CRU	0.872	0.873	0.908	0.898	0.895	0.919	0.863	0.865	0.882	0.886	0.883	0.896
	UDEL	0.837	0.844	0.881	0.861	0.862	0.887	0.821	0.828	0.846	0.844	0.843	0.860
	NCAR	0.985	0.985	0.989	0.989	0.988	0.991	0.983	0.982	0.984	0.987	0.986	0.987
	Variation Ratio	**R1**	**R2**	**R3**	**R4**	**R5**	**R6**	**R7**	**R8**	**R9**	**R10**	**R11**	**R12**
	CRU	3.022	3.001	2.993	2.929	2.882	2.898	2.873	2.866	2.852	2.914	2.900	2.903
	UDEL	3.154	3.132	3.124	3.057	3.008	3.024	2.999	2.991	2.976	3.041	3.027	3.030
	NCAR	0.952	0.946	0.943	0.923	0.908	0.913	0.906	0.903	0.899	0.918	0.914	0.915
	RMSE (degree)	**R1**	**R2**	**R3**	**R4**	**R5**	**R6**	**R7**	**R8**	**R9**	**R10**	**R11**	**R12**
	CRU	3.658	3.826	3.320	3.511	3.863	3.341	4.265	4.458	4.291	4.057	4.396	4.157
	UDEL	4.067	4.233	3.690	3.904	4.247	3.705	4.693	4.882	4.691	4.457	4.796	4.536
	NCAR	1.405	1.444	1.278	1.564	1.665	1.517	1.791	1.842	1.800	1.882	1.977	1.904
	Bias (°C)	**R1**	**R2**	**R3**	**R4**	**R5**	**R6**	**R7**	**R8**	**R9**	**R10**	**R11**	**R12**
	CRU	-2.850	-3.111	-2.743	-2.864	-3.317	-2.845	-3.560	-3.819	-3.723	-3.463	-3.857	-3.656
	UDEL	-3.272	-3.540	-3.078	-3.205	-3.651	-3.130	-3.957	-4.225	-4.086	-3.791	-4.194	-3.969
	NCAR	-0.544	-0.595	-0.548	-1.089	-1.187	-1.111	-1.121	-1.164	-1.166	-1.441	-1.507	-1.471
	Number of Yellow Box	7	6	15	6	4	10	2	4	2	4	6	6

3.4. Future Projections for Changes in Climatology of the CORDEX-AUSTRALASIA Domain

In this section, the 4.6 version of the regional climate model RegCM is run with a hydrostatic option to produce 50 km resolution climate data for the CORDEX-Australasia domain after determining the most suitable parameters for the domain in the previous section. RegCM4.6 is forced with the initial and boundary conditions of the global climate models MPI-ESM-MR and HadGEM2-ES. Climate projections are realized under the optimistic (RCP4.5) and pessimistic or business-as-usual (RCP8.5) scenarios. Projected seasonal changes for mean temperature, minimum temperature, maximum temperature, and precipitation are mapped by analyzing for three different future periods (i.e., 2011 - 2040, 2041 - 2070, 2071 - 2099) concerning the 1971 - 2000 baseline period. Seasonal results are defined as follows: December - January - February (DJF), March - April - May (MAM), June - July - August (JJA), and September - October - November (SON).

3.4.1. Projected Changes in Mean Temperature

Under the RCP4.5 scenario, the results obtained with both HadGEM2-ES (HGE-4.5) and MPI-ESM-MR (MPI-4.5) show that the mean temperature changes for Australasia in the near term (2011 - 2040) compared to the reference period (1971 - 2000) foresees an average warming of 0.5 - 1 ℃ throughout the region for all four seasons (Figure 3.49 and Figure 3.50). When viewed seasonally, it is seen that warming will increase towards the north of 30°S latitude, especially in DJF and MAM. Compared to MPI-4.5, HGE-4.5 predicts more warming in northeast Australia in DJF, in southern Australia and Tasmania in MAM, in northwest Australia in JJA, and in large part of northern Australia in SON.

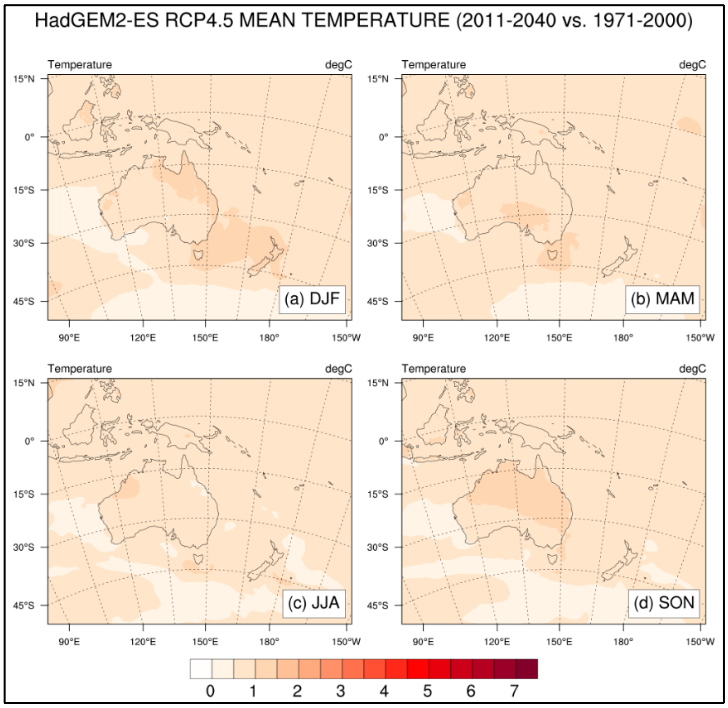

Figure 3.49. Projected changes in mean air temperature based on HadGEM2-ES driven RegCM4.6 under the RCP4.5 scenario for the period of 2011 - 2040 with respect to the reference period of 1971 - 2000: (a) December - January - February (DJF), (b) March - April - May (MAM), (c) June - July - August (JJA), and (d) September - October - November (SON) seasons.

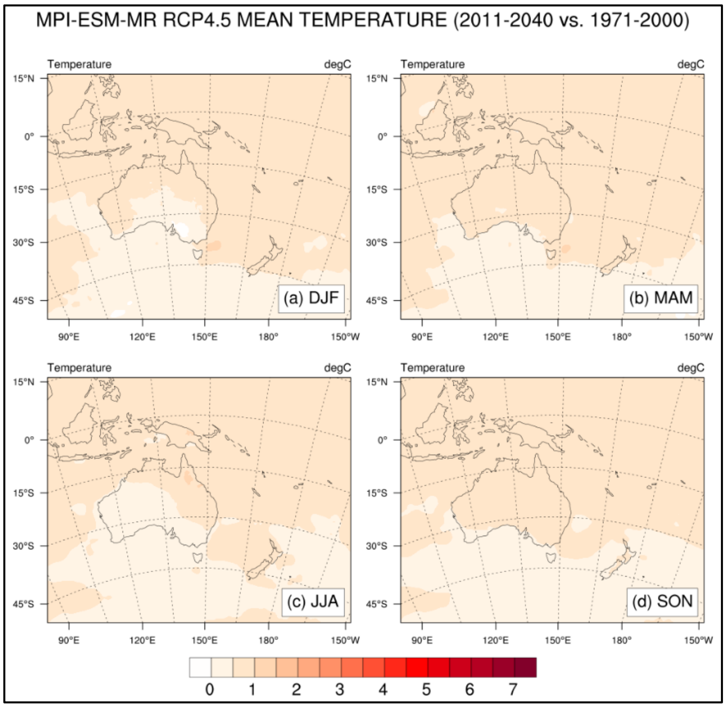

Figure 3.50. Projected changes in mean air temperature based on MPI-ESM-MR driven RegCM4.6 under the RCP4.5 scenario for the period of 2011 - 2040 with respect to the reference period of 1971 - 2000: (a) December - January - February (DJF), (b) March - April - May (MAM), (c) June - July - August (JJA), and (d) September - October - November (SON) seasons.

By looking at the change in mean temperature in the medium term (2041 - 2070), it is concluded that warming may reach an average of 1 - 1.5 °C which is higher than in the near term (Figure 3.51 and Figure 3.52). In this period, it is more evident that HGE-4.5 generally predicts more warming in the region than MPI-4.5. When both models are examined, warming in Tasmania and its surroundings during the summer-autumn period draws attention, especially according to HGE-4.5. Similarly, according to HGE-4.5 in all seasons and according to MPI-4.5 in all seasons except SON, it is expected that Micronesia and its surrounding area will be significantly warmer than other regions.

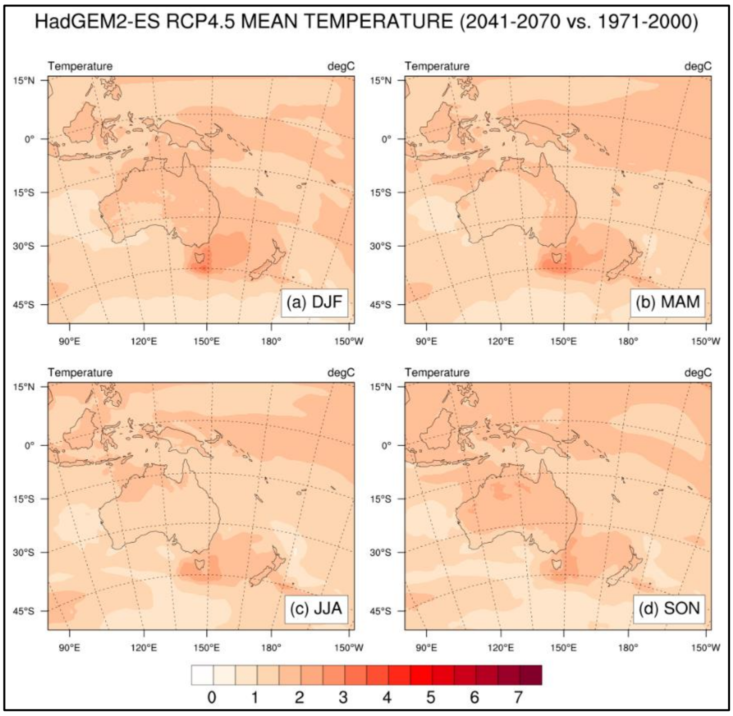

Figure 3.51. Projected changes in mean air temperature based on HadGEM2-ES driven RegCM4.6 under the RCP4.5 scenario for the period of 2041 - 2070 with respect to the reference period of 1971 - 2000: (a) December - January - February (DJF), (b) March - April - May (MAM), (c) June - July - August (JJA), and (d) September - October - November (SON) seasons.

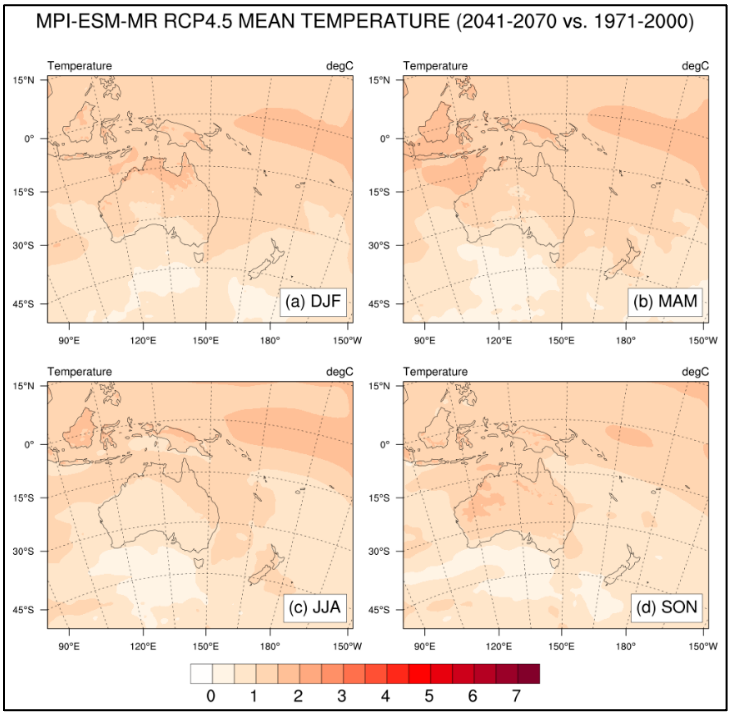

Figure 3.52. Projected changes in mean air temperature based on MPI-ESM-MR driven RegCM4.6 under the RCP4.5 scenario for the period of 2041 - 2070 with respect to the reference period of 1971 - 2000: (a) December - January - February (DJF), (b) March - April - May (MAM), (c) June - July - August (JJA), and (d) September - October - November (SON) seasons.

Under the RCP4.5 scenario, it is seen that according to MPI-4.5, temperature increases of up to 2 °C in the Australasia region in the long term (2071 -2099) may be around 3 °C according to HGE-4.5 (Figure 3.53 and Figure 3.54). Although the expected temperature increase in mean temperatures shows values similar to that in the medium term, the rise in the range of 1 - 1.5 °C according to MPI-4.5 and generally in the range of 1.5 - 4 °C according to HGE-4.5 in the medium term is expected to be around 2 °C according to MPI-4.5 and 3 °C according to HGE-4.5 at the end of the century. The expectation for an increase in mean temperature at the end of the century may be slightly higher in HGE-4.5 compared to MPI-4.5 in all four seasons for the whole region.

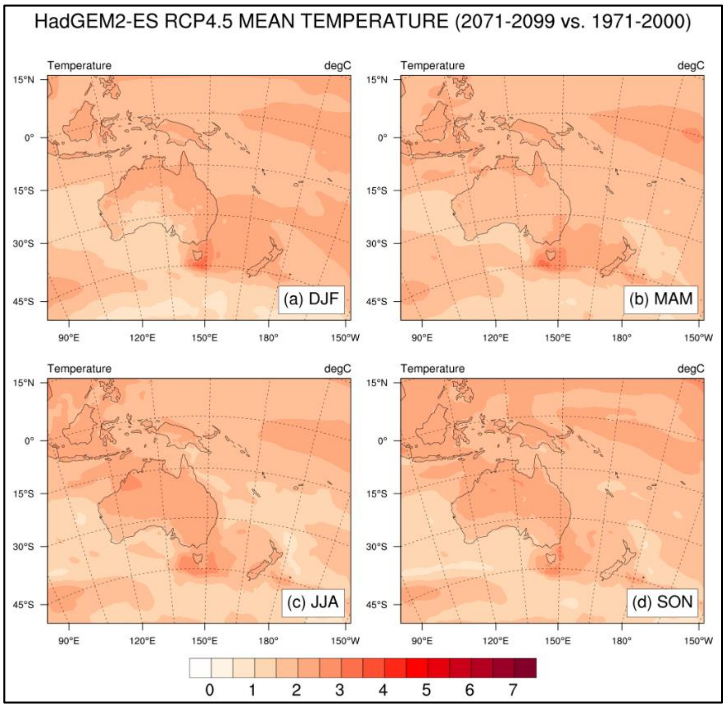

Figure 3.53. Projected changes in mean air temperature based on HadGEM2-ES driven RegCM4.6 under the RCP4.5 scenario for the period of 2071 - 2099 with respect to the reference period of 1971 - 2000: (a) December - January - February (DJF), (b) March - April - May (MAM), (c) June - July - August (JJA), and (d) September - October - November (SON) seasons.

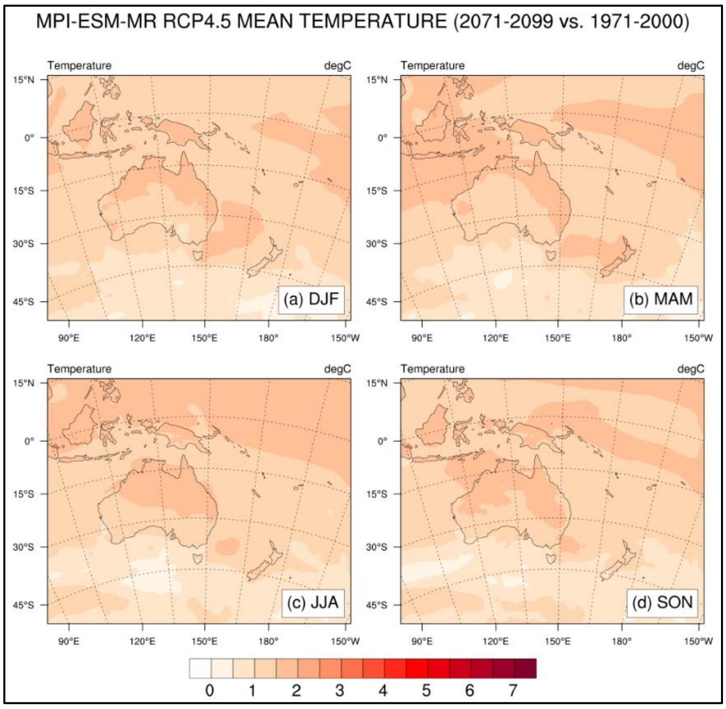

Figure 3.54. Projected changes in mean air temperature based on MPI-ESM-MR driven RegCM4.6 under the RCP4.5 scenario for the period of 2071 - 2099 with respect to the reference period of 1971 - 2000: (a) December - January - February (DJF), (b) March - April - May (MAM), (c) June - July - August (JJA), and (d) September - October - November (SON) seasons.

When the changes in mean temperatures are analyzed under the RCP8.5 scenario, it is seen that both models give similar results for the region and season in the near term (Figure 3.55 and Figure 3.56). In the near term, it can be said that the expectation of a temperature increase of about 1 ℃ in the HadGEM2-ES model (HGE-8.5), compared to the MPI-ESM-MR model (MPI-8.5), may increase a little more, especially in the DJF and MAM seasons and reach 2 ℃. According to HGE-8.5, the northern part of Australia in the summer and spring seasons of the southern hemisphere, the eastern part of Australia in the autumn season, and the western part of Australia in the winter season will be warmer than the other regions. Similarly, according to MPI-8.5, the temperature increase will become more evident in northeastern Australia in autumn and winter and in southeast Australia in spring. Besides, according to HGE-8.5, it seems that the warming will be higher along the Pacific Ocean in the northeastern part of the Australasia domain in MAM.

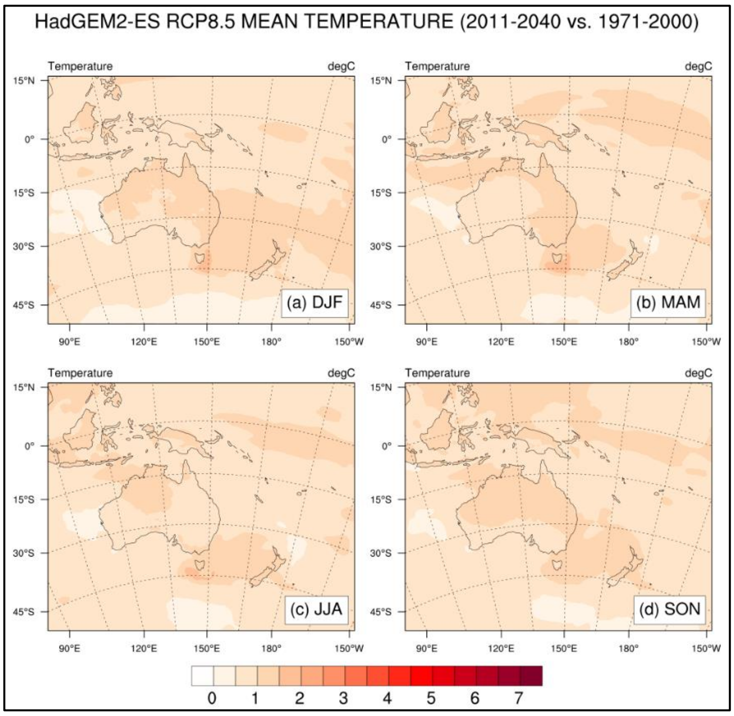

Figure 3.55. Projected changes in mean air temperature based on HadGEM2-ES driven RegCM4.6 under the RCP8.5 scenario for the period of 2011 - 2040 with respect to the reference period of 1971 - 2000: (a) December - January - February (DJF), (b) March - April - May (MAM), (c) June - July - August (JJA), and (d) September - October - November (SON) seasons.

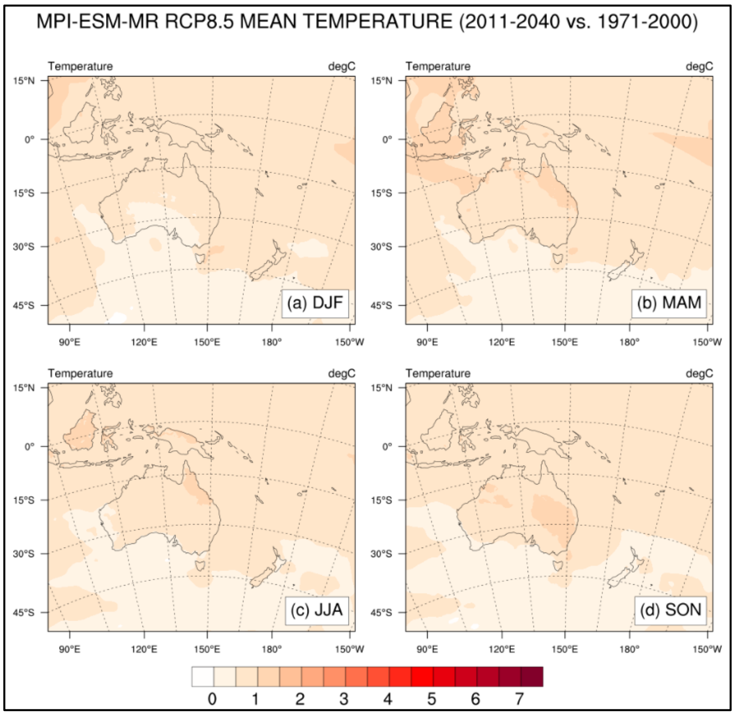

Figure 3.56. Projected changes in mean air temperature based on MPI-ESM-MR driven RegCM4.6 under the RCP8.5 scenario for the period of 2011 - 2040 with respect to the reference period of 1971 - 2000: (a) December - January - February (DJF), (b) March - April - May (MAM), (c) June - July - August (JJA), and (d) September - October - November (SON) seasons.

It is predicted that the mean temperature increase in Australasia in the medium term will be slightly higher in the near term (Figure 3.57 adn Figure 3.58). By considering both models, it can be said that the increases expected to be 2 ℃ on average will be higher in the HGE-8.5 model compared to MPI-8.5 and may reach 3.5 ℃. According to HGE-8.5, the temperature increase in Tasmania and its surroundings is remarkable in all four seasons. In both models, it is observed that the warming in the Australasia region will be more significant as we approach the equatorial region compared to the southern regions.

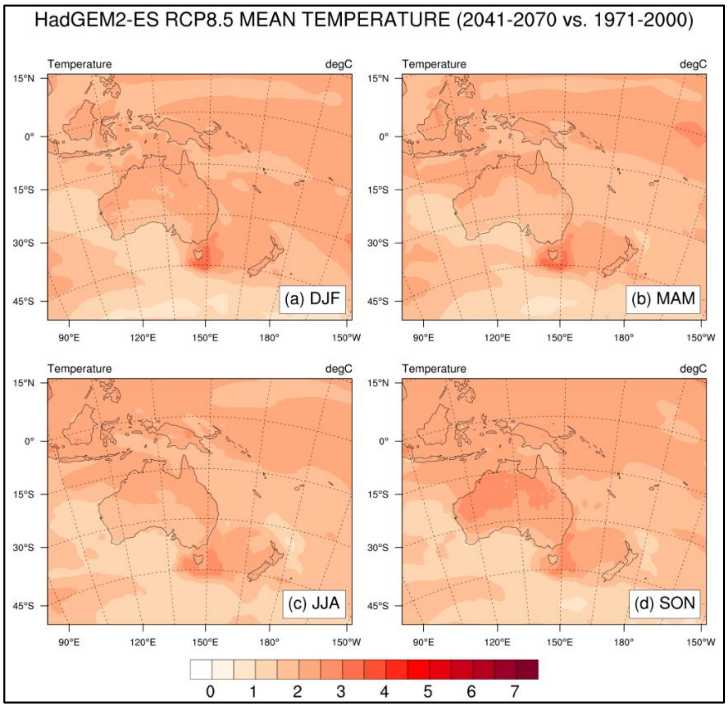

Figure 3.57. Projected changes in mean air temperature based on HadGEM2-ES driven RegCM4.6 under the RCP8.5 scenario for the period of 2041 - 2070 with respect to the reference period of 1971 - 2000: (a) December - January - February (DJF), (b) March - April - May (MAM), (c) June - July - August (JJA), and (d) September - October - November (SON) seasons.

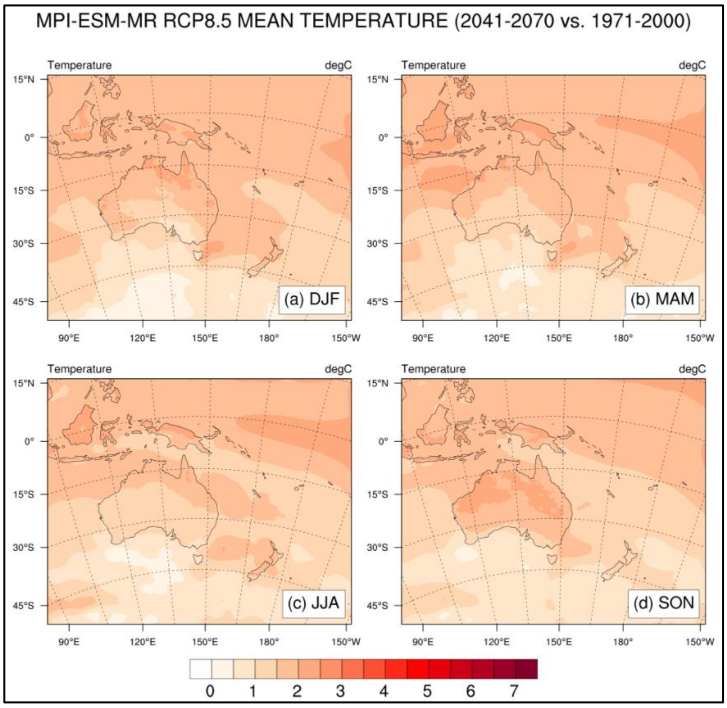

Figure 3.58. Projected changes in mean air temperature based on MPI-ESM-MR driven RegCM4.6 under the RCP8.5 scenario for the period of 2041 - 2070 with respect to the reference period of 1971 - 2000: (a) December - January - February (DJF), (b) March - April - May (MAM), (c) June - July - August (JJA), and (d) September - October - November (SON) seasons.

According to the RCP8.5 scenario, it is evident that the expected increase in the mean temperature values of Australasia in the long term will be higher compared to other periods (Figure 3.59 and Figure 3.60). By considering the region and season in general, it can be emphasized that the increases expected to be an average of 2.5 ℃, according to MPI-8.5, will increase more than 3 ℃ according to HGE-8.5. Furthermore, they may even reach 5 ℃ and above. Again, it is seen that the increase in DJF and MAM seasons may be slightly higher than in other seasons. According to HGE-8.5, the significant temperature increase in Tasmania and its surroundings in summer and autumn is similarly noticeable on the east coast of Papua New Guinea in winter. According to MPI-8.5, the temperature increase in Indonesia and its surroundings is more evident for all seasons than other regions.

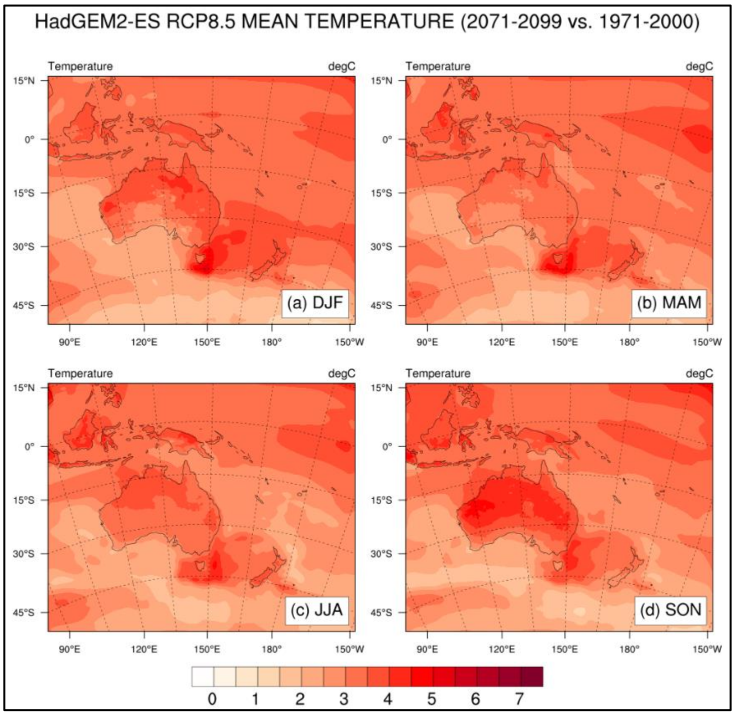

Figure 3.59. Projected changes in mean air temperature based on HadGEM2-ES driven RegCM4.6 under the RCP8.5 scenario for the period of 2071 - 2099 with respect to the reference period of 1971 - 2000: (a) December - January - February (DJF), (b) March - April - May (MAM), (c) June - July - August (JJA), and (d) September - October - November (SON) seasons.

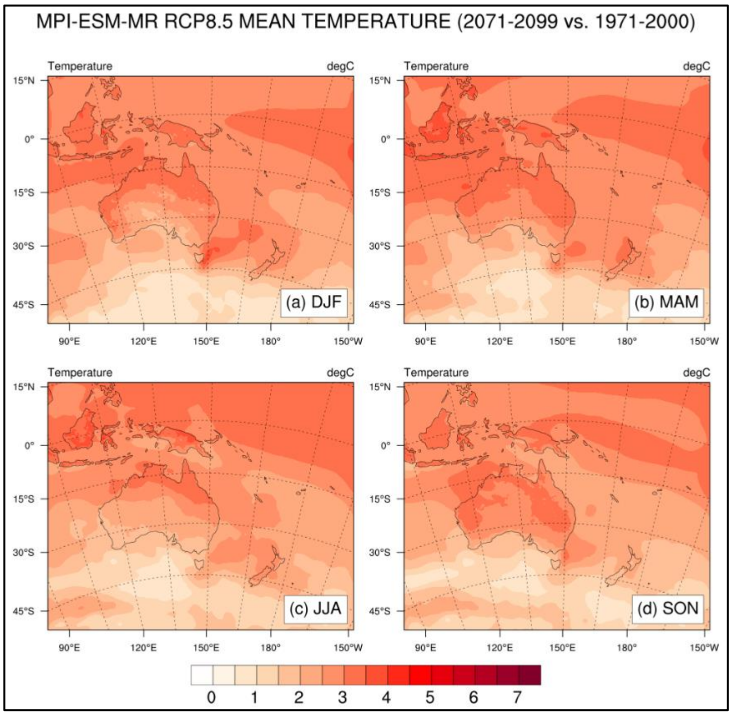

Figure 3.60. Projected changes in mean air temperature based on MPI-ESM-MR driven RegCM4.6 under the RCP8.5 scenario for the period of 2071 - 2099 with respect to the reference period of 1971 - 2000: (a) December - January - February (DJF), (b) March - April - May (MAM), (c) June - July - August (JJA), and (d) September - October - November (SON) seasons.

According to the dynamic downscaling results using the RegCM4.6 regional climate model, the mean temperatures for the CORDEX-Australasia domain will increase by at least about 1 ℃ in the future based on the optimistic scenario. This temperature increase may reach almost 3 ℃ in some seasons and places. In the pessimistic scenario, it is seen that the mean temperature increases of 1 to 3 ℃ across the region may reach 5 ℃ and slightly above towards the end of the century. According to the comparison of two global models based on RegCM4.6 as forcing data, the results of the model run with the HadGEM2-ES model predict a higher temperature increase compared to the model results run with the MPI-ESM-MR. The expected warming in all seasons is particularly striking in the southern hemisphere's summer and autumn seasons. In addition, the seasonally changing temperature increase of different regions of Australia will affect countries such as New Zealand, Papua New Guinea, and Indonesia, as well as small island countries in the sub-regions of Oceania, divided into Micronesia, Melanesia, and Polynesia, depending on the warming on the Pacific Ocean. In addition, it is clear that the warming, which intensifies as we move from the optimistic to the pessimistic scenario, will increase a lot as the end of the century approaches.

3.4.2. Projected Changes in Minimum Temperature

It is predicted that the minimum temperatures in the Australasia region may increase by 0.5 - 3 ℃ in the near future (Figure 3.61 and Figure 3.62). According to MPI-4.5, considering all seasons in the region, it is seen that the increase expected to be 0.5 - 1 ℃ can be predominantly 1 degree and above compared to HGE-4.5. It can be said that the increase in minimum temperatures, as in the case with mean temperatures, is more noticeable on the north of 30°S latitude. According to HGE-4.5, it is observed that the warming approaching 1.5 ℃ in the southern half of Australia in MAM will spread to the whole continent in the SON. Again, according to HGE-4.5, the minimum temperature increase on Papua New Guinea in DJF is also at these levels. According to MPI-4.5, the warming, which shows a more homogeneous spatial distribution in all four seasons, will reach 1.5 ℃ in JJA in the northeast of Australia.

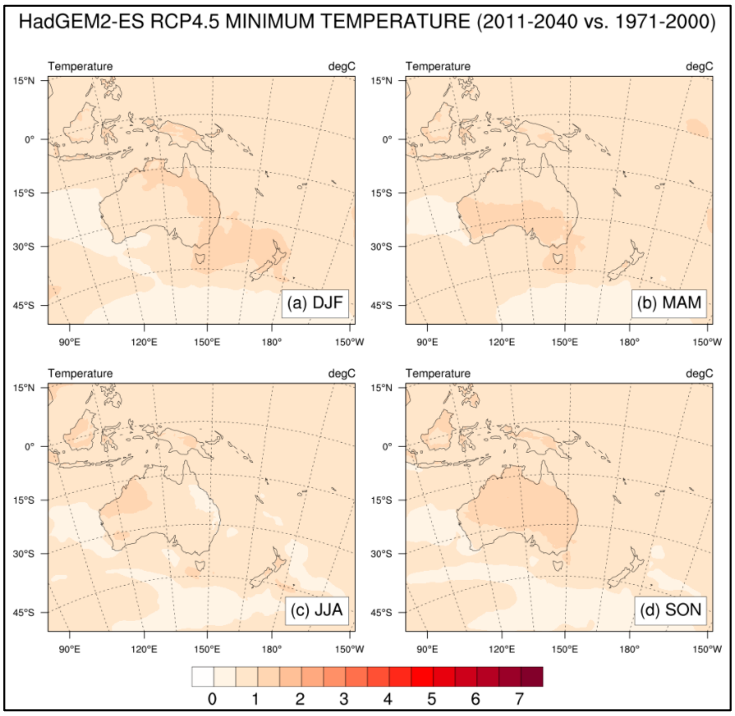

Figure 3.61. Projected changes in minimum air temperature based on HadGEM2-ES driven RegCM4.6 under the RCP4.5 scenario for the period of 2011 - 2040 with respect to the reference period of 1971 - 2000: (a) December - January - February (DJF), (b) March - April - May (MAM), (c) June - July - August (JJA), and (d) September - October - November (SON) seasons.

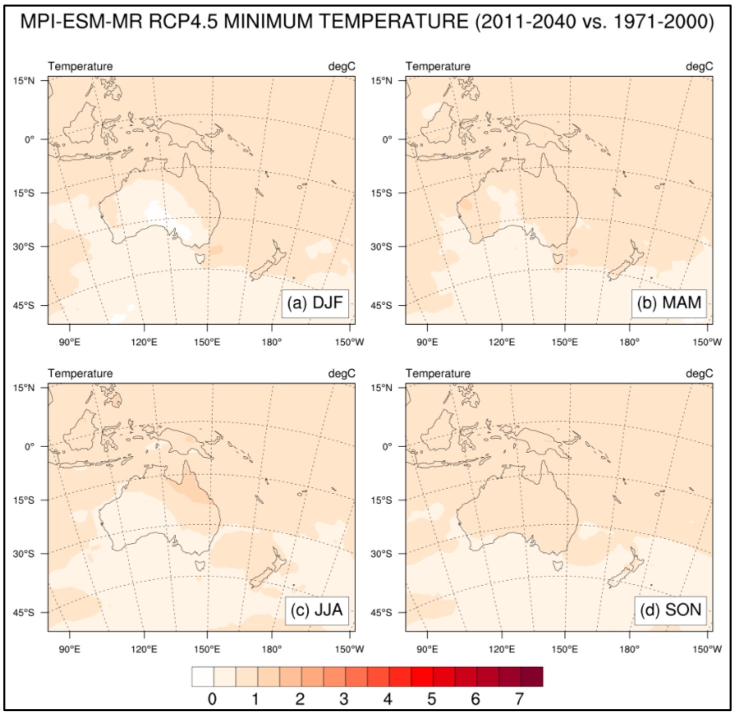

Figure 3.62. Projected changes in minimum air temperature based on MPI-ESM-MR driven RegCM4.6 under the RCP4.5 scenario for the period of 2011 - 2040 with respect to the reference period of 1971 - 2000: (a) December - January - February (DJF), (b) March - April - May (MAM), (c) June - July - August (JJA), and (d) September - October - November (SON) seasons.

From the results of both models, it is obvious that when we move from the near future to not too far future, the minimum temperature increases rise a little more (Figure 3.63 and Figure 3.64). It is seen that the minimum temperature increases in the near future may increase from 1 - 1.5 °C to 3 °C, especially compared to HGE-4.5. According to HGE-4.5, the minimum temperature increases over Australia, New Zealand, Papua New Guinea, and Indonesia will predominate in the range of 2.5 - 3 °C, especially during the DJF, MAM, and SON seasons. According to the MPI-4.5, it is expected that the minimum temperatures in most of Papua New Guinea will increase by approximately 3 °C during the summer and autumn seasons. Again, according to MPI-4.5, it is seen that the warming in the Indonesia islands, especially Borneo, can be around 2 °C in MAM.

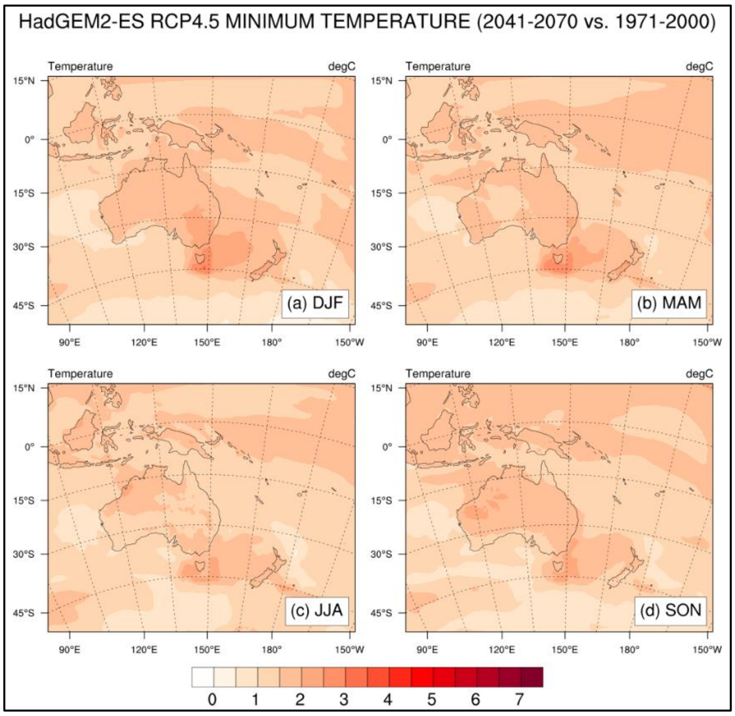

Figure 3.63. Projected changes in minimum air temperature based on HadGEM2-ES driven RegCM4.6 under the RCP4.5 scenario for the period of 2041 - 2070 with respect to the reference period of 1971 - 2000: (a) December - January - February (DJF), (b) March - April - May (MAM), (c) June - July - August (JJA), and (d) September - October - November (SON) seasons.

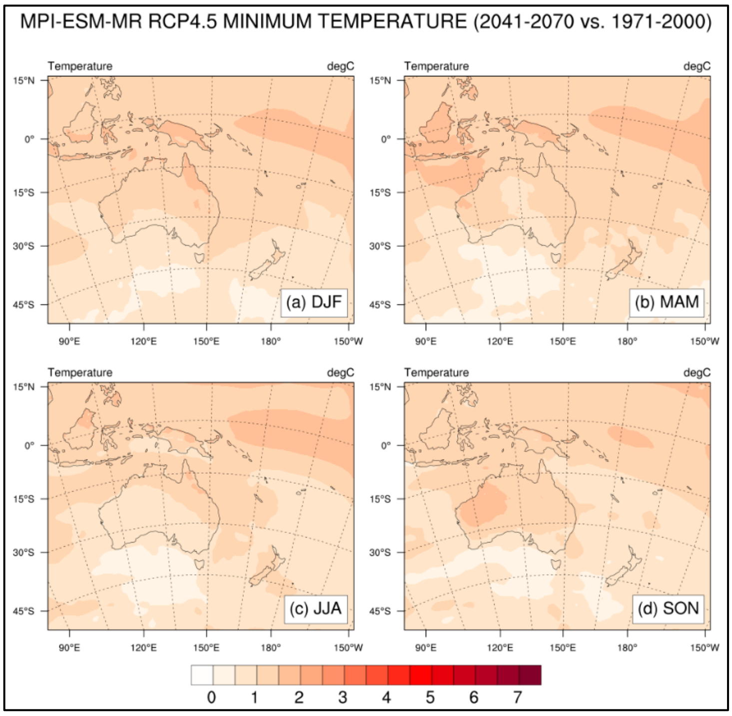

Figure 3.64. Projected changes in minimum air temperature based on MPI-ESM-MR driven RegCM4.6 under the RCP4.5 scenario for the period of 2041 - 2070 with respect to the reference period of 1971 - 2000: (a) December - January - February (DJF), (b) March - April - May (MAM), (c) June - July - August (JJA), and (d) September - October - November (SON) seasons.

When it comes to the last quarter of the century, it can be said that the spatial distribution of the high-temperature increase in the minimum temperature may expand a little more (Figure 3.65 and Figure 3.66). According to HGE-4.5, it is seen that the expectation of increase, which is generally 3 °C, may find 3.5 °C in some places (e.g., Tasmania and its surroundings in DJF and MAM). Again, according to HGE-4.5, the temperature increase in the western parts of Australia in JJA may rise to 3 °C and above. According to MPI-4.5, temperature increases of 2 - 2.5 °C are expected in DJF and MAM along with the north-northeast-east parts of Australia.

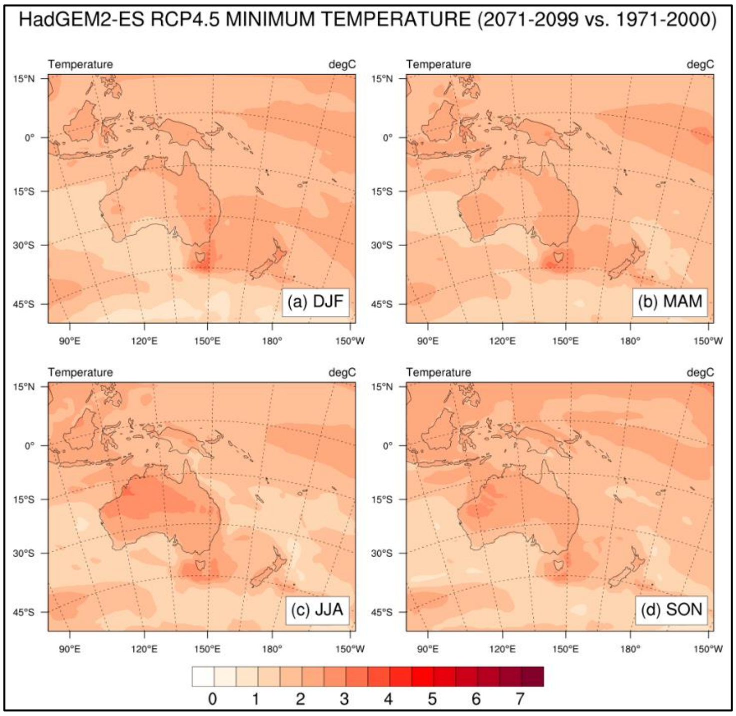

Figure 3.65. Projected changes in minimum air temperature based on HadGEM2-ES driven RegCM4.6 under the RCP4.5 scenario for the period of 2071 - 2099 with respect to the reference period of 1971 - 2000: (a) December - January - February (DJF), (b) March - April - May (MAM), (c) June - July - August (JJA), and (d) September - October - November (SON) seasons.

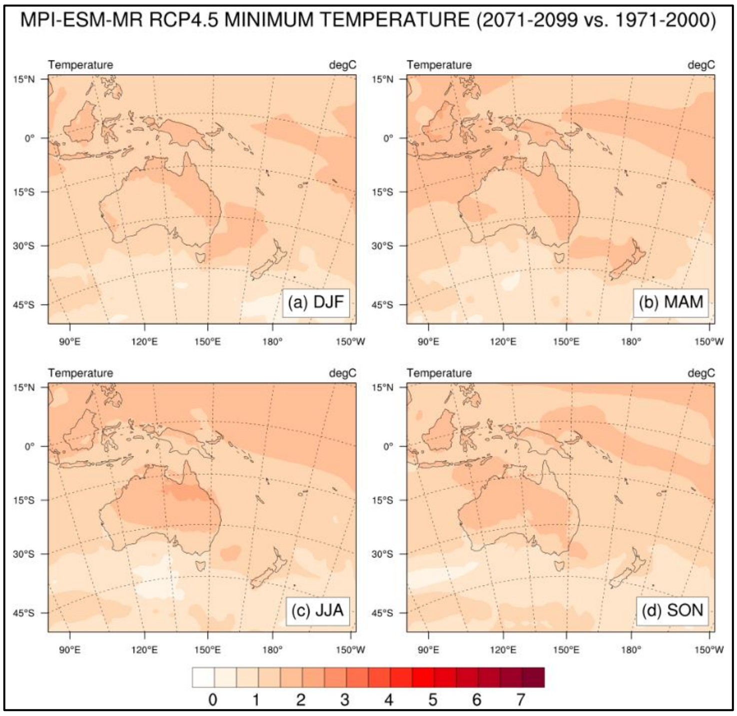

Figure 3.66. Projected changes in minimum air temperature based on MPI-ESM-MR driven RegCM4.6 under the RCP4.5 scenario for the period of 2071 - 2099 with respect to the reference period of 1971 - 2000: (a) December - January - February (DJF), (b) March - April - May (MAM), (c) June - July - August (JJA), and (d) September - October - November (SON) seasons.

According to the RCP8.5 scenario, it is expected that the minimum temperatures in Australasia will generally increase by around 1℃ in the near future (Figure 3.67 and Figure 3.68). According to HGE-8.5, it is seen that an increase of 2 ℃ in the South Pacific Ocean in DJF can show its effect towards the equatorial region, especially in MAM. According to HGE-8.5, approximately 2 ℃ of warming will be seen in entire Papua New Guinea during DJF and MAM seasons. On the other hand, according to MPI-8.5, the northeastern parts of Australia in MAM and JJA are expected to be slightly warmer than other regions. According to MPI-8.5, it is striking that with the high warming in the Tasman Sea, the minimum temperature increases (being more visible in DJF) in New Zealand will be higher.

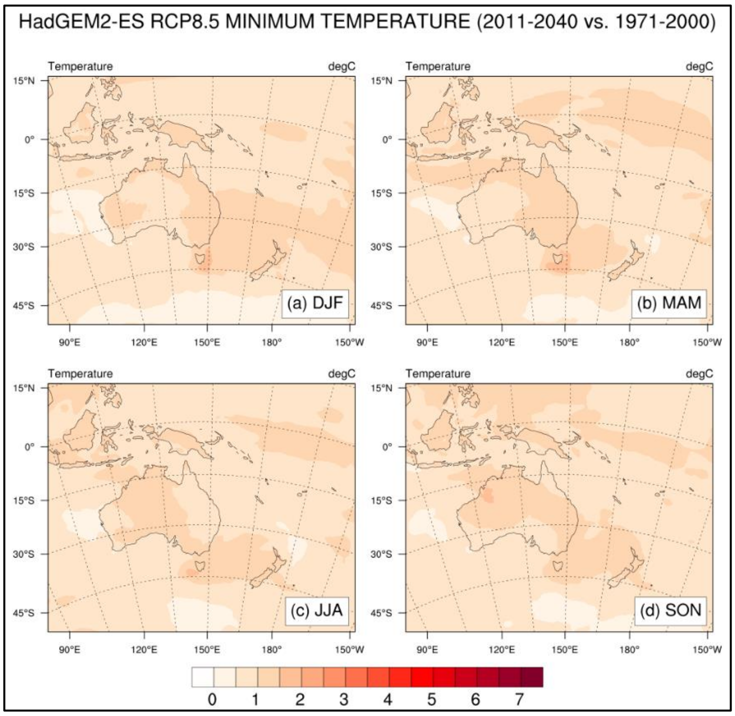

Figure 3.67. Projected changes in minimum air temperature based on HadGEM2-ES driven RegCM4.6 under the RCP8.5 scenario for the period of 2011 - 2040 with respect to the reference period of 1971 - 2000: (a) December - January - February (DJF), (b) March - April - May (MAM), (c) June - July - August (JJA), and (d) September - October - November (SON) seasons.

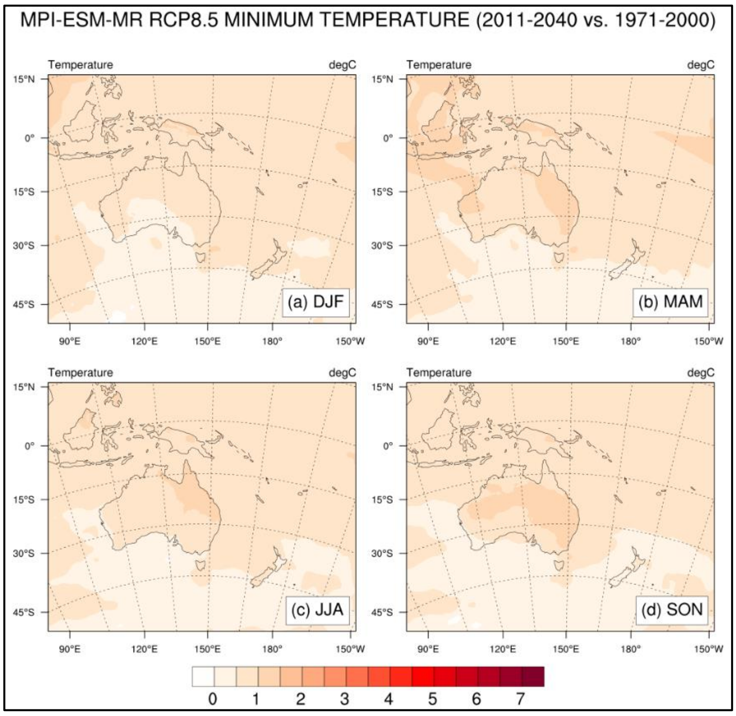

Figure 3.68. Projected changes in minimum air temperature based on MPI-ESM-MR driven RegCM4.6 under the RCP8.5 scenario for the period of 2011 - 2040 with respect to the reference period of 1971 - 2000: (a) December - January - February (DJF), (b) March - April - May (MAM), (c) June - July - August (JJA), and (d) September - October - November (SON) seasons.

By considering the change in the minimum temperatures in the medium term, it can be said that 1.5 - 2 °C increases will prevail in the Australasia domain throughout all four seasons (Figure 3.69 and Figure 3.70). According to HGE-8.5, there may be an increase of up to 3.5 °C around Tasmania, especially in DJF and MAM. According to the MPI-8.5 model, while the warming in Queensland, Australia is slightly higher in summer and winter than in other parts of the country, the minimum temperature increase is more noticeable in DJF and MAM over Indonesia and Papua New Guinea.

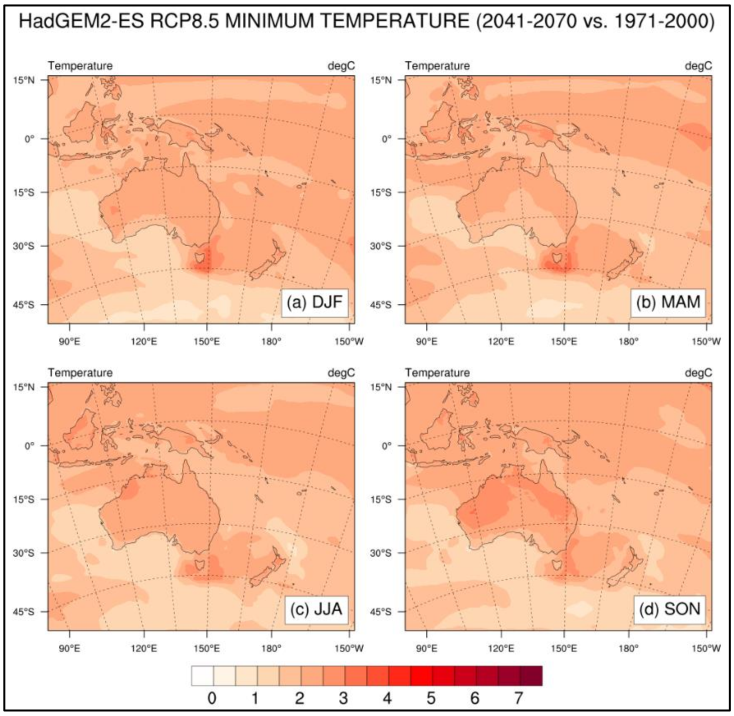

Figure 3.69. Projected changes in minimum air temperature based on HadGEM2-ES driven RegCM4.6 under the RCP8.5 scenario for the period of 2041 - 2070 with respect to the reference period of 1971 - 2000: (a) December - January - February (DJF), (b) March - April - May (MAM), (c) June - July - August (JJA), and (d) September - October - November (SON) seasons.

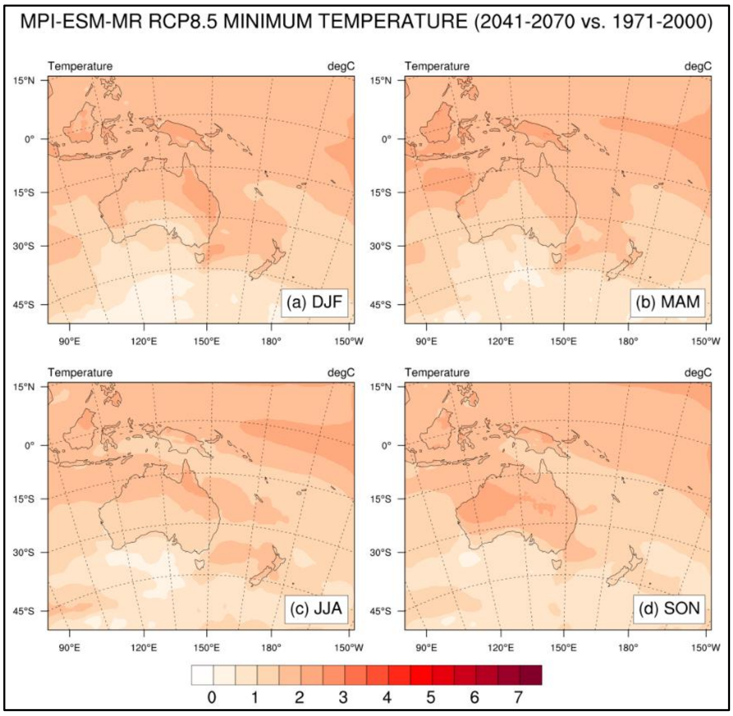

Figure 3.70. Projected changes in minimum air temperature based on MPI-ESM-MR driven RegCM4.6 under the RCP8.5 scenario for the period of 2041 - 2070 with respect to the reference period of 1971 - 2000: (a) December - January - February (DJF), (b) March - April - May (MAM), (c) June - July - August (JJA), and (d) September - October - November (SON) seasons.

When the projection results for Australasia are examined, it can be said that the increase in minimum temperatures will be seen much more in the far future in the region (Figure 3.71 and Figure 3.72). While the temperature increases according to MPI-8.5 may be 4 °C and above throughout the region, it is apparent that it may be 5 °C and above compared to HGE-8.5. For example, it can be seen that the minimum temperature increase in the western and inland parts of the Western Australia territory can exceed 5 °C in the spring season. According to the results of HGE-8.5, in addition to the warming in Tasmania and its surroundings in all four seasons, the warming in the northwest of Australia in JJA and in the west of Australia in SON is more obvious than in other regions. According to the MPI-8.5, while the north of the Australian continent will warm more noticeably in JJA, the northern island of New Zealand will warm more in DJF.

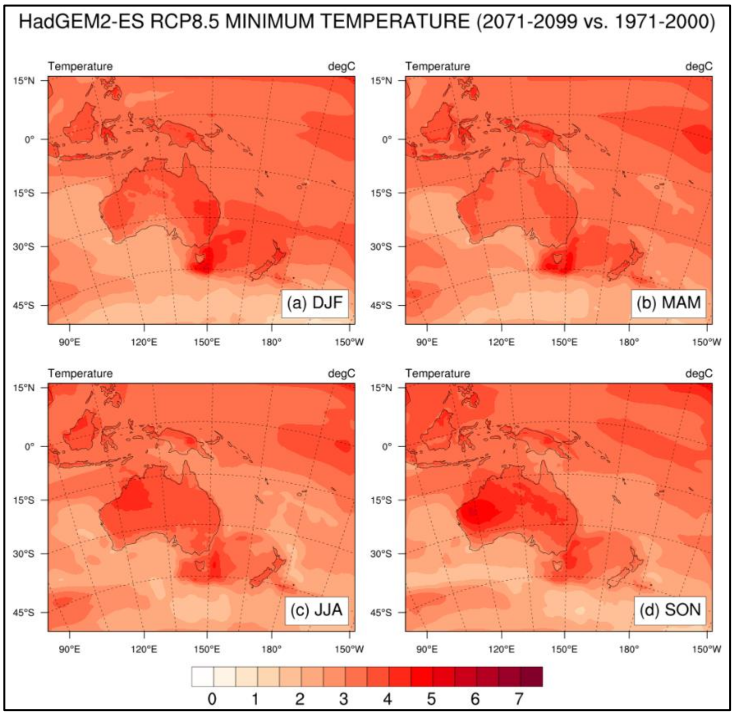

Figure 3.71. Projected changes in minimum air temperature based on HadGEM2-ES driven RegCM4.6 under the RCP8.5 scenario for the period of 2071 - 2099 with respect to the reference period of 1971 - 2000: (a) December - January - February (DJF), (b) March - April - May (MAM), (c) June - July - August (JJA), and (d) September - October - November (SON) seasons.

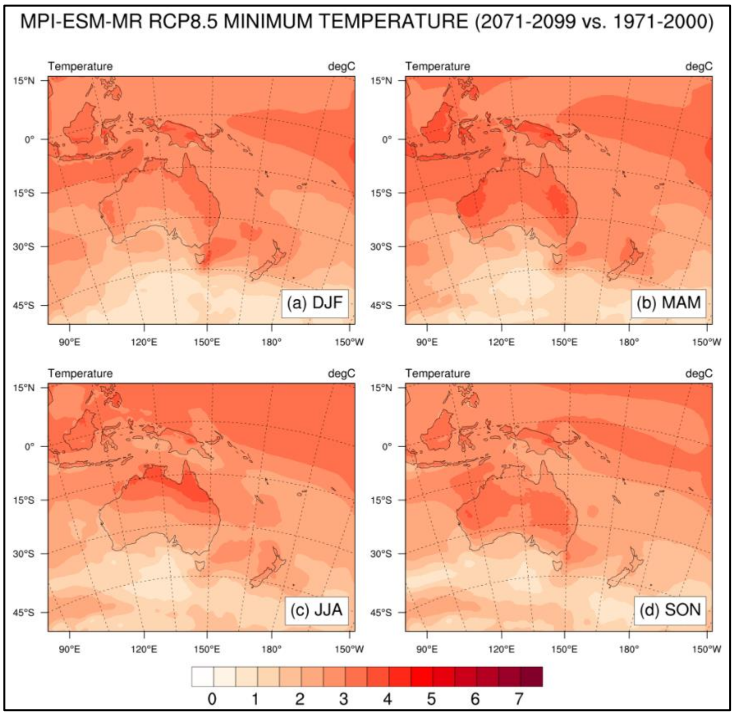

Figure 3.72. Projected changes in minimum air temperature based on MPI-ESM-MR driven RegCM4.6 under the RCP8.5 scenario for the period of 2071 - 2099 with respect to the reference period of 1971 - 2000: (a) December - January - February (DJF), (b) March - April - May (MAM), (c) June - July - August (JJA), and (d) September - October - November (SON) seasons.

Dynamic downscaling results using the RegCM4.6 regional climate model show that the minimum temperatures for the CORDEX-Australasia domain will increase by an average of 1 - 2 ℃ in the future due to the optimistic scenario. This temperature increase may increase up to 3 ℃ and above in some seasons and places. In the pessimistic scenario, it is predicted that the expected minimum temperature increases in the range of 1 - 3 ℃ across the region may exceed 3 ℃ and rise above 5 ℃ towards the end of the century. According to the comparison of two global models based on RegCM4.6 as forcing data, the results of the model run with the HadGEM2-ES model predict a greater increase in minimum temperatures compared to the results of the MPI-ESM-MR model. When considered seasonally, the increase in DJF and MAM seasons is slightly higher than in JJA and SON seasons. In addition, the minimum temperature increases will be higher, both as we move from the optimistic to the pessimistic scenario and as the time progresses from the near future to the distant future.

3.4.3. Projected Changes in Maximum Temperature

According to the RCP4.5 scenario, it is predicted that the maximum temperatures for Australasia in the near term may increase in the region of 0.5 - 1 ℃ (Figure 3.73 and Figure 3.74). According to HGE-4.5, it is seen that the maximum temperature increases in the Tasmania Sea in DJF, Tasmania in MAM, and in SON in northern Australia may be 1.5 ℃ and above. Again, according to HGE-4.5, DJF will experience a maximum temperature increase to exceed 1.5 ℃ in northern Borneo and Mindanao (Southern Philippines). According to MPI-4.5, it can be said that the increase in maximum temperatures shows a more homogeneous pattern for the Australasia domain for all four seasons.

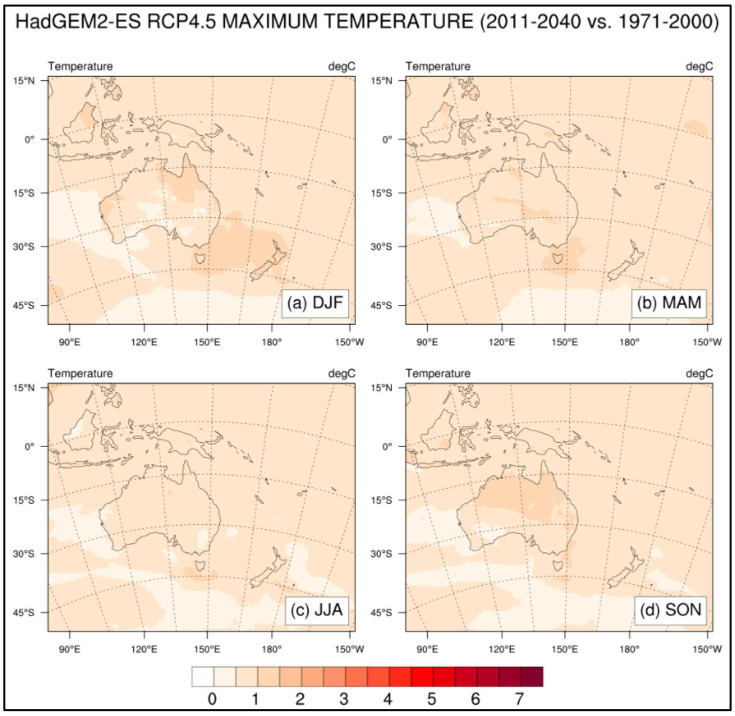

Figure 3.73. Projected changes in maximum air temperature based on HadGEM2-ES driven RegCM4.6 under the RCP4.5 scenario for the period of 2011 - 2040 with respect to the reference period of 1971 - 2000: (a) December - January - February (DJF), (b) March - April - May (MAM), (c) June - July - August (JJA), and (d) September - October - November (SON) seasons.

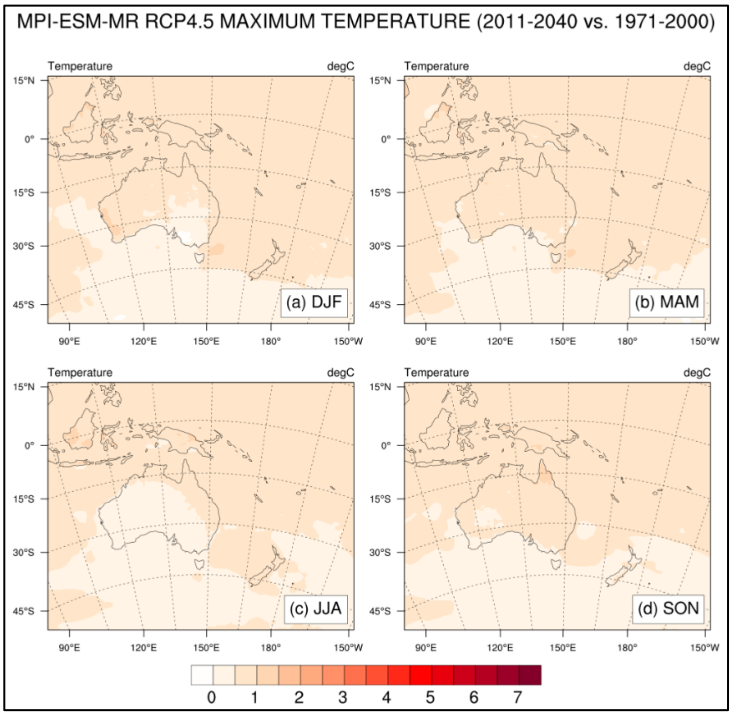

Figure 3.74. Projected changes in maximum air temperature based on MPI-ESM-MR driven RegCM4.6 under the RCP4.5 scenario for the period of 2011 - 2040 with respect to the reference period of 1971 - 2000: (a) December - January - February (DJF), (b) March - April - May (MAM), (c) June - July - August (JJA), and (d) September - October - November (SON) seasons.

It is seen that the increase in maximum temperatures may increase a little more in the medium term and reach at least 1 - 1.5 ℃ seasonally and spatially (Figure 3.75 and Figure 3.76). According to HGE-4.5, while the expected increase in DJF and MAM in Tasmania and its surroundings may exceed 3 ℃ and above, an average of 3 ℃ is expected towards the North Pacific Ocean. According to MPI-4.5, it can be said that the expectation of warming around 2.5 ℃ at maximum temperatures in DJF, MAM, and JJA seasons along the equatorial region east of 150°E longitude can be seen in JJA on the northeast coast of Papua New Guinea. Also, during the JJA season, the maximum temperature rise in Australia's north-northeast coasts may be slightly higher than in other parts of the continent.

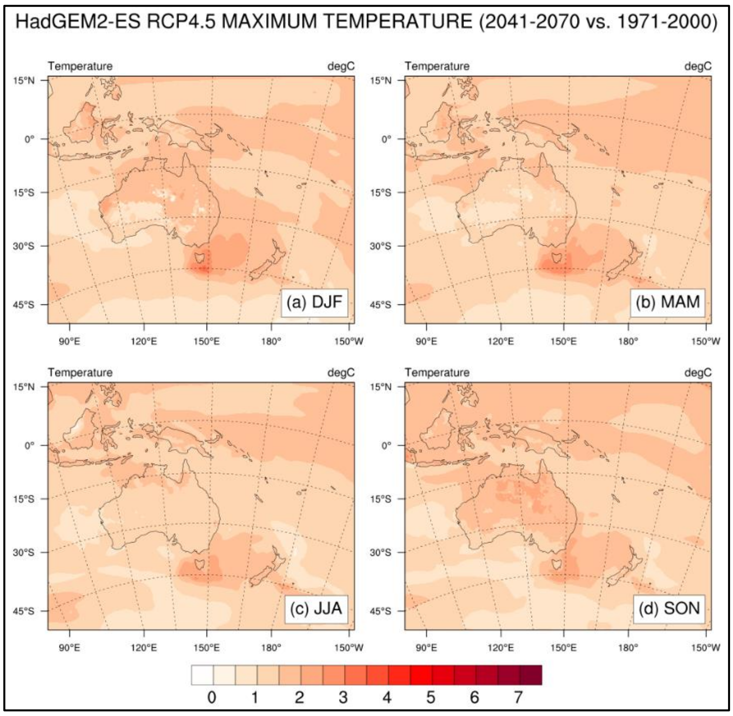

Figure 3.75. Projected changes in maximum air temperature based on HadGEM2-ES driven RegCM4.6 under the RCP4.5 scenario for the period of 2041 - 2070 with respect to the reference period of 1971 - 2000: (a) December - January - February (DJF), (b) March - April - May (MAM), (c) June - July - August (JJA), and (d) September - October - November (SON) seasons.

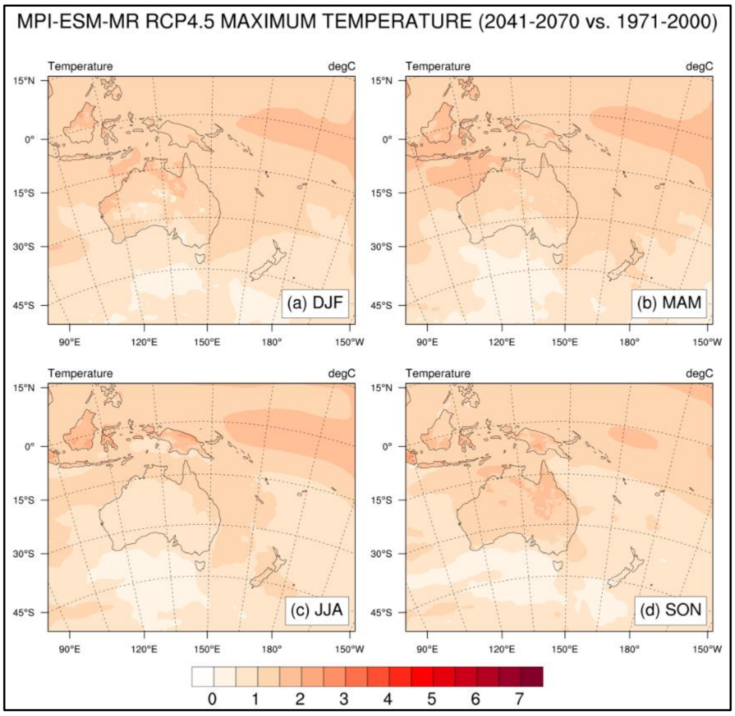

Figure 3.76. Projected changes in maximum air temperature based on MPI-ESM-MR driven RegCM4.6 under the RCP4.5 scenario for the period of 2041 - 2070 with respect to the reference period of 1971 - 2000: (a) December - January - February (DJF), (b) March - April - May (MAM), (c) June - July - August (JJA), and (d) September - October - November (SON) seasons.

It is seen that the maximum temperature increase in the long term may be slightly higher compared to the other two periods (Figure 3.77 and Figure 3.78). It can be said that the average warming of 1 - 2 °C shows a more heterogeneous pattern in both models. According to HGE-4.5, the regions where warming is most noticeable are Tasmania and its surroundings as well as the DJF's north of Borneo in all four seasons, and much less warming is expected in southwest Australia in the DJF. According to MPI-4.5, the predicted warming in the north of Australia is higher in all four seasons than other areas of the continent. Again, according to MPI-4.5, it is concluded that the expected increase in maximum temperatures will be slightly higher in the northern hemisphere of the Australasia domain in JJA, i.e., north of the equator line.

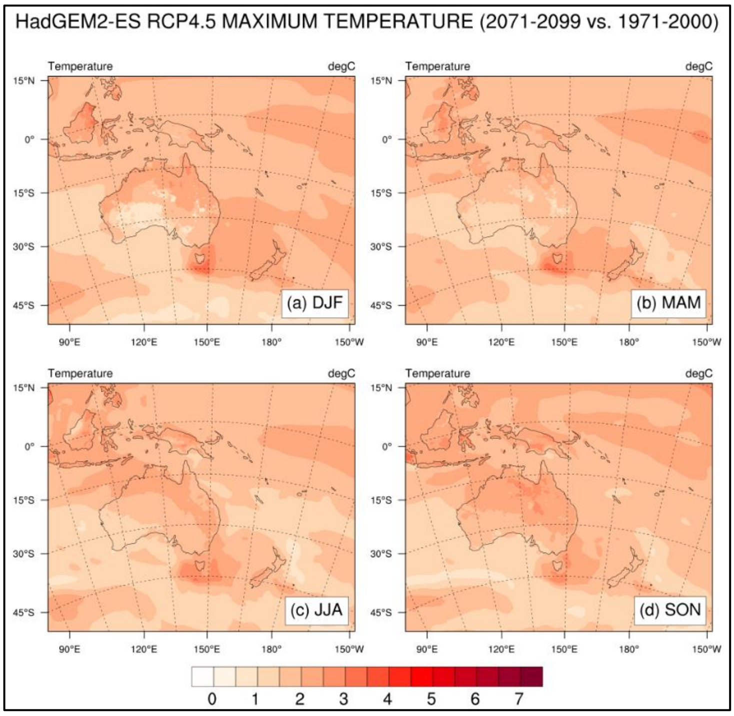

Figure 3.77. Projected changes in maximum air temperature based on HadGEM2-ES driven RegCM4.6 under the RCP4.5 scenario for the period of 2071 - 2099 with respect to the reference period of 1971 - 2000: (a) December - January - February (DJF), (b) March - April - May (MAM), (c) June - July - August (JJA), and (d) September - October - November (SON) seasons.

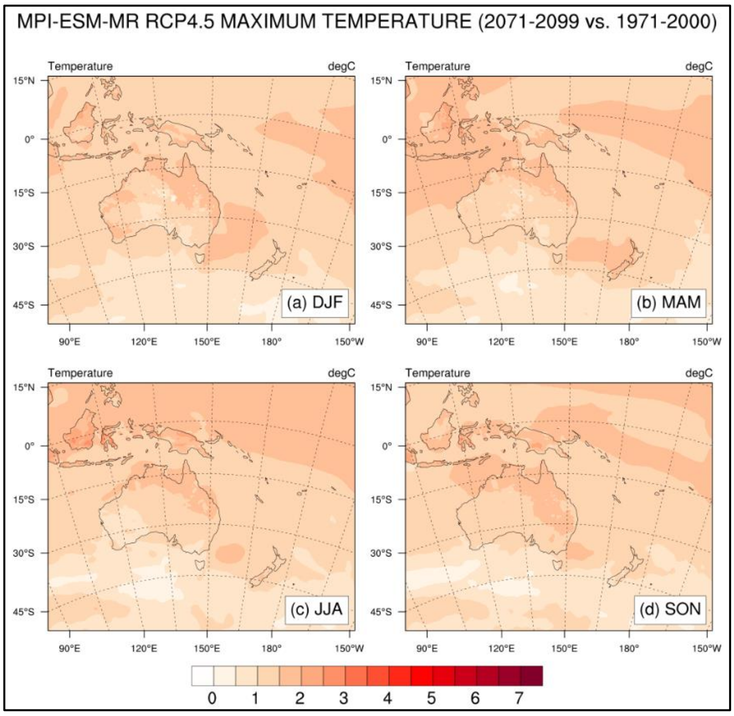

Figure 3.78. Projected changes in maximum air temperature based on MPI-ESM-MR driven RegCM4.6 under the RCP4.5 scenario for the period of 2071 - 2099 with respect to the reference period of 1971 - 2000: (a) December - January - February (DJF), (b) March - April - May (MAM), (c) June - July - August (JJA), and (d) September - October - November (SON) seasons.

Based on the RCP8.5 scenario, a minimum 0.5 - 1 ℃ temperature increase is expected at maximum temperatures in the near term (Figure 3.79 and Figure 3.80). The HGE-8.5 model states that the heating amount will be slightly higher than MPI-8.5. According to HGE-8.5, it is noteworthy that the maximum temperature increase will be higher in DJF between Australia and New Zealand at the Coral Sea and the Tasman Sea. It seems that this overheating will be more noticeable on the Tasman Sea in the other three seasons. It is also clear that the maximum temperature increase, which is predicted to be slightly above 0.5 ℃ throughout the season and region, according to the MPI-8.5, may be slightly more in southeast Australia in the SON.

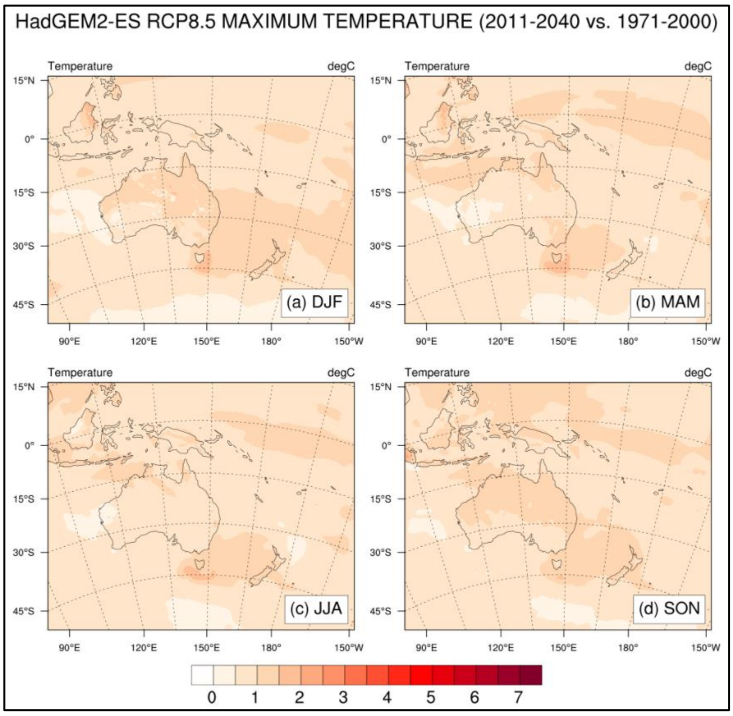

Figure 3.79. Projected changes in maximum air temperature based on HadGEM2-ES driven RegCM4.6 under the RCP8.5 scenario for the period of 2011 - 2040 with respect to the reference period of 1971 - 2000: (a) December - January - February (DJF), (b) March - April - May (MAM), (c) June - July - August (JJA), and (d) September - October - November (SON) seasons.

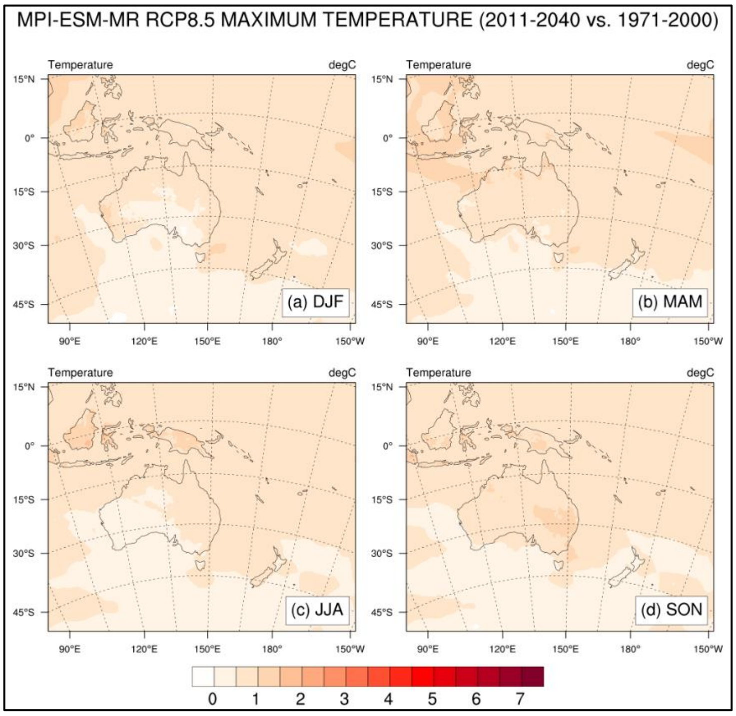

Figure 3.80. Projected changes in maximum air temperature based on MPI-ESM-MR driven RegCM4.6 under the RCP8.5 scenario for the period of 2011 - 2040 with respect to the reference period of 1971 - 2000: (a) December - January - February (DJF), (b) March - April - May (MAM), (c) June - July - August (JJA), and (d) September - October - November (SON) seasons.

It is seen that the maximum temperature increases may rise a little more (i.e., 1.5 - 2 °C) in the medium term (Figure 3.81 and Figure 3.82). The warming in and around Tasmania is slightly higher than HGE-8.5, and especially in DJF and MAM seasons, this warming is slightly higher than in the other two seasons. According to the MPI-8.5, warming is significantly higher in the regions north of 30°S latitude. Warming is a bit more noticeable than in other seasons, especially in JJA in the islands of Indonesia and Papua New Guinea.

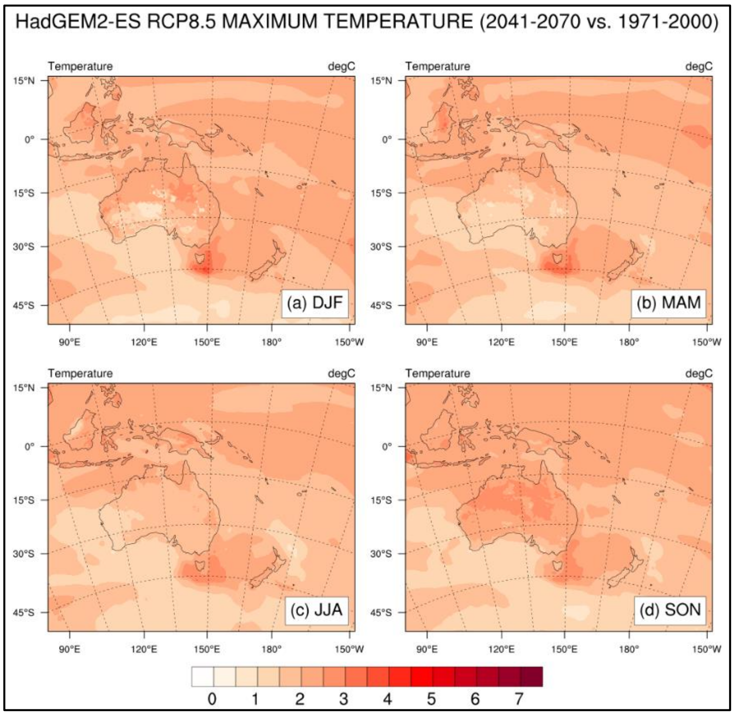

Figure 3.81. Projected changes in maximum air temperature based on HadGEM2-ES driven RegCM4.6 under the RCP8.5 scenario for the period of 2041 - 2070 with respect to the reference period of 1971 - 2000: (a) December - January - February (DJF), (b) March - April - May (MAM), (c) June - July - August (JJA), and (d) September - October - November (SON) seasons.

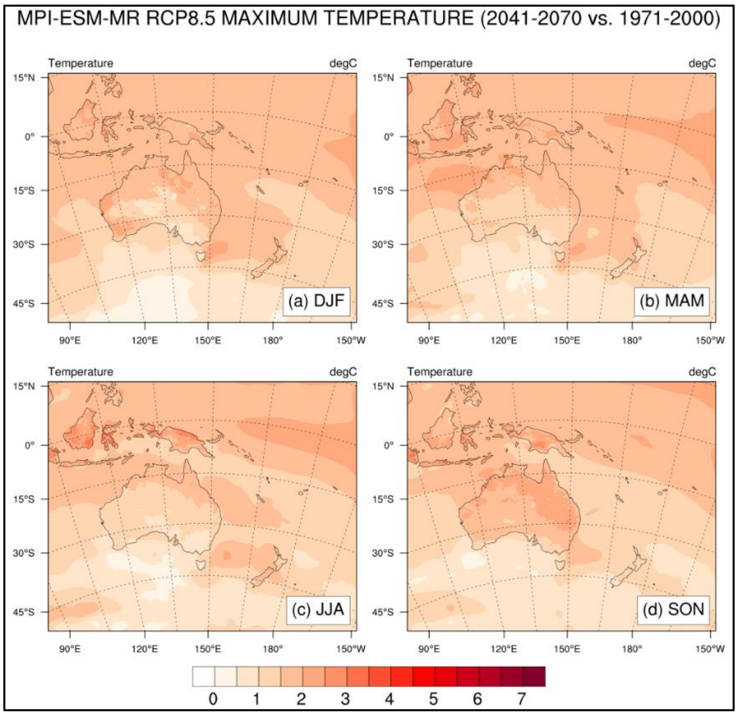

Figure 3.82. Projected changes in maximum air temperature based on MPI-ESM-MR driven RegCM4.6 under the RCP8.5 scenario for the period of 2041 - 2070 with respect to the reference period of 1971 - 2000: (a) December - January - February (DJF), (b) March - April - May (MAM), (c) June - July - August (JJA), and (d) September - October - November (SON) seasons.

By the end of the century, it is clear that the expectation of an increase in maximum temperatures will reach its highest values (Figure 3.83 and Figure 3.84), just like the mean temperature and minimum temperatures. It can also be said that the increase, which is expected to be 2.5 - 3 °C on average and can reach 7 °C, may be higher for the HGE-8.5 model than the MPI-8.5 model. It is estimated that the expected high-temperature increase for all four seasons may become most apparent in Australia in summer and spring seasons, especially according to HGE-8.5. In autumn and winter, the northern parts of Australia will experience higher maximum temperatures than the southern parts. According to MPI-8.5, a similar situation may be in question for Australia, and while the maximum temperature increase in Indonesia and Papua New Guinea islands in the north of the Australia continent is more striking, it can be said that this increase will become more explicit, especially in JJA and SON seasons.

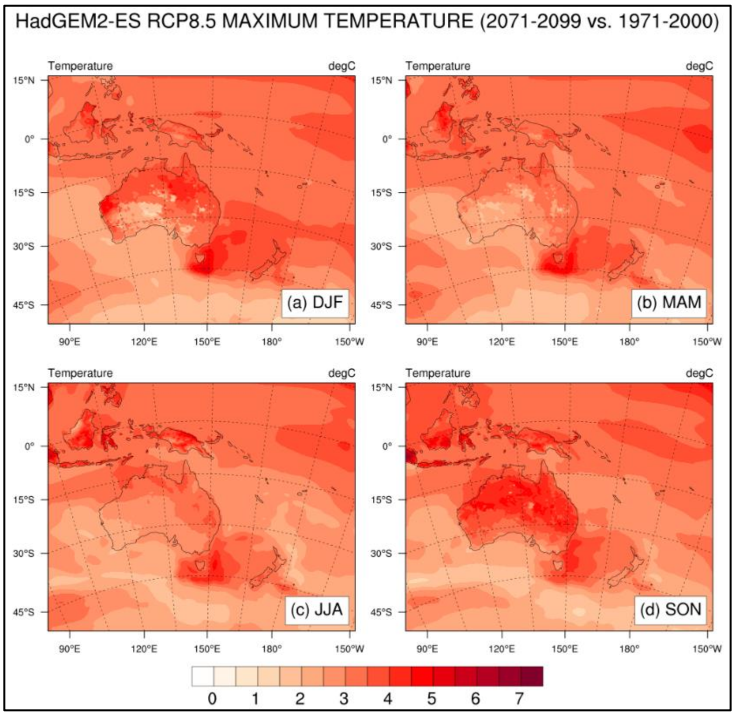

Figure 3.83. Projected changes in maximum air temperature based on HadGEM2-ES driven RegCM4.6 under the RCP8.5 scenario for the period of 2071 - 2099 with respect to the reference period of 1971 - 2000: (a) December - January - February (DJF), (b) March - April - May (MAM), (c) June - July - August (JJA), and (d) September - October - November (SON) seasons.

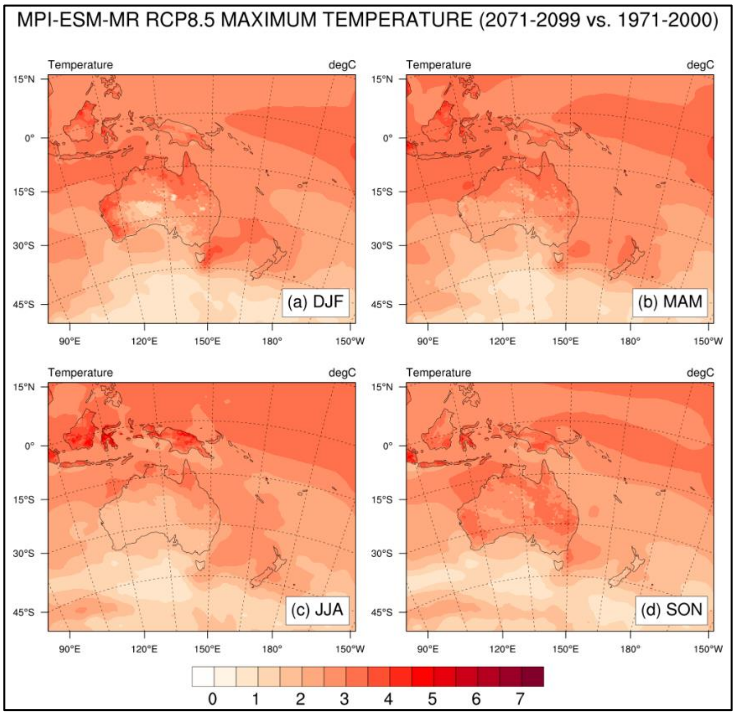

Figure 3.84. Projected changes in maximum air temperature based on MPI-ESM-MR driven RegCM4.6 under the RCP8.5 scenario for the period of 2071 - 2099 with respect to the reference period of 1971 - 2000: (a) December - January - February (DJF), (b) March - April - May (MAM), (c) June - July - August (JJA), and (d) September - October - November (SON) seasons.

It is anticipated that there will be a trend of increasing maximum temperatures in the future for the Australasia domain, as is the predicted change in mean temperatures and minimum temperatures. The expectation of an increase of at least 0.5 - 1 ℃ may increase to 7 ℃, depending on the area and time. It is seen that this expected increase for all four seasons may be slightly higher in DJF and MAM seasons. Again, in line with other predictions, it is seen that there is a spatial distribution in such a way that the expected increase in maximum temperatures will be slightly higher as time goes from the near term to the long term. In terms of comparing the two models, it should be noted that the maximum temperature increase is predicted to be higher in HGE than MPI, as in the other two variables.

3.4.4. Projected Changes in Precipitation

By considering all four seasons, according to the RCP4.5 scenario, it is seen that precipitation in Australasia will increase or decrease by 20 % compared to the previous period in the near term (Figure 3.85 and Figure 3.86). According to HGE-4.5, the expected increase (about 20 %) in DJF in the northwest and southeast regions of Australia is likely to be seen as a decrease at the same rate by the MAM season. In JJA, an increase in precipitation of up to 50 % is expected on the western coasts of Australia neighboring the Indian Ocean. Again, according to HGE-4.5, there may be an increase in precipitation of up to 50 % in the equatorial region in four seasons. The increase in precipitation at the level of 20 % in Papua New Guinea in DJF and New Zealand in JJA is also noteworthy. According to the MPI-4.5, a decrease in precipitation that can reach 35 % in the inner part of Australia in DJF and an increase in precipitation that can reach up to 50 % in the north-northeastern parts of Australia in JJA are predicted. In JJA, precipitation reductions of up to 50 % in the southern islands of Indonesia, as well as the expected 20 % reductions in most of Australia over four seasons, are also worth noting. Again, according to MPI-4.5, it is predicted that the precipitation will decrease by more than 50 % in the middle region of Pacific Ocean.

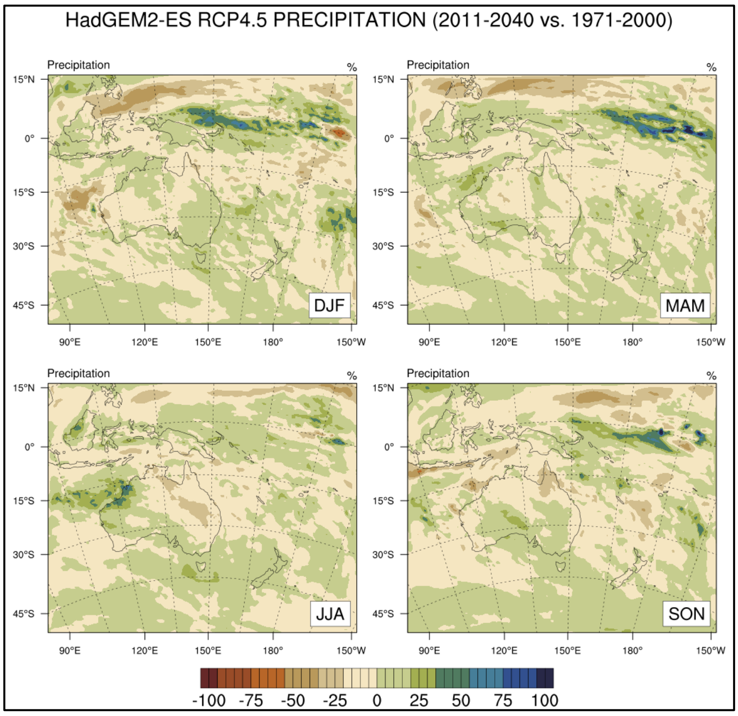

Figure 3.85. Projected changes in total precipitation based on HadGEM2-ES driven RegCM4.6 under the RCP4.5 scenario for the period of 2011 - 2040 with respect to the reference period of 1971 - 2000: (a) December - January - February (DJF), (b) March - April - May (MAM), (c) June - July - August (JJA), and (d) September - October - November (SON) seasons.

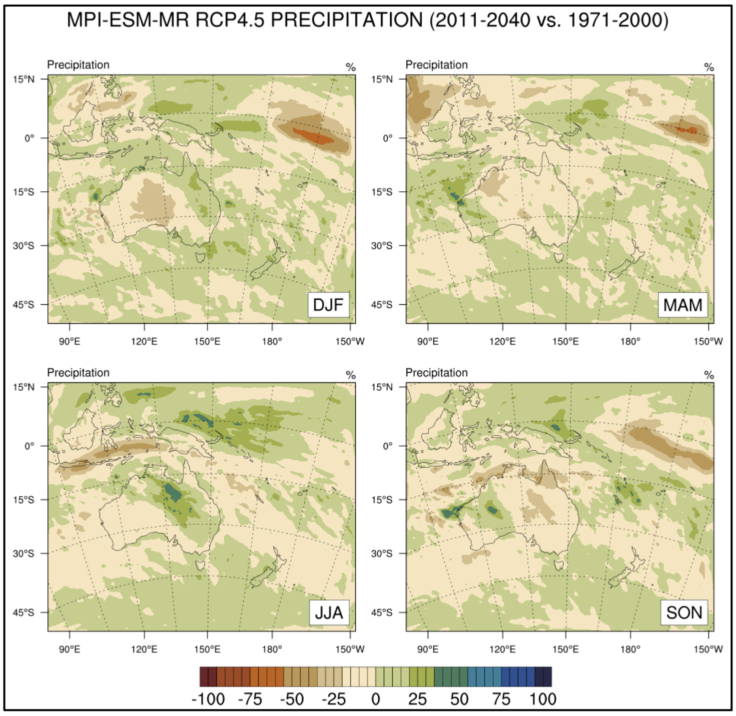

Figure 3.86. Projected changes in total precipitation based on MPI-ESM-MR driven RegCM4.6 under the RCP4.5 scenario for the period of 2011 - 2040 with respect to the reference period of 1971 - 2000: (a) December - January - February (DJF), (b) March - April - May (MAM), (c) June - July - August (JJA), and (d) September - October - November (SON) seasons.

When the medium-term change maps in the amount of precipitation are examined, the spatial distribution of the increase or decrease rates varies depending on the season and model, as in the short-term change (Figure 3.87 and Figure 3.88). Although increases and decreases of 20 % are predominantly dominant in both models, it can be said that excessive decrease and excessive increases will be at a higher level in the medium term compared to the short term. According to HGE-4.5, the expectation of a decrease of up to 75 % in the north of the equator in DJF can be seen as an increase in the same proportion towards 15°N latitude. In the same season, precipitation increase that may reach 20 % in the south of Australia may approach 100 % in the northwest of Australia in JJA. Again, according to HGE-4.5, the expected decrease of up to 50 % in the northeast of Australia stands out in the SON. The most striking part of the MPI-4.5 is the expectation of an increase of 100 % in the mid-Pacific Ocean off the northeast of Papua New Guinea in all four seasons. On the other hand, it is predicted that precipitation in the seas known as the Java Sea, the Banda Sea, the Arafura Sea, and the Timor Sea in the region between Australia and Papua New Guinea and Indonesia in JJA is expected to decrease by 60 %. Also, precipitation in the south of 30°S latitude will increase predominantly by 20 % in all four seasons.

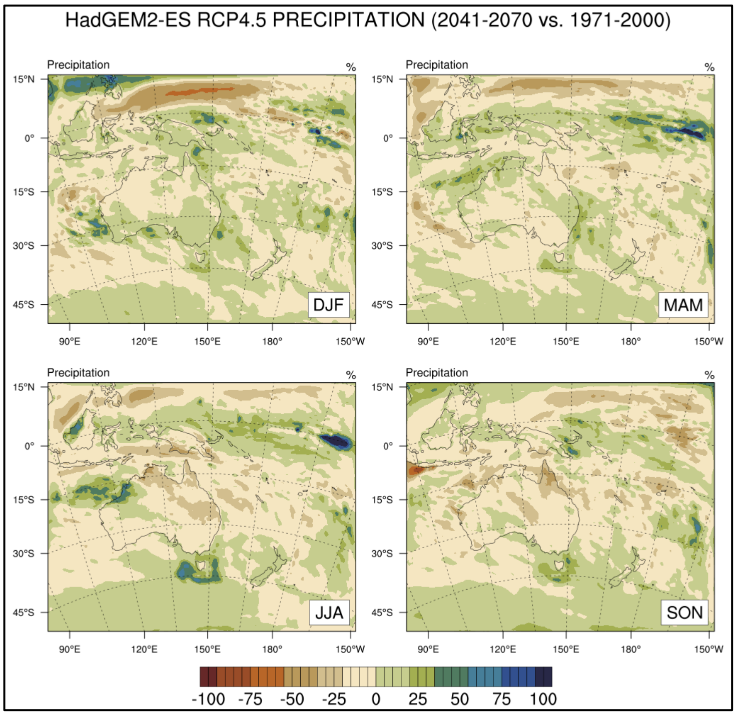

Figure 3.87. Projected changes in total precipitation based on HadGEM2-ES driven RegCM4.6 under the RCP4.5 scenario for the period of 2041 - 2070 with respect to the reference period of 1971 - 2000: (a) December - January - February (DJF), (b) March - April - May (MAM), (c) June - July - August (JJA), and (d) September - October - November (SON) seasons.

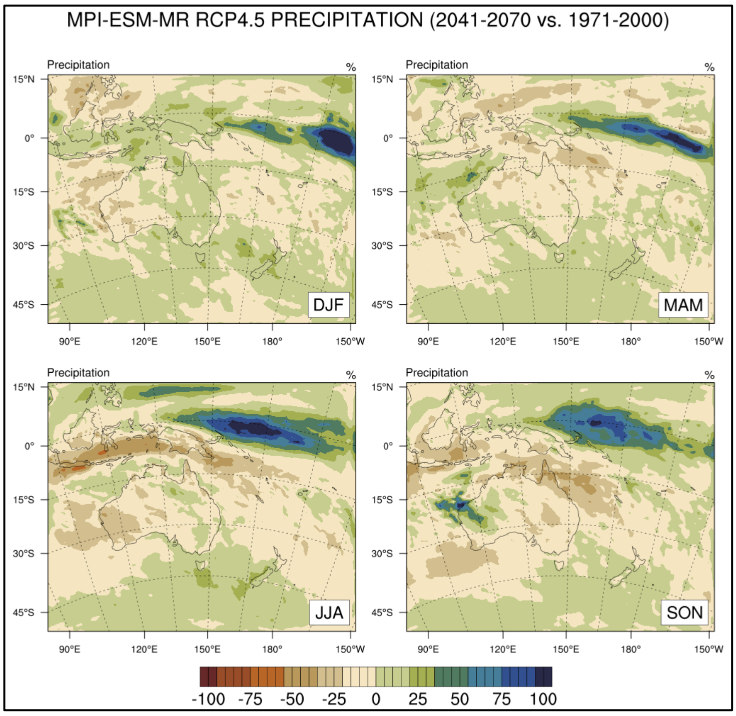

Figure 3.88. Projected changes in total precipitation based on MPI-ESM-MR driven RegCM4.6 under the RCP4.5 scenario for the period of 2041 - 2070 with respect to the reference period of 1971 - 2000: (a) December - January - February (DJF), (b) March - April - May (MAM), (c) June - July - August (JJA), and (d) September - October - November (SON) seasons.

Just as in the near- and medium-term precipitation changes, it can be said that according to the optimistic scenario, the long-term precipitation change for Australasia also varies seasonally and spatially (Figure 3.89 and Figure 3.90). Although both model simulations for all four seasons predict an increase and decrease of precipitation around 20 %, it can be stated that the increases and decreases in some regions show a similar pattern as in the previous periods, and the amount of change is higher. For example, according to HGE-4.5, an increase of 100 % is expected in the area extending along the equator between longitudes 150°E - 150°W. This increase is expected to become more severe in the SON, DJF, JJA, MAM seasons, respectively, and to spread to a broader area in MAM. In addition, decreases in the DJF and MAM seasons are predicted to reach 50 - 75 % levels north of the equator. Again, according to HGE4.5, it is seen that the expected 20 % increase in precipitation in DJF in southeast Australia may reach 50 % in JJA. In the SON, there may be a decrease in precipitation that can reach 50 % in the north-northeast parts of the continent. When the MPI-4.5 results are examined, it is seen that the expected precipitation increase in the range of 150°E - 150°W is now spread over a wider area in JJA, but the more severe increase expectation is in DJF and MAM seasons. Precipitation increases in the northeastern coastal and inland parts of Australia in the DJF, in the western, central, and eastern parts of Australia in the MAM, in the inner regions of Australia in the DJF, and in the west of Australia in the SON are noteworthy. It is expected that this rate, which is expected to be around 20 % on average, will increase even more in the west of Australia in the SON and reach 75 %.

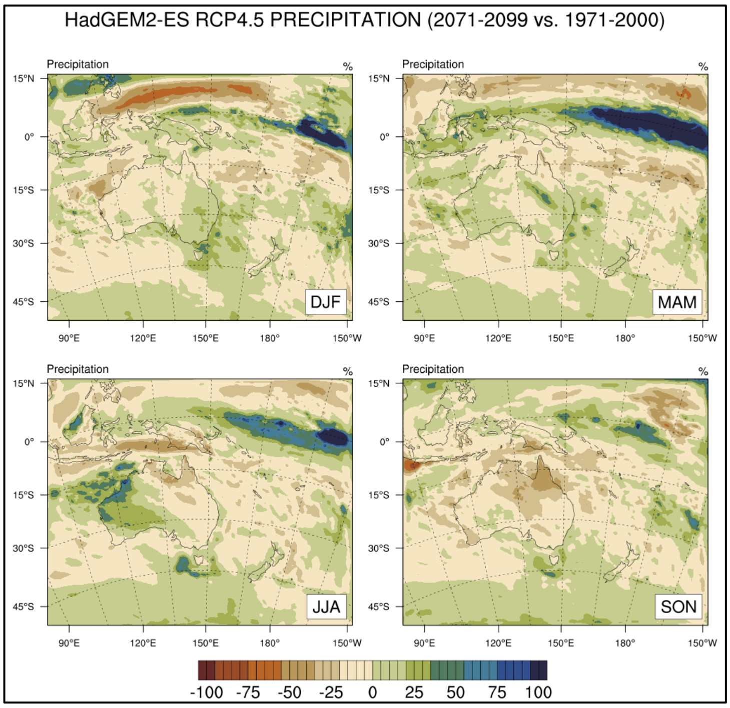

Figure 3.89. Projected changes in total precipitation based on HadGEM2-ES driven RegCM4.6 under the RCP4.5 scenario for the period of 2071 - 2099 with respect to the reference period of 1971 - 2000: (a) December - January - February (DJF), (b) March - April - May (MAM), (c) June - July - August (JJA), and (d) September - October - November (SON) seasons.

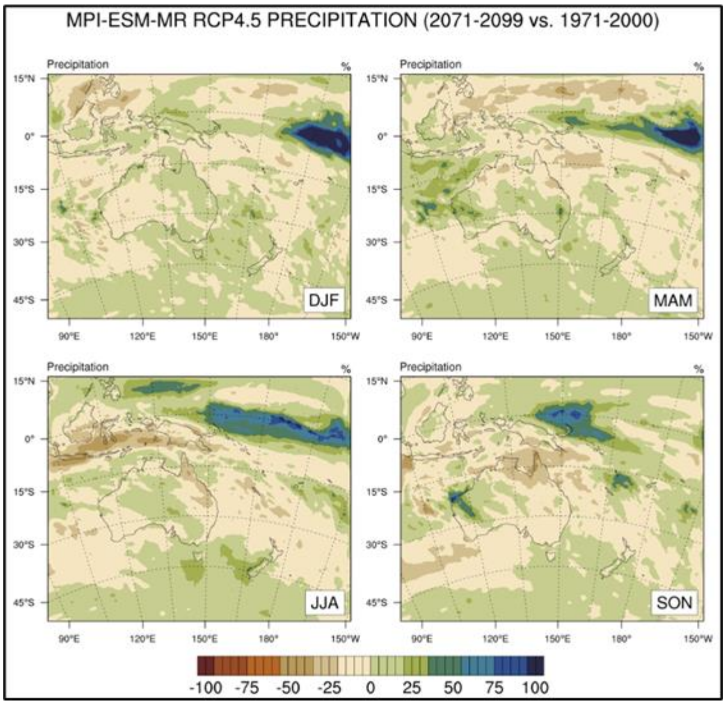

Figure 3.90. Projected changes in total precipitation based on MPI-ESM-MR driven RegCM4.6 under the RCP4.5 scenario for the period of 2071 - 2099 with respect to the reference period of 1971 - 2000: (a) December - January - February (DJF), (b) March - April - May (MAM), (c) June - July - August (JJA), and (d) September - October - November (SON) seasons.

When the precipitation change for the Australasia domain is examined according to the pessimistic scenario, it is seen that there may be both seasonal and spatial decreases and increases in the near term (Figure 3.91 and Figure 3.92). While increases and decreases of around 20 % seem to be dominant, the rates of increase and decrease in some regions are striking in the pessimistic scenario as in the optimistic scenario. For example, according to HGE-8.5, the increase in precipitation that can exceed 50 % or even 100 % in DJF and MAM between 150°E-150°W longitudes along the equatorial line seasons seems to have become more noticeable in all four seasons than MPI-8.5. This increase expectation becomes more intense towards the west, especially in DJF. According to HGE-8.5, an average precipitation increase of 60 % is noteworthy in the DJF in the north of the equator in the region up to 15°N latitude. According to the MPI-8.5, it is seen that the expectation of a 20 - 25 % increase in MAM in the west of Australia may exceed these values at some points. Again, according to MPI-8.5, precipitation decrease is expected in DJF and JJA in the west of Australia, and a precipitation increase is expected in the east.

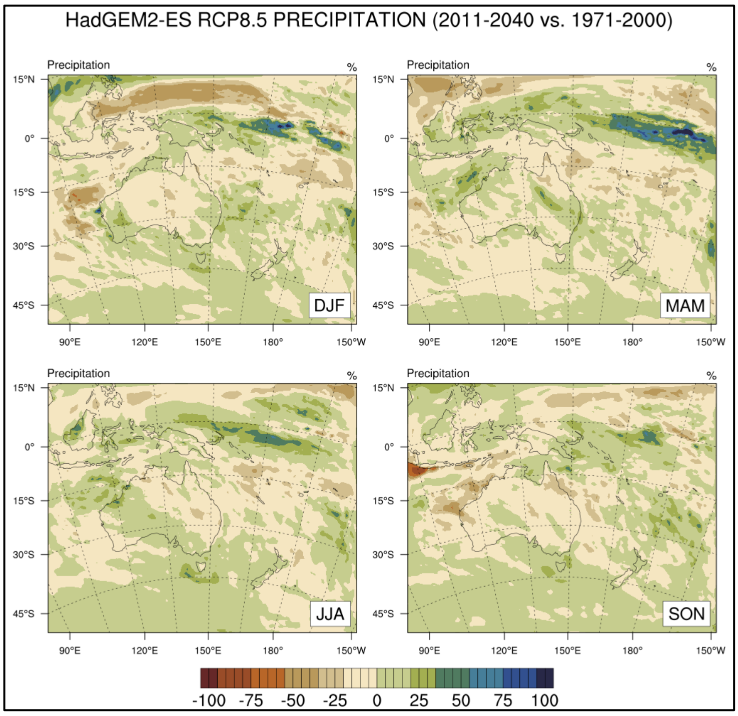

Figure 3.91. Projected changes in total precipitation based on HadGEM2-ES driven RegCM4.6 under the RCP8.5 scenario for the period of 2011 - 2040 with respect to the reference period of 1971 - 2000: (a) December - January - February (DJF), (b) March - April - May (MAM), (c) June - July - August (JJA), and (d) September - October - November (SON) seasons.

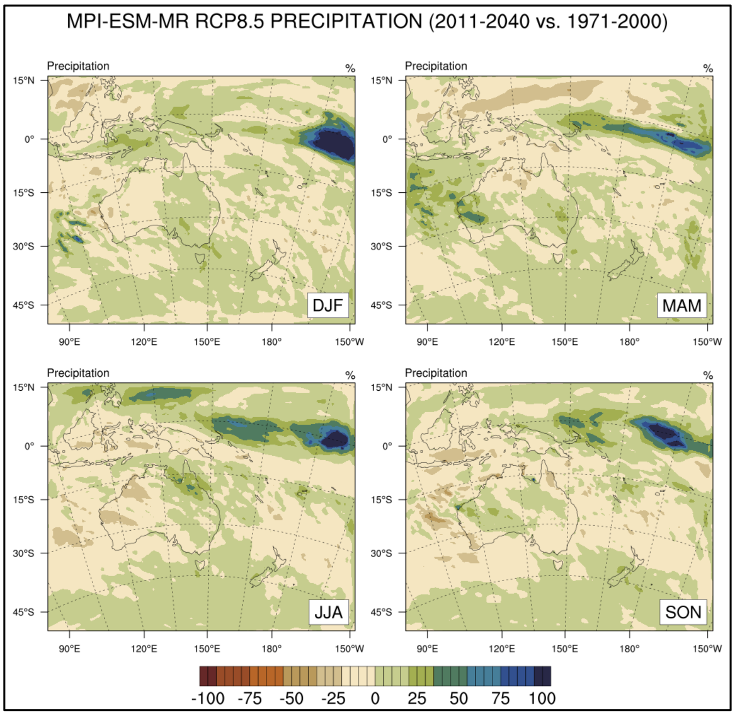

Figure 3.92. Projected changes in total precipitation based on MPI-ESM-MR driven RegCM4.6 under the RCP8.5 scenario for the period of 2011 - 2040 with respect to the reference period of 1971 - 2000: (a) December - January - February (DJF), (b) March - April - May (MAM), (c) June - July - August (JJA), and (d) September - October - November (SON) seasons.

When the precipitation change is analyzed based on the pessimistic scenario in the medium term, it is seen that the expected increase along the equatorial line between longitudes 150°E - 150°W for both models becomes more remarkable, despite the fact that it is similar to the previous results (Figure 3.93 and Figure 3.94). It can be said that this increase expectation, which can reach 100 %, will be more striking in MAM compared to HGE-8.5, and in JJA and SON compared to MPI-8.5. According to HGE-8.5, the increase in precipitation that can reach 50 % in the MAM season in the west of Australia can be seen as a decrease at the same rates in the north-northwest parts according to MPI-8.5. In addition, according to both models, it can be mentioned that there is a predominantly 20 % increase in precipitation towards the south of 45°S latitude. This increase expectation can be realized much more (around 50 %) in the JJA season than both models around Tasmania near 45°S latitude.

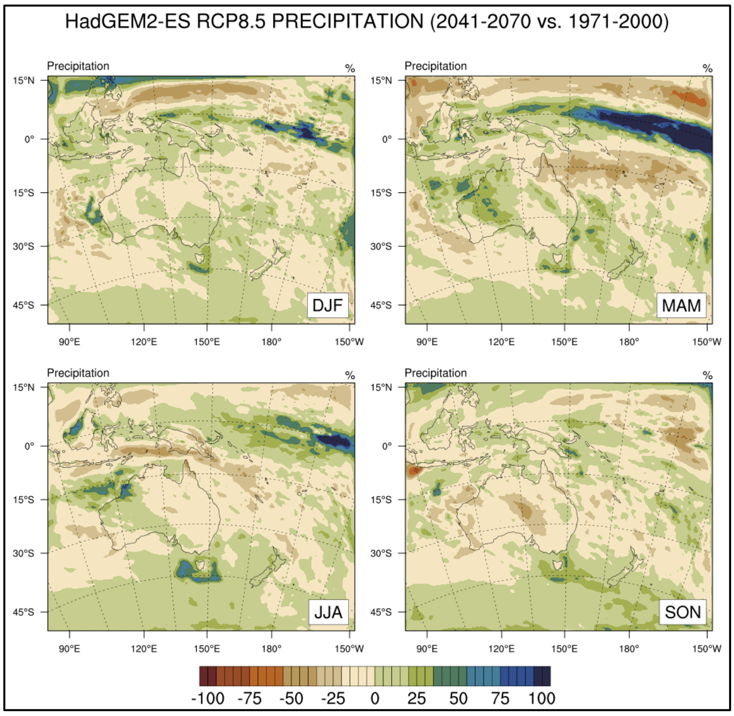

Figure 3.93. Projected changes in total precipitation based on HadGEM2-ES driven RegCM4.6 under the RCP8.5 scenario for the period of 2041 - 2070 with respect to the reference period of 1971 - 2000: (a) December - January - February (DJF), (b) March - April - May (MAM), (c) June - July - August (JJA), and (d) September - October - November (SON) seasons.

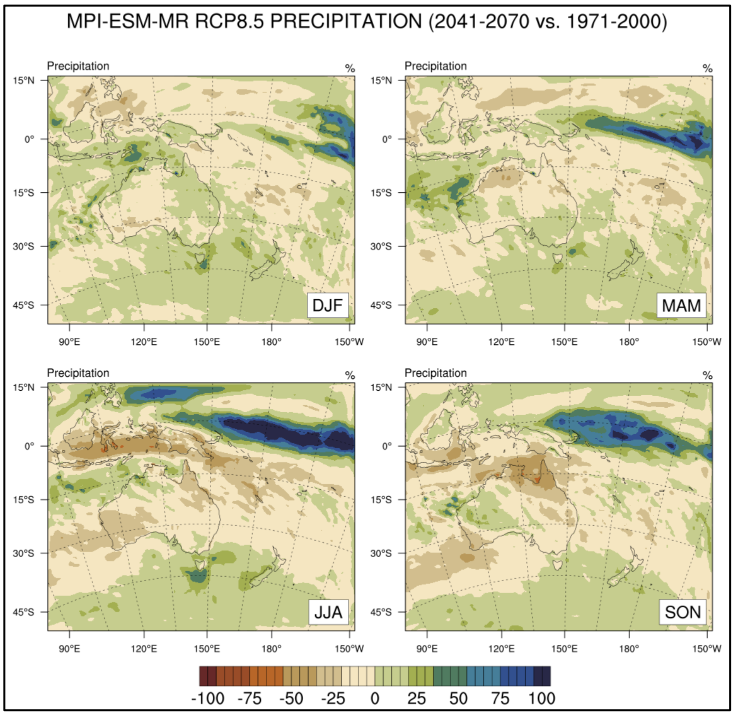

Figure 3.94. Projected changes in total precipitation based on MPI-ESM-MR driven RegCM4.6 under the RCP8.5 scenario for the period of 2041 - 2070 with respect to the reference period of 1971 - 2000: (a) December - January - February (DJF), (b) March - April - May (MAM), (c) June - July - August (JJA), and (d) September - October - November (SON) seasons.

When the precipitation variation for the Australasia domain is examined for the long term according to the pessimistic scenario, it is seen that the excessive increases and decreases in both models become more noticeable (Figure 3.95 and Figure 3.96). In the near and medium-term, it is anticipated that the expected excessive increases in precipitation along the equatorial region between 150°E -150°W longitudes will be expected in a broader region in all seasons in both models in the long term. According to HGE-8.5, a precipitation decrease is expected in the range of 50 - 75 % in DJF and MAM seasons in the north of the equator line. Again, according to HGE-8.5, precipitation in JJA in Indonesia and Papua New Guinea may decrease by up to 75 %. According to MPI-8.5, an increase of 20 % is expected in DJF in Australia in general. When it comes to the MAM season, it is seen that the expectation of an increase exceeding 25 % in the east of the continent has shifted to the northwestern parts of JJA. Although the expected decrease in precipitation for Australia in the SON season is dominant, it can be said that this decrease may range from 25 - 50 % towards the northeast coastal areas. In addition to all these, it is clear that precipitation expectation of 20 % or more from the south of the Australian continent is dominant in both models.

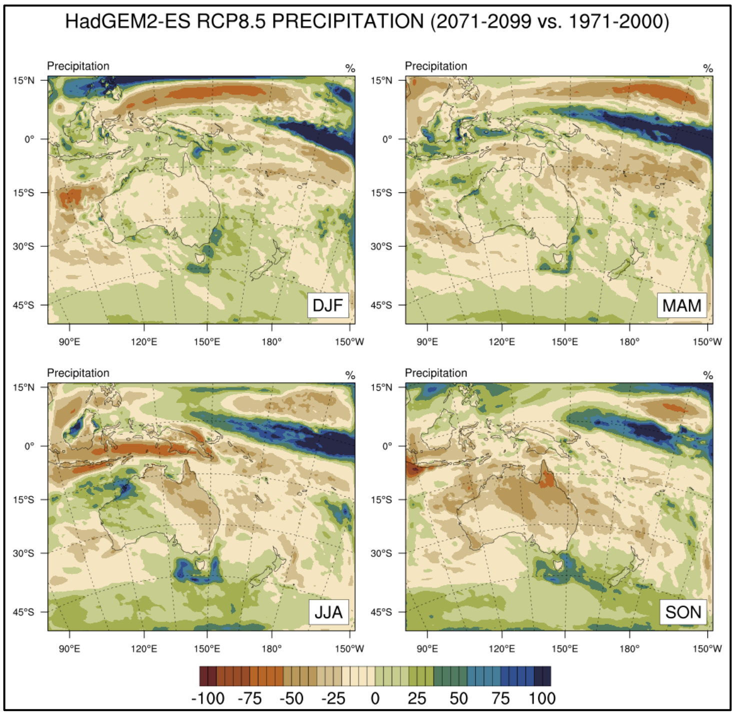

Figure 3.95. Projected changes in total precipitation based on HadGEM2-ES driven RegCM4.6 under the RCP8.5 scenario for the period of 2071 - 2099 with respect to the reference period of 1971 - 2000: (a) December - January - February (DJF), (b) March - April - May (MAM), (c) June - July - August (JJA), and (d) September - October - November (SON) seasons.

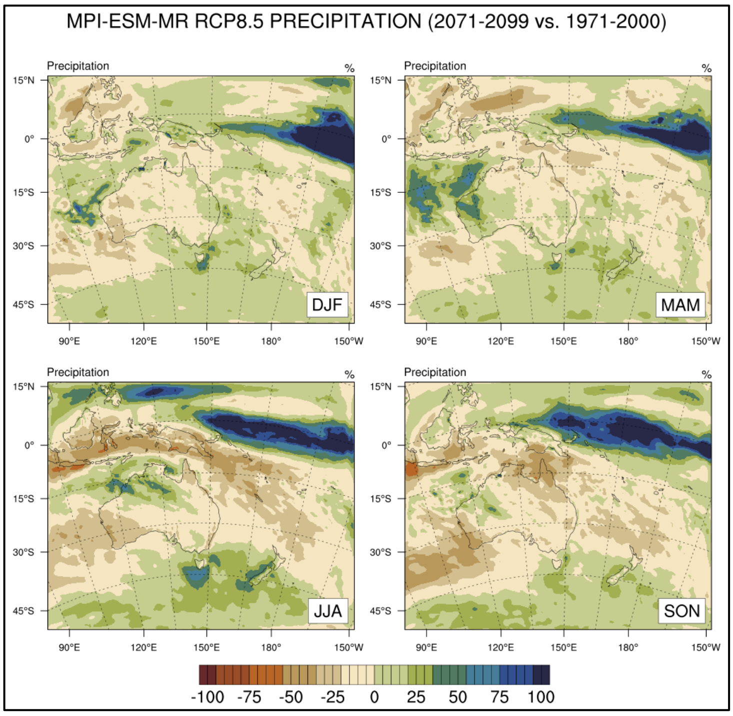

Figure 3.96. Projected changes in total precipitation based on MPI-ESM-MR driven RegCM4.6 under the RCP8.5 scenario for the period of 2071 - 2099 with respect to the reference period of 1971 - 2000: (a) December - January - February (DJF), (b) March - April - May (MAM), (c) June - July - August (JJA), and (d) September - October - November (SON) seasons.

The precipitation changes predicted for the CORDEX-Australasia domain show a very heterogeneous distribution depending on the period, season, and region, in contrast to the temperature changes. According to the precipitation simulation results, while there may be an increase in precipitation in some regions in the same period and the same season, it may decrease in another region. The increase and decrease rates are expected to be around 20 % throughout the domain. However, in some places, these rates may reach more extreme values that can reach up to 100 %. As the end of the century approaches and the scenario changes from optimistic to pessimistic, it can be said that the expectations for precipitation increases may rise even more in precipitation changes, just as in temperature changes.

4. DISCUSSION

Swedish scientist Svante August Arrhenius, one of the founders of physical chemistry, made the first calculation of global warming from anthropogenic emissions of CO_2 in 1896. Four decades after Arrhenius, British engineer Guy Stewart Callendar gathered data for the first time to show that the Earth was already getting warmer in line with emissions. Another four decades after Callender, carbon dioxide emission began to be declared as one of the most critical environmental problems. Today, climate change, which is considered as a “crisis” for all societies, is considered as one of the most vital threats in the world, far beyond being an environmental problem, and constitutes the main agenda of many scientific studies, administrative and political planning.

The rapidly increasing impacts of climate change have now made it compulsory for humanity to take more concrete steps in this regard. This essential situation triggers policy-makers in each sector to understand the sectoral effects of climate change much more comprehensively and take them into consideration in all strategy development and future planning. The joint efforts, first set in motion with the Kyoto Protocol and finally with the Paris Agreement, have now succeeded in making climate change mitigation and adaptation studies among the most urgent issues all over the world, even though it progresses more slowly than the experienced climate change. Impact studies have an important role in addressing the needs for the accurate implementation of mitigation and adaptation practices. At this point, climate modeling studies are also an important input source of impact studies in projecting the future climate.

Advances in climate science and computer science enable us to produce more realistic climate projections today. However, as the information detail in climate modeling improves and the models develop further, the required computational power and storage capacity also increase. In this context, climate models, which are tools in obtaining of future climate outputs with different spatial and temporal resolution, specific to various regions of the world under possible scenarios, require extensive international scientific collaborations. This study, which aims to contribute to this international cooperation under the roof of CORDEX, has enabled the production of alternative climate data for the Australasia region while evaluating the projected future climate change in terms of both average and extreme events.

In the first part of the thesis, global climate models with different resolutions in CMIP5 were tested in terms of both mean air temperature and precipitation climatology for the Australasia region, and also, the changes in mean air temperature and precipitation for the Australasia region until the end of the century were projected under three different scenarios (i.e., RCP2.6, RCP4.5, RCP8.5) with the multi-model ensemble mean approach. In this part, the use of the RCP2.6 scenario, which was not preferred much in climate change and climate change impact studies until the Paris Agreement, has been one of the most significant outputs of the study. The multi-model ensemble mean results indicate that, as theoretically expected, individual performances of each global model differ seasonally, but the multi-model ensemble mean approach minimizes the bias in the models. Model performances also vary widely in terms of geographical features of the locations, particularly in precipitation. Considering this, for RCP2.6, which is the most optimistic scenario, a warming of at least 0.5 ℃ in the Australia region is projected until the end of the century. This warming may be above 1.5 ℃ in some seasons (i.e., DJF and MAM). Although precipitation varies a lot on a local scale, it can be seen that it may increase by approximately 1 % in terms of spatial average. However, as mentioned before, there may be an increase of 50 % in some places in some seasons, and a decrease of up to 30 % is expected in some places. Multi-model ensemble results made under the RCP4.5 and RCP8.5 scenarios predict more warming compared to the RCP2.6 scenario. Under the RCP4.5 and RCP8.5 scenarios, it is seen that in the near future (2016 - 2035), the expectation of warming above 0.5 ℃ across the region may rise above 1 ℃ for RCP4.5 and 1.5 ℃ for RCP8.5 in the mid-century (2046 - 2065). At the end of the century, it can be said that the expected warming of around 1.5 ℃ for RCP4.5 and 3 ℃ for RCP8.5. These results are in line with the fact that the scenarios begin to diverge more discernibly by the mid-century. As can be seen very clearly, the expected warming intensifies as the scenarios move from optimistic to pessimistic and from the near future to the far future. This situation coincides with the theoretically expected findings. As in the RCP2.6 scenario, precipitation data shows more seasonal and spatial variability in future projections under the RCP4.5 and RCP8.5 scenarios. However, while it is predicted that there will be some increase in precipitation throughout the region, it is expected that this increase will be relatively higher in the pessimistic scenario from the mid-century towards the end of the century.

When all these results are compared with the AR5 results of IPCC (Christensen et al., 2013), the temperature projections for the region in general are similar in terms of spatial pattern and mean values. This thesis results also conforms to the AR5, revealing that a greater warming is expected as the scenario moves from optimistic to pessimistic and time moves from the near future to the far future. The differences between the findings of this study and the findings in the AR5 report are mostly in terms of maximum values. For example, according to the RCP8.5 scenario, it is stated that the temperature increase may approach 6 ℃ in some parts of Australasia. As in this study, the spatial and seasonal variability in AR5 is also wide in precipitation values, and for some places, there may be a decrease that exceeds 50 % in some periods and seasons, while there may be increases over 30 % in other places. In this thesis, using the same time periods as AR5 in the multi-model ensemble mean approach allows the temporal comparison of the results, but the differences in the domain and the models used cause partial discrepancies in the results. While CORDEX divides the world into 14 domains in total, AR5 examines the world in 26 domains. Additionally, Australasia domain is also defined with sub-regions such as north and south in AR5.

Since the low resolution of global climate models prevents us from obtaining very detailed information specific to the regions, it is a fact that we need much higher resolution model results. With the dynamic downscaling approach, which is the main method of this thesis, higher resolution climate data are produced for the CORDEX-Australasia domain, and the changes in temperature and precipitation climatology have been examined under two different scenarios (i.e., RCP4.5 and RCP8.5). In the analysis, not only the mean temperature but also the minimum and maximum temperatures that enable the determination of extreme climatic events were taken into account. Before the regional climate model RegCM4.6 used in the research was run for historical and future projections, several test runs were conducted to determine the suitable parameterizations. With this evaluation phase, it was concluded that RegCM4.6 should be run with Holtslag as PBL scheme and Tiedtke over lands and Emanuel over oceans as a convective cumulus scheme for the Australasia domain. Since the dependence of precipitation, which is the most difficult variable to model in climate studies, to many factors such as cloud microphysics, cumulus convection, large-scale circulation, planetary boundary processes and orography, meticulous implementation of this part reduces the uncertainty of the model and increases its reliability.

The RegCM4.6 regional climate model, operated with two different GCMs (i.e., HadGEM2-ES and MPI-ESM-MR) with appropriate parameterisations, was used to obtain 50 km high resolution climate data for the CORDEX-Australasia domain under scenarios that consider medium (RCP4.5) and very high (RCP8.5) greenhouse gas emissions. According to the dynamic downscaling results, it is seen that the mean temperature will increase between 1 - 3 ℃ in the Australasia region based on the RCP4.5 scenario and it may increase even more based on the RCP8.5 scenario which may be around 5 ℃ until the end of the century. In addition, RegCM4.6 results driven with HadGEM2-ES project a slightly higher warming than RegCM4.6 results driven with MPI-ESM-MR. This result is compatible with the high temperature sensitivity of the HadGEM2-ES model (Andrews et al., 2012; Caesar et al. 2013). While the average changes in the minimum and maximum temperature are similar to the mean temperature, it is seen that the maximum temperatures may reach 7 ℃ in

Australasia by the end of the century. In general, it is seen that the increases in temperature may be more siginificant in tropical regions and around Tasmania. Warming in tropical regions supports the continued warming observed in the Indo-Pacific Warm Pool region (Stevens, 2020), where sea surface temperatures remain above 28 ℃ year-round. Moreover, this hot zone, which has grown almost twice as much as in the last century (Stevens, 2020), can be expected to expand further in the future.

It is clear that the change in precipitation according to the change in temperature values shows a very heterogeneous pattern that was previously in the multi-model ensemble mean approach. In the same period, an increase in precipitation can be expected in one part of the region, and a decrease in another part. Considering the whole region, it can be said that these decrease and increase rates will be around 20 % on average. It should also be noted that when the scenario shifted from RCP4.5 to RCP8.5, the increase trend in the total amount of precipitation came into prominence. It is even seen that these increases are striking particularly along the equatorial belt and between 150°E - 150°W longitudes.

At this point, it will be useful to give a little more detailed information on the model performances in order to evaluate the climate model results more accurately. RegCM4.6 model shows a cold bias in terms of temperatures and an overestimation for precipitation (Appendix A, B, C, D). These results also coincide with the results of different models and configurations (Di Virgilio et al., 2019). Due to its geographical location, Australasia region is under the influence of climate drivers such as ENSO, IOD, MJO and AAO, as well as having different climate types, vegetation and elevation features. This situation makes the climate modeling of the region difficult and makes it very important to evaluate the model results within these factors. Although the use of a regional climate model has an added value compared to global climate models, and although parameterizations are made specific to the domain, the effect of uncertainties arising from global climate models cannot be eliminated to the desired extent. Specifically, the impacts of changes in ITCZ and the South Pacific Convergence Zone (SPCZ) become very crucial under a changing climate (Li and Xie, 2014; Brown et al., 2020). For example, 1 - 2 ℃ of warming in the tropics may cause an average of 6 % reduction in SPCZ precipitation, while a 3 ℃ warming reverses this situation, indicating more SPCZ precipitation (Widlansky et al., 2013). Apart from this, errors in global models such as the double ITCZ and the excessive equatorial Pacific cold tongue should also not be overlooked (Zheng et al., 2012; Li and Xie, 2014; Stouffer et al., 2017).

Finally, the impacts of climate change on extreme climate events as well as changes in Australasia's mean temperature and total precipitation amount have also been examined within the scope of this thesis. While an annual mean increase of 0-10 days is expected in the number of very hot days in Australasia in the future, it is predicted that the expected increase in the number of tropical nights, which is 20 days/year under the optimistic scenario (RCP4.5), will be 40 - 50 days/year in the pessimistic scenario (RCP8.5). Moreover, it is expected that there will be an annual average increase of 5-7 periods in the number of heatwaves in Australasia. The change in precipitation extremes shows spatial variation just like the mean precipitation values. For example, according to the RCP8.5 scenario outputs of the ACCESS1-0 model, the trend is predominantly expected to decrease in the inner parts of the continent of Australia, whereas the trend is predicted as an increase for the outputs of the RCP4.5 scenario and the MPI-ESM-LR model. Similarly, there is an increase expectation on the ocean. It is even projected that this increase may be more severe in the equatorial Pacific. In addition, it is seen that there will be an increase in precipitation intensity throughout the region. These two results reveal that the probability of heavy precipitation will increase in Australasia in the future. Also, while there were little changes in the consecutive dry days, in the central and southern regions of Australia this change is slightly more negative. This result in fact coincides with the projected rapid increase in daily precipitation extremes across Australia and the expectation of precipitation that increases with each degree of temperature increase (Bao et al., 2017). Furthermore, changes in the monsoons may cause significant changes in the precipitation regime in the region (Ashfaq et al., 2020). For instance, in the monsoon peak season, it is possible to see more precipitation in the north of Australia under both RCP2.6 and RCP8.5 scenarios in mid-century (Ashfaq et al., 2020). This increase projection is higher for the RCP8.5 scenario. Nevertheless, the impatcs of the processes that cause interseasonal and interannual variations in the precipitation extremes often make it difficult to generalize.

As a result, the Australasia region will be adversely affected by climate change, as is the case throughout the world. Both human health and agriculture will be most affected in all island countries, especially Australia, which has limited agricultural area, as well as sea level rise, increased ocean acidification, heatwave risk in densely populated cities, bushfire risk, other natural disaster such as heavy rainfall and storm events. It can be said to be an devastating threat to all habitats and ecosystems, particularly coastal settlements. In other words, not only rising temperatures and precipitation, which can be seen as both an increase and a decrease, but the expected increase in the number of extreme climate events will enhance the vulnerability of the region to climate change.

5. CONCLUSION

In this study, the performance of climate models for Australasia, which is one of the least studied regions within the scope of CORDEX, was tested with various approaches and datasets, and the changes in average climate conditions and extreme climate events at the regional scale were examined. By testing the individual performances of the low-resolution global climate model results, the changes in seasonal mean air temperature and total precipitation amount were revealed under the RCP2.6, RCP4.5 and RCP8.5 scenarios with the multi-model ensemble mean approach, and then HadGEM2-ES and MPI-ESM-MR models were dynamically downscaled to 50 km x 50 km horizontal resolution under RCP4.5 and RCP8.5 scenarios using RegCM4.6 regional climate model. According to the projection results obtained from RegCM4.6, the mean, minimum and maximum temperature values for Australasia, as well as seasonal changes in total precipitation were examined. In addition to these, changes in temperature and precipitation extremes were analyzed using the NEX-GDDP dataset, which is rarely used in the literature. As a result, it is clear that a warmer future awaits CORDEX-Australasia of up to 5 °C, and with increasing temperature, there will be an increase in the number of very hot days and tropical nights. It can be said that precipitation, which varies a lot in spatial terms, will increase more on average and the probability of heavy precipitation will be high. In general, towards the end of the century and moving from the most optimistic scenario to the pessimistic scenario, it is clear that the negative effects of climate change are much more severe.

Since there is no single accurate model approach or data set in climate change studies, and the projection results are region-specific, it is necessary to use as diverse and alternative approaches, models and data set as possible, taking into account all uncertainties. Therefore, three different datasets (i.e., low-resolution GCM output, statistically downscaled high-resolution data (NEX-GDDP), and dynamically downscaled high-resolution regional climate model (RegCM4.6) output) and three different approaches (multi-model ensemble, statistical downscaling, dynamical downscaling) were used in the study. These approaches, which constitute the three main pillars of climate modeling studies, have been tested for the Australasia domain. It has been seen that the results are generally compatible with each other and other studies in the literature in terms of approaches and findings. The overall findings of the study support the projected changes depending on the vulnerability of the intra-year and inter-year variations of the Indo-Pacific Warm Pool region and the ITCZ and SPCZ to climate change. HadGEM2-ES and MPI-ESM-MR global climate models, which were used as the parent GCMs for the dynamical downscaling approach part, were also found to be suitable models to be used for the domain according to the GCM comparisons at the multi-model ensemble mean stage. In addition, it has been revealed that dynamical downscaling, using higher resolution climate data, may result in better representation of the regional distribution of temperature increases. So much so that with the multi-model ensemble mean approach, temperature increases that can be around 3 ℃ at the most will actually reach much higher values, such as over 5 ℃. In addition, it can be said that the regional heterogeneous distribution of precipitation, which is the most difficult climate parameter to model, can be seen in a much sharper detail in high resolution climate data and the uncertainty of the change in precipitation is much higher. These results show the added value of the regional climate model to the Australasia domain due to its particular location. Moreover, the NEX-GDDP dataset, which provides high resolution climate data on a global scale, both temporally and spatially, is used in the calculation of temperature and precipitation extremes and presented as an alternative data set and approach in this study. The changes in daily maximum and minimum temperature and precipitation obtained from the regional climate model RegCM4.6 also support the changes in the temperature and precipitation extremes of NEX-GDDP. Since the NEX-GDDP outputs are also compatible with the results of similar studies with different data sets, it has revealed that it can be applied at the regional scale as an alternative data set.

In this study, it is seen once again that although the climate models are developing day by day, it is impossible to talk about a single perfect climate model. As each model has different uncertainties, these uncertainties arise from both the parent GCMs and the RCMs used. For this reason, it is necessary to use with more than one model in climate change studies. In addition, it is very important that the models used are run with the correct parameterization. In this study, the most suitable PBL scheme and convective parameterization for RegCM4.6 have been determined and all future projections have been realized with this configuration.

As in all climate modeling studies, there are some limitations within the scope of this study. The most critical of these is the high computing power and storage requirement, which is a technical limitation. This situation unfortunately makes it impossible to produce much higher resolution data in the study and to use with many more models. Obtaining open-source high temporal and spatial resolution data, which is shared within the scope of scientific cooperation, is also difficult due to these reasons, as well as the difficulties in remote data download. Apart from these technical problems, the fact that factors such as ITCZ, SPCZ, ENSO, IOD, MJO, and AAO cannot be represented in the most perfect way in the global climate models may cause too much bias in a region such as Australasia where these factors are highly effective. Finally, another limitation is that the region boundaries used by the IPCC in its reports and the regions within the scope of CORDEX are not exactly the same. This situation makes it difficult to make regional comparisons between different studies.

Australasia region is also under vital threat with climate change. Many effects such as increasing heatwaves, bushfire, excessive precipitation, rising sea level, acidification of the ocean endanger the health of all living things. For example, Australia, the mainland part of the region, is foremost an agricultural country, and its arable land is already narrow due to unfavorable climatic conditionsIn this narrow area, the impact to be exposed to agriculturally important areas such as the Murray-Darling Basin is very critical for the country. As a different example, the Malay peninsula including Papua New Guinea, Sumatra, Borneo and Sulawesi are among the places where the rainforest ecosystem is represented. These ecosystems and/or ecosystem services are also threatened by climate change. Lastly, the changes that will take place in the ITCZ and SPCZ under a changing climate will also have an impact on all climate regimes in the region.

Despite the limitations mentioned above, the RegCM4.6 model results can be said to be of acceptable accuracy and reliability for the CORDEX-Australasia domain. However, in the future, studying under new scenario sets (i.e., SSPs) with much higher resolutions at the scale of the sub-domains of the region and with the most appropriate configurations and models for each sub-domain in order to produce even more reasonable data for impact studies will improve the results much more. In this respect, although CMIP6 and CORDEX-CORE projects have recently been targeted and studied in global cooperation, it will be very beneficial to contribute to these studies with the use of convection-permitting regional climate models.

REFERENCES

Aguilar, E., Peterson, T. C., Ramírez Obando, P., Frutos, R., Retana, J. A., Solera, M., Soley, J., González García, I., Araujo, R. M., Rosa Santos, A., Valle, V. E., Brunet, M., Aguilar, L., Álvarez, L., Bautista, M., Castañón, C., Herrera, L., Ruano, E., Sinay, J. J., Sánchez, E., Hernández Oviedo, G. I., Obed, F., Salgado, J. E., Vázquez, J. L., Baca, M., Gutiérrez, M., Centella, C., Espinosa, J., Martínez, D., Olmedo, B., Ojeda Espinoza, C. E., Núñez, R., Haylock, M., Benavides, H., Mayorga, R., 2005. Changes in precipitation and temperature extremes in Central America and northern South America, 1961–2003. Journal of Geophysical Research, 110, D23107.

Ahmed, K., Sachindra, D. A., Shahid, S., Demirel, M. C., Chung, E.-S., 2019. Selection of multi-model ensemble of general circulation models for the simulation of precipitation and maximum and minimum temperature based on spatial assessment metrics. Hydrology and Earth System Sciences, 23, 4803-4824.

Ahrens, C. D., Henson, R., 2018. Essentials of Meteorology: An Invitation to the Atmosphere, Cengage Learning, Boston.

Aldrian, E., 2002. Spatial patterns of ENSO impact on Indonesian rainfall. Jurnal Sains & Teknologi Modifikasi Cuaca, 3, 5-15.

Alexander, L.V., Zhang, X., Peterson, T. C., Caesar, J., Gleason, B., Klein Tank, A. M. G., Haylock, M., Collins, D., Trewin, B., Rahimzadeh, F., Tagipour, A., Rupa Kumar, K., Revadekar, J., Griffiths, G., Vincent, L., Stephenson, D. B., Burn, J., Aguilar, E., Brunet, M., Taylor, M., New, M., Zhai, P., Rusticucci, M., Vazquez-Aguirre, J. L., 2006. Global observed changes in daily climate extremes of temperature and precipitation. Journal of Geophysical Research, 111, D05109.

Alexander, L. V., Arblaster, J. M., 2009. Assessing trends in observed and modelled climate extremes over Australia in relation to future projections. International Journal of Climatology, 29, 417-435.

Alexander, L. V., 2016. Global observed long-term changes in temperature and precipitation extremes: A review of progress and limitations in IPCC assessments and beyond. Weather and Climate Extremes, 11, 4-16.

Alexander, L. V., Arblaster, J. M., 2017. Historical and projected trends in temperature and precipitation extremes in Australia in observations and CMIP5. Weather and Climate Extremes, 15, 34-56.

Ali, H., Fowler, H. J., Lenderink, G., Lewis, E., Pritchard, D., 2021. Consistent large-scale response of hourly extreme precipitation to temperature variation over land. Geophysical Research Letters, 48, e2020GL090317.

Almazroui, M., 2012. Dynamical downscaling of rainfall and temperature over the Arabian Peninsula using RegCM4. Climate Research, 52, 49-62.

An, N., Turp, M. T., Akbaş, A., Öztürk, Ö., Kurnaz, M. L., 2018. Türkiye'nin değişen ikliminde ısıtma ve soğutma gün derecelerinin gelecek projeksiyonları [Future Projections of Heating and Cooling Degree Days in a Changing Climate of Turkey], Marmara Journal of Pure and Applied Sciences, 30, 227-240.

An, N., Turp, M. T., Türkeş, M., Kurnaz, M. L., 2020. Mid-term impact of climate change on hazelnut yield. Agriculture, 10, 159.

Andrews, T., Ringer, M. A., Doutriaux-Boucher, M., Webb, M. J., Collins, W. J., 2012. Sensitivity of an Earth system climate model to idealized radiative forcing. Geophysical Research Letters, 39, L10702.

Anthes, R. A., 1977. A cumulus parameterization scheme utilizing a one-dimensional cloud model. Monthly Weather Review, 105, 270-286.

Anthes, R. A., Hsie, E. Y., Kuo, Y. H., 1987. Description of the Penn State/NCAR Mesoscale Model version 4 (MM4), NCAR Technical Note TN-282-STR, USA.

Arakawa, A., 1972. Design of the UCLA General Circulation Model, UCLA Department of Meteorology Numerical Simulation of Weather and Climate Technical Report No. 7, Department of Meteorology, University of California, Los Angeles.

Arakawa, A., Schubert, W. H., 1974. Interaction of a cumulus cloud ensemble with the large-scale environment, Part I. Journal of Atmospheric Sciences, 31, 674-701.

Arakawa A., Cheng M. D., 1993. The Arakawa-Schubert Cumulus Parameterization. In Emanuel K. A., Raymond D. J. (Eds.), The Representation of Cumulus Convection in Numerical Models, 123-136, American Meteorological Society, Boston.

Arguez, A., Hurley, S., Inamdar, A., Mahoney, L., Sanchez-Lugo, A., Yang, L., 2020. Should we expect each year in the next decade (2019–28) to be ranked among the top 10 warmest years globally? Bulletin of the American Meteorological Society, 101, E655-E663.

Ashcroft, L., Karoly, D. J., Dowdy, A. J., 2019. Historical extreme rainfall events in southeastern Australia. Weather and Climate Extremes, 25, 100210.

Ashfaq, M., Cavazos, T., Reboita, M. S., Torres-Alavez, J. A., Im, E. S., Olusegun, C. F., Alves, L., Key, K., Adeniyi, M. O., Tall, M., Sylla, M. B., Mehmood, S., Zafar, Q., Das, S., Diallo, I., Coppola, E., Giorgi, F., 2020. Robust late twenty-first century shift in the regional monsoons in RegCM-CORDEX simulations. Climate Dynamics.

Bador, M., Donat, M. G., Geoffroy, O., & Alexander, L. V., 2018. Assessing the robustness of future extreme precipitation intensification in the CMIP5 ensemble. Journal of Climate, 31, 6505-6525.

Baldwin, J. W., Dessy, J. B., Vecchi, G. A., Oppenheimer, M., 2019. Temporally compound heat wave events and global warming: An emerging hazard. Earth's Future, 7, 411-427.

Bao, J., Sherwood, S. C., Alexander, L. V., Evans, J. P., 2017. Future increases in extreme precipitation exceed observed scaling rates. Nature Climate Change, 7, 128-132.

Bao, Y., Wen, X., 2017. Projection of China’s near-and long-term climate in a new high-resolution daily downscaled dataset NEX-GDDP. Journal of Meteorological Research, 31, 236-249.

Barron, E. J., 1987. Nuclear waste disposal: A climate problem? - An editorial. Climatic Change, 10, 107-109.

Barry, R. G., Chorley, R. J., 2009. Atmosphere, Weather and Climate, Routledge, London.

Batista, R. J., Gonçalves, F. L., da Rocha, R. P., 2016. Present climate and future projections of the thermal comfort index for the metropolitan region of São Paulo, Brazil. Climatic Change, 137, 439-454.

Bedia, J., Herrera, S., San Martín, D., Koutsias, N., Gutiérrez, J. M., 2013. Robust projections of Fire Weather Index in the Mediterranean using statistical downscaling. Climatic Change, 120, 229-247.

Beniston, M., 2003. Climatic change in mountain regions: A review of possible impacts. Climatic Change, 59, 5-31.

Bjerknes, V., 1904. Das Problem der Wettervorhers-age, betrachtet vom Standpunkte der Mechanik und der Physik. Meteorologische Zeitschrift, 21, 1-7.

BOM, n.d.-a. "Australian Climate Extremes: Time Series Graphs, Very Hot Days", http://www.bom.gov.au/cgi-bin/climate/change/extremes/timeseries.cgi?graph=HD40&ave_yr=T. (accessed April 2020).

BOM, n.d.-b. "Australian Climate Extremes: Time Series Graphs, Very Cold Days", http://www.bom.gov.au/cgi-bin/climate/change/extremes/timeseries.cgi?graph=CD10&ave_yr=T. (accessed April 2020).

BOM, n.d.-c. "El Niño Southern Oscillation (ENSO)", http://www.bom.gov.au/climate/about/australian-climate-influences.shtml?bookmark=enso. (accessed April 2020).

BOM, n.d.-d. "Indian Ocean", http://www.bom.gov.au/climate/about/australian-climate-influences.shtml?bookmark=iod. (accessed April 2020).

BOM, n.d.-e. "The Madden-Julian Oscillation", http://www.bom.gov.au/climate/about/australian-climate-influences.shtml?bookmark=mjo. (accessed April 2020).

BOM, n.d.-f. "Southern Annular Mode", http://www.bom.gov.au/climate/about/australian-climate-influences.shtml?bookmark=sam. (accessed April 2020).

BOM, n.d.-g. “Australian Climate Influences”, www.bom.gov.au/climate/about/. (accessed April 2020).

BOM, n.d.-h. “About the Climate Extremes Analyses”, http://www.bom.gov.au/climate/change/about/extremes.shtml#trend%20maps. (accessed April 2020).

Bretherton, C. S., McCaa, J. R., Grenier, H., 2004. A new parameterization for shallow cumulus convection and its application to marine subtropical cloud-topped boundary layers. Part I: Description and 1D results. Monthly Weather Review, 132, 864-882.

Briegleb, B. P., 1992. Delta-Eddington approximation for solar radiation in the NCAR Community Climate Model. Journal of Geophysical Research, 97, 7603-7612.

Brown, J. R., Lengaigne, M., Lintner, B. R., Widlansky, M. J., van der Wiel, K., Dutheil, C., Linsley, B. K., Matthews, A. J., Renwick, J., 2020. South Pacific Convergence Zone dynamics, variability and impacts in a changing climate. Nature Reviews Earth & Environment, 1, 530-543.

Caesar, J., Palin, E., Liddicoat, S., Lowe, J., Burke, E., Pardaens, A., Sanderson, M., Kahana, R., 2013. Response of the HadGEM2 Earth System Model to future greenhouse gas emissions pathways to the year 2300. Journal of Climate, 26, 3275-3284.

Cai, W., Santoso, A., Wang, G., Weller, E., Wu, L., Ashok, K., Ashok, K., Masumoto, Y., Yamagata, T., 2014. Increased frequency of extreme Indian Ocean Dipole events due to greenhouse warming. Nature, 510, 254-258.

Carter, L. J., 1987. Siting the nuclear waste repository: Last stand at Yucca Mountain. Environment: Science and Policy for Sustainable Development, 29, 8-32.

Case, M., Ardiansyah, F., Spector, E., 2007. Climate Change in Indonesia – Implications for Humans and Nature, World Wide Fund for Nature (WWF), Gland.

Charney, J. G., 1949. On a physical basis for numerical prediction of large-scale motions in the atmosphere. Journal of Meteorology, 6, 371-385.

Charney, J. G., 1951. Dynamic Forecasting by Numerical Process. In Malone T. F. (Ed.), Compendium of Meteorology, 470-482, American Meteorological Society, Boston.

Chen, M., Pollard, D., Barron, E. J., 2003. Comparison of future climate change over North America simulated by two regional models. Journal of Geophysical Research, 108, 4348.

Christensen, J. H., Carter, T. R., Rummukainen, M., Amanatidis, G., 2007. Evaluating the performance and utility of regional climate models: The PRUDENCE project. Climatic Change, 81, 1-6.

Christensen, J. H., Christensen, O. B., 2007. A summary of the PRUDENCE model projections of changes in European climate by the end of this century. Climatic Change, 81, 7-30.

Christensen, J. H., Krishna Kumar, K., Aldrian, E., An, S.-I., Cavalcanti, I. F. A., de Castro, M., Dong, W., Goswami, P., Hall, A., Kanyanga, J. K., Kitoh, A., Kossin, J., Lau, N.-C., Renwick, J., Stephenson, D. B., Xie, S.-P., Zhou, T., 2013. Climate Phenomena and Their Relevance for Future Regional Climate Change. In Stocker T. F., Qin D., Plattner G.-K., Tignor M., Allen S. K., Boschung J., Nauels A., Xia Y., Bex V., Midgley P. M. (Eds.), Climate Change 2013: The Physical Science Basis. Contribution of Working Group I to the Fifth Assessment Report of the Intergovernmental Panel on Climate Change, Cambridge University Press, Cambridge and New York.

Clarke, L. E., Edmonds, J. A., Jacoby, H. D., Pitcher, H. M., Reilly, J. M., Richels, R. G., 2007. Scenarios of Greenhouse Gas Emissions and Atmospheric Concentrations, Sub-Report 2.1A of Synthesis and Assessment Product 2.1 by the U.S. Climate Change Science Program and the Subcommittee on Global Change Research, Department of Energy, Office of Biological & Environmental Research, Washington DC.

Coates, L., Haynes, K., O’Brien, J., McAneney, J., de Oliveira, F. D., 2014. Exploring 167 years of vulnerability: An examination of extreme heat events in Australia 1844–2010. Environmental Science & Policy, 42, 33-44.

Collins, D. A., Della-Marta, P. M., Plummer, N., Trewin, B. C., 2000. Trends in annual frequencies of extreme temperature events in Australia. Australian Meteorological Magazine, 49, 277-292.

Coppola, E., Giorgi, F., Raffaele, F., Fuentes-Franco, R., Giuliani, G., Llopart-Pereira, M., Mamgain, A., Mariotti, L., Diro, G. T., Torma, C., 2014. Present and future climatologies in the phase I CREMA experiment. Climatic Change, 125, 23-38.

Coppola, E., Raffaele, F., Giorgi, F., 2018. Impact of climate change on snowmelt driven runoff timing over the Alpine region. Climate Dynamics, 51, 1259-1273.

Costs and benefits of carbon dioxide, 1979. Nature, 279, 1.

Cowan, T., Purich, A., Perkins, S., Pezza, A., Boschat, G., Sadler, K., 2014. More frequent, longer, and hotter heat waves for Australia in the twenty-first century. Journal of Climate, 27, 5851-5871.

CSIRO, 2007. Climate Change in Australia: Technical Report 2007, CSIRO Marine and Atmospheric Research, Aspendale.

CSIRO, 2010. Climate Variability and Change in South-Eastern Australia: A Synthesis of Findings From Phase 1 of the South Eastern Australian Climate Initiative (SEACI), South Eastern Australian Climate Initiative, Australia.

CSIRO, 2012. Climate and Water Availability in South-Eastern Australia: A Synthesis of Findings From Phase 2 of the South Eastern Australian Climate Initiative (SEACI), South Eastern Australian Climate Initiative, Australia.

CSIRO, BOM, 2020. State of the Climate 2020, CSIRO and BOM, Australia.

Deardorff, J. W., 1972. Parameterization of the planetary boundary layer for use in general circulation models. Monthly Weather Review, 100, 93-106.

Dee, D. P., Uppala, S. M., Simmons, A. J., Berrisford, P., Poli, P., Kobayashi, S., Andrae, U., Balmaseda, M. A., Balsamo, G., Bauer, P., Bechtold, P., Beljaars, A. C. M., van de Berg, L., Bidlot, J., Bormann, N., Delsol, C., Dragani, R., Fuentes, M., Geer, A. J., Haimberger, L., Healy, S. B., Hersbach, H., Hólm, E. V., Isaksen, L., Kållberg, P., Köhler, M., Matricardi, M., McNally, A. P., Monge-Sanz, B. M., Morcrette, J.-J., Park, B.-K., Peubey, C., de Rosnay, P., Tavolato, C., Thépaut, J.-N., Vitart, F., 2011. The ERA-Interim reanalysis: Configuration and performance of the data assimilation system. Quarterly Journal of the Royal Meteorological Society, 137, 553-597.

Demiroglu, O. C., Turp, M. T., Ozturk, T., Kurnaz, M. L., 2016a. Impact of climate change on natural snow reliability, snowmaking capacities, and wind conditions of ski resorts in Northeast Turkey: A dynamical downscaling approach. Atmosphere, 7, 52.

Demiroglu, O. C., Turp, M. T., Ozturk, T., An, N., Kurnaz, M. L., 2016b. Technical Climate Change Adaptation Options of the Major Ski Resorts in Bulgaria. In Koulov B., Zhelezov G. (Eds.), Sustainable Mountain Regions: Challenges and Perspectives in Southeastern Europe, 77-88, Springer, Basel.

Demiroglu, O. C., Akbas, A., Turp, M. T., Ozturk, T., An, N., Kurnaz, M. L., 2018. Case Study Turkey: Climate Change and Coastal Tourism: Impacts of Climate Change on the Turquoise Coast. In Jones A., Phillips, M. (Eds.), Global Climate Change and Coastal Tourism: Recognizing Problems, Managing Solutions & Future Expectations, 247-262, Centre for Agriculture and Biosciences International (CABI), Oxfordshire.

Demiroglu, O. C., Turp, M. T., Kurnaz, M. L., Abegg, B., 2021. The Ski Climate Index (SCI): fuzzification and a regional climate modeling application for Turkey. International Journal of Biometeorology, 65, 763-777.

Demory, M.-E., Berthou, S., Sørland, S. L., Roberts, M. J., Beyerle, U., Seddon, J., Haarsma, R., Schär, C., Christensen, O. B., Fealy, R., Fernandez, J., Nikulin, G., Peano, D., Putrasahan, D., Roberts, C. D., Steger, C., Teichmann, C., Vautard, R., 2020. Can high-resolution GCMs reach the level of information provided by 12–50 km CORDEX RCMs in terms of daily precipitation distribution? Geoscientific Model Development Discussions, 1-33.

Dey, R., Lewis, S. C., Abram, N. J., 2019. Investigating observed northwest Australian rainfall trends in Coupled Model Intercomparison Project phase 5 detection and attribution experiments. International Journal of Climatology, 39, 112-127.

Dey, R., Lewis, S. C., Arblaster, J. M., Abram, N. J., 2019. A review of past and projected changes in Australia's rainfall. WIREs Climate Change, 10, e577.

Di Virgilio, G., Evans, J. P., Di Luca, A., Olson, R., Argüeso, D., Kala, J., Andrys, J., Hoffmann, P., Katzfey, J. J., Rockel, B., 2019. Evaluating reanalysis-driven CORDEX regional climate models over Australia: Model performance and errors. Climate Dynamics, 53, 2985-3005.

Dickinson, R. E., Henderson-Sellers A., Kennedy, P. J., Wilson, M. F., 1986. Biosphere-Atmosphere Transfer Scheme (BATS) for the NCAR Community Climate Model (No. NCAR/TN-275-+STR), National Center for Atmospheric Research, Colorado.

Dickinson, R. E., Errico, R. M., Giorgi, F., Bates, G. T., 1989. A regional climate model for the western United States. Climatic Change, 15, 383-422.

Dickinson, R. E., Henderson-Sellers, A., Kennedy, P. J., 1993. Biosphere-Atmosphere Transfer Scheme (BATS) Version 1e as Coupled to the NCAR Community Climate Model (No. NCAR/TN-387+STR), National Center for Atmospheric Research, Colorado.

Diffenbaugh, N. S., Giorgi, F., 2012. Climate change hotspots in the CMIP5 global climate model ensemble. Climatic Change, 114, 813-822.

Donat, M. G., Alexander, L. V., Yang, H., Durre, I., Vose, R., Dunn, R. J. H., Willett, K. M., Aguilar, E., Brunet, M., Caesar, J., Hewitson, B., Jack, J., Klein Tank, A. M. G., Kruger, A. C., Marengo, J., Peterson, T. C., Renom, M., Oria Rojas, C., Rusticucci, M., Salinger, J., Elrayah, A. S., Sekele, S. S., Srivastava, A. K., Trewin, B., Villarroel, C., Vincent, L. A., Zhai, P., Zhang, X., Kitching, S., 2013. Updated analyses of temperature and precipitation extreme indices since the beginning of the twentieth century: The HadEX2 dataset. Journal of Geophysical Research: Atmospheres, 118, 2098-2118.

Donat, M. G., Sillmann, J., Wild, S., Alexander, L. V., Lippmann, T., Zwiers, F. W., 2014. Consistency of temperature and precipitation extremes across various global gridded in situ and reanalysis datasets. Journal of Climate, 27, 5019-5035.

Donat, M. G., Lowry, A. L., Alexander, L. V., O'Gorman, P. A., Maher, N., 2016. More extreme precipitation in the world's dry and wet regions. Nature Climate Change, 6, 508-513.

Dudhia, J., Gill, D., Manning, K., Wang, W., Bruyere, C., Kelly, S., Lackey, K., 2005. PSU/NCAR Mesoscale Modeling System Tutorial Class Notes and User's Guide: MM5 Modeling System Version 3, National Center for Atmospheric Research, Colorado.

Edwards, P. N., 2011. History of climate modeling. WIREs Climate Change, 2, 128-139.

Elguindi, N., Bi, X., Giorgi, F., Nagarajan, B., Pal, J., Solmon, F., Rauscher, S., Zakey, A., O'Brien, T., Nogherotto, R., Giuliani, G., 2014. Regional Climate Model RegCM Reference Manual Version 4.6, The Abdus Salam International Centre for Theoretical Physics Earth System Physics Section, Trieste.

Emanuel, K. A., 1991. A scheme for representing cumulus convection in large-scale models. Journal of Atmospheric Sciences, 48, 2313-2329.

Emanuel, K. A., Živković-Rothman, M., 1999. Development and evaluation of a convection scheme for use in climate models. Journal of the Atmospheric Sciences, 56, 1766-1782.

Endler, C., Matzarakis, A., 2011. Analysis of high-resolution simulations for the Black Forest region from a point of view of tourism climatology–a comparison between two regional climate models (REMO and CLM). Theoretical and Applied Climatology, 103, 427-440.

Evans, J. P., McCabe, M. F., 2010. Regional climate simulation over Australia's Murray-Darling basin: A multitemporal assessment. Journal of Geophysical Research, 115, D14114.

Evans, J. P., 2011. CORDEX–An International Climate Downscaling Initiative, Proceedings of the 19th International Congress on Modelling and Simulation, 2705-2711, Perth, 12-16 December 2011, 2705-2711.

Evans, J. P., Ekström, M., Ji, F., 2012. Evaluating the performance of a WRF physics ensemble over South-East Australia. Climate Dynamics, 39, 1241-1258.

Evans, J. P., McCabe, M. F., 2013. Effect of model resolution on a regional climate model simulation over southeast Australia. Climate Research, 56, 131-145.

Evans, J. P., Ji, F., Lee, C., Smith, P., Argüeso, D., Fita, L., 2014. Design of a regional climate modelling projection ensemble experiment–NARCliM. Geoscientific Model Development, 7, 621-629.

Ezer, A., Ozturk, T., Turp, M. T., Kurnaz, M. L., 2017. Projections for Changes in Precipitation Extremes of the CORDEX-Central Asia Domain Using RegCM4.3.5 Under RCP8.5 Scenario, EGU General Assembly 2017 Conference Abstracts, Vienna, 23-28 April 2017, 5440.

Flato, G., Marotzke, J., Abiodun, B., Braconnot, P., Chou, S. C., Collins, W., Cox, P., Driouech, F., Emori, S., Eyring, V., Forest, C., Gleckler, P., Guilyardi, E., Jakob, C., Kattsov, V., Reason, C., Rummukainen, M., 2013. Evaluation of Climate Models. In Stocker T. F., Qin D., Plattner G.-K., Tignor M., Allen S. K., Boschung J., Nauels A., Xia Y., Bex V., Midgley P. M. (Eds.), Climate Change 2013: The Physical Science Basis. Contribution of Working Group I to the Fifth Assessment Report of the Intergovernmental Panel on Climate Change, Cambridge University Press, Cambridge and New York.

Frey-Buness, F., Heimann, D., Sausen, R., 1995. A statistical-dynamical downscaling procedure for global climate simulations. Theoretical and Applied Climatology, 50, 117-131.

Frich, P., Alexander, L. V., Della-Marta, P., Gleason, B., Haylock, M., Klein Tank, A. M. G., Peterson, T., 2002. Observed coherent changes in climatic extremes during the second half of the twentieth century. Climate Research, 19, 193-212.

Fritsch, J. M., Chappell, C. F., 1980. Numerical prediction of convectively driven mesoscale pressure systems. Part I: Convective parameterization. Journal of Atmospheric Sciences, 37, 1722-1733.

Fritsch J. M., Kain J. S., 1993. Convective Parameterization for Mesoscale Models: The Fritsch-Chappell Scheme. In Emanuel K. A., Raymond D.J. (Eds.), The Representation of Cumulus Convection in Numerical Models, 165-170, American Meteorological Society, Boston.

Fuentes, U., Heimann, D., 2000. An improved statistical-dynamical downscaling scheme and its application to the Alpine precipitation climatology. Theoretical and Applied Climatology, 65, 119-135.

Fujino, J., Nair, R., Kainuma, M., Masui, T., Matsuoka, Y., 2006. Multi-gas mitigation analysis on stabilization scenarios using AIM global model. The Energy Journal, 27, 343-354.

Gao, X., Zhao, Z., Giorgi, F., 2002. Changes of extreme events in regional climate simulations over East Asia. Advances in Atmospheric Sciences, 19, 927-942.

Gao, Y., Ma, S., Wang, T., 2019. The impact of climate change on wind power abundance and variability in China. Energy, 189, 116215.

Giorgi, F., Bates, G. T., 1989. The climatological skill of a regional model over complex terrain. Monthly Weather Review, 117, 2325-2347.

Giorgi, F., 1990. Simulation of regional climate using a limited area model nested in a general circulation model. Journal of Climate, 3, 941-963.

Giorgi, F., Marinucci, M. R., Visconti, G., 1990. Use of a limited area model nested in a general circulation model for regional climate simulation over Europe. Journal of Geophysical Research, 95, 18413-18431.

Giorgi, F., Mearns, L. O., 1991. Approaches to the simulation of regional climate change: A review. Reviews of Geophysics, 29, 191-216.

Giorgi, F., Bates, G. T., Nieman, S. J., 1993a. The multiyear surface climatology of a regional atmospheric model over the western United States. Journal of Climate, 6, 75-95.

Giorgi, F., Marinucci, M. R., Bates, G. T., 1993b. Development of a second generation regional climate model (RegCM2). Part I: Boundary layer and radiative transfer processes. Monthly Weather Review, 121, 2794-2813.

Giorgi, F., Marinucci, M. R., Bates, G. T., de Canio, G., 1993c. Development of a second generation regional climate model (RegCM2). Part II: Convective processes and assimilation of lateral boundary conditions. Monthly Weather Review, 121, 2814-2832.

Giorgi, F., Shields Brodeur, C., Bates, G. T., 1994. Regional climate change scenarios over the United States produced with a nested regional climate model. Journal of Climate, 7, 375-399.

Giorgi, F., 1995. Perspectives for regional earth system modeling. Global and Planetary Change, 10, 23-42.

Giorgi, F., Jones, C., Asrar, G. R., 2009. Addressing climate information needs at the regional level: the CORDEX framework. World Meteorological Organization (WMO) Bulletin, 58, 175-183.

Giorgi, F., Coppola, E., Solmon, F., Mariotti, L., Sylla, M. B., Bi, X., Elguindi, N., Diro, G. T., Nair, V., Giuliani, G., Turuncoglu, U. U., Cozzini, S., Güttler, I., O'Brien, T. A., Tawfik, A. B., Shalaby, A., Zakey, A. S., Steiner, A. L., Stordal, F., Sloan, L. C., Brankovic, C., 2012. RegCM4: model description and preliminary tests over multiple CORDEX domains. Climate Research, 52, 7-29.

Giorgi, F., 2014. Introduction to the special issue: the phase I CORDEX RegCM4 hyper-matrix (CREMA) experiment. Climatic Change, 125, 1, 1-5.

Giorgi, F., Coppola, E., Raffaele, F., Diro, G. T., Fuentes-Franco, R., Giuliani, G., Mamgain, A., Llopart, M. P., Mariotti, L., Torma, C., 2014. Changes in extremes and hydroclimatic regimes in the CREMA ensemble projections. Climatic Change, 125, 1, 39-51.

Giorgi, F., Gutowski Jr, W. J., 2015. Regional dynamical downscaling and the CORDEX initiative. Annual Review of Environment and Resources, 40, 467-490.

Giorgi, F., Solmon, F., Giuliani, G., 2016. Regional Climatic Model RegCM User's Guide Version 4.5, The Abdus Salam International Centre for Theoretical Physics Earth System Physics Section, Trieste.

Giorgi, F., Coppola, E., Giuliani, G., 2017. Plans for RegCM4 CORDEX-CORE Simulations, EGU General Assembly 2017 Conference Abstracts, Vienna, 23-28 April 2017, 2195.

Giorgi, F., Gao, X. J., 2018. Regional earth system modeling: Review and future directions. Atmospheric and Oceanic Science Letters, 11, 189-197.

Giorgi, F., 2019. “30-Years of Regional Climate Modeling: Where Are We, How Did We Get There and Where Are We Going?”, https://icrc-cordex2019.cordex.org/wp-content/uploads/sites/2/2019/10/Giorgi-ICRC-2019-30-years_LR.pdf. (accessed May 2020).

Gramelsberger, G., 2009. Conceiving Meteorology as the exact science of the atmosphere: Vilhelm Bjerknes's paper of 1904 as a milestone. Meteorologische Zeitschrift, 18, 669-673.

Grell, G. A., 1993. Prognostic evaluation of assumptions used by cumulus parameterizations. Monthly Weather Review, 121, 764-787.

Grell, G. A., Dudhia, J. M., Stauffer, D. R., 1994. Description of the Fifth-Generation Penn State/NCAR Mesoscale Model (MM5) (No. NCAR/TN-398+STR), National Center for Atmospheric Research, Colorado.

Grenier, H., Bretherton, C.S., 2001. A moist PBL parameterization for large-scale models and its application to subtropical cloud-topped marine boundary layers. Monthly Weather Review, 129, 357-377.

Gu, H., Wang, G., Yu, Z., Mei, R., 2012. Assessing future climate changes and extreme indicators in east and south Asia using the RegCM4 regional climate model. Climatic Change, 114, 301-317.

Gutowski Jr., W. J., Giorgi, F., Timbal, B., Frigon, A., Jacob, D., Kang, H.-S., Raghavan, K., Lee, B., Lennard, C., Nikulin, G., O’Rourke, E., Rixen, M., Solman, S., Stephenson, T., Tangang, F., 2016. WCRP coordinated regional downscaling experiment (CORDEX): A diagnostic MIP for CMIP6. Geoscientific Model Development, 9, 4087-4095.

Hack, J. J, Boville, B.A., Briegleb, B. P., Kiehl, J. T., Rasch, P. J., Williamson, D. L., 1993. Description of the NCAR Community Climate Model (CCM2) (No. NCAR/TN-382+STR), National Center for Atmospheric Research, Colorado.

Hansen, J., Fung, I., Lacis, A., Rind, D., Lebedeff, S., Ruedy, R., Russell, G., Stone, P., 1988. Global climate changes as forecast by Goddard Institute for Space Studies three-dimensional model. Journal of Geophysical Research, 93, 9341-9364.

Harris, I., Osborn, T. J., Jones, P., Lister, D., 2020. Version 4 of the CRU TS monthly high-resolution gridded multivariate climate dataset. Scientific Data, 7, 1-18.

Hausfather, Z., Drake, H. F., Abbott, T., Schmidt, G. A., 2020. Evaluating the performance of past climate model projections. Geophysical Research Letters, 47, e2019GL085378.

Haylock, M. R., Peterson, T. C., Alves, L. M., Ambrizzi, T., Anunciação, Y. M. T., Baez, J., Barros, V. R., Berlato, M. A., Bidegain, M., Coronel, G., Corradi, V., Garcia, V. J., Grimm, A. M., Karoly, D., Marengo, J. A., Marino, M. B., Moncunill, D. F., Nechet, D., Quintana, J., Rebello, E., Rusticucci, M., Santos, J. L., Trebejo, I., Vincent, L. A., 2006. Trends in total and extreme South American rainfall in 1960–2000 and links with sea surface temperature. Journal of Climate, 19, 1490-1512.

Heimann, D., 1986. Estimation of regional surface layer wind field characteristics using a three-layer mesoscale model. Beitraege zur Physik der Atmosphaere, 59, 518-537.

Heimann, D., 2001. A model-based wind climatology of the eastern Adriatic coast. Meteorologische Zeitschrift, 10, 5-16.

Hendrawan, I. G., Asai, K., Triwahyuni, A., Lestari, D. V., 2019. The interanual rainfall variability in Indonesia corresponding to El Niño Southern Oscillation and Indian Ocean Dipole. Acta Oceanologica Sinica, 38, 57-66.

Herger, N., Abramowitz, G., Knutti, R., Angélil, O., Lehmann, K., Sanderson, B. M., 2018. Selecting a climate model subset to optimise key ensemble properties. Earth System Dynamics, 9, 135-151.

Herold, N., Ekström, M., Kala, J., Goldie, J., Evans, J. P., 2018. Australian climate extremes in the 21st century according to a regional climate model ensemble: Implications for health and agriculture. Weather and Climate Extremes, 20, 54-68.

Hewitson, B. C., Crane, R. G., 1996. Climate downscaling: techniques and application. Climate Research, 7, 85-95.

Hijioka, Y., Matsuoka, Y., Nishimoto, H., Masui, M., Kainuma, M., 2008. Global GHG emissions scenarios under GHG concentration stabilization targets. Journal of Global Environmental Engineering, 13, 97-108.

Hoffmann, P., Schoetter, R., Schlünzen, H., 2018. Statistical-dynamical downscaling of the urban heat island in Hamburg, Germany. Meteorologische Zeitschrift, 27, 89-109.

Holton, J. H., 2004. An Introduction to Dynamic Meteorology, Elsevier Academic Press, Massachusetts.

Holtslag, A. A. M., De Bruijn, E. I. F., Pan, H.-L., 1990. A high resolution air mass transformation model for short-range weather forecasting. Monthly Weather Review, 118, 1561-1575.

Holtslag, A. A. M., Boville, B. A., 1993. Local versus nonlocal boundary-layer diffusion in a global climate model. Journal of Climate, 6, 1825-1842.

Houghton, J., 2009. Global Warming: The Complete Briefing, Fourth Edition, Cambridge University Press, New York.

IPCC, 1990. The IPCC Scientific Assessment, Cambridge University Press, Cambridge, New York, Melbourne.

IPCC, 1996. Climate Change 1995: The Science of Climate Change. Contribution of Working Group I to the Second Assessment Report of the Intergovernmental Panel on Climate Change, Cambridge University Press, Cambridge, New York, Melbourne.

IPCC, 2001. Climate Change 2001: The Scientific Basis. Contribution of Working Group I to the Third Assessment Report of the Intergovernmental Panel on Climate Change, Cambridge University Press, Cambridge and New York.

IPCC, 2007. Climate Change 2007: The Physical Science Basis. Working Group I Contribution to the Fifth Assessment Report of the Intergovernmental Panel on Climate Change, Cambridge University Press, Cambridge and New York.

IPCC, 2012. Managing the Risks of Extreme Events and Disasters to Advance Climate Change Adaptation. A Special Report of Working Groups I and II of the Intergovernmental Panel on Climate Change, Cambridge University Press, Cambridge and New York.

IPCC, 2013. Climate Change 2013: The Physical Science Basis. Contribution of Working Group I to the Fifth Assessment Report of the Intergovernmental Panel on Climate Change, Cambridge University Press, Cambridge and New York.

Jacobson, M. Z., 2005. Fundamentals of Atmospheric Modeling, Second Edition, Cambridge University Press, New York.

Jakob, D., Walland, D., 2016. Variability and long-term change in Australian temperature and precipitation extremes. Weather and Climate Extremes, 14, 36-55.

Jewell, R., 1984. The meteorological judgment of Vilhelm Bjerknes. Social Research, 51, 783-807.

Johnson, F., White, C. J., van Dijk, A., Ekstrom, M., Evans, J. P., Jakob, D., Kiem, A. S., Leonard, M., Rouillard, A., Westra, S., 2016. Natural hazards in Australia: floods. Climatic Change, 139, 21-35.

Jones, R. G., Murphy, J. M., Noguer, M., 1995. Simulation of climate change over Europe using a nested regional-climate model. I: Assessment of control climate, including sensitivity to location of lateral boundaries. Quarterly Journal of the Royal Meteorological society, 121, 1413-1449.

Jones, P. W., 1998. A User’s Guide for SCRIP: A Spherical Coordinate Remapping and Interpolation Package: Version 1.5, University of California, Los Alamos National Laboratory (LANL), New Mexico.

Joseph, J. H., Wiscombe, W. J., Weinman, J. A., 1976. The delta-Eddington approximation for radiative flux transfer. Journal of Atmospheric Sciences, 33, 2452-2459.

Kain, J. S., Fritsch, J. M., 1990. A one-dimensional entraining/detraining plume model and its application in convective parameterization. Journal of Atmospheric Sciences, 47, 2784-2802.

Kain J. S., Fritsch J. M., 1993. Convective Parameterization for Mesoscale Models: The Kain-Fritsch Scheme. In Emanuel K. A., Raymond D. J. (Eds.), The Representation of Cumulus Convection in Numerical Models, 159-164, American Meteorological Society, Boston.

Kain, J. S., 2004. The Kain–Fritsch convective parameterization: An update. Journal of Applied Meteorology, 43, 170-181.

Kalnay, E., Kanamitsu, M., Kistler, R., Collins, W., Deaven, D., Gandin, L., Iredell, M., Saha, S., White, G., Woollen, J., Zhu, Y., Chelliah, M., Ebisuzaki, W., Higgins, W., Janowiak, J., Mo, K. C., Ropelewski, C., Wang, J., Leetmaa, A., Reynolds, R., Jenne, R., Joseph, D. 1996. The NCEP/NCAR 40-year reanalysis project. Bulletin of the American Meteorological Society, 77, 437-472.

Kanamitsu, M., Ebisuzaki, W., Woollen, J., Yang, S.K., Hnilo, J. J., Fiorino, M., Potter, G. L., 2002. NCEP–DOE AMIP-II Reanalysis (R-2). Bulletin of the American Meteorological Society, 83, 1631-1644.

Karl, T. R., Nicholls, N., Ghazi, A., 1999. Clivar/GCOS/WMO workshop on indices and indicators for climate extremes workshop summary. Climatic Change, 42, 3-7.

Kasahara, A., Washington, W. M., 1967. NCAR global general circulation model of the atmosphere. Monthly Review Weather, 95, 389-402.

Kiehl, J. T., Hack, J. J, Bonan, G. B., Boville, B. A., Briegleb, B. P., Williamson, D. L., Rasch, P. J., 1996. Description of the NCAR Community Climate Model (CCM3) (No. NCAR/TN-420+STR), National Center for Atmospheric Research, Colorado.

King, A. D., Klingaman, N. P., Alexander, L. V., Donat, M. G., Jourdain, N. C., Maher, P., 2014. Extreme rainfall variability in Australia: Patterns, drivers, and predictability. Journal of Climate, 27, 6035-6050.

Klein Tank, A. M. G., 2004. Changing Temperature and Precipitation Extremes in Europe's Climate of the 20th Century, Ph.D. Dissertation, Utrecht University.

Klein Tank, A. M. G., Zwiers, F. W., Zhang, X.. 2009. Guidelines on Analysis of Extremes in a Changing Climate in Support of Informed Decisions for Adaptation, World Meteorological Organization, Geneva.

Kriegler, E., O'Neill, B. C., Hallegatte, S., Kram, T., Lempert, R. J., Moss, R. H., Wilbanks, T., 2012. The need for and use of socio-economic scenarios for climate change analysis: A new approach based on shared socio-economic pathways. Global Environmental Change, 22, 807-822.

Kumar, P., Kumar, S., Barat, A., Sarthi, P. P., Sinha, A. K., 2020. Evaluation of NASA's NEX-GDDP-simulated summer monsoon rainfall over homogeneous monsoon regions of India. Theoretical and Applied Climatology, 141, 525-536.

Kuo, H. L., 1965. On formation and intensification of tropical cyclones through latent heat release by cumulus convection. Journal of Atmospheric Sciences, 22, 40-63.

Kuo, H. L., 1974. Further studies of the parameterization of the influence of cumulus convection on large-scale flow. Journal of Atmospheric Sciences, 31, 1232-1240.

Lanzante, J. R., Dixon, K. W., Nath, M. J., Whitlock, C. E., Adams-Smith, D., 2018. Some pitfalls in statistical downscaling of future climate. Bulletin of the American Meteorological Society, 99, 791-803.

Legates, D. R., Willmott, C. J., 1990a. Mean seasonal and spatial variability in global surface air temperature. Theoretical and Applied Climatology, 41, 11-21.

Legates, D. R., Willmott, C. J., 1990b. Mean seasonal and spatial variability in gauge-corrected, global precipitation. International Journal of Climatology, 10, 111-127.

Leggett, J., Pepper, W. J., Swart, R. J., 1992. Emissions Scenarios for the IPCC: An Update. In Houghton J. T., Callander B. A., Varney S. K. (Eds.), Climate Change 1992: The Supplementary Report to the IPCC Scientific Assessment, 75-95, Cambridge University Press, Cambridge.

Lenton, A., Matear, R. J., Mongin, M., 2018. Effects of Climate Change on Ocean Acidification Relevant to the Pacific Islands, Pacific Marine Climate Change Report Card 2018, 31-42, Commonwealth Marine Economies Programme, UK.

Li, G., Xie, S. P., 2014. Tropical biases in CMIP5 multimodel ensemble: The excessive equatorial Pacific cold tongue and double ITCZ problems. Journal of Climate, 27, 1765-1780.

Li, C., Fang, Y., Caldeira, K., Zhang, X., Diffenbaugh, N. S., Michalak, A. M., 2018. Widespread persistent changes to temperature extremes occurred earlier than predicted. Scientific Reports, 8, 1-8.

Li, M., Guo, J., He, J., Xu, C., Li, J., Mi, C., Tao, S., 2020. Possible impact of climate change on apple yield in Northwest China. Theoretical and Applied Climatology, 139, 191-203.

Loughran, T. F., Pitman, A. J., Perkins-Kirkpatrick, S. E., 2019. The El Niño–Southern Oscillation's effect on summer heatwave development mechanisms in Australia. Climate Dynamics, 52, 6279-6300.

Lynch, P., 2006. The Emergence of Numerical Weather Prediction: Richardson's Dream, Cambridge University Press, New York.

Lynch, P., 2008. The origins of computer weather prediction and climate modeling. Journal of Computational Physics, 227, 3431-3444.

Mahony, M., 2017. The (Re)Emergence of Regional Climate: Mobile Models, Regional Visions and the Government of Climate Change. In Heymann M., Gramelsberger G., Mahony M. (Eds.), Cultures of Prediction in Atmospheric and Climate Science: Epistemic and Cultural Shifts in Computer-Based Modelling and Simulation, 139-158, Routledge, Oxfordshire.

Manabe, S., Bryan, K., 1969. Climate calculations with a combined ocean-atmosphere model. Journal of the Atmospheric Sciences, 26, 786-789.

Manabe, S., Bryan, K., Spelman, M. J., 1975. A global ocean-atmosphere climate model. Part I. The atmospheric circulation. Journal of Physical Oceanography, 5, 3-29.

Manabe, S., Wetherald, R. T., 1975. The effects of doubling the CO_2 concentration on the climate of a general circulation model. Journal of the Atmospheric Sciences, 32, 3-15.

Manabe, S., Stouffer, R. J. 1980. Sensitivity of a global climate model to an increase of CO_2 concentration in the atmosphere. Journal of Geophysical Research, 85, 5529-5554.

Maraun, D., Wetterhall, F., Ireson, A. M., Chandler, R. E., Kendon, E. J., Widmann, M., Brienen, S., Rust, H. W., Sauter, T., Themeßl, M., Venema, V. K. C., Chun, K. P., Goodess, C. M., Jones, R. G., Onof, C. Vrac, M., Thiele-Eich, I., 2010. Precipitation downscaling under climate change: Recent developments to bridge the gap between dynamical models and the end user. Reviews of Geophysics, 48, RG3003.

Maraun, D., Widmann, M., 2018. Statistical Downscaling and Bias Correction for Climate Research, Cambridge University Press, Cornwall.

Marin, M., Feng, M., Phillips, H. E., Bindoff, N. L., 2021. A global, multiproduct analysis of coastal marine heatwaves: Distribution, characteristics, and long-term trends. Journal of Geophysical Research: Oceans, 126, e2020JC016708.

Mariotti, L., Diallo, I., Coppola, E., Giorgi, F., 2014. Seasonal and intraseasonal changes of African monsoon climates in 21st century CORDEX projections. Climatic Change, 125, 53-65.

Maurer, E. P., Hidalgo, H. G., 2008. Utility of daily vs. monthly large-scale climate data: An intercomparison of two statistical downscaling methods. Hydrology and Earth System Sciences, 12, 551-563.

McCaa, J. R., Bretherton, C. S., 2004. A new parameterization for shallow cumulus convection and its application to marine subtropical cloud-topped boundary layers. Part II: Regional simulations of marine boundary layer clouds. Monthly Weather Review, 132, 883-896.

Mearns, L. O., Bogardi, I., Giorgi, F., Matyasovszky, I., Palecki, M., 1999. Comparison of climate change scenarios generated from regional climate model experiments and statistical downscaling. Journal of Geophysical Research, 104, 6603-6621.

Mearns, L. O., Gutowski, W., Jones, R., Leung, R., McGinnis, S., Nunes, A., Qian, Y., 2009. A regional climate change assessment program for North America. Eos, Transactions, American Geophysical Union, 90, 311-311.

Measey, M., 2010. Indonesia: A vulnerable country in the face of climate change. Global Majority E-Journal, 1, 31-45.

Meinshausen, M., Smith, S. J., Calvin, K., Daniel, J. S., Kainuma, M. L. T., Lamarque, J.-F., Matsumoto, K., Montzka, S. A., Raper, S. C. B., Riahi, K., Thomson, A.,Velders, G. J. M., van Vuuren, D. P. P., 2011. The RCP greenhouse gas concentrations and their extensions from 1765 to 2300. Climatic Change, 109, 213-241.

Meleux, F., Solmon, F., Giorgi, F., 2007. Increase in summer European ozone amounts due to climate change. Atmospheric Environment, 41, 7577-7587.

Menéndez, C. G., De Castro, M., Sorensson, A., Boulanger, J. P., 2010. CLARIS project: Towards climate downscaling in South America. Meteorologische Zeitschrift, 19, 357-362.

Mengelkamp, H. T., Kapitza, H., Pflüger, U., 1997. Statistical-dynamical downscaling of wind climatologies. Journal of Wind Engineering and Industrial Aerodynamics, 67, 449-457.

Meyers, G., McIntosh, P., Pigot, L., Pook, M., 2007. The years of El Niño, La Niña, and interactions with the tropical Indian Ocean. Journal of Climate, 20, 2872-2880.

Ministry of Foreign Affairs of the Netherlands, 2018. "Climate Change Profile: Indonesia", https://www.government.nl/documents/publications/2019/02/05/climate-change-profiles. (accessed January 2021).

Mlawer, E. J., Taubman, S. J., Brown, P. D., Iacono, M. J., Clough, S. A., 1997. Radiative transfer for inhomogeneous atmospheres: RRTM, a validated correlated-k model for the longwave. Journal of Geophysical Research, 102, 16663-16682.

Moss, R. H., Edmonds, J. A., Hibbard, K. A., Manning, M. R., Rose, S. K., van Vuuren, D. P., Carter, T. R., Emori, S., Kainuma, M., Kram, T., Meehl, G. A., Mitchell, J. F., Nakicenovic, N., Riahi, K., Smith, S. J., Stouffer, R. J., Thomson, A. M., Weyant, J. P., Wilbanks, T. J., 2010. The next generation of scenarios for climate change research and assessment. Nature, 463, 747-756.

Murphy, J., 1999. An evaluation of statistical and dynamical techniques for downscaling local climate. Journal of Climate, 12, 2256-2284.

Murphy, B. F., Timbal, B., 2008. A review of recent climate variability and climate change in southeastern Australia. International journal of Climatology, 28, 859-879.

Nakićenović, N., Alcamo, J., Davis, G., de Vries, B., Fenhann, J., Gaffin, S., Gregory, K., Grübler, A., Jung, T. Y., Kram, T., La Rovere, E.L., Michaelis, L., Mori, S., Morita, T., Pepper, W., Pitcher, H., Price, L., Raihi, K., Roehrl, A., Rogner, H.-H., Sankovski, A., Schlesinger, M., Shukla, P., Smith, S., Swart, R., van Rooijen, S., Victor, N., Dadi, Z., 2000. Emissions Scenarios. A Special Report of Working Group III of the Intergovernmental Panel on Climate Change, Cambridge University Press, New York.

NASA, 2021a. "Facts: Global Temperature. Global Climate Change: Vital Signs of the Planet", https://climate.nasa.gov/vital-signs/global-temperature/. (accessed March 2021).

NASA, 2021b. "Facts: Carbon Dioxide. Global Climate Change: Vital Signs of the Planet", https://climate.nasa.gov/vital-signs/carbon-dioxide/. (accessed March 2021).

National Research Council, 2012. A National Strategy for Advancing Climate Modeling, The National Academies Press, Washington.

Nebeker, F., 1995. Calculating the Weather: Meteorology in the 20th Century, Academic Press, San Diego.

Neelin, J. D., 2011. Climate Change and Climate Modeling, Cambridge University Press, New York.

NOAA NCEI, 2021. "Climate at A Glance: Global Time Series. Climate Monitoring", https://www.ncdc.noaa.gov/cag/. (accessed March 2021).

Null, J. 2021. "El Niño and La Niña Years and Intensities: Based on Oceanic Niño Index (ONI)", https://ggweather.com/enso/oni.htm. (accessed March 2021).

Nur'utami, M. N., Hidayat, R., 2016. Influences of IOD and ENSO to Indonesian rainfall variability: role of atmosphere-ocean interaction in the Indo-Pacific sector. Procedia Environmental Sciences, 33, 196-203.

Office of the Prime Minister's Science Advisory Committee, 2013. New Zealand's Changing Climate and Oceans: The Impact of Human Activity and Implications for the Future. An Assessment of the Current State of Scientific Knowledge by the Office of the Chief Science Advisor, Office of the Prime Minister's Science Advisory Committee, Auckland.

Olesen, J. E., Carter, T. R., Diaz-Ambrona, C. H., Fronzek, S., Heidmann, T., Hickler, T., Holt, T., Minguez, M. I., Morales, P., Palutikof, J. P., Quemada, M., Ruiz-Ramos, M., Rubæk, G. H., Sau, F., Smith, B., Sykes, M. T., 2007. Uncertainties in projected impacts of climate change on European agriculture and terrestrial ecosystems based on scenarios from regional climate models. Climatic Change, 81, 123-143.

Oleson, K. W., Lawrence, D. M., Bonan, G. B., Drewniak, B., Huang, M., Koven, C. D., Levis, S., Li, F., Riley, W. J., Subin, Z. M., Swenson, S. C., Thornton, P. E., Bozbiyik, A., Fisher, R., Heald, C. L., Kluzek, E., Lamarque, J.-F., Lawrence, P. J., Leung, L. R., Lipscomb, W., Muszala, S., Ricciuto, D. M., Sacks, W., Sun, Y., Tang, J., Yang, Z.-L., 2013. Technical Description of Version 4.5 of the Community Land Model (CLM) (No. NCAR/TN-503+STR), National Center for Atmospheric Research, Colorado.

O'Neill, B. C., Kriegler, E., Riahi, K., Ebi, K. L., Hallegatte, S., Carter, T. R., Mathur, R., van Vuuren, D. P., 2014. A new scenario framework for climate change research: The concept of shared socioeconomic pathways. Climatic Change, 122, 387-400.

Ozturk, T., Altinsoy, H., Türkeş, M., Kurnaz, M. L., 2012. Simulation of temperature and precipitation climatology for the Central Asia CORDEX domain using RegCM 4.0. Climate Research, 52, 63-76.

Ozturk, T., Turp, M. T., Türkeş, M., Kurnaz, M. L., 2017. Projected changes in temperature and precipitation climatology of Central Asia CORDEX Region 8 by using RegCM4.3.5. Atmospheric Research, 183, 296-307.

Ozturk, T., Turp, M. T., Türkeş, M., Kurnaz, M. L., 2018. Future projections of temperature and precipitation climatology for CORDEX-MENA domain using RegCM4.4. Atmospheric Research, 206, 87-107.

Öztürk, T., Türkeş, M., Kurnaz, M. L., 2011. RegCM4.3.5 iklim modeli benzetimleri kullanılarak Türkiye'nin gelecek hava sıcaklığı ve yağış klimatolojilerindeki değişikliklerin çözümlenmesi [Analysing projected changes in future air temperature and precipitation climatology of Turkey by using RegCM4.3.5 climate simulations]. Aegean Geographical Journal, 20, 17-27.

PACCSAP, 2015. Current and Future Climate of Papua New Guinea, Pacific-Australia Climate Change Science and Adaptation Planning Program (PACCSAP) Partners, Australia.

Pal, J. S., Giorgi, F., Bi, X., Elguindi, N., Solmon, F., Rauscher, S. A., Gao, X., Francisco, R., Zakey, A., Winter, J., Ashfaq, M., Syed, F. S., Sloan, L.C., Bell, J. L., Diffenbaugh, N. S., Karmacharya, J., Konaré, A., Martinez, D., Da Rocha, R. P., Steiner, A. L., 2007. Regional climate modeling for the developing world: The ICTP RegCM3 and RegCNET. Bulletin of the American Meteorological Society, 88, 1395-1409.

Pal, J. S., Eltahir, E. A., 2016. Future temperature in southwest Asia projected to exceed a threshold for human adaptability. Nature Climate Change, 6, 197-200.

Parker, W. S., 2013. Ensemble modeling, uncertainty and robust predictions. WIREs Climate Change, 4, 213-223.

Peel, M. C., Finlayson, B. L., McMahon, T. A., 2007. Updated world map of the Köppen-Geiger climate classification. Hydrology and Earth System Sciences Discussions, 4, 439-473.

Perkins, S. E., Pitman, A. J., Holbrook, N. J., McAneney, J., 2007. Evaluation of the AR4 climate models' simulated daily maximum temperature, minimum temperature, and precipitation over Australia using probability density functions. Journal of Climate, 20, 4356-4376.

Perkins, S. E., Alexander, L. V., Nairn, J. R., 2012. Increasing frequency, intensity and duration of observed global heatwaves and warm spells. Geophysical Research Letters, 39, L20714.

Perkins, S. E., Argüeso, D., White, C. J., 2015. Relationships between climate variability, soil moisture, and Australian heatwaves. Journal of Geophysical Research: Atmospheres, 120, 8144-8164.

Perkins-Kirkpatrick, S. E., White, C. J., Alexander, L. V., Argüeso, D., Boschat, G., Cowan, T., Evans, J. P., Ekström, M., Oliver, E. C. J., Phatak A., Purich, A., 2016. Natural hazards in Australia: Heatwaves. Climatic Change, 139, 101-114.

Persaud, E., Levison, J., MacRitchie, S., Berg, S. J., Erler, A.R., Parker, B., Sudicky, E., 2020. Integrated modelling to assess climate change impacts on groundwater and surface water in the Great Lakes Basin using diverse climate forcing. Journal of Hydrology, 584, 124682.

Peterson, T., Folland, C., Gruza, G., Hogg, W., Mokssit, A., Plummer, N., 2001. Report on the Activities of the Working Group on Climate Change Detection and Related Rapporteurs 1998-2001, World Meteorological Organization, Geneva.

Peterson, T. C., Taylor, M. A., Demeritte, R., Duncombe, D. L., Burton, S., Thompson, F., Porter, A., Mercedes, M., Villegas, E., Semexant Fils, R., Klein Tank, A., Martis, A., Warner, R., Joyette A., Mills, W., Alexander, L., Gleason, B., 2002. Recent changes in climate extremes in the Caribbean region. Journal of Geophysical Research, 107, 4601.

Phillips, N. A., 1956. The general circulation of the atmosphere: A numerical experiment. Quarterly Journal of the Royal Meteorological Society, 82, 123-164.

Pinto, J. G., Neuhaus, C. P., Leckebusch, G. C., Reyers, M., Kerschgens, M., 2010. Estimation of wind storm impacts over Western Germany under future climate conditions using a statistical—dynamical downscaling approach. Tellus A: Dynamic Meteorology and Oceanography, 62, 188-201.

Raghavan, S. V., Hur, J., Liong, S. Y., 2018. Evaluations of NASA NEX-GDDP data over Southeast Asia: Present and future climates. Climatic Change, 148, 503-518.

Raymond, D. J., Emanuel, K. A., 1993. The Kuo Cumulus Parameterization. In Emanuel K. A., Raymond D. J. (Eds.), The Representation of Cumulus Convection in Numerical Models, 145-147, American Meteorological Society, Boston.

Reboita, M. S., Amaro, T. R., De Souza, M. R., 2018. Winds: intensity and power density simulated by RegCM4 over South America in present and future climate. Climate Dynamics, 51, 187-205.

Reichler, T., Kim, J., 2008. How well do coupled models simulate today's climate? Bulletin of the American Meteorological Society, 89, 303-312.

Remedio, A. R., Teichmann, C., Buntemeyer, L., Sieck, K., Weber, T., Rechid, D., Hoffmann, P., Nam, C., Kotova, L., Jacob, D., 2019. Evaluation of New CORDEX Simulations Using an Updated Köppen–Trewartha Climate Classification. Atmosphere, 10, 726.

Reyers, M., Pinto, J. G., Moemken, J., 2015. Statistical–dynamical downscaling for wind energy potentials: evaluation and applications to decadal hindcasts and climate change projections. International Journal of Climatology, 35, 229-244.

Riahi, K., Gruebler, A., Nakićenović, N., 2007. Scenarios of long-term socio-economic and environmental development under climate stabilization. Technological Forecasting and Social Change, 74, 887-935.

Riahi, K., Rao, S., Krey, V., Cho, C., Chirkov, V., Fischer, G., Kindermann, G., Nakićenović, N., Rafaj, P., 2011. RCP 8.5—A scenario of comparatively high greenhouse gas emissions. Climatic Change, 109, 33-57.

Richardson, L. F., 1922. Weather Prediction by Numerical Process, Cambridge University Press, Cambridge.

Rockel, B., 2015. The regional downscaling approach: A brief history and recent advances. Current Climate Change Reports, 1, 22-29.

Rodó, X., Pascual, M., Doblas-Reyes, F. J., Gershunov, A., Stone, D. A., Giorgi, F., Hudson, P. J., Kinter, J., Rodríguez-Arias, M. A., Stenseth, N. C., Alonso, D., García-Serrano, J., Alonso, D., 2013. Climate change and infectious diseases: Can we meet the needs for better prediction? Climatic Change, 118, 625-640.

Rummukainen, M., 2010. State-of-the-art with regional climate models. WIREs Climate Change, 1, 82-96.

Sahany, S., Mishra, S. K., Salunke, P., 2019. Historical simulations and climate change projections over India by NCAR CCSM4: CMIP5 vs. NEX-GDDP. Theoretical and Applied Climatology, 135, 1423-1433.

Salinger, M. J., Basher, R. E., Fitzharris, B. B., Hay, J. E., Jones, P. D., Macveigh, J. P., Schmidely-Leleu, I., 1995. Climate trends in the South-west Pacific. International Journal of Climatology, 15, 285-302.

Salinger, M. J., Mullan, A. B., 1999. New Zealand climate: Temperature and precipitation variations and their links with atmospheric circulation 1930–1994. International Journal of Climatology, 19, 1049-1071.

Salinger, M. J., Griffiths, G. M., 2001. Trends in New Zealand daily temperature and rainfall extremes. International Journal of Climatology, 21, 1437-1452.

Schewe, J., Gosling, S. N., Reyer, C., Zhao, F., Ciais, P., Elliott, J., Francois, L., Huber, V., Lotze, H. K., Seneviratne, S. I., van Vliet, M. T. H., Vautard, R., Wada, Y., Breuer, L., Büchner, M., Carozza, D. A., Chang, J., Coll, M., Deryng, D., de Wit, A., Eddy, T. D., Folberth, C., Frieler, K., Friend, A. D., Gerten, D., Gudmundsson, L., Hanasaki, N., Ito, A., Khabarov, N., Kim, H., Lawrence, P., Morfopoulos, C., Müller, C., Schmied, H. M., Orth, R., Ostberg, S., Pokhrel, Y., Pugh, T. A. M., Sakurai, G., Satoh, Y., Schmid, E., Stacke, T., Steenbeek, J., Steinkamp, J., Tang, Q., Tian, H., Tittensor, D. P., Volkholz, J., Wang, X., Warszawski, L., 2019. State-of-the-art global models underestimate impacts from climate extremes. Nature Communications, 10, 1005.

Schubert, D., van der Linden, R., Reyers, M., Fink, A. H., Massmeyer, K., Pinto, J. G., 2017. Statistical-dynamical downscaling of precipitation for Vietnam: Methodology and evaluation for the recent climate. International Journal of Climatology, 37, 4211-4228.

Schulzweida, U., 2020. CDO User Guide: Climate Data Operator Version 1.9.9, Max-Planck Institute (MPI) for Meteorology, Hamburg.

Seneviratne, S. I., Nicholls, N., Easterling, D., Goodess, C. M., Kanae, S., Kossin, J., Luo, Y., Marengo, J., McInnes, K., Rahimi, M., Reichstein, M., Sorteberg, A., Vera, C., Zhang, X., 2012. Changes in Climate Extremes and Their Impacts on the Natural Physical Environment. In Field C. B., Barros V., Stocker T. F., Qin D., Dokken D. J., Ebi K. L., Mastrandrea M. D., Mach K. J., Plattner G.-K., Allen S. K., Tignor M., Midgley P. M. (Eds.), Managing the Risks of Extreme Events and Disasters to Advance Climate Change Adaptation. A Special Report of Working Groups I and II of the Intergovernmental Panel on Climate Change (IPCC), 109-230, Cambridge University Press, Cambridge and New York.

Sharples, J. J., Cary, G. J., Fox-Hughes, P., Mooney, S., Evans, J. P., Fletcher, M.-S., Fromm, M., Grierson, P. F., McRae, R., Baker, P., 2016. Natural hazards in Australia: Extreme bushfire. Climatic Change, 139, 85-99.

Sheffield, J., Goteti, G., Wood, E. F., 2006. Development of a 50-year high-resolution global dataset of meteorological forcings for land surface modeling. Journal of Climate, 19, 3088-3111.

Shepard, D., 1968. A Two-Dimensional Interpolation Function for Irregularly-Spaced Data, Proceedings of the 1968 23rd ACM National Conference, New York, 27-29 August 1968, 517-524.

Sillmann, J., Kharin, V. V., Zhang, X., Zwiers, F. W., Bronaugh, D., 2013a. Climate extremes indices in the CMIP5 multimodel ensemble: Part 1. Model evaluation in the present climate. Journal of Geophysical Research: Atmospheres, 118, 1716-1733.

Sillmann, J., Kharin, V. V., Zwiers, F. W., Zhang, X., Bronaugh, D., 2013b. Climate extremes indices in the CMIP5 multimodel ensemble: Part 2. Future climate projections. Journal of Geophysical Research: Atmospheres, 118, 2473-2493.

Simmons, A., Uppala, S., Dee, D., Kobayashi. S., 2006. ERA-Interim: New ECMWF reanalysis products from 1989 onwards. ECMWF Newsletter, 110, 26-35.

Smith, S. J., Wigley, T. M. L., 2006. Multi-Gas Forcing Stabilization with the MiniCAM. The Energy Journal, 27, 373-391.

Smith, I., Chandler, E., 2010. Refining rainfall projections for the Murray Darling Basin of south-east Australia—the effect of sampling model results based on performance. Climatic Change, 102, 377-393.

Song, Y., Wang, C., Linderholm, H. W., Tian, J., Shi, Y., Xu, J., Liu, Y., 2019. Agricultural adaptation to global warming in the Tibetan Plateau. International Journal of Environmental Research and Public Health, 16, 3686.

Stainforth, D. A., Allen, M. R., Tredger, E. R., Smith, L. A., 2007. Confidence, uncertainty and decision-support relevance in climate predictions. Philosophical Transactions of the Royal Society A: Mathematical, Physical and Engineering Sciences, 365, 2145-2161.

Steffen, W., Hughes, L., Perkins, S., 2014. Heatwaves: Hotter, Longer, More Often, Climate Council of Australia, Sydney.

Steiner, J. T., 1980. The Climate of the South-West Pacific Region. A Review for Pilots, New Zealand Meteorological Service Miscellaneous Publication 166, New Zealand Meteorological Service, Wellington.

Stevens, A., 2020. “A Warm Pool in The Indo-Pacific Ocean Has Almost Doubled in Size, Changing Global Rainfall Patterns”, https://www.climate.gov/news-features/featured-images/warm-pool-indo-pacific-ocean-has-almost-doubled-size-changing-global. (accessed March 2021).

Stouffer, R. J., Eyring, V., Meehl, G. A., Bony, S., Senior, C., Stevens, B., Taylor, K. E., 2017. CMIP5 scientific gaps and recommendations for CMIP6. Bulletin of the American Meteorological Society, 98, 95-105.

Sylla, M. B., Pal, J. S., Wang, G. L., Lawrence, P. J., 2016. Impact of land cover characterization on regional climate modeling over West Africa. Climate Dynamics, 46, 637-650.

Tapiador, F. J., Navarro, A., Moreno, R., Sánchez, J. L., García-Ortega, E., 2020. Regional climate models: 30 years of dynamical downscaling. Atmospheric Research, 235, 104785.

Tawfik, A. B., Steiner, A. L., 2011. The role of soil ice in land-atmosphere coupling over the United States: A soil moisture–precipitation winter feedback mechanism. Journal of Geophysical Research, 116, D02113.

Taylor, K. E., 2001. Summarizing multiple aspects of model performance in a single diagram. Journal of Geophysical Research, 106, 7183-7192.

Tebaldi, C., Knutti, R., 2007. The use of the multi-model ensemble in probabilistic climate projections. Philosophical Transactions of the Royal Society A: Mathematical, Physical and Engineering Sciences, 365, 2053-2075.

Teutschbein, C., Seibert, J., 2010. Regional climate models for hydrological impact studies at the catchment scale: a review of recent modeling strategies. Geography Compass, 4, 834-860.

Thrasher, B., Nemani, R., 2015. NASA Earth Exchange Global Daily Downscaled Projections (NEX-GDDP), NASA Ames Research Center, California.

Thrasher, B., Maurer, E. P., McKellar, C., Duffy, P. B., 2012. Technical note: Bias correcting climate model simulated daily temperature extremes with quantile mapping. Hydrology and Earth System Sciences, 16, 3309-3314.

Thrasher, B., Xiong, J., Wang, W., Melton, F., Michaelis, A., Nemani, R., 2013. Downscaled climate projections suitable for resource management. Eos, Transactions, American Geophysical Union, 94, 321-323.

Tiedtke, M., 1989. A comprehensive mass flux scheme for cumulus parameterization in large-scale models. Monthly Weather Review, 117, 1779-1800.

Tiedtke, M., 1996. An extension of cloud-radiation parameterization in the ECMWF model: The representation of subgrid-scale variations of optical depth. Monthly Weather Review, 124, 745-750.

Tobin, I., Vautard, R., Balog, I., Bréon, F. M., Jerez, S., Ruti, P. M., Thais, F., Vrac, M., Yiou, P., 2015. Assessing climate change impacts on European wind energy from ENSEMBLES high-resolution climate projections. Climatic Change, 128, 99-112.

Tozer, C. R., Risbey, J. S., Monselesan, D. P., Squire, D. T., Chamberlain, M. A., Matear, R. J., Ziehn, T., 2020. Assessing the representation of Australian regional climate extremes and their associated atmospheric circulation in climate models. Journal of Climate, 33, 1227-1245.

Trenberth, K. E., Dai, A., Rasmussen, R. M., Parsons, D. B., 2003. The changing character of precipitation. Bulletin of the American Meteorological Society, 84, 1205-1218.

Turp, M. T., Öztürk, T., Türkeş, M., Kurnaz, M. L., 2014a. RegCM4.3.5 bölgesel iklim modelini kullanarak Türkiye ve çevresi bölgelerin yakın gelecekteki hava sıcaklığı ve yağış klimatolojileri için öngörülen değişikliklerin incelenmesi [Investigation of projected changes for near future air temperature and precipitation climatology of Turkey and surrounding regions by using the regional climate model RegCM4.3.5]. Aegean Geographical Journal, 23, 1-24.

Turp, M. T., Ozturk, T., Türkeş, M., Kurnaz, M. L., 2014b. Assessment of Simulated Changes in Air Temperature and Precipitation Over Central Asia via Multi-Model Ensemble Means of CMIP5 Models, EGU General Assembly 2014 Conference Abstracts, Vienna, 27 April-2 May 2014, 7409.

Turp, M. T., Ozturk, T., Türkeş, M., Kurnaz, M. L., 2015. Assessment of projected changes in air temperature and precipitation over the Mediterranean Region via multi-model ensemble mean of CMIP5 models. Journal of the Black Sea/Mediterranean Environment, 21, 93-96.

Turp, M. T., Ozturk, T., Kurnaz, M. L., 2016a. Assessment of Projected Changes in Temperature and Precipitation Climatology Over the CORDEX-Region 9 via Multi-Model Ensemble Mean of CMIP5 Models, EGU General Assembly 2016 Conference Abstracts, Vienna, 17-22 April 2016, 12946.

Turp, M. T., Collu, K., Deler, F. B., Ozturk, T., Kurnaz, M. L., 2016b. Impacts of Climate Change on the Climate Extremes of the Middle East, EGU General Assembly 2016 Conference Abstracts, Vienna, 17-22 April 2016, 14225.

Turp, M. T., Kurnaz, M. L., 2017. CMIP5 Multi-Model Projection of the Changes in Air Temperature and Precipitation Climatology Over the CORDEX-Australasia Domain Under the RCP2.6 Scenario, EGU General Assembly 2017 Conference Abstracts, Vienna, 23-28 April 2017, 10802.

Turp, M. T., An, N., Kurnaz, M. L., 2017. Evaluation of Prospective Changes in Temperature Extremes for the CORDEX-Australasia Domain Using the NEX-GDDP Dataset, EGU General Assembly 2017 Conference Abstracts, Vienna, 23-28 April 2017, 10531.

Türkeş, M., 2010. Klimatoloji ve Meteoroloji, Birinci Baskı, Kriter Yayınevi, İstanbul.

Türkeş, M., 2013. IPCC İklim Değişikliği 2013: Fiziksel Bilim Temeli Politikacılar İçin Özet Raporundaki Yeni Bulgu ve Sonuçların Bilimsel Bir Değerlendirmesi. In İklim Değişikliğinde Son Gelişmeler: IPCC 2013 Raporu, 8-18, Sabancı Üniversitesi İstanbul Politikalar Merkezi (İPM), İstanbul.

Ummenhofer, C. C., England, M. H., 2007. Interannual extremes in New Zealand precipitation linked to modes of Southern Hemisphere climate variability. Journal of Climate, 20, 5418-5440.

Ummenhofer, C. C., Gupta, A. S., England, M. H., 2009. Causes of late twentieth-century trends in New Zealand precipitation. Journal of Climate, 22, 3-19.

UNFCCC, 1992. United Nations Framework Convention on Climate Change, United Nations, New York.

United Nations, 2015. “Paris Agreement”, https://unfccc.int/files/essential_background/convention/application/pdf/english_paris_agreement.pdf. (accessed May 2020).

van der Linden P., Mitchell J. F. B. (Eds.), 2009. ENSEMBLES: Climate Change and Its Impacts: Summary of Research and Results from The ENSEMBLES Project, Met Office Hadley Centre, Exeter.

van Vuuren, D. P., Den Elzen, M. G., Lucas, P. L., Eickhout, B., Strengers, B. J., Van Ruijven, B., Wonink, S., van Houdt, R., 2007. Stabilizing greenhouse gas concentrations at low levels: An assessment of reduction strategies and costs. Climatic Change, 81, 119-159.

van Vuuren, D. P., Edmonds, J., Kainuma, M., Riahi, K., Thomson, A., Hibbard, K., Hurtt, G. C., Kram, T., Krey, V., Lamarque, J. F., Masui, T., Meinshausen, M., 2011a. The representative concentration pathways: An overview. Climatic Change, 109, 5-31.

van Vuuren, D. P., Stehfest, E., Den Elzen, M. G. J., Kram, T., van Vliet, J., Deetman, S., Morna, I., Goldewijk, K. K., Hof, A., Beltran, A. M., Oostenrijk, R., van Ruijven, B., 2011b. RCP2.6: exploring the possibility to keep global mean temperature increase below 2°C. Climatic Change, 109, 95-116.

Vautard R., 2018. Regional Climate Projections. In Troccoli A. (Ed.), Weather & Climate Services for the Energy Industry, Palgrave Macmillan, Cham.

Vaze, J., Teng, J., Chiew, F. H. S., 2011. Assessment of GCM simulations of annual and seasonal rainfall and daily rainfall distribution across south-east Australia. Hydrological Processes, 25, 1486-1497.

Venetsanou, P., Anagnostopoulou, C., Loukas, A., Voudouris, K., 2020. Hydrological impacts of climate change on a data-scarce Greek catchment. Theoretical and Applied Climatology, 140, 1017-1030.

Vincent, L. A., Peterson, T. C., Barros, V. R., Marino, M. B., Rusticucci, M., Carrasco, G., Ramirez, E., Alves, L. M., Ambrizzi, T., Berlato, M. A., Grimm, A. M., Marengo, J. A., Molion, L., Moncunill, D. F., Rebello, E., Anunciação, Y. M. T., Quintana, J., Santos, J. L., Baez, J., Coronel, G., Garcia, J., Trebejo, I., Bidegain, M., Haylock, M. R., Karoly, D., 2005. Observed trends in indices of daily temperature extremes in South America 1960–2000. Journal of Climate, 18, 5011-5023.

Volken, E., Brönnimann, S., 2009. The problem of weather prediction, considered from the viewpoints of mechanics and physics. Meteorologische Zeitschrift, 18, 663-667.

Vose, R. S., Schmoyer, R. L., Steurer, P. M., Peterson, T. C., Heim, R., Karl, T. R., Eischeid, J., 1992. The Global Historical Climatology Network: Long-Term Monthly Temperature, Precipitation, Sea Level Pressure, and Station Pressure Data, Carbon Dioxide Information Analysis Center (CDIAC), Berkeley.

Walsh, K., White, C. J., McInnes, K., Holmes, J., Schuster, S., Richter, H., Evans, J. P., Di Luca, A., Warren, R. A., 2016. Natural hazards in Australia: Storms, wind and hail. Climatic Change, 139, 55-67.

Washington, W. M., Meehl, G. A., 1984. Seasonal cycle experiment on the climate sensitivity due to a doubling of CO_2 with an atmospheric general circulation model coupled to a simple mixed-layer ocean model. Journal of Geophysical Research, 89, 9475-9503.

Weart, S. R., 2004. The Discovery of Global Warming, Harvard University Press, Massachusetts.

Westra, S., White, C. J., Kiem, A. S., 2016. Introduction to the special issue: Historical and projected climatic changes to Australian natural hazards. Climatic Change, 139, 1-19.

White, C. J., Grose, M. R., Corney, S. P., Bennett, J. C., Holz, G. K., Sanabria, L. A., McInnes, K. L., Cechet, R. P., Gaynor, S. M., Bindoff, N. L., 2010. Climate Futures for Tasmania: Extreme Events Technical Report, Antarctic Climate and Ecosystems Cooperative Research Centre, Tasmania.

Widlansky, M. J., Timmermann, A., Stein, K., McGregor, S., Schneider, N., England, M. H., Matthieu, L., Cai, W., 2013. Changes in South Pacific rainfall bands in a warming climate. Nature Climate Change, 3, 417-423.

Wilby, R. L., Wigley, T. M. L., 1997. Downscaling general circulation model output: a review of methods and limitations. Progress in Physical Geography, 21, 530-548.

Wilby, R. L., Charles, S. P., Zorita, E., Timbal, B., Whetton, P., Mearns, L. O., 2004. “Guidelines for Use of Climate Scenarios Developed From Statistical Downscaling Methods”, https://www.ipcc-data.org›dgm_no2_v1_09_2004. (accessed April 2020).

Williamson, D. L., Kiehl, J. T., Ramanathan, V., Dickinson, R. E., Hack, J. J., 1987. Description of NCAR Community Climate Model (CCM1) (No. NCAR/TN-285+STR), National Center for Atmospheric Research, Colorado.

Willmott, C. J., Matsuura, K., 2001. “Terrestrial Air Temperature and Precipitation: Monthly and Annual Time Series (1950–1999) Version 1.02”, http://climate.geog.udel.edu/~climate/html_pages/README.ghcn_ts2.html. (accessed January 2020).

Wilson, C. A., Mitchell, J. F. B., 1987. A doubled CO_2 climate sensitivity experiment with a global climate model including a simple ocean. Journal of Geophysical Research, 92, 13315-13343.

Wippermann, F., Gross, G., 1981. On the construction of orographically influenced wind roses for given distributions of the large-scale wind. Beiträge zur Physik der Atmosphäre, 54, 492-501.

Wise, M. A., Calvin, K. V., Thomson, A. M., Clarke, L. E., Bond-Lamberty, B., Sands, R. D., Smith, S. J., Janetos, A. C., Edmonds, J. A., 2009. Implications of limiting CO_2 concentrations for land use and energy. Science, 324, 1183-1186.

WMO, 1979. World Climate Conference: A Conference of Experts on Climate and Mankind, World Meteorological Organization, Geneva.

Wood, A. W., Maurer, E. P., Kumar, A., Lettenmaier, D. P., 2002. Long-range experimental hydrologic forecasting for the eastern United States. Journal of Geophysical Research, 107, 4429.

Wood, A. W., Leung, L. R., Sridhar, V., Lettenmaier, D. P., 2004. Hydrologic implications of dynamical and statistical approaches to downscaling climate model outputs. Climatic Change, 62, 189-216.

World Bank Group, 2021a. "Country: Indonesia, Climate Data: Historical", https://climateknowledgeportal.worldbank.org/country/indonesia/climate-data-historical. (accessed February 2021).

World Bank Group, 2021b. "Country: Indonesia, Climate Data: Projections", https://climateknowledgeportal.worldbank.org/country/indonesia/climate-data-projections. (accessed February 2021).

Woth, K., Weisse, R., von Storch, H., 2006. Climate change and North Sea storm surge extremes: an ensemble study of storm surge extremes expected in a changed climate projected by four different regional climate models. Ocean Dynamics, 56, 3-15.

Zaninelli, P. G., Menéndez, C. G., Falco, M., López-Franca, N., Carril, A. F., 2019. Future hydroclimatological changes in South America based on an ensemble of regional climate models. Climate Dynamics, 52, 819-830.

Zhang, X., Aguilar, E., Sensoy, S., Melkonyan, H., Tagiyeva, U., Ahmed, N., Kutaladze, N., Rahimzadeh, F., Taghipour, A., Hantosh, T. H., Albert, P., Semawi, M., Ali, M. K., Al-Shabibi, M. H. S., Al-Oulan, Z., Zatari, T., Khelet, I. A. D., Hamoud, S., Sagir, R., Demircan, M., Eken, M., Adiguzel, M., Alexander, L., Peterson, T. C., Wallis, T., 2005. Trends in Middle East climate extreme indices from 1950 to 2003. Journal of Geophysical Research, 110, D22104.

Zheng, Y., Lin, J. L., Shinoda, T., 2012. The equatorial Pacific cold tongue simulated by IPCC AR4 coupled GCMs: Upper ocean heat budget and feedback analysis. Journal of Geophysical Research, 117, C05024.

Zorita, E., von Storch, H., 1999. The analog method as a simple statistical downscaling technique: comparison with more complicated methods. Journal of Climate, 12, 2474-2489.

APPENDIX A: SEASONAL SPATIAL PATTERN OF THE DIFFERENCE BETWEEN RegCM4.6 OUTPUT AND CRU DATA FOR MEAN AIR TEMPERATURE

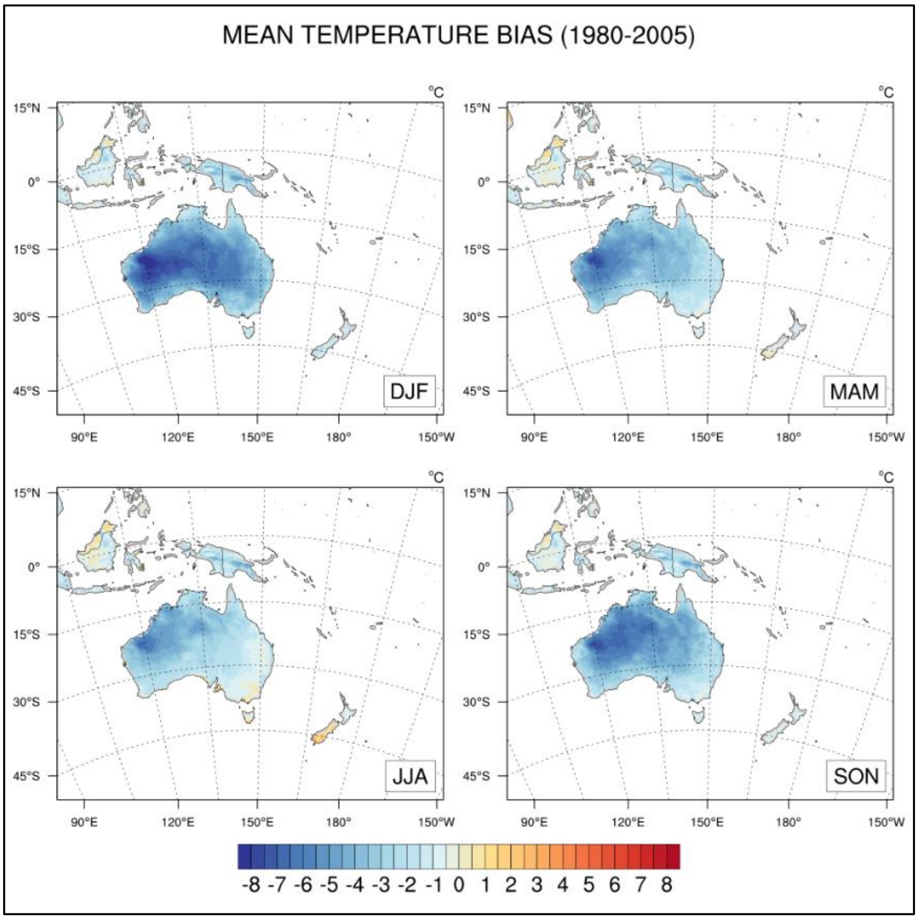

APPENDIX B: SEASONAL SPATIAL PATTERN OF THE DIFFERENCE BETWEEN RegCM4.6 OUTPUT AND CRU DATA FOR MAXIMUM AIR TEMPERATURE

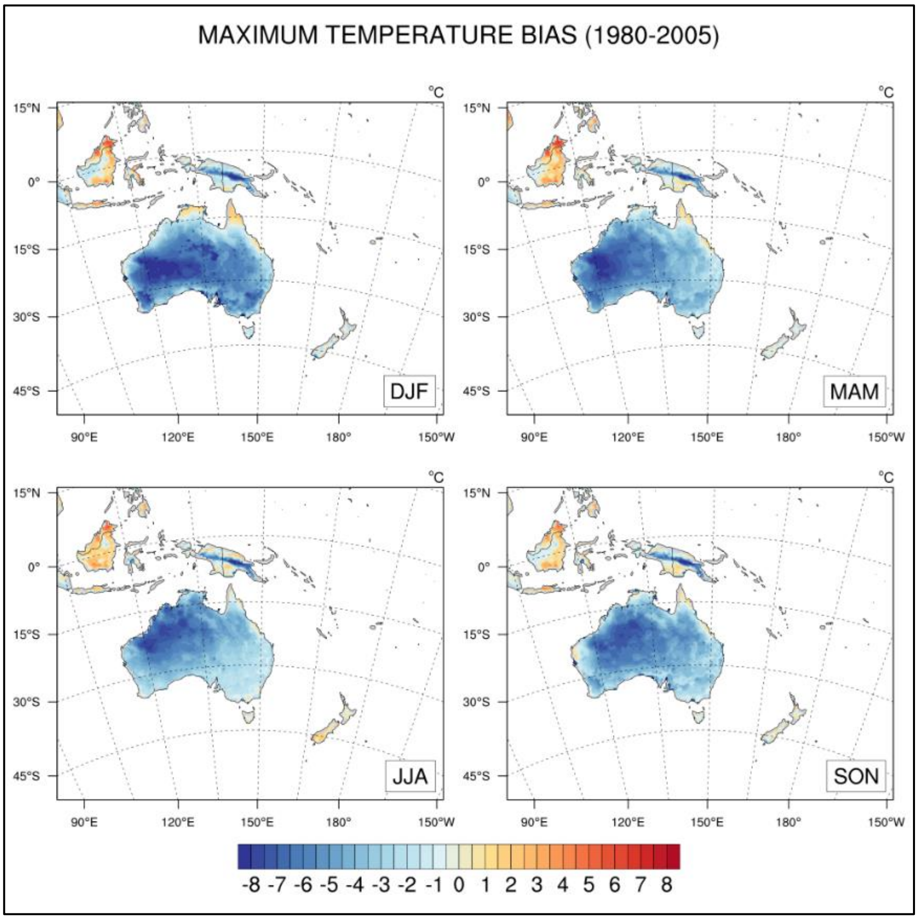

APPENDIX C: SEASONAL SPATIAL PATTERN OF THE DIFFERENCE BETWEEN RegCM4.6 OUTPUT AND CRU DATA FOR MINIMUM AIR TEMPERATURE

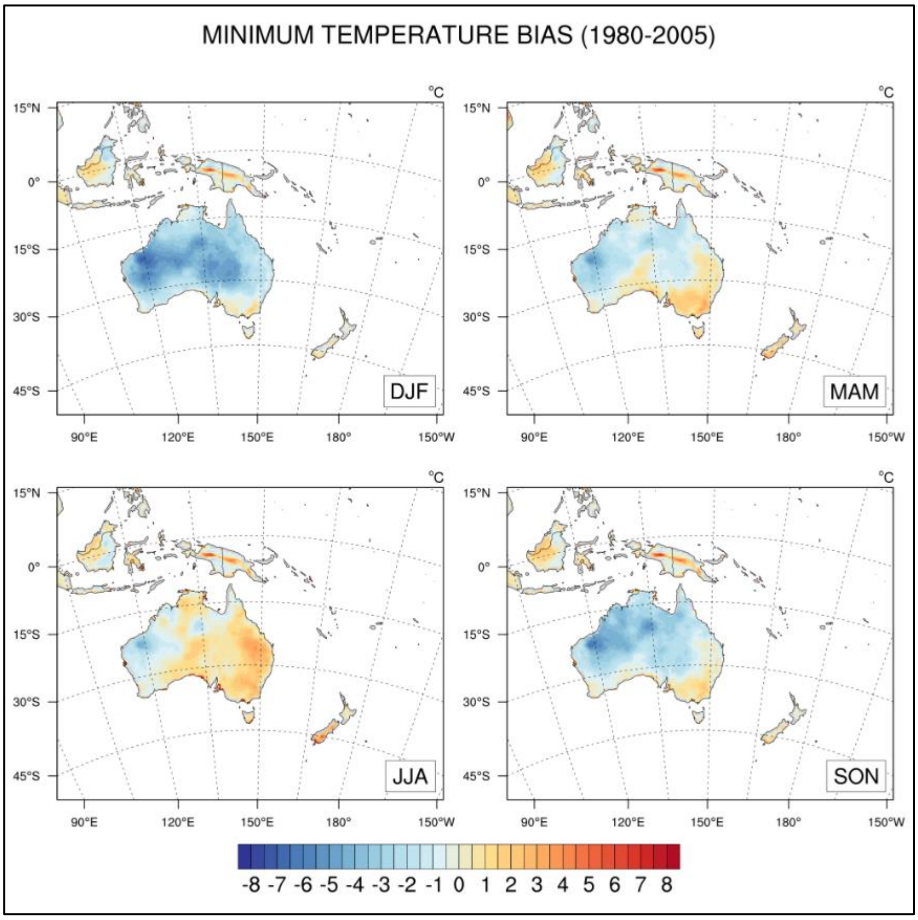

APPENDIX D: SEASONAL SPATIAL PATTERN OF THE DIFFERENCE BETWEEN RegCM4.6 OUTPUT AND CRU DATA FOR PRECIPITATION